Numerical analysis and discrete approximation of a dispersive shallow water model

Nora Aïssiouene

Université Pierre et Marie Curie

Institut National de Recherche en Informatique et Automatique

École doctorale de sciences mathématiques de Paris centre

Thèse de doctorat

Discipline : Mathématiques

présentée par

Nora Aïssiouene

Numerical analysis and discrete approximation of a dispersive shallow water model

---

dirigée par Edwige Godlewski et Jacques Sainte-Marie

soutenue le 06 Décembre 2016 devant le jury composé de :

M. Michael Dumbser	Professeur	Rapporteur
M. Robert Eymard	Professeur	Rapporteur
M^{me} Marie-Odile Bristeau	Directeur de recherche	Examinatrice
M. Yvon Maday	Professeur	Examinateur
M^{me} Anne Mangeney	Professeur	Examinatrice
M. Fabien Marche	Maître de Conférence	Examinateur
M^{me} Edwige Godlewski	Professeur	Directrice
M. Jacques Sainte-Marie	Directeur de recherche	Directeur

Equipe-projet Inria ANGE (Analyse numérique appliquée à la géophysique et à l'écologie)

Institut National de Recherche en Informatique et Automatique de Paris.
2 rue Simone Iff, CS 42112
75 589 Paris Cedex 12

—

Laboratoire Jacques Louis Lions
4 place Jussieu
75005 Paris

Université Pierre et Marie Curie.
École doctorale de sciences mathématiques de Paris centre.
Boîte courrier 290
4 place Jussieu
75 252 Paris Cedex 05

Résumé

Dans cette thèse, on s'intéresse à l'approximation numérique d'un modèle d'écoulement dispersif en eau peu profonde. Les applications visées par ce type de modélisation sont nombreuses (écoulement dans les océans, les rivières, etc) et cette thèse est motivée en particulier par les risques naturels et la production d'énergie renouvelable. Le modèle étudié a été dérivé par moyenne selon la verticale des équations d'Euler et prend en compte la pression non-hydrostatique. Cette contribution non hydrostatique apporte des précisions cruciales pour comprendre les phénomènes, notamment lorsque les effets dispersifs sont importants. Il est alors nécessaire de résoudre un système de type incompressible; ce qui nous amène à résoudre une équation elliptique en pression.
Nous proposons une méthode numérique pour résoudre le système dispersif avec topographie pour les modèles 1D et 2D. L'approche développée est basée sur un schéma de type prediction-correction, initialement introduit par Chorin-Temam pour les équations de Navier-Stokes. Nous définissons un cadre générique qui permet de concevoir un schéma valable en 1D et 2D et aussi de pouvoir augmenter l'ordre de précision. Par ailleurs, la méthode proposée garantit les propriétés de stabilité telles que la positivité de la hauteur d'eau, la conservation de l'entropie discrète et la condition inf-sup. L'étape de prédiction du schéma implique de résoudre les équations de Saint-Venant avec terme source, cette partie est réalisée avec la méthode des volumes finis, tandis que la partie correction nous amène à résoudre un problème mixte en vitesse/pression. Ainsi, nous proposons une formulation variationnelle qui nous permet d'appliquer la méthode des éléments finis avec des choix d'espaces compatibles. Par ailleurs, cela nous permet d'établir des conditions aux limites compatibles entre l'étape de prédiction et l'étape de correction. Cette méthode est appliquée pour le problème en 1D et 2D pour des maillages non structurés. Le travail effectué étant destiné à simuler des processus géophysiques réels, la méthode a été conçue pour pouvoir traiter les transitions de sol sec/mouillé et cette propriété a été confirmée par plusieurs tests numériques. Par ailleurs, pour palier les problèmes liés aux coûts de calculs, nous utilisons des méthodes itératives pour la résolution de l'équation en pression. Afin de valider la méthode, nous présentons la comparaison entre certaines solutions analytiques et leurs simulations numériques. Nous avons également réalisé des tests comparant les solutions calculées et les données obtenues lors d'expériences en laboratoire.

Mots-clés

Ecoulements à surface libre, dispersion, pression non hydrostatique, propagation des ondes, schéma prediction-correction, différences finies, volumes finis, éléments finis.

Abstract

In this PhD thesis we are interested in the numerical approximation of a dispersive shallow water system, aimed at modeling the free surface flows (*e.g.* ocean and rivers) and motivated by applications for natural hazards and sustainable energy resources. This model is a depth-averaged Euler system and takes into account a non-hydrostatic pressure which brings crucial information for understanding the behavior of the flow, particularly when dispersion occur. However this dispersive contribution suggests solving an incompressible type system, and this leads us to solve an elliptic equation in the pressure.
We develop a numerical method for the one- and the two-dimensional dispersive shallow water system with a topography. The approach is based on a prediction-correction method initially introduced by Chorin-Temam, and we establish a global framework in order to easily increase the order of accuracy of the method. Moreover, the proposed method guarantees good stability properties such as positivity, entropy inequality, and inf-sup condition. The prediction part leads to solving a shallow water system for which we use finite volume methods, while the correction part leads to solving a mixed problem in velocity and pressure. We propose a variational formulation of the mixed problem which allows us to apply a finite element method with compatible spaces. In this framework we establish compatible boundary conditions between the prediction part and the correction part. The method is performed for the one-dimensional model and for the two-dimensional problem on unstructured grids. In order to make the method practical for real geophysical cases, we have derived a scheme able to treat wet/dry interfaces and to this end we give many examples to test its performance. In addition, to deal with the significant computational cost for the two-dimensional problem, an iterative method is used.
A validation of the method is established using stationary and non-stationary analytical solutions for the one- and the two-dimensional problem. Moreover, we provide a comparison of simulated solutions with data from laboratory experiments.

Keywords

free surface flows, depth-averaged Euler, dispersion, non-hydrostatic pressure, Shallow Water, splitting scheme, waves, finite volume, finite element.

Contents

List of Figures

Chapter 1

Introduction

1.1 General issues

A good understanding of geophysical flows behavior is essential in order to make accurate predictions about natural events such as tsunamis, wave interactions or sustainable energy resources. Gaining this understanding is a major challenge that requires close cooperation between geophysicists, mathematicians and researchers in fluid mechanics. The environmental stakes are high since these predictions deal with natural hazards like tsunamis, coastal volcano eruptions, erosion, flooding and rises in sea level. Moreover, faced with global climate change, having a better knowledge and understanding of these natural phenomena makes it possible to adapt to environmental changes in an appropriate and efficient way. These problems do not only concern natural hazards. To take the example of energy production, in addition to coastal and off-shore wind turbines, new and innovative ways must be found to harness natural resources like marine energies or fuel produced by microalgae.

To understand these processes, many laboratory experiments are performed by geophysicists in an attempt to reproduce phenomena, and these experiments provide a large amount of exploitable data. From the mathematical side, having an accurate model to represent a real phenomenon is still an important research field and is essential in order to provide technical tools to help us understand and make predictions. Although there are now a number of ways to predict many phenomena, it is essential to better understand their origins. For instance, the arrival of a tsunami wave on the coast line can be quite well predicted, but our knowledge of the source signal from the seismic remains far from complete.

In this context, numerical simulation provides a good approach to represent the physics involved, which clearly makes improving mathematical models together with numerical methods a crucial issue. In addition, high computing resources are being increasingly developed, allowing the scientific community to propose more complex methods for complex models that have a significant computational cost.

In this work, we are interested in modeling flow propagation in shallow water. In this introduction, we give a state of the art of existing models and methods, drawing a clear distinction between hydrostatic and non-hydrostatic models. Then we present a global overview of our work. Finally, we present our conclusion and outline for future work.

1.2 Applications and motivations

It is clear that a vast number of applications that require hydrodynamic simulations exist and the dispersive contributions of the models can modify the conclusions of a study drastically. In this section, we focus on two important issues: renewable energy production and coastal area.

Sustainable energy

The evolution of energy production is forcing us to find new ways to explore the power of natural resources. This PhD thesis is done in the context of the Inria Project lab **Algae in Silicio**. This project brings together biologists and mathematicians who aim at working towards a new generation of bio fuel (see [49]). To allow the culture of micro-algae, laboratories use photobioreactors or raceway ponds.
Among the possibilities to produce energy from biology, we are interested in the ability of some micro-algae species to store a large amount of lipids. The objective is to optimize the production of the biomass. To do so, the micro-algae culture is done in raceway, which is equipped with a paddle wheel, which helps the circulation of the micro-algae. In this context, the aim of the hydrodynamic simulation is to predict the trajectories of the micro-algae in the raceway and to propose ways to optimize the production rate. Several parameters can be tested like the dimensions of the raceway and the paddle wheels together with their velocity. In a more general case, the conception of the infrastructure can be optimized. A first study has been done in the ANGE team to simulate the behavior of the micro-algae in the raceway with a multilayer hydrostatic model [6]. One of the objectives of this PhD thesis is to improve the accuracy of the results concerning the micro-algae's trajectories by using a non-hydrostatic model with the biological model to predict the Lagrangian trajectories of the particles. Figure 1.1 shows a raceway with the paddle wheels (1.1a) and a simulation (1.1b) where we can see the trajectories of the micro-algae in this raceway computed by a multi-layer hydrostatic system (we give the details of the models in the next section). With the hydrostatic model, we neglect the vertical acceleration, but in the case of the raceway, the fluid can be extremely rough and we expect a large acceleration near the paddle wheel. In these cases, the dispersion can have an effect on the hydrodynamics and then on the trajectories. We expect to observe a modification in the velocity if we use a multi-layer model with dispersion. In addition, we expect a modification of the free surface and then, an impact on the refraction of the light, which

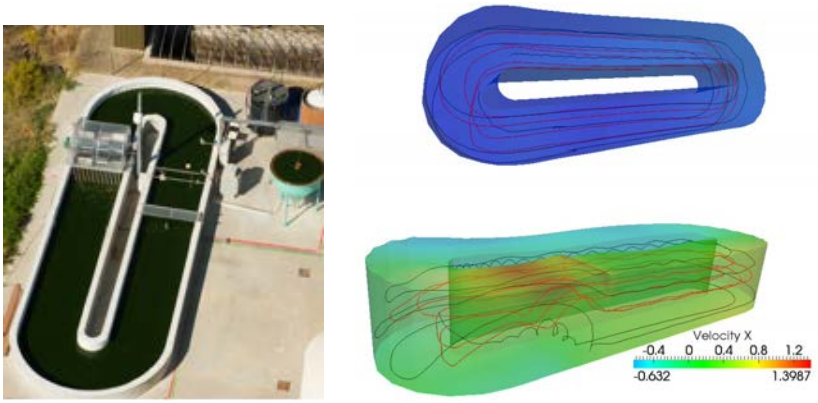

(a) Raceway (INRA Narbonne)

(b) Simulation of Lagrangian trajectories in the Raceway

Figure 1.1: Raceway illustration and simulation.

has consequences on the behavior of the micro-algae.

Coastal oceanography

Among coastal engineering concerns, the study of tsunamis and large wavelength propagation is one issue which needs a good model to be able to predict and understand this phenomenon. From the seisimic activity to the flooding, there are different geophysical regimes, so attempting to simulate a tsunami by means of only one simplified model is not a realistic proposition. In the context of the MIMOSA ANR (analysis, modeling and applications of seismic noise: from microseisms to earth normal mode). Another motivation of this work is to use a dispersive shallow water model for the propagation of tsunamis and wave interactions. The challenge is to have a better understanding of the seismic perturbation generating a tsunami. A previous study carried out in the team with the collaboration of IPGP used the hydrostatic model to simulate the main waves of the observed data. The objective now is to evaluate the impact of the dispersive effect for a real case like a tsunami.

1.3 Geophysical models

The most comonly used model giving a mathematical description of the fluid dynamic is the incompressible Navier-Stokes Equations (1848) for a Newtonian fluid [80]. It is clear that the real phenomena is always much more complicated, but in practice, the Navier-Stokes Equations (NSE) provide a relevant mathematical model to approach the reality of

oceans and river flows. We recall below the system in three dimensions:

$$\begin{aligned}
\frac{\partial \rho}{\partial t} + \frac{\partial \rho u}{\partial x} + \frac{\partial \rho v}{\partial y} + \frac{\partial \rho w}{\partial z} &= 0, && (1.1)\\
\frac{\partial \rho u}{\partial t} + \frac{\partial \rho u^2}{\partial x} + \frac{\partial \rho uv}{\partial y} + \frac{\partial \rho uw}{\partial z} + \frac{\partial p}{\partial x} &= \frac{\partial \Sigma_{xx}}{\partial x} + \frac{\partial \Sigma_{xy}}{\partial y} + \frac{\partial \Sigma_{xz}}{\partial z}, && (1.2)\\
\frac{\partial \rho v}{\partial t} + \frac{\partial \rho uv}{\partial x} + \frac{\partial \rho v^2}{\partial y} + \frac{\partial \rho vw}{\partial z} + \frac{\partial p}{\partial y} &= \frac{\partial \Sigma_{yx}}{\partial x} + \frac{\partial \Sigma_{yy}}{\partial y} + \frac{\partial \Sigma_{yz}}{\partial z}, && (1.3)\\
\frac{\partial \rho w}{\partial t} + \frac{\partial \rho uw}{\partial x} + \frac{\partial \rho vw}{\partial y} + \frac{\partial \rho w^2}{\partial z} + \frac{\partial p}{\partial z} &= -\rho g + \frac{\partial \Sigma_{zx}}{\partial x} + \frac{\partial \Sigma_{zy}}{\partial y} + \frac{\partial \Sigma_{zz}}{\partial z}, && (1.4)
\end{aligned}$$

where (u, v, w), p are the velocity (resp. the pressure), ρ the density of the fluid, g the gravity acceleration, and the Cauchy stress tensor Σ is given by:

$$\Sigma_{xx} = 2\mu \frac{\partial u}{\partial x}, \quad \Sigma_{xz} = \Sigma_{zx} = \mu(\frac{\partial u}{\partial z} + \frac{\partial w}{\partial x}), \tag{1.5}$$

$$\Sigma_{yy} = 2\mu \frac{\partial v}{\partial y}, \quad \Sigma_{xy} = \Sigma_{yx} = \mu(\frac{\partial u}{\partial z} + \frac{\partial w}{\partial x}), \tag{1.6}$$

$$\Sigma_{zz} = 2\mu \frac{\partial u}{\partial z}, \quad \Sigma_{yz} = \Sigma_{zy} = \mu(\frac{\partial u}{\partial z} + \frac{\partial w}{\partial x}), \tag{1.7}$$

with μ the dynamic viscosity. Equation (1.1) is the continuity equation and Equations (1.2)-(1.4) are the momentum equations. To model the free surface and the bottom of the flow, the system (1.2)-(1.1) is completed with kinematic boundary conditions (specified in the next section).

Although the theoritical issues surrounding the NSE represent an on-going research topic, the NSE are widely used as the reference model. In fluid mechanics, we often reduce the model to some specific regime to allow the model to be studied and solved numerically.

If we neglect the viscosity, considering a perfect fluid with $\rho_0 = 1$, we have the incompressible Euler system with a constant density:

$$\begin{aligned}
\frac{\partial u}{\partial x} + \frac{\partial v}{\partial y} + \frac{\partial w}{\partial z} &= 0, && (1.8)\\
\frac{\partial u}{\partial t} + \frac{\partial u^2}{\partial x} + \frac{\partial uv}{\partial y} + \frac{\partial uw}{\partial z} + \frac{\partial p}{\partial x} &= 0, && (1.9)\\
\frac{\partial v}{\partial t} + \frac{\partial uv}{\partial x} + \frac{\partial v^2}{\partial y} + \frac{\partial vw}{\partial z} + \frac{\partial p}{\partial y} &= 0, && (1.10)\\
\frac{\partial w}{\partial t} + \frac{\partial uw}{\partial x} + \frac{\partial vw}{\partial y} + \frac{\partial w^2}{\partial z} + \frac{\partial p}{\partial z} &= -g. && (1.11)
\end{aligned}$$

Both analytical and numerical difficulties arise when solving this system. One of them comes from the incompressibility of the fluid, the pressure p being a Lagrange multiplier of this condition. Other constraints arise at the numerical level for real applications, especially when one wants to model the free surface on a domain with large dimensions (*eg.*

oceans, lakes, rivers, etc.). One of the possibility to approach free surface flow behavior consists in using the numerical methods for the Navier Stokes model and detecting the free surface. Many techniques have been proposed to approach this issue. For instance, bi-phasic models [149] use the Navier Stokes equations with two fluids, the water and the air. The surface is tracked by detecting the air/water interface. The Navier-Stokes equations can also be used in a moving domain to avoid solving equations for the air domain. This method also requires detecting the surface with a level set method for instance, and re-meshing the domain at each iteration of the computation [135]. We are interested in model where the dimensions are reduced and where we avoid to re-mesh a domain during the computations. This implies reducing the models according to the considered geophysical phenomenon. Models for the propagation of waves have been studied by both physicists and mathematicians. From the mathematical point of view, simpler geophysical free surface models can be derived from the Navier-Stokes system under some assumptions. In the following section, we give a classification of the most commonly used free surface geophysical models.

1.3.1 Hydrostatic models

Hydrostatic Navier-Stokes

The Hydrostatic Navier-Stokes free surface model is determined by assuming that the pressure is hydrostatic [13, 39, 88, 122]. This means in the NSE (1.2)-(1.4), Equation (1.4) is replaced by:

$$\frac{\partial p}{\partial z} = -g + \frac{\partial \Sigma_{zx}}{\partial x} + \frac{\partial \Sigma_{zy}}{\partial y} + \frac{\partial \Sigma_{zz}}{\partial z}. \tag{1.12}$$

Thus, we complete Equations (1.2)-(1.3) and (1.12) with the kinematic boundary conditions at the surface

$$\frac{\partial \eta}{\partial t} + u_s \frac{\partial \eta}{\partial x} + v_s \frac{\partial \eta}{\partial y} - w_s = 0, \tag{1.13}$$

and the non penetration boundary conditions at the bottom:

$$u_b \frac{\partial z_b}{\partial x} + v_b \frac{\partial z_b}{\partial y} - w_b = 0, \tag{1.14}$$

where η is the free surface elevation, $z_b = z_b(x, z)$ is the topography and (u_s, v_s, w_s) (resp. (u_b, v_b, w_b)) is the velocity at the surface (resp. at the bottom). We also denote the water depth by:

$$H = \eta - z_b \tag{1.15}$$

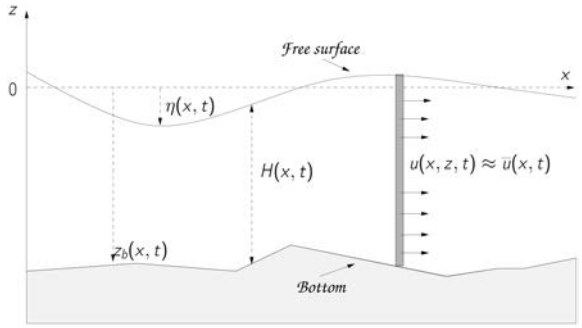

Figure 1.2: Notations for the one-dimensional Shallow Water system

For the hydrostatic Navier Stokes equations, the pressure is a function of the other variables mainly, neglecting the viscosity terms (1.7), it reads $p = g(\eta - z) + p^a$, with p^a the atmospheric pressure and with suitable boundary conditions specified later. Therefore hydrostatic models have some common features with compressible models. This highlights the fact that considering the hydrostatic pressure, we avoid the inconvenience related to the incompressible property. However, the issue related to the size of the domain and the moving domain is still present with this model.

The Shallow Water (or Saint-Venant) model

The Shallow Water system was introduced in 1871 by the physicist Adhémar Jean Claude Barré de Saint-Venant [21, 20]. This is the classical model used in practice to represent the flow behavior in rivers (see [32, 111, 109, 110]) and, as the name implies, it is essentially based on the assumption that the water depth is shallow. This assumption implies that the model is hydrostatic and states that the velocity is constant with the depth, which is valid for rivers, lakes or coastal flows. Classically, the two-dimensional Shallow Water model can be written as:

$$\frac{\partial H}{\partial t} + \frac{\partial H\overline{u}}{\partial x} + \frac{\partial H\overline{v}}{\partial y} = 0, \tag{1.16}$$

$$\frac{\partial H\overline{u}}{\partial t} + \frac{\partial}{\partial x}(H\overline{u}^2) + \frac{\partial}{\partial y}(H\overline{uv}) + \frac{\partial}{\partial x}(g\frac{H^2}{2}) = -gH\frac{\partial z_b}{\partial x}, \tag{1.17}$$

$$\frac{\partial H\overline{v}}{\partial t} + \frac{\partial}{\partial x}(H\overline{uv}) + \frac{\partial}{\partial y}(H\overline{v}^2) + \frac{\partial}{\partial y}(g\frac{H^2}{2}) = -gH\frac{\partial z_b}{\partial y}. \tag{1.18}$$

where we denote $(\overline{u}, \overline{v})$ an average of the velocity (u, v) over the depth:

$$\overline{u} = \frac{1}{H}\int_{z_b}^{\eta} u\, dz, \quad \overline{v} = \frac{1}{H}\int_{z_b}^{\eta} v\, dz. \tag{1.19}$$

This is illustrated for the one-dimensional model in Figure 1.2. There are different ways (from physics or mathematics) to derive a hydrostatic model like the Saint-Venant model.

In the following, we briefly recall a way to derive the Shallow Water system (1.16)-(1.18) from the Euler equations, which shows why the Shallow Water system is hydrostatic. We give the derivation starting from the Euler system in three dimensions to obtain the Shallow Water equations in two dimensions. To do so, we use a dimensionless system and make the necessary assumptions on the parameters. It is very classical to use these kinds of techniques for partial differential equations to simplify the models. If we introduce the characteristic values L, h, and

$$\epsilon = \frac{h}{L}, \tag{1.20}$$

the shallow water assumption is satisfied when $\epsilon << 1$, where L is the wave length characteristic and h is the water depth characteristic. In addition to the definition of L, h and ϵ given by (1.20), we introduce the following characteristic values

$$c = \sqrt{gh}, \quad U = c, \quad W = \epsilon c, \quad P = c^2, \quad T = \frac{\lambda}{c},$$

where c represents the characteristic wave speed. Then, we introduce the dimensionless parameters

$$\tilde{x} = \frac{x}{L}, \quad \tilde{u} = \frac{u}{U}, \quad \tilde{v} = \frac{v}{U}, \quad \tilde{p} = \frac{p}{P}, \quad \tilde{g} = \frac{gH}{U^2}, \quad \tilde{z} = \frac{z}{h}, \quad \tilde{\eta} = \frac{\eta}{h},$$

and we obtain the dimensionless Euler equations:

$$\frac{\partial \tilde{u}}{\partial x} + \frac{\partial \tilde{w}}{\partial z} = 0, \tag{1.21}$$

$$\frac{\partial \tilde{u}}{\partial t} + \frac{\partial \tilde{u}^2}{\partial x} + \frac{\partial \tilde{u}\tilde{v}}{\partial y} + \frac{\partial \tilde{u}\tilde{w}}{\partial z} + \frac{\partial \tilde{p}}{\partial x} = 0, \tag{1.22}$$

$$\frac{\partial \tilde{u}}{\partial t} + \frac{\partial \tilde{u}\tilde{v}}{\partial x} + \frac{\partial \tilde{v}^2}{\partial y} + \frac{\partial \tilde{u}\tilde{w}}{\partial z} + \frac{\partial \tilde{p}}{\partial y} = 0, \tag{1.23}$$

$$\epsilon^2 \left(\frac{\partial \tilde{w}}{\partial t} + \frac{\partial \tilde{u}\tilde{w}}{\partial x} + \frac{\partial \tilde{v}\tilde{w}}{\partial y} + \frac{\partial \tilde{w}^2}{\partial z} \right) + \frac{\partial \tilde{p}}{\partial z} = -1. \tag{1.24}$$

Under the shallow water assumption $\epsilon << 1$, and with the dimensionalized variables, the terms

$$\frac{\partial w}{\partial t} + \frac{\partial uw}{\partial x} + \frac{\partial vw}{\partial y} + \frac{\partial w^2}{\partial z}, \tag{1.25}$$

are neglected and we deduce the hydrostatic assumption:

$$\frac{\partial p}{\partial z} = -g. \tag{1.26}$$

After integration over the depth, we deduce the hydrostatic pressure:

$$p(x,y,z,t) = g(\eta(x,y,t) - z) + p^a \tag{1.27}$$

where p^a is the pressure at the surface, assumed to be equal to the atmospheric pressure, is neglected. Then $p = g(\eta - z)$ and the averaged pressure is :

$$\bar{p} = g\frac{H}{2}. \tag{1.28}$$

After determining closure relations between $\int u^2$ and $(\int \bar{u})^2$ we find the inviscid Shallow Water system (1.16)-(1.18). This assumption is valid in many geophysical situations, so we obtain a compressible type system with a source term. The shallowness hypothesis makes this model appropriate to simulate the propagation of a tsunami for instance, where the characteristic depth of the ocean is between 1 and 4 km and the characteristic length is greater than 200 km (see [64]). However, when one wants to study the waves involved in the origins of the tsunami, it is necessary to go further in the asymptotic derivation to have more accurate results.

Remark 1.3.1. *The 2D Shallow Water model is derived from the 3D Navier-Stokes system thanks to the vertical average, the dimension is reduced to two, yet the vertical velocity is not neglected and is obtained using the divergence-free condition. We obtain an explicit equation for* $\bar{w}$

$$\bar{w} = -\frac{1}{2}\frac{\partial H\bar{u}}{\partial x} - \frac{1}{2}\frac{\partial H\bar{v}}{\partial y} + \frac{\bar{u}}{2}\frac{\partial(H+2z_b)}{\partial x} + \frac{\bar{v}}{2}\frac{\partial(H+2z_b)}{\partial y}, \tag{1.29}$$

that completes Equations (1.16)-(1.18). *Extensive literature exists for the SW system, both from the theoritical and numerical points of view.*

1.3.2 State of the art of non-hydrostatic models

In usual shallow water equations, the vertical acceleration is neglected, thus dispersive effects due to the terms (1.25) are not modeled. Even though the hydrostatic system is suitable for many practical cases, the validity domain is still an important research field. The difficulties dealing with a non-hydrostatic model appear both at the continuous and numerical levels. Thus, many dispersive systems have been developed to take the dispersion into account, such as the unidirectional equation to model the propagation of solitary waves above a flat bottom called the Korteweg-de Vries equation (1895) presented in [100] (see also [101, 55, 123]). Then, Boussinesq (1871) studied non-linear systems for wave propagation in a channel [36, 37, 38]), followed by Peregrine (1967) in [131], then Green and Naghdi (1976) in [86, 87], see also [104, 95, 142] for other formulations of the Green-Naghdi equations. We also refer to Nwogu (1993) for reduced models for

coastal engineering in [129], and in 2003, Saut studied non-linear wave equations with dispersion [27, 28]. Although a large class of models is available, other non-hydrostatic models have been proposed more recently, by among, others Sainte-Marie [44, 141, 43], Lannes [106, 104], Yamazaki [152], Gavrilyuk [108].
In the following section, we outline some reference dispersive models to understand the difficulty of taking this vertical acceleration into account (1.25). The models we present can be derived from the Navier-Stokes (1.1)-(1.4) or the Euler (1.8)-(1.11) systems. One can use geophysical criteria and linear theory [1] to approximate the dispersion relation, the minimization of energy or the asymptotic expansion [104, 52]. In the case of approximation by asymptotic expansion, we often distinguish the different regimes like Shallow Water (i.e when $kh << 1$, k is the wave number and h is the characteristic value as used in (1.20)) with small or large amplitude regimes. Furthermore, it is possible to derive many free surface systems depending on the regime, for instance by introducing other characteristic values like the typical amplitude or the variation of the bottom. This leads to asymptotic models with dimensionless parameters such as nonlinearity ($\frac{a_{surf}}{h}$, where a_{surf} is the characteristic amplitude wave), shallowness (defined by (1.20)), topography and transversality for the two-dimensional model. When we derive a symplified system starting from the Euler equations keeping high order terms, i.e keeping the terms in $O(\epsilon^k)$, $k \geq 2$, then the system includes high order derivatives and this makes the equation hard to study both analytically and numerically. Some other criteria are also used to calibrate parameters in order to fit with data both from laboratory experiments or observations of a real phenomenon like a tsunami. There is also a class of models where we consider the potential flow ϕ such that $(u, v, w) = \nabla\phi$, and we refer to the Bernoulli equations, for example (see [104]).
The challenge concerns how to reduce a model from NSE or Euler equations with good properties and for which we can develop a practicable numerical method. The goal of this section is not to compare the different models but to give a range of models from which one can start to study dispersive effects. We also stress that there is not a single satisfcatory model which is valid for many regimes with a good mathematical structure. Each of them has a limited range of validity. Many of them are still being studied in order to be improved thanks to several criteria (both mathematical and geophysical). Despite the existing literature on these subjects, there is a real need to develop good mathematical models and robust and stable numerical methods.

The Green Nagdhi model

The Green-Naghdi (GN in the following) model, also known as the Fully non linear Boussinesq equations, was introduced by Serre [142], then Green and Naghdi [86], and is the reference model to represent dispersion despite its complexity, both to analyze and solve numerically. We give the one-dimensional system with a variable topography and we refer to [104] for a fully justified asymptotic model with dimensionless parameters. It has been

widely studied by Lannes *et al.* ([29, 104]) by distinguishing several asymptotic regimes (long wave, small amplitude, small perturbation of the bottom, etc.). It is given in [104, 48] with the formulation:

$$\frac{\partial H}{\partial t} + \frac{\partial H\bar{u}}{\partial x} = 0, \tag{1.30}$$

$$\frac{\partial H\bar{u}}{\partial t} + \frac{\partial H\bar{u}^2}{\partial x} + (1 + H\mathcal{T}\frac{1}{H})^{-1}\left[gH\frac{\partial}{\partial x}(H - H_0) + h\mathcal{Q}(\bar{u})\right] = 0, \tag{1.31}$$

where $H(x,t), z_b(x)$ are defined as in (1.15) and $H_0(x)$ is the water depth at rest, and $\mathcal{T}$ and $\mathcal{Q}$ are the differential operators defined by :

$$\begin{aligned}
\mathcal{T}w &= -\frac{H^2}{3}\frac{\partial^2 w}{\partial x^2} - H\partial_x H\partial_x w + \left(\partial_x(H - H_0)\partial_x^2 b + \frac{H}{2}\partial^3 z_b\right)\bar{u}^2, \\
\mathcal{Q}(\bar{u}) &= 2H\partial_x\left(H + \frac{b}{2}\right)\left(\partial_x^2\bar{u}\right)^2 + \frac{4}{3}H^2\partial_x\bar{u}\partial_x^2\bar{u} + H\partial_x^2 z_b\bar{u}\partial_x u \\
&\quad + \left(\partial_x(H - H0)\partial_x^2 z_b + \frac{H}{2}\partial_x^3 z_b\right)\bar{u}
\end{aligned}$$

This model has also been provided in two dimensions in [106]. The fact that the bottom is not flat leads to a complex model, which is still an important field of investigation. Furthermore, in [48], Chazel *et al.* proposed an improvement of the GN system in two dimensions based on linear theory [1]. The idea is to establish common properties of the linearized system of (1.30)-(1.31) for a flat bottom around a given state. More precisely, the parameters are chosen to have an optimal dispersion relation. Among the reduced models that depend on regimes (small amplitude, small perturbation of the bottom etc), it is often possible to write the system in a more suitable formulation, so Equation (1.31) can be written :

$$\frac{\partial H\bar{u}}{\partial t} + \frac{\partial H\bar{u}^2}{\partial x} + \mathcal{D} = 0, \tag{1.32}$$

where $\mathcal{D}$ is the non-hydrostatic contribution containing differential operators (in space and time) in terms of $\bar{u}$, which depends on the regime. This formulation is especially more convenient to provide a relevant numerical method, but the expression of $\mathcal{D}$ can be very complex depending on the regime and contains high order derivative terms.

The depth-averaged Euler Systems

In the ANGE team, several non-hydrostatic models, generally derived from the Euler equations, have been proposed. We recall some of them briefly here and we focus on the depth-averaged Euler (DAE in the following) system for which the numerical method presented in this PhD thesis was developed.

- In 2008, in [44], a derivation of non-hydrostatic models was proposed with an asymp-

totic analysis to model long wave propagation. It led to a model that is similar to a Boussinesq-type model [27, 28].

- In 2009, in [141], J. Sainte-Marie proposed an extension to the one-dimensional Shallow Water system with dispersive terms and presented a multilayer version of the model.

- In 2011, in [42], a model similar to the Yamazaki model [152] was presented. It does not take into consideration the advective terms of the vertical velocity $\frac{\partial uw}{\partial x}+\frac{\partial vw}{\partial y}+\frac{\partial w^2}{\partial z}$ in (1.25), hence in the Euler system, the momentum equation is taken as:

$$\frac{\partial w}{\partial t}+\frac{\partial p}{\partial z}=-g. \tag{1.33}$$

For this PhD thesis, we consider the non-hydrostatic depth-averaged model introduced in 2013 by Bristeau *et al.* in [43] (we do not give the details of the complete derivation of the model). We denote by $(\bar{u},\bar{v},\bar{w})^T$ the three-dimensional averaged velocity and $\bar{p}_{nh}$, the non-hydrostatic pressure. The idea is to derive a free surface model which keeps the vertical acceleration (1.25). In [43], the model is written in one dimension but its extension to two dimensions is straightforward and reads:

$$\begin{aligned}
\frac{\partial H}{\partial t}+\frac{\partial H\bar{u}}{\partial x}+\frac{\partial H\bar{v}}{\partial y} &= 0, && (1.34)\\
\frac{\partial H\bar{u}}{\partial t}+\frac{\partial}{\partial x}(H\bar{u}^2)+\frac{\partial}{\partial y}(H\bar{u}\bar{v})+\frac{\partial}{\partial x}(g\frac{H^2}{2}+H\bar{p}_{nh}) &= -(gH+2\bar{p}_{nh})\frac{\partial z_b}{\partial x}, && (1.35)\\
\frac{\partial H\bar{v}}{\partial t}+\frac{\partial}{\partial x}(H\bar{u}\bar{v})+\frac{\partial}{\partial y}(H\bar{v}^2)+\frac{\partial}{\partial y}(g\frac{H^2}{2}+H\bar{p}_{nh}) &= -(gH+2\bar{p}_{nh})\frac{\partial z_b}{\partial y}, && (1.36)\\
\frac{\partial H\bar{w}}{\partial t}+\frac{\partial H\bar{u}\bar{w}}{\partial x}+\frac{\partial H\bar{v}\bar{w}}{\partial y} &= 2\bar{p}_{nh}, && (1.37)
\end{aligned}$$

completed with the incompressibility condition:

$$\frac{\partial H\bar{u}}{\partial x}+\frac{\partial H\bar{v}}{\partial y}-\bar{u}\frac{\partial(H+2z_b)}{\partial x}-\bar{v}\frac{\partial(H+2z_b)}{\partial y}+2\bar{w} = 0. \tag{1.38}$$

Furthermore, denoting the averaged energy by:

$$\bar{E}=\frac{H(\bar{u}^2+\bar{v}^2+\bar{w}^2)}{2}+\frac{gH(\eta+z_b)}{2}, \tag{1.39}$$

the following energy balance is satisfied for smooth solutions:

$$\frac{\partial\bar{E}}{\partial t}+\operatorname{div}\left(\bar{\mathbf{u}}\left(\bar{E}+\frac{g}{2}H^2+H\bar{p}_{nh}\right)\right)=0, \tag{1.40}$$

with $\bar{\mathbf{u}} = (\bar{u}, \bar{v})^T$. In Equations (1.35)-(1.36), we can decompose the total pressure of the fluid into two parts: the averaged hydrostatic part $\bar{p}_{hyd} = g\frac{H}{2}$ and the non-hydrostatic part $\bar{p}_{nh}$ which is an unknown of the problem. Thus, the total pressure can be written:

$$p_{total} = \bar{p}_{hyd} + \bar{p}_{nh}. \tag{1.41}$$

As in incompressible models, and in contrast to hydrostatic models, the difficulty of dispersive equations comes from the pressure, which is no longer given by an algebraic expression as in the Shallow Water model (1.16)-(1.18). The pressure, and more precisely the non-hydrostatic pressure has to be determined under the constraint (1.38), which comes from the divergence-free constraint of the Euler system and is now considered as the incompressibility relation. So the model we study has no high order derivative term, which is different of the formulation (1.32). In contrast to the Shallow Water model (1.16)-(1.18), the velocity $\bar{w}$ is an unknown of the system and is governed by the advection equation (1.38).

Equation for the pressure The governing equation for $\bar{p}_{nh}$ in the model (1.34)-(1.38) can be obtained by applying the Shallow Water expression of the divergence-free operator (1.38) to the momentum equations (1.35)-(1.36). For the sake of simplicity, we give here the pressure equation in one dimension :

$$\begin{aligned} -\frac{\partial}{\partial x}\left(H\frac{\partial \bar{p}_{nh}}{\partial x}\right) + \frac{1}{H}\left(4 - H\frac{\partial^2 H + 2z_b}{\partial x^2} + \left(\frac{\partial H + 2z_b}{\partial x}\right)^2\right)\bar{p}_{nh} = \\ 2H\left(\frac{\partial \bar{u}}{\partial x}\right)^2 + 2\bar{u}^2\frac{\partial^2 z_b}{\partial x^2} + gH\frac{\partial^2 (H + z_b)}{\partial x^2} - 2g\frac{\partial z_b}{\partial x}\frac{\partial H + z_b}{\partial x}, \end{aligned} \tag{1.42}$$

This is a Sturm-Liouville type equation, with second order differential operators, which is complicated to study and solve, particularly numerically.

Derivation of the DAE model The derivation of the DAE (1.34)-(1.37) model given in [43] differs from the classical methods mentioned above (asymptotic expansion, linear theory, etc.) and for the sake of clarity, we give the main steps of the derivation in one dimension. The depth-averaged model has been derived using a moment closure principle introduced by Levermore [113] in the context of kinetic models. It involves closure relations to minimize the energy. Starting from the Euler System (1.9)-(1.11) and performing the average over the depth, we search for closure relations between the quantities appearing in the system after averaging and without any approximation: $\int_{z_b}^{\eta} u^2\ dz$, $\int_{z_b}^{\eta} u\,w\ dz$, $\int_{z_b}^{\eta} u\,z\ dz$ and $\left(\int_{z_b}^{\eta} u\ dz\right)^2$, such that it minimizes the averaged energy:

$$\int_{z_b}^{\eta}\left(\frac{u^2 + w^2}{2} + gz\right)\ dz. \tag{1.43}$$

We obtain the following closure relations:

$$\int_{z_b}^{\eta} u^2\, dz \simeq \frac{1}{H}\left(\int_{z_b}^{\eta} u\, dz\right)^2, \tag{1.44}$$

$$\int_{z_b}^{\eta} u\, w\, dz \simeq \frac{1}{H}\left(\int_{z_b}^{\eta} u\, dz\right)\left(\int_{z_b}^{\eta} w\, dz\right), \tag{1.45}$$

$$\int_{z_b}^{\eta} u\, z\, dz \simeq \frac{1}{H}\left(\int_{z_b}^{\eta} z\, dz\right)\left(\int_{z_b}^{\eta} u\, dz\right). \tag{1.46}$$

In addition, denoting $p_{nh}|_b$ the non-hydrostatic pressure at the bottom, we find the following relation

$$\overline{p}_{nh}|_b = 2\overline{p}_{nh}, \tag{1.47}$$

to obtain the energy balance (1.40). We refer to [43] for details of the minimization.

A comparison of the DAE model and the Green-Naghdi model These two models differ slightly in one coefficient of the non-hydrostatic pressure in the vertical momentum equation. Indeed, with a flat bottom, the GN model can be written exactly like the DAE model (1.34)-(1.38), except for the advection equation in $\bar{w}$ which is replaced in the GN model by:

$$\frac{\partial H\bar{w}}{\partial t} + \frac{\partial Hw\bar{u}v}{\partial x} + \frac{\partial Hw\bar{u}v}{\partial y} = \frac{3}{2}\bar{p}. \tag{1.48}$$

For a flat topography, the method proposed in this PhD thesis is developed for the DAE model but can be easily adapted for the GN model. Only the constant term in the Sturm-Liouville equation (1.42) **changes. A numerical comparison is proposed in Chapter 3 using two analytical solitary waves of the DAE and the GN models.** However, for a variable bottom in space, it is much more complicated to give a comparison of the two models and the method should be readapted to take into consideration a non-flat bottom for the GN model.

The Madsen-Sorensen model

This dispersive model is widely used for coastal engineering ([117]) and is typically used for weakly dispersive water waves and small amplitude waves. Madsen-Sorensen's model (1992) can be written as:

$$\frac{\partial H}{\partial t} + \frac{\partial H\bar{u}}{\partial x} = 0, \tag{1.49}$$

$$\frac{\partial H\bar{u}}{\partial t} + \frac{\partial}{\partial x}\left(H\bar{u}^2 + g\frac{H^2}{2}\right) + gH\frac{\partial z_b}{\partial x} + \tau = \psi, \tag{1.50}$$

where τ denotes the friction and

$$\psi = (\beta + \frac{1}{3}){z_b}^2(H\bar{u})_{xxt} - \beta g {z_b}^3 \eta_{xxx} + z_b \frac{\partial z_b}{\partial x}\left(\frac{1}{3}(H\bar{u})_{xt} - 2\beta g z_b \eta_{xx}\right),$$

where β is a real empirical parameter chosen to approach the dispersion relation defined by the linear wave theory [1], like in [48] for the Green Naghdi model. In addition, this model is suitable for the coastal zone, since, due to its mathematical structure, the breaking wave process can be easily applied. Although this model is widely used for applications, it is only suitable for weakly dispersive waves and does not admit an energy. Nwogu's model (1993) is also used for coastal engineering (see [129]). **These kinds of models can be seen as an approximation of the non-hydrostatic model** (1.34)-(1.38)**. If we replace $\bar{p}_{nh}$ given by Equation** (1.37) **in Equations** (1.35)-(1.36)**, and using** (1.34)**, it leads to an equation with high order derivative terms in space and time in H, $H\bar{u}$. If one part of the high order derivative terms is neglected, we can derive Madsen-Sorenen's or Nwogu's models.**

1.3.3 About multi-layer models

To begin with, it is worth mentioning that the multi-layer principle for hydrostatic Navier-Stokes consists in discretizing the model along the vertical. It has been developed to approach the hydrostatic Navier-Stokes equations with a free surface. The interest is to propose numerical schemes using extensions of the numerical method developed for the Shallow Water system (1.16)-(1.18) and which does not require moving meshes. For the hydrostatic case, it has been studied, by among others, Fernandez-Nieto [76] and Sainte-Marie [13]. For the non-hydrostatic case, recent models have been developed to extend the DAE system to a non-hydrostatic multilayer model [74].

1.3.4 Hydro vs non-hydro

In the previous section, we have introduced the different kinds of free surface models and have distinguished two families : hydrostatic models and non-hydrostatic models. In this section, we give an illustration of the dispersive effect on a numerical simulation. We consider a flow in channel with a bump. In Figure 1.3a, we have reproduced the hydrostatic hydraulic jump, which is an analytical solution of the Saint-Venant system (1.16)-(1.18), and we compare the solution obtained for the same geometry, initial water depth, inflow and outflow with the non-hydrostatic model (1.34)-(1.36) in Figure 1.3b. The dispersive effects are clearly identifiable in Figure 1.3b by the oscillations occurring after the bump, while we can observe the shock of the hydrostatic solution in Figure 1.3a. This specific solution is investigated in this PhD thesis and is presented in Chapter 5.

(a) Simulation with a hydrostatic model (Saint-Venant)

(b) Simulation with a non-hydrostatic model (a depth-averaged model)

Figure 1.3: Comparison of a hydrostatic and non-hydrostatic model on a hydraulic jump.

1.4 Numerical methods

Just as we have made a clear distinction between hydrostatic models like the Saint-Venant system (1.16)-(1.18) and non-hydrostatic models, the numerical methods must also be distinguished. The Shallow Water model (1.16)-(1.18) is hyperbolic and has been widely studied both in one and two dimensions. Robust and stable numerical schemes are now available to approach these kinds of models accurately (see [82, 34, 110]). A dispersive model of the form (1.32) can be viewed as a hydrostatic model with a complementary contribution, leading to a system which is no longer hyperbolic. Among the methods proposed for dispersive models (for which we give a state of the art in the next section), some of them still require solving a hyperbolic system, so in this section we present the main ways to solve the hyperbolic part and we detail the kinetic scheme applied in our work. Then, we set out the main existing numerical methods for non-hydrostatic models.

1.4.1 Numerical methods for hyperbolic systems

The Saint-Venant system (1.16)-(1.18) is a hyperbolic system of conservation laws with source terms. It is classical to discretize the conservative part using a finite volume framework. Many well-known numerical fluxes are available such as, for instance HLL (Harten, Lax, Van Leer), Roe and Rusanov, see also the Godunov-type schemes consisting in solving a Riemann solver at each interface in the discretization of the conservative

part [110, 83, 140, 32]. The difficulty of the Saint-Venant model arises in the treatment of the source term containing the topography term $H\nabla z_b$ in Equations (1.17)-(1.18) in a non conservative form. This leads to difficulty in preserving non-trivial equilibria of the system. Nevertheless, this issue has been extensively studied [32, 140] to obtain a robust numerical scheme with good properties. The numerical approximation of conservation with source terms is often performed using finite volumes techniques. But when considering more complex systems with a coupling between advection and e.g. diffusion terms, the finite volumes have to be coupled with finite elements type approximations. Such a coupling raises in general important issues [73]. We refer to [10] for the discretization of the two-dimensional Shallow Water system (1.16)-(1.18) on unstructured meshes. In this part, we describe the finite volume framework together with the kinetic scheme which we have used in this PhD thesis.

Kinetic interpretation

The kinetic approach applied to the Shallow Water system with a source term (1.16)-(1.18), detailed in [132, 133] and [14] consists in using a description of the microscopic behavior of the system. In this method, fictitious particles are introduced and the equations are considered at the microscopic scale, where no discontinuity occur. The kinetic interpretation of the system allows its transformation into a linear transport equation, to which an upwinding discretization is naturally applicable. We introduce a real function χ defined on $\mathbb{R}$, compactly supported and having the following properties

$$\begin{cases} \chi(-\omega) = \chi(\omega) \geq 0 \\ \int_{\mathbb{R}} \chi(\omega)\ d\omega = \int_{\mathbb{R}} w^2 \chi(\omega)\ d\omega = 1. \end{cases} \tag{1.51}$$

Let us construct the density of particles $M(x,t,\xi)$ defined by a Gibbs equilibrium: the microscopic density of particles present at time t, at the abscissa x and with velocity ξ given by

$$M(x,t,\xi) = \frac{H}{c}\chi\left(\frac{\xi - \bar{u}}{c}\right), \tag{1.52}$$

with $c = \sqrt{\frac{gH}{2}}$. Then we have the following theorem

Theorem 1.4.1. *The functions (H,u) are strong solutions of the Saint-Venant system described by* (1.16)-(1.18) *if and only if the equilibrium $M(x,t,\xi)$ is a solution of the Boltzmann equation*

$$(\mathcal{B}) \qquad \frac{\partial M}{\partial t} + \xi\frac{\partial M}{\partial x} - g\frac{\partial z_b}{\partial x}\frac{\partial M}{\partial \xi} = Q(x,t,\xi), \tag{1.53}$$

where $Q(x,t,\xi)$ is a "collision term" satisfying

$$\int_{\mathbb{R}} Q \; d\xi = \int_{\mathbb{R}} \xi Q \; d\xi = 0. \tag{1.54}$$

Proof of theorem 1.4.1. From the definitions (1.51) and (1.54), the proof is obvious by calculating the quantities

$$\int_{\mathbb{R}} (\mathcal{B}) \; d\xi, \quad \int_{\mathbb{R}} \xi(\mathcal{B}) \; d\xi$$

and using (1.54). We notice that:

$$\int_{\mathbb{R}} M d\xi = H \quad , \quad \int_{\mathbb{R}} \xi M d\xi = H\overline{u} \quad , \quad \int_{\mathbb{R}} \xi^2 M d\xi = H\overline{u}^2 + c^2 H, \tag{1.55}$$

and

$$\int_{\mathbb{R}} \frac{\partial M}{\partial \xi} d\xi = 0 \quad , \quad \int_{\mathbb{R}} \xi \frac{\partial M}{\partial \xi} d\xi = H. \tag{1.56}$$

□

This theorem produces a very useful consequence. The non-linear shallow water system can be treated as a single linear equation on a non-linear quantity M, for which it is easier to find simple numerical schemes with good theoretical properties.

Finite volume method

We apply a one-dimensional finite volume method on the Boltzmann equation which is a transport equation where ξ is a velocity. We consider the domain $\mathbb{R}$ sub-divided into N control cells $C_i = [x_{i-1/2}, x_{i+1/2}]$ centered in x_i, $i = 1, N$. We denote Δx_i the length of C_i and $t^{n+1} = t^n + \Delta t^n$, $k > 0$ where t^0 is the initial time and Δt^n is the time step depending on the stability property (CFL).
We define the average values of a function f by:

$$f_i = \frac{1}{\Delta x_i} \int_{x_{i-1/2}}^{x_{i+1/2}} f \; dx. \tag{1.57}$$

Likewise, a time average is considered:

$$f^n = \frac{1}{\Delta t} \int_{\Delta t} f \; dt. \tag{1.58}$$

Using the hydrostatic reconstruction technique [7], we define the reconstructed water depth $H_{i+1/2^+}$ and $H_{i+1/2^-}$ for each interface $x_{i+1/2}$ by:

$$H_{i+1/2^+} = \max(0, H_{i+1} + (z_{bi+1} - z_{bi+1/2})) \quad H_{i+1/2^-} = \max(0, H_i + (z_{bi} - z_{bi+1/2})) \tag{1.59}$$

with the reconstructed topography:

$$z_{bi+1/2} = \max(z_{bi}, z_{bi+1}). \tag{1.60}$$

The discretization of the density M defined by (1.52) reads:

$$M_{i+1/2^+}(\xi) = \frac{H_{i+1/2^+}}{c_{i+1/2^+}}\chi(\frac{\xi - u_{i+1}}{c_{i+1/2^+}}) \quad \text{and} \quad M_{i+1/2^-}(\xi) = \frac{H_{i+1/2^-}}{c_{i+1/2^-}}\chi(\frac{\xi - u_i}{c_{i+1/2^-}}). \tag{1.61}$$

We apply an upwind scheme for the transport part, setting the following definition of $M_{i+1/2}$ at the interface:

$$M_{i+1/2}(\xi) = \begin{cases} M_{i+1/2^+}(\xi) & \text{if } \xi \leq 0 \\ M_{i+1/2^-}(\xi) & \text{if } \xi \geq 0 \end{cases} \tag{1.62}$$

Then, the Boltzmann equation (1.53) is discretized as :

$$\begin{aligned} f_i^{n+1^-}(\xi) &= M_i(\xi) - \frac{\Delta t^n}{\Delta x_i}\big(\xi M_{i+1/2}(\xi) - \xi M_{i-1/2}(\xi) \\ &\quad + (\xi - u_i)(M_i - M_{i+1/2^-}) - (\xi - u_i)(M_i - M_{i-1/2^+})\Big). \end{aligned} \tag{1.63}$$

Thanks to the property of χ, the scheme satisfies :

$$\int_R (\xi - u_i)(M_i - M_{i+1/2^-}) - (\xi - u_i)(M_i - M_{i-1/2^+})d\xi = 0, \tag{1.64}$$

and

$$\int_R \xi(\xi - u_i)(M_i - M_{i+1/2^-})d\xi = g\frac{{H_i}^2 - H^2_{i+1/2^-}}{2}, \tag{1.65}$$

$$\int_{\mathbb{R}} \xi(\xi - u_i)(M_i - M_{i-1/2^+})d\xi = g\frac{{H_i}^2 - H^2_{i-1/2^+}}{2}, \tag{1.66}$$

where H_i is the average value of H on the cell C_i defined as (1.57). Therefore using the properties (1.55)-(1.56) in (1.63), the final scheme reads:

$$\begin{pmatrix} H^{n+1} \\ (H\overline{u})^{n+1} \end{pmatrix} = \int_{\mathbb{R}} \begin{pmatrix} 1 \\ \xi \end{pmatrix} f^{n+1^-}(\xi)\, d\xi. \tag{1.67}$$

We have given the standard kinetic scheme for the Shallow Water system, however the kinetic scheme has been adapted for the two-dimensional model in [14]. In this PhD thesis, we have used the above kinetic scheme for the hydrostatic part for the one- and the two-dimensional problems, see Chapters 2, 3, and 4. These schemes admit a fully discrete entropy inequality and one can prove its convergence [114].

1.4.2 State of the art of numerical methods for dispersive models

Including dispersive effects in a model adds significant difficulties to derive a robust algorithm. Indeed, these additional terms change the class of equation, and new numerical approaches need to be developed. The dispersive models (1.30)-(1.31), (1.34)-(1.38), (1.49)-(1.50) presented in Section 1.3.2, can often be written under the following condensed formulation:

$$\frac{\partial X}{\partial t} + \mathrm{div} F(X) + \mathcal{D} = S(X), \tag{1.68}$$

where X is defined by

$$X = \begin{pmatrix} H, \\ H\bar{u} \\ H\bar{v}, \\ H\bar{w} \end{pmatrix}, \tag{1.69}$$

F is the associated flux, and S is the topography source term. We denote by $\mathcal{D}$ the additional dispersive terms which may contain differential operators depending on the model. Thus for $\mathcal{D} = 0$ we come back to the Shallow Water equations, which can be solved with the method previously presented in Section 1.4.1. For $\mathcal{D} \neq 0$, the difficulties arise in two dimensions, and more specifically for unstructured grids. Many strategies have been investigated in one or two dimensions, and we give here a brief review of existing techniques.

Determining $\mathcal{D}$ depends on the formulation of the model, and usually $\mathcal{D}$ contains derivative terms up to third order, it is then necessary to apply a high order scheme to discretize $\mathcal{D}$. Several techniques have been proposed to solve this problem, some techniques use a change of variables to include the term $\mathcal{D}$ in the whole scheme designed for the model [108]. Some other techniques decouple the two parts of (1.68) and use a different scheme for each part, namely one method to discretize the flux F together with the source term S and one method to discretize the dispersive terms present in $\mathcal{D}$. In [48], F. Chazel *et al.* (2010) use a high-order finite volume scheme (WENO [151]) and a finite difference scheme for the one-dimensional Green-Naghdi model (1.30)-(1.31). Similarly, in [108] O. Le Métayer, S. Gavrilyuk and S. Hankuses (2010) use a HLL scheme for the hyperbolic part for a flat bottom (without source terms) and discretize the high order derivative terms present in

$\mathcal{D}$ by finite difference approximation. The finite difference scheme has been performed for many dispersive models [30]. These approaches are also used on models of Madsen-Sorensen (1.49)-(1.50) and Nwogu types (see Section 1.3.2) in [72, 116]. Mitsotakis *et al.* performed a Galerkin Finite-Element Method for the one-dimensional GN model [52, 65].

The method described above can be written as a generalization of a splitting scheme to solve the dispersive part. Writing the model in the form (1.68), we describe the principle of the splitting scheme which consists in computing the dispersive part $\mathcal{D}$ of (1.68) separately from the hyperbolic part at the discrete level. This method can be summarized by the semi-discretization in time of Equation (1.68):

$$X^{n+1/2} = X^n - \Delta t^n \left(\text{div}F(X^n) - S(X^n)\right), \tag{1.70}$$

$$X^{n+1} = X^{n+1/2} - \Delta t^n \mathcal{D}^k, \tag{1.71}$$

where $k = n$ or $k = n + 1$ (depending on the method) and where step (1.71) consists in correcting the state $X^{n+1/2}$ with the dispersive part $\mathcal{D}$, which depends on the derivatives of X. For these kinds of methods, it is classical to apply a different numerical scheme for the two parts (1.70) and (1.71).

Recently (2014), a discontinuous-Galerkin discretization was proposed by A. Duran and F. Marche in [62] for the Green-Naghdi model. The idea is to determine first the equation governed by $\mathcal{D}$ defined by (1.68), this step is done at the continuous level and provides a high order differential equation. Then, after giving a weak formulation of the problem written under the form (1.68), a discontinuous Galerkin scheme is applied, with a high order of space derivatives. This approach is also performed for the system on a flat bottom in [124] with the one-dimensional Boussinesq equations. The discontinuous Galerkin approach has bee also used by M. Dumbser and M. Facchini on Boussinesq type models [61]. More recently (2016), A. Duran and F. Marche performed an hybrid method [63] for the two-dimensional GN model.
Another algorithm has been investigated in [23] by S. Bellec *et al.* (2016) based on the derivation of discrete asymptotic equations. The idea is to start with a discretization of the incompressible Euler equations, and using asymptotic expensions (like in [4]), it gives a numerical method describing the free surface. This has been tested for the Peregrine equations in [23] using a Galerkin method on the two-dimensional Euler system.

Notice that one of the issues of the dispersive models presented in paragraph 1.3.2 and their numerical approaches described above, concerns the capability to manage the transition between wet and dry domains. Few available methods in the literature are able to treat the vacuum for these kinds of models. In our work, we propose a scheme able to satisfy

this property.

The method proposed in this PhD thesis is a splitting approach of the Chorin-Temam type (1969) combining two numerical methods: the finite volume method for the hyperbolic part with a source term, and the finite element method for the dispersive part. This method is detailed in Section 1.5.1..

1.5 Outline of the main contributions of this PhD thesis

The main purpose of our work is to design with a judicious numerical method for a non-hydrostatic model (1.34)-(1.36) in order to capture the dispersive effect mentioned in the previous section. This PhD thesis is organized in five chapters and one appendix. Chapters 2, 3 and 4 are composed of the three following papers:

- A robust and stable numerical scheme for a depth-averaged Euler system. Submitted, 2016.
- A combined finite volume - finite element scheme for a dispersive shallow water system. Networks and Heterogeneous Media, 11(1):1– 27, 2016.
- A two-dimensional method for a dispersive shallow water model on unstructured meshes. Submitted, 2016.

The fifth chapter presents several additional results concerning the model. Finally, the appendix presents the result of collaborative work carried out at the Cemracs 2015 and published in the proceedings:

- A coupled model for unsteady Stokes/Exner equations and numerical results with feel++ library. Submitted, CEMRACS 2015, 2015, Marseille, France.

In the following part, we propose a summary of the PhD thesis pointing out the main contributions. We gather Chapters 2, 3 and 4 in the following section to explain our numerical method in a general way.

1.5.1 Overview of Chapters 2, 3 and 4

Chapters 2, 3 and 4 deal with the numerical method of the DAE model (1.34)-(1.38). The objective is to give a global framework that could also be applied to dispersive models of the GN, Boussinesq types etc. We emphasize the fact that the method has been developed for the DAE model (1.34)-(1.38) but could be adapted for the Green-Naghdi model by choosing appropriate dual operators (detailed in the following). In order to achieve this goal, this work is organized in three parts with increasing difficulty. In the second chapter, we propose a finite difference scheme with good properties and give numerical validations

of the method. Having in mind to extend the method to the two-dimensional model on unstructured meshes, so the third chapter proposes a variational formulation of the one-dimensional model with a finite element approximation scheme. The fourth chapter extends the method to two dimensions with additional properties related to the finite element framework (inf-sup condition, etc.).
In this part, we highlight the main contributions that lead to obtaining a robust numerical method for the DAE model and we present the results in a more general case.

Splitting method In one or two dimensions, the starting point of the scheme is to use the Chorin-Temam splitting scheme [50], also called the prediction-projection method, to treat the hyperbolic part and the dispersive part independently, using the incompressibility condition as for the Navier-Stokes Equations [138]. Using the notations of the condensed system (1.68), we can summarize the model by the following:

$$\frac{\partial X}{\partial t} + \mathrm{div} F(X) + \mathcal{D}(p) = S(X), \tag{1.72}$$

$$\mathcal{B}(\bar{\mathbf{u}}) = 0, \tag{1.73}$$

where $\bar{\mathbf{u}} = (\bar{u}, \bar{v}, \bar{w})^T$ is the velocity and X is defined by (1.69), the dispersive part $\mathcal{D}$ is an operator depending on the non-hydrostatic pressure p. The operators $\mathcal{B}$ and $\mathcal{D}$ corresponding to the divergence and the gradient operators have to satisfy the duality relation:

$$\int_\Omega \mathcal{B}(\mathbf{v}) q d\mathbf{x} = -\int_\Omega \mathcal{D}(q) \cdot \mathbf{v} d\mathbf{x} + BC \tag{1.74}$$

with BC containing the boundary terms, and $\mathbf{v} = (v_1, v_2, v_3)^T$, q are taken in appropriate spaces. We do not give details on the spaces and the boundary terms here and we refer to Chapter 2 where we show that this relation is satisfied for the shallow water version of the operators $\mathcal{B}$ and $\mathcal{D}$. Notice that with this formulation, the pressure p is an unknown of the system, while in the condensed formulation (1.68), the "shallow water incompressibility constraint" has been taken into consideration in the dispersive part, hence high order derivative terms depending on H, $\mathbf{u}$ appear in (1.68) and it leads to the numerical schemes mentioned in Section 1.4.2.
In contrast to the Navier-Stokes equations where the primitive variables of the system are the velocity and the pressure, the DAE system (1.34)-(1.37) is written in terms of the variables $(H\bar{u}, H\bar{v}, H\bar{w})$ and p, while the shallow water version of the incompressibility constraint (1.38) is applied to the velocity $\bar{\mathbf{u}}$ (we will specify the expression of the operators in the next part). Writing the incompressibility constraint according to the velocity $\bar{\mathbf{u}}$ instead of the discharge $H\bar{\mathbf{u}}$ is necessary to have the duality between the operators $\mathcal{B}$ and $\mathcal{D}$, and the numerical method is based on this duality. This implies that we need an

operator to obtain the velocity from the discharge $\mathbf{u} = \frac{1}{H}(H\bar{\mathbf{u}})$. The splitting scheme can be written as:

$$\begin{aligned} X^{n+1/2} &= X^n - \Delta t^n \left(\mathrm{div} F(X^n) - S(X^n)\right), && (1.75)\\ X^{n+1} &= X^{n+1/2} - \Delta t^n \mathcal{D}\left(p^{n+1}\right), && (1.76)\\ \mathcal{B}\left(\bar{\mathbf{u}}^{n+1}\right) &= 0, && (1.77) \end{aligned}$$

where the predicted state $X^{n+1/2}$ is obtained by applying the finite volume scheme (based on the kinetic scheme [14] and detailed in Section 1.4.1). The predicted velocity is computed by $\bar{\mathbf{u}}^{n+1/2} = \frac{1}{H^{n+1/2}}(H\mathbf{u})^{n+1/2}$ and does not satisfy the divergence-free condition (1.38). This is the purpose of the correction step (1.76). To obtain the contribution of the dispersive part $\mathcal{D}(p^{n+1})$ such that the final corrected step X^{n+1} satisfies the divergence-free condition (1.77), we have to solve an elliptic equation in p.
After writing Equation (1.76) in terms of $\bar{\mathbf{u}}^{n+1}$:

$$\bar{\mathbf{u}}^{n+1} = \bar{\mathbf{u}}^{n+1/2} - \Delta t^n \frac{1}{H^{n+1/2}} \mathcal{D}\left(p^{n+1}\right). \tag{1.78}$$

We derive the elliptic equation governing the non-hydrostatic pressure by applying the operator $\mathcal{B}$ to Equation (1.78) and using (1.77). We obtain the following equation in p^{n+1}:

$$\mathcal{B}\left(\frac{1}{H^{n+1/2}} \mathcal{D}\left(p^{n+1}\right)\right) = \frac{1}{\Delta t^n} \mathcal{B}\left(\bar{\mathbf{u}}^{n+1/2}\right) \tag{1.79}$$

This last equation ensures that we obtain a pressure p^{n+1} that allows the divergence-free condition to be satisfied by the velocity $\bar{\mathbf{u}}^{n+1}$.
One of the interests of the technique is to keep the numerical method developed for the hyperbolic part, which has good stability properties, such as the preservation of:

- The positivity of H
- The Well-balanced property
- The entropy inequalities at the discrete level

The operators $\mathcal{D}$ and $\mathcal{B}$ corresponding to the non-hydrostatic model (1.34)-(1.38) are denoted by ∇_{sw} and div_{sw} and are defined for f and $\mathbf{v} = (v_1, v_2, v_3)^T$ smooth enough, by:

$$\nabla_{sw} f = \begin{pmatrix} H\frac{\partial f}{\partial x} + f\frac{\partial (H+2z_b)}{\partial x} \\ H\frac{\partial f}{\partial y} + f\frac{\partial (H+2z_b)}{\partial y} \\ -2f \end{pmatrix}, \tag{1.80}$$

$$\mathrm{div}_{sw}(\mathbf{v}) = \frac{\partial H v_1}{\partial x} + \frac{\partial H v_2}{\partial y} - v_1 \frac{\partial (H+2z_b)}{\partial x} - v_2 \frac{\partial (H+2z_b)}{\partial y} + 2v_3, \tag{1.81}$$

and the DAE model can be written in a more condensed form:

$$\frac{\partial H}{\partial t} + \nabla_0 \cdot (H\bar{\mathbf{u}}) = 0, \tag{1.82}$$

$$\frac{\partial H\bar{\mathbf{u}}}{\partial t} + \nabla_0 \cdot (H\bar{\mathbf{u}} \otimes \bar{\mathbf{u}}) + \nabla_0(\frac{g}{2}H^2) + \nabla_{sw}(p) = -gH\nabla_0(z_b), \tag{1.83}$$

$$\mathrm{div}_{sw}(\bar{\mathbf{u}}) = 0, \tag{1.84}$$

where we define

$$\nabla_0 = \begin{pmatrix} \frac{\partial}{\partial x} \\ \frac{\partial}{\partial y} \\ 0 \end{pmatrix}, \quad \mathrm{div}_0 = \nabla_0 \cdot \tag{1.85}$$

Mixed problem in velocity-pressure and boundary conditions As we have highlighted above, by using the splitting scheme we obtain a correction step (1.76) with a shallow water divergence-free condition (1.77) and this naturally leads us to consider this problem as a mixed problem in velocity-pressure. In addition, one of the difficulties of taking a fully non-linear dispersive model with a non-hydrostatic pressure comes from the treatment of the boundary conditions on the pressure. It is a general problem when using prediction-correction scheme since p defined by (1.79) does not satisfy the natural boundary conditions. The mixed problem considered allows us to impose compatible boundary conditions for the pressure and the velocity in accordance with the hyperbolic part. The interest of the mixed problem for the boundary conditions is to impose the velocity instead of the pressure. Nevertheless, the associated boundary conditions for the pressure are studied. This is presented in Chapter 3 for the one-dimensional case, and is then used for the method extended to the two-dimensional case. We give here the boundary conditions of the two-dimensional problem presented in Chapter 4. We denote by Ω the bounded model domain (see Figure 1.4) and $\Gamma = \Gamma_{in} \cup \Gamma_s \cup \Gamma_{out}$ its boundaries (for the inlet, the wall and the outlet), and $\mathbf{n}$ the outward normal vector of Γ. We complete the mixed problem composed of (1.76) and (1.77) with the following compatibility conditions:

- If we impose a discharge at the hyperbolic system on the boundary Γ_{in}, then we impose the normal component of the velocity in the mixed problem:

$$\bar{\mathbf{u}}^{n+1} \cdot \mathbf{n} = \bar{\mathbf{u}}^{n+1/2} \cdot \mathbf{n} \text{ on } \Gamma_{in}. \tag{1.86}$$

- If we impose slip boundary conditions at Γ_s, then we conserve this condition for the mixed problem

$$\bar{\mathbf{u}}^{n+1} \cdot \mathbf{n} = 0 \text{ on } \Gamma_s. \tag{1.87}$$

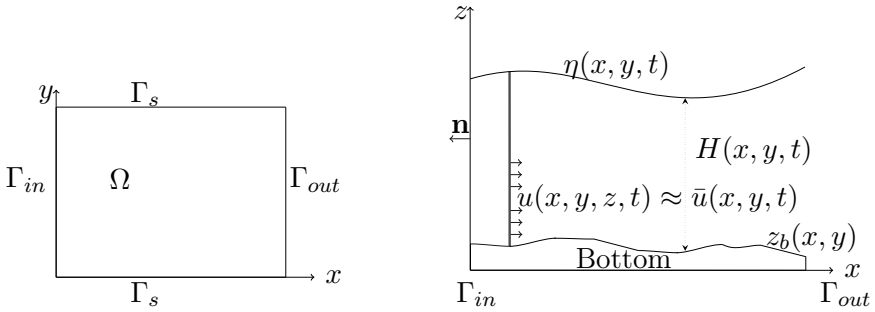

(a) View from above. (b) Vertical cross section.

Figure 1.4: Model domain and notations.

- If we consider Γ_{out} the outlet of the domain and if we have imposed a water depth in the Shallow Water system, then we impose a homogeneous Dirichlet condition for the pressure:

$$p = 0 \text{ on } \Gamma_{out}. \tag{1.88}$$

The two-dimensional case is general and can be specified for the one-dimensional model. The procedure has been studied by J.-L. Guermond in [90] for the Chorin-Temam scheme applied on the Navier-Stokes problem.
In order to perform a Finite element method, we give the variational formulation of the mixed problem (1.76)-(1.77), completed with the boundary conditions (1.86),(1.87),(1.88). It reads:

- Find $p \in Q_0$, $\mathbf{u} \in \mathbf{V}$ such that,

$$a(\bar{\mathbf{u}}^{n+1}, \mathbf{v}) + \Delta t\, b(\mathbf{v}, p^{n+1}) = a(\bar{\mathbf{u}}^{n+1/2}, \mathbf{v}), \quad \forall \mathbf{v} \in \mathbf{V}_0, \tag{1.89}$$

$$b(\bar{\mathbf{u}}^{n+1}, q) = < H\bar{\mathbf{u}}^{n+1/2}, q >_{\Gamma_{in}}, \quad \forall q \in Q_0, \tag{1.90}$$

where $< \cdot, \cdot >_{\Gamma_{in}}$ represents the duality between $H^{-1/2}(\Gamma_{in})$ and $H^{1/2}(\Gamma_{in})$.

$$a(\mathbf{u}, \mathbf{v}) = \int_\Omega H\mathbf{u} \cdot \mathbf{v} d\mathbf{x}, \quad \forall \mathbf{u}\,, \mathbf{v} \in \mathbf{V}, \tag{1.91}$$

$$b(\mathbf{v}, q) = \int_\Omega \nabla_{sw}\,(q) \cdot \mathbf{v}\, d\mathbf{x}, \quad \forall \mathbf{v} \in \mathbf{V},\ \forall q \in 0, \tag{1.92}$$

and

$$\mathbf{V} = \{\mathbf{v} \in L^2(\Omega)^3, \}, \tag{1.93}$$

$$Q = \{q \in L^2(\Omega),\ , \nabla_{sw}\,(q) \in (L^2(\Omega))^3\}, \tag{1.94}$$

$$Q_0 \quad = \quad \{q \in Q \ , \ q|_{\Gamma_{out}} = 0\}. \tag{1.95}$$

The operators ∇_{sw} and div_{sw} are defined by (1.80) and (1.81). Several variational formulations are proposed in Chapter 2, 3 and 4 depending on the dimension of the problem and on the boundary conditions. In addition, we give the equivalent formulation of the problem using the equation in pressure corresponding to (1.79).

Finite difference scheme and finite element for the dispersive part First we study the one-dimensional model and we develop a coupled method using the splitting scheme in time. The hyperbolic part is solved with a finite volume scheme and the dispersive part is solved with a finite difference scheme. This approach is suitable in one dimension and allows us to choose a good approximation for the non-hydrostatic contribution such that the properties at the hyperbolic level are still valid (discrete positivity, entropy inequality, lake at rest, etc). This is the subject of the Chapter 2. However, this method is not adapted to simulation on unstructured meshes. Thus, in Chapter 3 we consider the correction step as a mixed problem in velocity-pressure and we give the corresponding variational formulation. This allows us to apply a finite element method that satisfies the same properties as the finite difference scheme. The purpose is to establish a framework to extend the method to two dimensions. This is the subject of Chapter 4 where the finite element method is applied to the two-dimensional DAE model on an unstructured grid with two possible choices of approximation spaces. We summarize the implemented methods by the following:

- In one dimension : finite difference method on a staggered grid of the shallow water version of the Sturm-Liouville equation (1.42), see Chapter 2.
- In one dimension : finite element method with P1/P0 and P1-iso-P2/P1 approximations, see Chapter 3.
- In two dimensions: finite element method with P1/P1 and P1-isoP2/P1 approximations satisfying the discrete inf-sup condition, see Chapter 4.
- Numerical treatment for the wet/dry interfaces for each method, see Chapters 2, 3, and 4.

The one-dimensional implementation has been performed in Fortran, and the two-dimensional method has been implemented in the software Freshkiss3d [1] developed in the Ange team.

Entropy inequality As mentioned in the previous section, one of the interests of the kinetic scheme involves the stability properties of the scheme. In the context of conservation

[1] FRESHKISS is a code developed in C++ and stands for FREe Surface Hydrodynamics using KInetic SchemeS. It simulates 3D incompressible Navier-Stokes equations with free surface (see https://team.inria.fr/ange/research/software/).

law, the energy of the system is an entropy function and satisfies an energy balance. The kinetic scheme guarantees this property at the discrete level for the Shallow Water system. Moreover, using a splitting scheme for the dispersive part with the duality of the operators ∇_{sw} and div_{sw} allows us to preserve this property and we can establish an entropy inequality for the semi-discrete scheme in time and for the fully discrete scheme in space with an estimation of the error.

- A proposition (see Chapter 2, Section 2.5), states that the finite difference approximation of the operators ∇_{sw} and div_{sw} leads to conserving the energy balance consistency at the discrete level in time, that is to say a discretization in time of Equation (1.40):

$$\bar{E}^{n+1} - \bar{E}^n + \Delta t^n \frac{\partial}{\partial x}\left(u^n\left(E^n + g\frac{(H^n)^2}{2}\right) + (Hu)^{n+1}p^{n+1}\right) \leq (\Delta t^2)\left(||F'(X) + S(X)||_2^2\right), \tag{1.96}$$

  where $\bar{E}^n$ is the discretization in time of the energy (1.39), X is defined by (1.69), F is the flux of the hyperbolic part in one dimension of the system (1.34)-(1.37) and S is the topography source term.

- The second property (see Chapter 2, section 2.5) states that an in-cell entropy inequality can be established with an error term depending on the space step of the finite difference scheme.

- We deduce a global entropy inequality in space over the spacial domain (see Chapter 2).

This property has been studied in one dimension (see Chapter 2) and can be extended to two dimensions, which is the object of future work.

Wet / dry interface An important issue in the numerical method of a fully non-linear shallow water model of type (1.34)-(1.37) is its capability to treat the wet/dry front, that is to say when H tends to zero, which is a crucial issue in coastal engineering. In the finite volume method applied to the Shallow Water system (1.16)-(1.18), we have a natural numerical treatment for the dry zones thanks to the hydrostatic reconstruction [7]. However, for the non-hydrostatic model (1.34)-(1.37), a special treatment is required to treat the transition between wet and dry zones. From the continuous point of view, the non-hydrostatic model is defined for a positive water depth. Regarding the mixed problem, we recall that the incompressibility constraint is computed in the velocity variable $\mathbf{u}$, while the momentum equations (1.35)-(1.36) are computed in $H\mathbf{u}$ and this leads to dividing by H in Equation (1.79) of p. In the method proposed for the one-dimensional case and for the two-dimensional case as well, we propose to set the pressure to zero in the dry zone.

Since we use an iterative solver for the mixed problem and since the wet/dry interface varies, we opt to solve the problem on the whole domain setting p to zero in the dry area. This technique has been approved by the validation of the method and the validation of the model (see paragraphs 1.5.1 and 1.5.1).

Inf-sup condition Regarding the mixed problem in velocity-pressure, the inf-sup stability property has to be verified. This property, added to the ellipticity and the coercivity of the bilinear forms a and b defined by (1.91)-(1.92) of the mixed problem, guarantees the well-posedness of the continuous problem and the stability of the scheme.
Notice that the inf-sup condition is satisfied for $H \geq H_0 > 0$, but when the water depth tends to zero, this property still needs to be proved.

Validation of the numerical method

Before applying the method to any real cases, it is necessary to ensure that the numerical method behaves well on some analytical solutions of the model (1.34)-(1.36). Thus, a first step is to evaluate the capability of the scheme to simulate some typical solutions of the model. The tests are performed for several meshes to evaluate the convergence rate of the method.

- **Solitary wave** First we propose a solitary wave for the one-dimensional model. This solution can be used for the validation of the two-dimensional method, in which the wave propagates only in the x direction. Notice that for the similar model of Yamazaki [152], it is not possible to find a solitary wave as an analytical solution of the model. This solution has been used in one dimension in Chapters 2 and 3, and in two dimensions in Chapter 4.

- **Parabolic bowl in one and two dimensions** We propose a version of the parabolic bowl for the one-dimensional model. This is an adaptation of Thacker's parabolic basin for the dispersive scheme. To have a plane surface for the non-hydrostatic model, we add a source term to the advection equation of w. This solution is not given explicitly and requires solving a simple ODE numerically. This test allows us to validate the code in one dimension, see Chapter 2. We succeeded in extending this analytical solution to the two-dimensional model. In this case, the solution is given explicitly (without needing to solve an ODE). This extension has been computed numerically in Chapter 4, allowing us to validate the finite element method. This is considered crucial because it tests the wet-dry/ dry-wet interfaces.

Validation of the model

Numerical validation with analytical solutions does not ensure the validity of the model. In order to test the ability of the model to represent some psysical phenomena, one can

compare the numerical results with experimental data. A famous test case was proposed by Dinguemans in 1994 (see [57]) and consists in generating small amplitude waves over a specific geometry. The one-dimensional method is validated using this test in Chapter 3. Another validation with observation data for the one-dimensional model is proposed in Chapter 5. The experiment simulates a wave arriving at the coast line. To do so, a solitary wave is generated in a channel where a slope represents the shore.

- **Dinguemans experiment**: comparison with the observed data and comparison with the hydrostatic model (see Chapter 3).
- **Experiment of a solitary wave**: reaching land to test the wet/dry interface (see Chapter 5).
- **Dam break** : We perform a simulation of a dam break with a comparison between the Shallow Water and the depth-averaged model to illustrate the dispersive effects. For this case, we compare the simulated results with results provided in literature where a simulation with a Green-Naghdi model is performed and is compared with the numerical result using the Euler system in [108] (see Chapter 3).

1.5.2 Overview of Chapter 5

In the fifth chapter, we propose some additional results to evaluate the proposed method with regard to specific issues and applications.

Analytical stationary solution We give a validation of the numerical method in one dimension for a stationary solution. To do so, we compare the numerical and the analytical solution for a specific case. Then we simulate an hydraulic jump for hydrostatic and the non-hydrostatic case in order observe the dispersion occurring in this case.

Breaking wave Non-hydrostatic models of the type (1.34)-(1.36) are no longer valid when a breaking wave occurs, see [98] for the regularity of the solutions of models with dispersion and viscosity. A classical solution consists in detecting the breaking wave and switching to another model, like the Shallow Water model which is more suitable, or adding an artificial viscosity after the detection. There are different ways to perform such techniques. In this part, we apply one of the methods which consists in adding an artificial viscosity for the one-dimensional model and we compare the numerical results with data obtained from a laboratory experiment.

Dispersion relation We give the dispersion relation associated to the linearized DAE model (1.34)-(1.37) and give a comparison with the dispersion relation of the Airy theory [1].

1.5.3 Overview of the appendix

The appendix is devoted to the modeling of sediment transport in a fluid flow and presents a work carried out at the CEMRACS 2015 summer school on Coupling Multi-Physics Models involving Fluids. In this study, we model the fluid by a Stokes equation rather than the usual Shallow Water equation. For the transport of sediment, the classical Exner equation governs the topography behavior. To do so, the model is inspired by the fluid-structure interaction (FSI) theory together with the numerical method developed for the FSI equations. Hence, from the point of view of FSI theory, the topography plays the role of a moving structure.

1.6 Outline of the conclusion

In this work, we provide a general framework to develop a robust and stable numerical scheme for dispersive models written in the form (1.70)-(1.71). A validation with analytical solutions is proposed for the one- and the two-dimensional models. Similarly, the numerical method is validated using experimental data. The treatment of the wet/dry interfaces allows the method to be applied to real geophysical problems, for instance in coastal engineering. We propose an efficient method to solve the one-layer problem, and the work presented in this PhD thesis represents an intermediate step towards solving multi-layer models, *i.e.* an approximation of the three-dimensional Navier-Stokes system. Finally the main contributions of this work can be summarized as:

- A judicious rewriting of the dispersive model which **takes into account the non-hydrostatic pressure instead of high order derivative terms**
  - Definition of **dual operators** which leads to solving the problem with classical methods introduced first for the Euler or Navier-Stokes systems
  - Treatment of the **boundary conditions** to maintain consistency with the boundary conditions imposed in the hyperbolic part, and choose physical boundary conditions
- Discrete **entropy inequality** property for the fully discrete scheme in space for the one-dimensional method
- Treatment of the **dry/wet interfaces**
- Extension of the method to the two-dimensional model on **unstructured meshes**
- **Validation of the numerical method** with analytical solutions for the one- and two -dimensional model
- **Validation of the model** using comparisons with data provided from experiments, with wet/dry areas

1.7 Future work

This work addresses various issues both at the continuous level and at the numerical level. We point out some important aspects which can be improved on the method.

1.7.1 Optimization of the method

The method presented in this Phd thesis involves a significant computational cost to solve a real problem. It can be optimized by constructing an efficient preconditioner for the iterative method presented in Chapter 4. This requires studying the Sturm Liouville operator and finding a way to approach the inverse of the elliptic operator at the discrete level. In terms of accuracy, the interest of using a finite element method is that it allows us to increase the order of the method by constructing new pairs of approximation spaces for the mixed problem in velocity-pressure.
The method including a breaking wave criterion has been presented for the one-dimensional case and can be easily extended to two-dimensional case, which will be done in a forthcoming development.

1.7.2 Coupling models and methods

Another possible investigation consists in solving the elliptic problem only for a selected period and domain. This implies coupling different models, a hydrostatic multilayer model on one region and a dispersive model for another region. This is a tricky task and depends on the case being simulated, however, it could be useful to simulate a real phenomenon over a long period of time and a significant domain size.

1.7.3 Multi layer version

The multilayer model described in [74] has been derived by discretizing the Euler model in the vertical direction. The resulting model presents good properties. It admits an energy balance and involves a total pressure for each layer composed with a hydrostatic and a non-hydrostatic part as for the one layer model (1.41). Therefore, the method presented in this work for the DAE model (1.34)-(1.38) can be extended to solve the multi-layer model. It implies solving the elliptic equation for each layer taking into consideration the exchange terms at the interfaces of the layers. As stated in paragraph 1.2, dispersive models and their numerical simulation can improve our knowledge of coastal oceanography modeling and they can have applications in the development of sustainable energies. As we expect a different behavior regarding the micro-algae if we use a multi-layer model with dispersion, we plan to use a multi-layer dispersive model with an extended method to predict and optimize the trajectories of micro-algae in a raceway.

Chapter 2

A robust and stable numerical scheme for a depth-averaged Euler system

This work has been done in collaboration with Marie-Odile Bristeau, Edwige Godlewski and Jacques Sainte-Marie. It has been submitted.

2.1 Introduction

Non-linear shallow water equations model the dynamics of a shallow, rotating layer of homogeneous incompressible fluid and are typically used to describe vertically averaged flows in two or three dimensional domains in terms of horizontal velocity and depth variations. The classical Saint-Venant system [21] with viscosity and friction [77, 79, 121] is particularly well-suited for the study and numerical simulations of a large class of geophysical phenomena such as rivers, lava flows, ice sheets, coastal domains, oceans or even run-off or avalanches when being modified with adapted source terms [33, 35, 119]. But the Saint-Venant system is built on the hydrostatic assumption consisting in neglecting the vertical acceleration of the fluid. This assumption is valid for a large class of geophysical flows but is restrictive in various situations where the dispersive effects cannot be neglected. As an example, neglecting the vertical acceleration in granular flows or landslides leads to significantly overestimate the initial flow velocity [120, 115], with strong implication for hazard assessment.

The derivation of shallow water type models including the non-hydrostatic effects has received an extensive coverage [86, 45, 26, 129, 131, 44, 43] and numerical techniques for the approximation of these models have been recently proposed [106, 62, 42, 108]

In [43], some of the authors have presented an original derivation process of a non-hydrostatic shallow water-type model approximating the incompressible Euler and Navier-Stokes systems with free surface where the closure relations are obtained by a minimal energy constraint instead of an asymptotic expansion. The model slightly differs from the well-known Green-Naghdi model [86]. The purpose of this paper is to propose a robust and efficient numerical scheme for the model described in [43] and related systems. The numerical procedure, based on a projection-correction strategy [50], is endowed with properties such as consistency, positivity, well-balancing and satisfies a fully discrete entropy inequality. The proof of this last property is technical – it is far from being obvious to obtain this inequality for the classical Saint-Venant system – but it is a strong stability property. Notice also that the proposed numerical scheme can be applied to other similar dispersive systems satisfying a "symmetry" relation between the gradient pressure and divergence operators.

We emphasize that the scheme we introduce behaves well when the water depth tends to zero and hence is able to treat wet/dry interfaces. As far as the authors know, few numerical methods endowed with such stability properties have been proposed for such dispersive models extending the shallow water equations.

The paper is organized as follows. In Section 2.2, we recall the non-hydrostatic model proposed in [43] and we give a rewritting of the system. A kinetic description of the model is given in Section 2.3 and it is used to derive the numerical procedure and to prove the properties that are detailed in Sections 2.4 and 2.5. The numerical scheme consists in a

combined finite volume and finite difference strategy. In Section 2.4, we first study the semi-discrete schemes (in space and in time) and then we establish some properties of the fully discrete scheme. In Section 2.5, we prove the entropy inequality for the fully discrete scheme. Stationary/transient analytical solutions of the model are proposed in Section 2.6 and finally the numerical scheme is confronted with analytical solutions.

2.2 A depth-averaged Euler system

Several strategies are possible for the derivation of shallow water type models extending the Saint-Venant system. A usual process is to assume potential flows and an extensive literature exists concerning these models [29, 48, 105, 4, 5, 66]. An asymptotic expansion, going one step further than the classical Saint-Venant system is also possible [79, 44, 141] but such an approach does not always lead to properly defined unique closure relations. In this paper, we start from a non-hydrostatic model derived and studied in [43], where the closure relations are obtained by a minimal energy constraint.

The non-hydrostatic model we intend to discretize in this paper has several interesting properties

- the model formulation only involves first order partial derivatives and appears as a depth-averaged version of the Euler system,
- the proposed model is similar to the well-known Green-Naghdi model [86] but keeps a natural expression of the topography source term.

2.2.1 The model

So we start from the system (see Fig. 2.1 for the notations)

$$\frac{\partial H}{\partial t} + \frac{\partial}{\partial x}\big(H\overline{u}\big) = 0, \tag{2.1}$$

$$\frac{\partial}{\partial t}(H\overline{u}) + \frac{\partial}{\partial x}\left(H\overline{u}^2 + \frac{g}{2}H^2 + H\overline{p}_{nh}\right) = -(gH + 2\overline{p}_{nh})\frac{\partial z_b}{\partial x}, \tag{2.2}$$

$$\frac{\partial}{\partial t}(H\overline{w}) + \frac{\partial}{\partial x}(H\overline{w}\overline{u}) = 2\overline{p}_{nh}, \tag{2.3}$$

$$\frac{\partial(H\overline{u})}{\partial x} - \overline{u}\frac{\partial(H + 2z_b)}{\partial x} + 2\overline{w} = 0. \tag{2.4}$$

We consider this system for

$$t > t_0 \quad \text{and} \quad x \in [0, L],$$

$\overline{\mathbf{u}} = (\overline{u}, \overline{w})^T$ denotes the velocity vector and $\overline{p}_{nh}$ the non-hydrostatic part of the pressure. The total pressure is given by

$$\overline{p} = \frac{g}{2}H + \overline{p}_{nh}. \tag{2.5}$$

The quantities $(\overline{u}, \overline{w}, \overline{p})$ correspond to vertically averaged values of the variables (u, w, p) arising in the incompressible Euler system.

Figure 2.1: Notations: water depth $H(x,t)$, free surface $H + z_b(x,t)$ and bottom $z_b(x,t)$.

The smooth solutions H, $\overline{u}$, $\overline{w}$, $\overline{p}_{nh}$ of the system (2.1)-(2.4) also satisfy the energy conservation law

$$\frac{\partial}{\partial t}(\eta + gHz_b) + \frac{\partial}{\partial x}\Big(\overline{u}\big(\eta + gHz_b + \frac{g}{2}H^2 + H\overline{p}_{nh}\big)\Big) = 0, \tag{2.6}$$

where

$$\eta = \frac{H(\overline{u}^2 + \overline{w}^2)}{2} + \frac{g}{2}H^2. \tag{2.7}$$

We can rewrite (2.6) under the form

$$\frac{\partial \tilde{\eta}}{\partial t} + \frac{\partial \widehat{G}}{\partial x} = 0, \tag{2.8}$$

with

$$\tilde{\eta} = \eta + gHz_b, \qquad G = \overline{u}\big(\eta + \frac{g}{2}H^2\big), \qquad \tilde{G} = G + gHz_b\overline{u}, \qquad \widehat{G} = \widetilde{G} + H\overline{p}_{nh}\overline{u}. \tag{2.9}$$

In the sequel, we will also use the definitions

$$\eta_{hyd} = \frac{H}{2}\overline{u}^2 + \frac{g}{2}H^2, \tag{2.10}$$

$$\tilde{\eta}_{hyd} = \eta_{hyd} + gHz_b, \tag{2.11}$$

$$G_{hyd} = \overline{u}(\eta_{hyd} + \frac{g}{2}H^2), \tag{2.12}$$

$$\tilde{G}_{hyd} = \overline{u}(\tilde{\eta}_{hyd} + \frac{g}{2}H^2), \tag{2.13}$$

which are functions of the unknowns. The entropic solutions of the system (2.1)-(2.4) correspond to an inequality in the r.h.s. of Eqs. (2.6),(2.8).

The system (2.1)-(2.4) is completed with initial and boundary conditions that will be precised later.

Remark 2.2.1. *Notice that simple computations from Eqs.* (2.1) *and* (2.4) *lead to the relation*

$$\frac{\partial}{\partial t}\left(H\frac{H + 2z_b}{2}\right) + \frac{\partial}{\partial x}\left(H\frac{H + 2z_b}{2}\overline{u}\right) = H\overline{w}, \tag{2.14}$$

and Eq. (2.4) *could be replaced by* (2.14)*. In this paper we use* (2.4) *which leads to keep the analogy with the divergence operator in the Navier-Stokes equations as shown in the following paragraph.*

2.2.2 A rewriting

The model we study is a depth-averaged approximation of the incompressible Euler system and in fact we can rewrite it with shallow water type versions of the gradient and divergence operators. Let us formally define the operator ∇_{sw} by

$$\nabla_{sw} f = \begin{pmatrix} H\frac{\partial f}{\partial x} + \frac{\partial (H+2z_b)}{\partial x} f \\ -2f \end{pmatrix}, \tag{2.15}$$

that is a shallow water version of the gradient operator. Likewise, we define a shallow water version of the divergence operator div_{sw} under the form

$$\mathrm{div}_{sw}\, \mathbf{u} = \frac{\partial (Hu)}{\partial x} - u\frac{\partial (H+2z_b)}{\partial x} + 2w, \tag{2.16}$$

where $\mathbf{u} = (u, w)^T$. In definitions (2.15) and (2.16), we assume the considered quantities are smooth enough. The definition of the operators ∇_{sw} and div_{sw} implies that we have the identity

$$\int_I \nabla_{sw}\, p.\mathbf{u}\; dx = [Hup]_{\partial I} - \int_I p\mathrm{div}_{sw}\, \mathbf{u}\; dx, \quad \forall\; p,\; \forall \mathbf{u}, \tag{2.17}$$

where I is any interval of $\mathbb{R}$. Notice that ∇_{sw} and div_{sw} are H and z_b dependent operators and when necessary we will use the notations $\nabla_{sw}\,(.; H)$ and $\mathrm{div}_{sw}\,(.; H)$.

The system (2.1)-(2.4) can be rewritten under the compact form

$$\frac{\partial H}{\partial t} + \frac{\partial}{\partial x}\big(H\overline{u}\big) = 0, \tag{2.18}$$

$$\frac{\partial}{\partial t}(H\overline{\mathbf{u}}) + \frac{\partial}{\partial x}\left(\overline{u}.H\overline{\mathbf{u}}\right) + \nabla_0\left(\frac{g}{2}H^2\right) + \nabla_{sw}\,\overline{p}_{nh} = -gH\nabla_0 z_b, \tag{2.19}$$

$$\mathrm{div}_{sw}\,\overline{\mathbf{u}} = 0, \tag{2.20}$$

with the notation

$$\nabla_0 f = \begin{pmatrix} \frac{\partial f}{\partial x} \\ 0 \end{pmatrix}.$$

Then the system (2.18)-(2.20) appears as a 1d shallow water version of the 2d incompressible Euler system.

2.2.3 Pressure equation

For $H > 0$, Eq. (2.19) can also be written in the nonconservative form

$$\frac{\partial \overline{\mathbf{u}}}{\partial t} + \overline{u}\frac{\partial \overline{\mathbf{u}}}{\partial x} + g\nabla_0 H + \frac{1}{H}\nabla_{sw}\,\overline{p}_{nh} = -g\nabla_0 z_b, \tag{2.21}$$

and applying (2.16) to Eq. (2.21) leads together with (2.20) to the relation

$$-\frac{\partial}{\partial x}\left(H\frac{\partial \overline{p}_{nh}}{\partial x}\right)+\frac{1}{H}\left(4-H\frac{\partial^2(H+2z_b)}{\partial x^2}+\left(\frac{\partial(H+2z_b)}{\partial x}\right)^2\right)\overline{p}_{nh}=$$
$$2H\left(\frac{\partial \overline{u}}{\partial x}\right)^2+2\overline{u}^2\frac{\partial^2 z_b}{\partial x^2}+gH\frac{\partial^2(H+z_b)}{\partial x^2}-2g\frac{\partial z_b}{\partial x}\frac{\partial(H+z_b)}{\partial x}. \quad (2.22)$$

Notice that Eq. (2.22) also reads

$$-\Delta_{sw}\,\overline{p}_{nh}=2H\left(\frac{\partial \overline{u}}{\partial x}\right)^2+2\overline{u}^2\frac{\partial^2 z_b}{\partial x^2}+gH\frac{\partial^2(H+z_b)}{\partial x^2}-2g\frac{\partial z_b}{\partial x}\frac{\partial(H+z_b)}{\partial x}, \quad (2.23)$$

with

$$\Delta_{sw}=\mathrm{div}_{sw}\left(\frac{1}{H}\nabla_{sw}\right).$$

Conversely, Eq. (2.21) with (2.23) gives the divergence free condition (2.20). The resolution of Eq. (2.23) – requiring the inversion of a non local operator – gives the expression for the non-hydrostatic pressure term $\overline{p}_{nh}$. A discrete approximation of Δ_{sw} will be defined in paragraph 2.4.3 and used for the numerical solution of (2.18)-(2.20).

Remark 2.2.2. *In all the writings of the model, the pressure term $\overline{p}_{nh}$ appears as the Lagrange multiplier of the divergence free condition. As in the incompressible Euler system, it is not possible to derive a priori bounds for the pressure terms. And hence, it is possible to obtain nonpositive values for the total pressure $\overline{p}$ defined by* (2.5).

Such a situation means the fluid is no longer in contact with the bottom and the formulation of the proposed model is no longer valid since in that case the bottom of the fluid has to be considered as a free surface.

Even if the proposed model can be modified to take into account these situations (nonpositive presure), we do not consider them in this paper and we will propose in paragraph 2.4.6 a modification ensuring that the total pressure remains nonnegative.

2.2.4 A more general formulation

There exists a wide family of shallow water type dispersive models. One of the most popular models for the description of long, dispersive water waves is the Green-Naghdi model [86]. Several derivations of the Green-Naghdi model have been proposed in the literature [86, 87, 146, 123]. For the mathematical justification of the model, the reader can refer to [4, 118] and for its numerical approximation to [108, 29, 48, 42].

Following [108] (see also [43]), the Green-Naghdi model writes

$$\frac{\partial H}{\partial t}+\frac{\partial}{\partial x}\big(H\overline{u}\big)=0, \quad (2.24)$$
$$\frac{\partial (H\overline{u})}{\partial t}+\frac{\partial}{\partial x}\left(H\overline{u}^2+\frac{g}{2}H^2+H\overline{p}_{gn}\right)=-(gH+2\overline{p}_{gn})\frac{\partial z_b}{\partial x}, \quad (2.25)$$
$$\frac{\partial}{\partial t}(H\overline{w})+\frac{\partial}{\partial x}(H\overline{uw})=\frac{3}{2}\overline{p}_{gn}, \quad (2.26)$$

$$\frac{\partial(H\overline{u})}{\partial x} - \overline{u}\frac{\partial(H+2z_b)}{\partial x} + \frac{3}{2}\overline{w} = 0. \tag{2.27}$$

And hence it appears that the proposed model and the Green-Naghdi system share a similar form. Indeed, introducing a parameter α we consider a more general system

$$\frac{\partial H}{\partial t} + \frac{\partial}{\partial x}\big(H\overline{u}\big) = 0, \tag{2.28}$$

$$\frac{\partial}{\partial t}(H\overline{\mathbf{u}}) + \frac{\partial}{\partial x}\left(\overline{u}.H\overline{\mathbf{u}}\right) + \nabla_0\left(\frac{g}{2}H^2\right) + \nabla_{sw}^{\alpha}\,\overline{p}_{nh} = -gH\nabla_0 z_b, \tag{2.29}$$

$$\mathrm{div}_{sw}^{\alpha}\,\overline{\mathbf{u}} = 0, \tag{2.30}$$

with

$$\nabla_{sw}^{\alpha} f = \begin{pmatrix} H\frac{\partial f}{\partial x} + \frac{\partial(H+2z_b)}{\partial x} f \\ -\alpha f \end{pmatrix},$$

and

$$\mathrm{div}_{sw}^{\alpha}\,\mathbf{u} = \frac{\partial(Hu)}{\partial x} - u\frac{\partial(H+2z_b)}{\partial x} + \alpha w. \tag{2.31}$$

The value $\alpha = 2$ in Eqs. (2.28)-(2.30) gives exactly the model (2.1)-(2.4) whereas for $\alpha = 3/2$ we recover the system (2.24)-(2.27). The system (2.28)-(2.30) is completed with the energy balance

$$\frac{\partial\tilde{\eta}^{\alpha}}{\partial t} + \frac{\partial}{\partial x}\left(\overline{u}\big(\tilde{\eta}^{\alpha} + \frac{g}{2}H^2 + H\overline{p}_{nh}\big)\right) = 0, \tag{2.32}$$

where

$$\tilde{\eta}^{\alpha} = \frac{H}{2}\left(\overline{u}^2 + \frac{2\alpha-1}{3}\overline{w}^2\right) + \frac{g}{2}H^2 + gHz_b. \tag{2.33}$$

Notice that the fundamental duality relation

$$\int_I \overline{p}_{nh}\mathrm{div}_{sw}^{\alpha}\,\overline{\mathbf{u}}\;dx = [H\overline{u}\overline{p}_{nh}]_{\partial I} - \int_I \nabla_{sw}^{\alpha}\,\overline{p}_{nh}.\overline{\mathbf{u}}\;dx,$$

holds for any interval I.

Remark 2.2.3. *It is not in the scope of this paper to compare the Green-Naghdi model and the proposed system. We only notice the range of validity of the two models differs, the first being more appropriate for long wave propagation (Airy waves) and the second being adapted for advection dominated flows, see [43, Section 5].*

Remark 2.2.4. *In the sequel, we propose a numerical approximation of the system* (2.28)-(2.30) *for the value $\alpha = 2$ but the numerical scheme remains valid for any value of $\alpha > 0$.*

2.3 Kinetic description

In this section, we propose a kinetic interpretation for the system (2.1)-(2.3) completed with (2.6). The kinetic description will be used in Section 2.4 to derive a stable, accurate

and robust numerical scheme.

The kinetic approach consists in using a description of the microscopic behavior of the system [132]. In this method, a fictitious density of particles is introduced and the equations are considered at the microscopic scale, where no discontinuity occurs. The kinetic interpretation of a system allows its transformation into a family of linear transport equations, to which an upwinding discretization is naturally applicable.

Following [132], we introduce a real function χ defined on $\mathbb{R}$, compactly supported and which has the following properties

$$\begin{cases} \chi(-w) = \chi(w) \geq 0 \\ \int_{\mathbb{R}} \chi(w)\ dw = \int_{\mathbb{R}} w^2 \chi(w)\ dw = 1. \end{cases} \tag{2.34}$$

Among all the functions χ satisfying (2.34), one plays an important role. Indeed, the choice

$$\chi(z) = \frac{1}{\pi}\left(1 - \frac{z^2}{4}\right)_+^{1/2}, \tag{2.35}$$

with $x_+ \equiv \max(0, x)$, allows to ensure important stability properties [133, 8]. In the following, we keep this special choice for χ.

2.3.1 Kinetic interpretation of the Saint-Venant system

The classical Saint-Venant system [21, 79] corresponds to the hydrostatic part of the model (2.1)-(2.3), it reads

$$\frac{\partial H}{\partial t} + \frac{\partial}{\partial x}\big(H\overline{u}\big) = 0, \tag{2.36}$$

$$\frac{\partial}{\partial t}(H\overline{u}) + \frac{\partial}{\partial x}\left(H\overline{u}^2 + \frac{g}{2}H^2\right) = -gH\frac{\partial z_b}{\partial x}, \tag{2.37}$$

completed with the entropy inequality

$$\frac{\partial \tilde{\eta}_{hyd}}{\partial t} + \frac{\partial \tilde{G}_{hyd}}{\partial x} \leq 0, \tag{2.38}$$

with $\tilde{\eta}_{hyd}$ and $\tilde{G}_{hyd}$ defined by (2.11),(2.13).

Let us construct the density of particles $M(x, t, \xi)$ playing the role of a Maxwellian: the microscopic density of particles present at time t, at the abscissa x and with velocity ξ is given by

$$M(H, \overline{u}, \xi) = \frac{H}{c}\chi\left(\frac{\xi - \overline{u}}{c}\right) = \frac{1}{g\pi}\Big(2gH - (\xi - \overline{u})^2\Big)_+^{1/2}, \tag{2.39}$$

with $c = \sqrt{\frac{gH}{2}}$, $\xi \in \mathbb{R}$. The equilibrium defined by (2.39) corresponds to the classical kinetic Maxwellian equilibrium, used in [133] for example. It satisfies the following moment

relations

$$\begin{aligned}\int_{\mathbb{R}} \begin{pmatrix} 1 \\ \xi \end{pmatrix} M(H,\overline{u},\xi)\, d\xi &= \begin{pmatrix} H \\ H\overline{u} \end{pmatrix}, \\ \int_{\mathbb{R}} \xi^2 M(H,\overline{u},\xi)\, d\xi &= H\overline{u}^2 + g\frac{H^2}{2}.\end{aligned} \tag{2.40}$$

The interest of the particular form (2.39) lies in its link with a kinetic entropy, see [8] where the properties of $H_K(f,\xi,z)$ are studied, H_K refers to the kinetic entropy used in [8]. Consider the kinetic entropy,

$$H_K(f,\xi,z) = \frac{\xi^2}{2} f + \frac{g^2\pi^2}{6} f^3 + gzf, \tag{2.41}$$

where $f \geq 0$, $\xi \in \mathbb{R}$ and $z \in \mathbb{R}$, and its version without topography

$$H_{K,0}(f,\xi) = \frac{\xi^2}{2} f + \frac{g^2\pi^2}{6} f^3. \tag{2.42}$$

Then one can check the relations

$$\int_{\mathbb{R}} H_K\big(M(H,\overline{u},\xi),\xi,z_b\big)\, d\xi = \tilde{\eta}_{hyd}, \tag{2.43}$$

$$\int_{\mathbb{R}} \xi H_K\big(M(H,\overline{u},\xi),\xi,z_b\big)\, d\xi = \tilde{G}_{hyd}. \tag{2.44}$$

These definitions allow us to obtain a kinetic representation of the Saint-Venant system [133].

Proposition 2.3.1. *The pair of functions $(H, H\overline{u})$ is a strong solution of the Saint-Venant system* (2.36)-(2.37) *if and only if $M(H,\overline{u},\xi)$ satisfies the kinetic equation*

$$(\mathcal{B}) \qquad \frac{\partial M}{\partial t} + \xi\frac{\partial M}{\partial x} - g\frac{\partial z_b}{\partial x}\frac{\partial M}{\partial \xi} = Q, \tag{2.45}$$

for some "collision term" $Q(x,t,\xi)$ which satisfies, for a.e. (x,t),

$$\int_{\mathbb{R}} Q\ d\xi = \int_{\mathbb{R}} \xi Q\ d\xi = 0. \tag{2.46}$$

Proof of prop. 2.3.1. Using (2.40), the proof relies on a very simple computation. □

Remark 2.3.2. *The proposition 2.3.1 remains valid if, instead of* (2.35)*, the equilibrium M is built with any function satisfying* (2.34)*.*

This proposition has a very useful consequence : the non-linear shallow water system can be viewed as a family of linear equations for a scalar function M depending nonlinearly

on H and $\overline{u}$, for which it is easier to find simple numerical schemes with good theoretical properties.

2.3.2 Kinetic interpretation of the depth-averaged Euler system

Since we take into account the non-hydrostatic effects of the pressure, the microscopic vertical velocity γ of the particles has to be considered and we now construct the new density of particles $M(x,t,\xi,\gamma)$ defined by a Gibbs equilibrium: the microscopic density of particles present at time t, abscissa x and with microscopic horizontal velocity ξ and microscopic vertical velocity γ is given by

$$M(x,t,\xi,\gamma) = \frac{H}{c}\chi\left(\frac{\xi-\overline{u}}{c}\right)\delta\left(\gamma-\overline{w}\right), \tag{2.47}$$

where δ is the Dirac distribution and $c=\sqrt{\frac{gH}{2}}$. We will also use the notations $M(H,\overline{u},\xi)$.

Then we have the following proposition.

Proposition 2.3.3. *For a given $\overline{p}_{nh}$, the functions $(H,\overline{u},\overline{w})$ satisfying the divergence free condition* (2.16)*, are strong solutions of the depth-averaged Euler system described in* (2.1)-(2.3),(2.6) *if and only if the equilibrium $M(x,t,\xi,\gamma)$ is solution of the kinetic equations*

$$(\mathcal{B}_{nh}) \qquad \frac{\partial M}{\partial t}+\xi\frac{\partial M}{\partial x}-\left(\left(g+\frac{2\overline{p}_{nh}}{H}\right)\frac{\partial z_b}{\partial x}+\frac{1}{H}\frac{\partial}{\partial x}(H\overline{p}_{nh})\right)\frac{\partial M}{\partial \xi} + \frac{2\overline{p}_{nh}}{H}\frac{\partial M}{\partial \gamma} = Q_{nh}, \tag{2.48}$$

where $Q_{nh}=Q_{nh}(x,t,\xi,\gamma)$ is a "collision term" satisfying

$$\int_{\mathbb{R}^2} Q_{nh}\ d\xi d\gamma = \int_{\mathbb{R}^2} \xi Q_{nh}\ d\xi d\gamma = \int_{\mathbb{R}^2} \gamma Q_{nh} d\xi d\gamma = 0. \tag{2.49}$$

Additionally, the solution is an entropy solution if

$$\int_{\mathbb{R}^2}\left(\frac{\xi^2+\gamma^2}{2}+\frac{g^2\pi^2}{2}M^2+gz_b\right)Q_{nh}d\gamma d\xi \leq 0. \tag{2.50}$$

Notice that in the case of the Saint-Venant system (2.36)-(2.37), the particular choice of M defined by (2.39) ensures

$$\int_{\mathbb{R}}\left(\frac{\xi^2}{2}+\frac{g^2\pi^2}{2}M^2+gz_b\right)Qd\xi = 0,$$

with Q satisfying (2.46).

Proof of prop. 2.3.3. From the definitions (2.34),(2.47) and (2.49), the proof results from easy computations, namely by integrating the relation (2.48)

$$\int_{\mathbb{R}^2} (\mathcal{B}_{nh})\ d\xi d\gamma, \quad \int_{\mathbb{R}^2} \xi(\mathcal{B}_{nh})\ d\xi d\gamma, \quad \text{and} \quad \int_{\mathbb{R}^2} \gamma(\mathcal{B}_{nh})\ d\xi d\gamma.$$

Likewise, the energy balance is obtained calculating the quantity

$$\int_{\mathbb{R}^2} \left(\frac{\xi^2+\gamma^2}{2} + \frac{g^2\pi^2}{2} M^2 + g z_b \right) (\mathcal{B}_{nh})\ d\xi d\gamma.$$

□

Equation (2.4) is a kinematic constraint, it is not easy to describe it at the kinetic level.

2.4 Numerical scheme

In this section we propose a discretization for the system (2.18)-(2.20). In order to proceed step by step, we first establish some properties for the semi-discrete schemes in time and then in space. Then we study the fully discrete scheme.

For the sake of simplicity, the notations with $^-$ are dropped. We write the system (2.18)-(2.19) in a condensed form

$$\frac{\partial X}{\partial t} + \frac{\partial}{\partial x} F(X) + R_{nh} = S(X), \tag{2.51}$$

with

$$X = \begin{pmatrix} H \\ Hu \\ Hw \end{pmatrix}, \quad F(X) = \begin{pmatrix} Hu \\ Hu^2 + \frac{g}{2}H^2 \\ Huw \end{pmatrix}, \quad S(X) = \begin{pmatrix} 0 \\ -gH\nabla_0 z_b \end{pmatrix}, \tag{2.52}$$

and

$$R_{nh} = \begin{pmatrix} 0 \\ \nabla_{sw}\, p_{nh} \end{pmatrix},$$

with $\nabla_{sw}\, p_{nh}$ defined by (2.15). The expression of p_{nh} satisfies (2.23) and ensures the divergence free condition (2.20) is satisfied.

2.4.1 Fractional step scheme

For the time discretization, we denote $t^n = \sum_{k\leq n} \Delta t^k$ where the time steps Δt^k will be precised later though a CFL condition. Following [50], we use an operator splitting

technique resulting in a two step scheme

$$\frac{X^{n+1/2}-X^n}{\Delta t^n}+\frac{\partial}{\partial x}F(X^n)=S(X^n), \tag{2.53}$$

$$\frac{X^{n+1}-X^{n+1/2}}{\Delta t^n}+R_{nh}^{n+1}=0. \tag{2.54}$$

The non-hydrostatic part of the pressure p_{nh}^{n+1} is defined by (2.23) and ensures, as already said, that the divergence free constraint (2.20) is satisfied i.e.

$$\mathrm{div}_{sw}\,\mathbf{u}^{n+1}=0. \tag{2.55}$$

The discretization of Eq. (2.23) is given hereafter. The system (2.53)-(2.54) has to be completed with suitable boundary conditions that will be precised later, see paragraph 2.4.3.

The prediction step (2.53) consists in the resolution of Saint-Venant type equations and a transport equation for $(Hw)^{n+1/2}$ i.e.

$$H^{n+1/2}=H^n-\Delta t^n\frac{\partial (Hu)^n}{\partial x}, \tag{2.56}$$

$$(Hu)^{n+1/2}=(Hu)^n-\Delta t^n\frac{\partial}{\partial x}\left(Hu^2+\frac{g}{2}H^2\right)^n-\Delta t^n gH^n\frac{\partial z_b}{\partial x}, \tag{2.57}$$

$$(Hw)^{n+1/2}=(Hw)^n-\Delta t^n\frac{\partial (Hwu)^n}{\partial x}, \tag{2.58}$$

and the correction step (2.54) writes

$$H^{n+1}=H^{n+1/2}, \tag{2.59}$$

$$\mathbf{u}^{n+1}=\mathbf{u}^{n+1/2}-\frac{\Delta t^n}{H^{n+1}}\nabla_{sw}\,p_{nh}^{n+1}, \tag{2.60}$$

with

$$\mathbf{u}^{n+1}=\left(\frac{(Hu)^{n+1}}{H^{n+1}},\frac{(Hw)^{n+1}}{H^{n+1}}\right)^T.$$

More precisely, due to the expression of the operator ∇_{sw} given in (2.15), the notations $\nabla_{sw}\,p_{nh}^{n+1}$ means $\nabla_{sw}\,(p_{nh}^{n+1};H^{n+1})$ and the same remark holds for the operator div_{sw}. Then inserting $\mathbf{u}^{n+1}=(u^{n+1},w^{n+1})$ satisfying (2.60) in relation (2.55) gives the governing equation for p_{nh}^{n+1}

$$\mathrm{div}_{sw}\left(\frac{1}{H^{n+1}}\nabla_{sw}\,p_{nh}^{n+1}\right)=\frac{1}{\Delta t^n}\mathrm{div}_{sw}\left(\frac{(Hu)^{n+1/2}}{H^{n+1/2}},\frac{(Hw)^{n+1/2}}{H^{n+1/2}}\right)^T, \tag{2.61}$$

that is a discrete version of (2.23). Notice also that in Eq. (2.60) we have used the fact that $H^{n+1}=H^{n+1/2}$. It appears that the right hand side of (2.61) can be evaluated by the conservative variables $(H,Hu,Hw)^{n+1/2}$ given by (2.56)-(2.58), the first step of the time scheme.

Proposition 2.4.1. *The scheme* (2.53)-(2.55) *satisfies a semi-discrete (in time) entropy inequality of the form*

$$\tilde{\eta}^{n+1} \leq \tilde{\eta}^n - \Delta t^n \frac{\partial}{\partial x}\left(\tilde{G}^n + (Hu)^{n+1} p_{nh}^{n+1}\right) + (\Delta t^n)^2 \mathcal{O}\left(\left\|F'(X^n) + S(X^n)\right\|_2^2\right), \quad (2.62)$$

with

$$\tilde{\eta}^n = \tilde{\eta}(X^n) = \frac{H^n}{2}\Big((u^n)^2 + (w^n)^2\Big) + \frac{g}{2}(H^n)^2 + gH^n z_b,$$

defined by (2.9). *Equation* (2.62) *appears as a discretization of* (2.8).

Proof of prop. 2.4.1. Multiplying Eq. (2.57) by u^n, we obtain after classical manipulations

$$\tilde{\eta}_{hyd}^{n+1/2} = \tilde{\eta}_{hyd}^n - \Delta t^n \frac{\partial}{\partial x}\left(u^n\left(\tilde{\eta}_{hyd}^n + \frac{g}{2}(H^n)^2\right)\right) + \frac{g}{2}(H^{n+1/2} - H^n)^2 + \frac{H^{n+1/2}}{2}(u^{n+1/2} - u^n)^2, \quad (2.63)$$

with

$$\tilde{\eta}_{hyd}^n = \tilde{\eta}_{hyd}(X^n) = \frac{H^n}{2}(u^n)^2 + \frac{g}{2}(H^n)^2 + gH^n z_b,$$

defined by (2.11). Likewise, multiplying Eq. (2.58) by w^n leads to

$$\frac{H^{n+1/2}}{2}(w^{n+1/2})^2 = \frac{H^n}{2}(w^n)^2 - \Delta t^n \frac{\partial}{\partial x}\left(u^n \frac{H^n}{2}(w^n)^2\right) + \frac{H^{n+1/2}}{2}(w^{n+1/2} - w^n)^2. \quad (2.64)$$

Notice that the last terms appearing in Eq. (2.63) and in Eq. (2.64) are non negative. These error terms are due to the explicit time scheme. The sum of the two previous equations gives the inequality

$$\tilde{\eta}^{n+1/2} \leq \tilde{\eta}^n - \Delta t^n \frac{\partial \tilde{G}^n}{\partial x} + (\Delta t^n)^2 \mathcal{O}\left(\left\|F'(X^n) + S(X^n)\right\|_2^2\right). \quad (2.65)$$

Now we multiply (2.60) by $(H\mathbf{u})^{n+1}$ and after simple computations it comes

$$\frac{H^{n+1}}{2}(u^{n+1})^2 = \frac{H^{n+1/2}}{2}(u^{n+1/2})^2 - \Delta t^n \left(\frac{\partial}{\partial x}\big((Hu)^{n+1} p_{nh}^{n+1}\big) + p_{nh}^{n+1}\left(\frac{\partial}{\partial x}(Hu)^{n+1} - u^{n+1}\frac{\partial}{\partial x}(H^{n+1} + 2z_b)\right)\right) - \frac{H^{n+1/2}}{2}(u^{n+1} - u^{n+1/2})^2, \quad (2.66)$$

and

$$\frac{H^{n+1}}{2}(w^{n+1})^2 = \frac{H^{n+1/2}}{2}(w^{n+1/2})^2 + 2\Delta t^n p_{nh}^{n+1} w^{n+1} - \frac{H^{n+1/2}}{2}(w^{n+1} - w^{n+1/2})^2. \quad (2.67)$$

In Eqs. (2.66) and (2.67), the error terms due to the time discretization are non-positive. Using the two previous equations and (2.55) gives the inequality

$$\tilde{\eta}^{n+1} \leq \tilde{\eta}^{n+1/2} - \Delta t^n \frac{\partial}{\partial x}\left((Hu)^{n+1} p_{nh}^{n+1}\right). \tag{2.68}$$

Finally Eq. (2.68) coupled with Eq. (2.65) gives the result. □

2.4.2 The semi-discrete (in space) scheme

To approximate the solution $X = (H, Hu, Hw)^T$ of the system (2.51), we use a combined finite volume/finite element framework. We assume that the computational domain is discretized with I nodes x_i, $i = 1, \ldots, I$. We denote C_i the cell $(x_{i-1/2}, x_{i+1/2})$ of length $\Delta x_i = x_{i+1/2} - x_{i-1/2}$ with $x_{i+1/2} = (x_i + x_{i+1})/2$. We denote $X_i = (H_i, q_{x,i}, q_{z,i})^T$ with

$$X_i \approx \frac{1}{\Delta x_i} \int_{C_i} X(x,t)dx,$$

the approximate solution at time t on the cell C_i with $q_{x,i} = H_i u_i$, $q_{z,i} = H_i w_i$. Likewise, for the topography, we define

$$z_{b,i} = \frac{1}{\Delta x_i} \int_{C_i} z_b(x)dx.$$

The non-hydrostatic part of the pressure is discretized on a staggered grid (in fact the dual mesh if we consider the 2d case)

$$p_{nh,i+1/2} \approx \frac{1}{\Delta x_{i+1/2}} \int_{x_i}^{x_{i+1}} p_{nh}(x,t)dx,$$

$\Delta x_{i+1/2} = x_{i+1} - x_i$.

Now we propose and study the semi-discrete (in space) scheme approximating the model (2.51) and the divergence free condition (2.20). The semi-discrete scheme writes

$$\Delta x_i \frac{\partial X_i}{\partial t} + \left(F_{i+1/2-} - F_{i-1/2+}\right) + R_{nh,i} = 0, \tag{2.69}$$

$$\mathrm{div}_{sw,i+1/2}\left(\{\mathbf{u}_j\}\right) = 0, \tag{2.70}$$

where (2.70) is a discretized version of the divergence free condition (2.20) which we detail below and with the numerical fluxes

$$F_{i+1/2+} = \mathcal{F}(X_i, X_{i+1}, z_{b,i}, z_{b,i+1}) + \mathcal{S}_{i+1/2+}$$
$$F_{i+1/2-} = \mathcal{F}(X_i, X_{i+1}, z_{b,i}, z_{b,i+1}) + \mathcal{S}_{i+1/2-}.$$

$\mathcal{F}$ is a numerical flux for the conservative part of the system, $\mathcal{S}$ is a convenient discretization

of the topography source term, see paragraph 2.4.3.

Since the first two lines of (2.53) correspond to the classical Saint-Venant system, the numerical fluxes

$$F_{i+1/2\pm} = \begin{pmatrix} F_{H,i+1/2} \\ F_{q_x,i+1/2\pm} \\ F_{q_z,i+1/2} \end{pmatrix}, \tag{2.71}$$

can be constructed using any numerical solver for the Saint-Venant system. More precisely for $F_{H,i+1/2}$,$F_{q_x,i+1/2\pm}$ we adopt numerical fluxes suitable for the Saint-Venant system with topography. Notice that from the definition (2.52), since only the second component of $S(X)$ is non zero, only F_{q_x} has two interface values under the form $F_{q_x,i+1/2\pm}$. For the definition of $F_{q_z,i+1/2}$, the formula (see [9])

$$F_{q_z,i+1/2} = F_{H,i+1/2} w_{i+1/2}, \tag{2.72}$$

with

$$w_{i+1/2} = \begin{cases} w_i & \text{if } F_{H,i+1/2} \geq 0 \\ w_{i+1} & \text{if } F_{H,i+1/2} < 0 \end{cases} \tag{2.73}$$

can be used.

Combining the finite volume approach for the hyperbolic part with a finite difference strategy for the parabolic part, the non-hydrostatic part $R_{nh,i}$ is defined by

$$R_{nh,i} = \begin{pmatrix} 0 \\ \nabla_{sw,i}\, p_{nh} \end{pmatrix},$$

where the two components of $\nabla_{sw,i}\, p_{nh}$ are defined (see (2.15)) by

$$\begin{aligned} \Delta x_i\, \nabla_{sw,i}\, p_{nh}|_1 &= H_i(p_{nh,i+1/2} - p_{nh,i-1/2}) \\ &\quad + p_{nh,i+1/2}\big(\zeta_{i+1} - \zeta_i\big) + p_{nh,i-1/2}\big(\zeta_i - \zeta_{i-1}\big), \qquad (2.74) \\ \Delta x_i\, \nabla_{sw,i}\, p_{nh}|_2 &= -\Big(\Delta x_{i+1/2} p_{nh,i+1/2} + \Delta x_{i-1/2} p_{nh,i-1/2}\Big), \qquad (2.75) \end{aligned}$$

with

$$\zeta_i = \frac{H_i + 2z_{b,i}}{2}.$$

And in (2.70), $\mathrm{div}_{sw,i+1/2}\,(\mathbf{u})$ is defined (see (2.16)) by

$$\begin{aligned} \Delta x_{i+1/2} \mathrm{div}_{sw,i+1/2}\,(\mathbf{u}) = (Hu)_{i+1} - (Hu)_i - (u_i + u_{i+1})\big(\zeta_{i+1} - \zeta_i\big) \\ + \Delta x_{i+1/2}\big(w_{i+1} + w_i\big). \end{aligned} \tag{2.76}$$

Notice that in the definitions (2.74)-(2.75) and in the sequel, the quantity p_{nh} means

$\{p_{nh,j}\}$. Likewise in Eq. (2.76) and in the sequel, $\mathbf{u}$ means $\{\mathbf{u}_j\}$.

In a first step, we assume we have for the resolution of the hyperbolic part i.e. the calculus of $F_{i+1/2-}$,$F_{i-1/2+}$, a robust and efficient numerical scheme. Since this step mainly consists in the resolution of the Saint-Venant equations there exist several solvers endowed with such properties (HLL, Rusanov, relaxation, kinetic,...), see [32].

We assume we have for the prediction step a numerical scheme which is

(i) consistent with the Saint-Venant system (2.36)-(2.37),

(ii) well-balanced i.e., at rest, $\frac{\partial X_i}{\partial t} = 0 \; \forall i$ (see (2.69)),

(iii) satisfying an in-cell entropy of the form

$$\Delta x_i \frac{\partial \tilde{\eta}_{hyd,i}}{\partial t} + \left(\tilde{G}_{hyd,i+1/2} - \tilde{G}_{hyd,i-1/2}\right) \leq 0,$$

with (see (2.11),(2.13))

$$\tilde{\eta}_{hyd,i} = \frac{H_i}{2}(u_i)^2 + \frac{g}{2}(H_i)^2 + gH_i z_b,$$

and $\tilde{G}_{hyd,i+1/2}$ is the entropy flux associated with the chosen finite volume solver.

Then the following proposition holds.

Proposition 2.4.2. *The numerical scheme* (2.69),(2.70)

(i) is consistent with the model (2.1)-(2.4),

(ii) preserves the same steady state as the lake at rest,

(iii) satisfies an in-cell entropy inequality associated with the entropy $\tilde{\eta}(t)$ *analogous to the continuous one defined in* (2.8)

$$\Delta x_i \frac{\partial \tilde{\eta}_i}{\partial t} + \left(\hat{G}_{i+1/2} - \hat{G}_{i-1/2}\right) \leq d_i, \quad \text{in } C_i, \tag{2.77}$$

with

$$\begin{aligned} \tilde{\eta}_i &= \tilde{\eta}(X_i) = \tilde{\eta}_{hyd,i} + H_i \frac{w_i^2}{2}, \\ \hat{G}_{i+1/2} &= \tilde{G}_{hyd,i+1/2} + F_{H,i+1/2} w_{i+1/2}^2/2 + (Hu)_{i+1/2} p_{nh,i+1/2}, \end{aligned}$$

and d_i *is an error term satisfying* $d_i = \mathcal{O}(\Delta x^3)$,

(iv) ensures a decrease of the total energy under the form

$$\frac{\partial}{\partial t} \sum_i \Delta x_i \tilde{\eta}_i \leq 0. \tag{2.78}$$

The inequality (2.77) is obtained by multiplying (scalar product) the two momenta equations of (2.69) by $\mathbf{u}_i$ which corresponds to a piecewise constant discretization. For the hyperbolic part it allows to derive a semi-discrete entropy, see [7, 8].

The error term d_i in the r.h.s. of (2.77) comes from the discretization of the non-hydrostatic part corresponding to the incompressible part of the model. In order to eliminate d_i, a more accurate discretization of the velocity field – in accordance with the approximation of the divergence free condition – would be necessary.

Proof of prop. 2.4.2. (i) Since we have assumed that the numerical scheme for the prediction part is consistent, we have (with the same notations as in [32])

$$\mathcal{F}(X, X, z, z) = F(X).$$

Likewise $\mathcal{S}$ is a consistent discretization of the topography source term. It is easy to prove that the non-hydrostatic terms given by (2.74),(2.75) are a consistent discretization of R_{nh} proving the result.

(ii) When $\mathbf{u}_j = (0, 0)^T$ for $j = i-1, i, i+1$, the hyperbolic part being discretized using a well-balanced scheme we have

$$F_{i+1/2-} = F_{i-1/2+} = 0,$$

and the scheme (2.69),(2.70) reduces to

$$R_{nh,i} = (0, 0, 0)^T, \qquad \frac{\partial X_i}{\partial t} = 0,$$

ensuring the scheme is well-balanced.

(iii) Multiplying the first two equations of system (2.69) by the first two components of $\tilde{\eta}'(X_i)$ with

$$\tilde{\eta}'(X_i) = \begin{pmatrix} gH_i - \frac{u_i^2+w_i^2}{2} \\ u_i \\ w_i \end{pmatrix},$$

we obtain

$$\Delta x_i \frac{\partial \tilde{\eta}_{hyd,i}}{\partial t} + \left(\tilde{G}_{hyd,i+1/2-} - \tilde{G}_{hyd,i-1/2+}\right) + u_i \, \nabla_{sw,i} \, p_{nh}|_1 \leq 0. \tag{2.79}$$

In Eq. (2.79), the three first terms are obtained as in [7]. The proof of theorem 2.1 in [7] can be used without any change, except for the vertical kinetic energy, namely

$$H\frac{w^2}{2},$$

that is not considered in [7] since the model is hydrostatic. In order to obtain the contri-

bution of the vertical kinetic energy in Eq. (2.79), we proceed as follows.

Multiplying the third component of Eq. (2.69) by w_i i.e. by the third component of $\tilde{\eta}'(X_i)$, we obtain

$$\Delta x_i \frac{\partial H_i w_i}{\partial t} w_i + \Big(F_{H,i+1/2} w_{i+1/2} - F_{H,i-1/2} w_{i-1/2}\Big) w_i + \Delta x_i \, \nabla_{sw,i} \, p_{nh}|_2 \, w_i = 0.$$

The first term in the above equation also writes

$$\frac{\partial H_i w_i}{\partial t} w_i = \frac{\partial}{\partial t}\left(\frac{H_i}{2} w_i^2\right) + \frac{w_i^2}{2}\frac{\partial H_i}{\partial t}. \tag{2.80}$$

For the fluxes, it comes

$$\begin{aligned}\Big(F_{H,i+1/2} w_{i+1/2} - F_{H,i-1/2} w_{i-1/2}\Big) w_i = F_{H,i+1/2}\frac{w_{i+1/2}^2}{2} - F_{H,i-1/2}\frac{w_{i-1/2}^2}{2} \\ + F_{H,i+1/2} w_{i+1/2}\left(w_i - \frac{w_{i+1/2}}{2}\right) - F_{H,i-1/2} w_{i-1/2}\left(w_i - \frac{w_{i-1/2}}{2}\right).\end{aligned} \tag{2.81}$$

Using the first equation of (2.69) and the definition (2.73), the sum of Eqs. (2.80) and (2.81) gives

$$\begin{aligned}\Delta x_i \frac{\partial}{\partial t}\left(\frac{H_i}{2} w_i^2\right) + F_{H,i+1/2}\frac{w_{i+1/2}^2}{2} - F_{H,i-1/2}\frac{w_{i-1/2}^2}{2} + \Delta x_i \, \nabla_{sw,i} \, p_{nh}|_2 \, w_i = \\ \frac{1}{2}\left[F_{H,i+1/2}\right]_- (w_{i+1} - w_i)^2 - \frac{1}{2}\left[F_{H,i-1/2}\right]_+ (w_i - w_{i-1})^2,\end{aligned}$$

with the notations $[a]_+ = max(a, 0)$, $[a]_- = min(a, 0)$ $a = [a]_+ + [a]_-$. Therefore it yields

$$\Delta x_i \frac{\partial}{\partial t}\left(\frac{H_i}{2} w_i^2\right) + F_{H,i+1/2}\frac{w_{i+1/2}^2}{2} - F_{H,i-1/2}\frac{w_{i-1/2}^2}{2} + \Delta x_i \, \nabla_{sw,i} \, p_{nh}|_2 \, w_i \leq 0, \tag{2.82}$$

and the left hand side of the above equation is exactly the contribution of the vertical kinetic energy over the energy balance (2.79).

Adding (2.79) to (2.82) gives

$$\Delta x_i \frac{\partial \tilde{\eta}_i}{\partial t} + \Big(\tilde{G}_{i+1/2-} - \tilde{G}_{i-1/2+}\Big) + \begin{pmatrix} u_i \\ w_i \end{pmatrix} . \nabla_{sw,i} \, p_{nh} \leq 0, \tag{2.83}$$

with $\tilde{G}_{i+1/2-} = \tilde{G}_{hyd,i+1/2-} + F_{H,i+1/2}\frac{w_{i+1/2}^2}{2}$ and it remains to rewrite the last term in Eq. (2.83). Using the definitions (2.74),(2.75), we have

$$\begin{aligned}\Delta x_i \, \nabla_{sw,i} \, p_{nh}|_2 \, w_i &= -\Big(\Delta x_{i+1/2} p_{nh,i+1/2} + \Delta x_{i-1/2} p_{nh,i-1/2}\Big) w_i, \\ \Delta x_i \, \nabla_{sw,i} \, p_{nh}|_1 \, u_i &= H_i (p_{nh,i+1/2} - p_{nh,i-1/2}) u_i\end{aligned} \tag{2.84}$$

$$
\begin{aligned}
& +p_{nh,i+1/2}\big(\zeta_{i+1}-\zeta_i\big)u_i + p_{nh,i-1/2}\big(\zeta_i-\zeta_{i-1}\big)u_i \\
= \;& (Hu)_{i+1/2}p_{nh,i+1/2} - (Hu)_{i-1/2}p_{nh,i-1/2} \\
& +p_{nh,i+1/2}\big(\zeta_{i+1}-\zeta_i\big)u_i + p_{nh,i-1/2}\Big(\zeta_i-\zeta_{i-1}\Big)u_i \\
& -\frac{(Hu)_{i+1}-(Hu)_i}{2}p_{nh,i+1/2} - \frac{(Hu)_i-(Hu)_{i-1}}{2}p_{nh,i-1/2},
\end{aligned} \tag{2.85}
$$

with

$$
(Hu)_{i+1/2} = \frac{(Hu)_{i+1}+(Hu)_i}{2}.
$$

The divergence free condition (2.70) multiplied by $p_{nh,i+1/2}/2$ leads to

$$
\begin{aligned}
\frac{p_{nh,i+1/2}}{2}\Big((Hu)_{i+1}-(Hu)_i\Big) - \frac{u_i+u_{i+1}}{2}p_{nh,i+1/2}\,(\zeta_{i+1}-\zeta_i) & \\
+ \Delta x_{i+1/2}\frac{p_{nh,i+1/2}}{2}(w_{i+1}+w_i) = 0. &
\end{aligned} \tag{2.86}
$$

The sum of relations (2.84), (2.85) and (2.86) gives

$$
\Delta x_i \nabla_{sw,i}\, p_{nh}.\begin{pmatrix} u_i \\ w_i \end{pmatrix} = \Big((Hu)_{i+1/2}p_{nh,i+1/2} - (Hu)_{i-1/2}p_{nh,i-1/2}\Big) + d_{i+1/2} - d_{i-1/2}, \tag{2.87}
$$

with

$$
d_{i+1/2} = \frac{p_{nh,i+1/2}}{2}\Big(\Delta x_{i+1/2}(w_{i+1}-w_i) - (u_{i+1}-u_i)\big(\zeta_{i+1}-\zeta_i\big)\Big), \tag{2.88}
$$

$$
d_{i-1/2} = \frac{p_{nh,i-1/2}}{2}\Big(\Delta x_{i-1/2}(w_i-w_{i-1}) - (u_i-u_{i-1})\big(\zeta_i-\zeta_{i-1}\big)\Big). \tag{2.89}
$$

Assuming the variables are smooth enough, the quantity $d_i = d_{i+1/2} - d_{i-1/2}$ satisfies $d_i = \mathcal{O}(\Delta x^3)$ and we have

$$
\Delta x_i \begin{pmatrix} u_i \\ w_i \end{pmatrix}.\nabla_{sw,i}\, p_{nh} = \Big((Hu)_{i+1/2}p_{nh,i+1/2} - (Hu)_{i-1/2}p_{nh,i-1/2}\Big) + \mathcal{O}(\Delta x)^3,
$$

which together with (2.83) proves *(iii)*.

(iv) With a suitable choice of the boundary conditions, typically $p_{nh,i+1/2} = 0$ for $i = 0$ or $i = N$ – when the inflow is prescribed – or a convenient definition of the vertical velocities w_0 or w_{N+1} – when the water depth is given – see paragraph 2.4.3, then the sum for $i = 1, \ldots, N$ of (2.83) with (2.87)-(2.89) proves *(iv)*. □

2.4.3 The fully discrete scheme

Now we examine the fully discrete scheme that consists in the combination of the semi-discrete schemes described in paragraphs 2.4.1 and 2.4.2.

Prediction step

Using the space discretization defined in paragraph 2.4.2, we adopt, for the system (2.53), the discretization

$$X_i^{n+1/2} = X_i^n - \sigma_i^n (F_{i+1/2-}^n - F_{i-1/2+}^n), \tag{2.90}$$

where $\sigma_i^n = \Delta t^n / \Delta x_i$ is the ratio between the space and time steps and $F_{i+1/2\pm}$ are given by a robust and efficient discretization of the hyperbolic part with the topography.

For the discretization of the topography source term in the Saint-Venant system, several techniques are available. In this paper, we use the hydrostatic reconstruction (HR scheme for short) [7], leading to the following expressions for the numerical fluxes

$$\begin{aligned} F_{i+1/2-}^n &= \begin{pmatrix} \mathcal{F}_H(X_{i+1/2-}^n, X_{i+1/2+}^n) \\ \mathcal{F}_{q_x}(X_{i+1/2-}^n, X_{i+1/2+}^n) \\ \mathcal{F}_H(X_{i+1/2-}^n, X_{i+1/2+}^n) w_{i+1/2} \end{pmatrix} + \begin{pmatrix} 0 \\ g\frac{(H_i^n)^2}{2} - \frac{g(H_{i+1/2-}^n)^2}{2} \\ 0 \end{pmatrix}, \\ F_{i+1/2+}^n &= \begin{pmatrix} \mathcal{F}_H(X_{i+1/2-}^n, X_{i+1/2+}^n) \\ \mathcal{F}_{q_x}(X_{i+1/2-}^n, X_{i+1/2+}^n) \\ \mathcal{F}_H(X_{i+1/2-}^n, X_{i+1/2+}^n) w_{i+1/2}^n \end{pmatrix} + \begin{pmatrix} 0 \\ g\frac{(H_{i+1}^n)^2}{2} - \frac{g(H_{i+1/2+}^n)^2}{2} \\ 0 \end{pmatrix}, \end{aligned} \tag{2.91}$$

where (2.72) has been used and $\mathcal{F} = (\mathcal{F}_H, \mathcal{F}_{q_x})^T$ is a numerical flux for the Saint-Venant system without topography. The reconstructed states

$$X_{i+1/2-}^n = (H_{i+1/2-}^n, H_{i+1/2-}^n u_i^n), \qquad X_{i+1/2+}^n = (H_{i+1/2+}^n, H_{i+1/2+}^n u_{i+1}^n), \tag{2.92}$$

are defined by

$$H_{i+1/2-}^n = (H_i^n + z_{b,i} - z_{b,i+1/2})_+, \qquad H_{i+1/2+}^n = (H_{i+1}^n + z_{b,i+1} - z_{b,i+1/2})_+, \tag{2.93}$$

and

$$z_{b,i+1/2} = \max(z_{b,i}, z_{b,i+1}). \tag{2.94}$$

Correction step

For the system (2.54),(2.55), we adopt the discretization

$$H_i^{n+1} = H_i^{n+1/2}, \tag{2.95}$$

$$\mathbf{u}_i^{n+1} = \mathbf{u}_i^{n+1/2} - \frac{\Delta t^n}{H_i^{n+1}} \nabla_{sw,i}\, p_{nh}^{n+1}, \tag{2.96}$$

$$\mathrm{div}_{sw,i+1/2}\left(\mathbf{u}^{n+1}\right) = 0, \tag{2.97}$$

with $\nabla_{sw,i}\, p_{nh}^{n+1} = \nabla_{sw,i}\,(p_{nh}^{n+1}; H^{n+1/2})$ and $\mathrm{div}_{sw,i+1/2}\left(\mathbf{u}^{n+1}\right) = \mathrm{div}_{sw,i+1/2}\left(\mathbf{u}^{n+1}; H^{n+1/2}\right)$ defined by Eqs. (2.74)-(2.76). Then, applying $\mathrm{div}_{sw,i+1/2}$ to (2.96) and using (2.97) gives

the expression for the elliptic equation under the form

$$\mathrm{div}_{sw,i+1/2}\left(\frac{1}{H^{n+1}}\nabla_{sw}\, p_{nh}^{n+1}\right) = \frac{1}{\Delta t^n}\mathrm{div}_{sw,i+1/2}\left(\mathbf{u}^{n+1/2}\right). \tag{2.98}$$

The solution of (2.98) gives p_{nh}^{n+1} and allows to calculate $(H\mathbf{u})_i^{n+1}$ using (2.96).

Omitting the superscript $^{n+1}$, the expression of

$$\Delta_{sw,i+1/2}p_{nh} = \mathrm{div}_{sw,i+1/2}\left(\frac{1}{H}\nabla_{sw}\, p_{nh}\right),$$

is given by

$$\begin{aligned}
-\Delta x_{i+1/2}\Delta_{sw,i+1/2}p_{nh} =& -\frac{H_{i+1}}{\Delta x_{i+1}}\Big(p_{nh,i+3/2}-p_{nh,i+1/2}\Big)+\frac{H_i}{\Delta x_i}\Big(p_{nh,i+1/2}-p_{nh,i-1/2}\Big)\\
&-\frac{p_{nh,i+3/2}}{\Delta x_{i+1}}\big(\zeta_{i+2}-\zeta_{i+1}\big)-\frac{p_{nh,i+1/2}}{\Delta x_{i+1}}\big(\zeta_{i+1}-\zeta_i\big)\\
&+\frac{p_{nh,i+1/2}}{\Delta x_i}\big(\zeta_{i+1}-\zeta_i\big)+\frac{p_{nh,i-1/2}}{\Delta x_i}\big(\zeta_i-\zeta_{i-1}\big)\\
&+\left(\frac{p_{nh,i+3/2}-p_{nh,i+1/2}}{\Delta x_{i+1}}+\frac{p_{nh,i+1/2}-p_{nh,i-1/2}}{\Delta x_i}\right)\big(\zeta_{i+1}-\zeta_i\big)\\
&+\frac{p_{nh,i+3/2}}{H_{i+1}\Delta x_{i+1}}\big(\zeta_{i+2}-\zeta_{i+1}\big)\big(\zeta_{i+1}-\zeta_i\big)\\
&+\frac{p_{nh,i+1/2}}{H_{i+1}\Delta x_{i+1}}\big(\zeta_{i+1}-\zeta_i\big)^2+\frac{p_{nh,i+1/2}}{H_i\Delta x_i}\big(\zeta_{i+1}-\zeta_i\big)^2\\
&+\frac{p_{nh,i-1/2}}{H_i\Delta x_i}\big(\zeta_{i+1}-\zeta_i\big)\big(\zeta_i-\zeta_{i-1}\big)\\
&+\Delta x_{i+1/2}\Bigg(\frac{\Delta x_{i+3/2}p_{nh,i+3/2}+\Delta x_{i+1/2}p_{nh,i+1/2}}{\Delta x_{i+1}H_{i+1}}\\
&+\frac{\Delta x_{i+1/2}p_{nh,i+1/2}+\Delta x_{i-1/2}p_{nh,i-1/2}}{\Delta x_i H_i}\Bigg).
\end{aligned}$$

And it remains to prove that the previous relation is consistent with the left hand side of

Eq. (2.22). We rewrite $\Delta_{sw,i+1/2}p_{nh}$ under the form

$$\begin{aligned}
-\Delta x_{i+1/2}\Delta_{sw,i+1/2}p_{nh} =& -\frac{H_{i+1}}{\Delta x_{i+1}}\Big(p_{nh,i+3/2}-p_{nh,i+1/2}\Big)+\frac{H_i}{\Delta x_i}\Big(p_{nh,i+1/2}-p_{nh,i-1/2}\Big)\\
&-\frac{p_{nh,i+3/2}}{\Delta x_{i+1}}\Big(\zeta_{i+2}-2\zeta_{i+1}+\zeta_i\Big)\\
&-\left(\frac{1}{\Delta x_{i+1}}-\frac{1}{\Delta x_i}\right)p_{nh,i+1/2}\Big(\zeta_{i+1}-\zeta_i\Big)\\
&-\frac{p_{nh,i-1/2}}{\Delta x_i}\Big(\zeta_{i+1}-2\zeta_i+\zeta_{i-1}\Big)\\
&+\frac{p_{nh,i+3/2}}{H_{i+1}\Delta x_{i+1}}\Big(\zeta_{i+2}-\zeta_{i+1}\Big)\Big(\zeta_{i+1}-\zeta_i\Big)\\
&+p_{nh,i+1/2}\left(\frac{1}{H_{i+1}\Delta x_{i+1}}+\frac{1}{H_i\Delta x_i}\right)\Big(\zeta_{i+1}-\zeta_i\Big)^2\\
&+\frac{p_{nh,i-1/2}}{H_i\Delta x_i}\Big(\zeta_{i+1}-\zeta_i\Big)\Big(\zeta_i-\zeta_{i-1}\Big)\\
&+\Delta x_{i+1/2}\Bigg(\frac{\Delta x_{i+3/2}p_{nh,i+3/2}+\Delta x_{i+1/2}p_{nh,i+1/2}}{\Delta x_{i+1}H_{i+1}}\\
&+\frac{\Delta x_{i+1/2}p_{nh,i+1/2}+\Delta x_{i-1/2}p_{nh,i-1/2}}{\Delta x_iH_i}\Bigg),
\end{aligned}$$

that is indeed a consistent discretization of the left hand side of Eq. (2.22).

In the case of a regular mesh $\Delta x_i=\Delta x=cst$, the above expression of $\Delta_{sw,i+1/2}p_{nh}$ reduces to

$$\begin{aligned}
-\Delta x^2\Delta_{sw,i+1/2}p_{nh} =& -H_{i+1}\Big(p_{nh,i+3/2}-p_{nh,i+1/2}\Big)+H_i\Big(p_{nh,i+1/2}-p_{nh,i-1/2}\Big)\\
&-p_{nh,i+3/2}\Big(\zeta_{i+2}-2\zeta_{i+1}+\zeta_i\Big)\\
&-p_{nh,i-1/2}\Big(\zeta_{i+1}-2\zeta_i+\zeta_{i-1}\Big)\\
&+\frac{p_{nh,i+3/2}}{H_{i+1}}\Big(\zeta_{i+2}-\zeta_{i+1}\Big)\Big(\zeta_{i+1}-\zeta_i\Big)\\
&+p_{nh,i+1/2}\left(\frac{1}{H_i}+\frac{1}{H_{i+1}}\right)\Big(\zeta_{i+1}-\zeta_i\Big)^2\\
&+\frac{p_{nh,i-1/2}}{H_i}\Big(\zeta_{i+1}-\zeta_i\Big)\Big(\zeta_i-\zeta_{i-1}\Big)\\
&+\Delta x^2\left(\frac{p_{nh,i+3/2}+p_{nh,i+1/2}}{H_{i+1}}+\frac{p_{nh,i+1/2}+p_{nh,i-1/2}}{H_i}\right).
\end{aligned}$$

Remark 2.4.3. *The numerical scheme proposed in this paragraph for the correction step is based on a finite difference strategy and hence cannot be extended to unstructured meshes in higher dimension. But, based on a variational formulation of the correction step, the authors have obtained a finite element version of the scheme* (2.96)-(2.97) *with piecewise polynomial approximations of the velocities and the pressure satisfying the discrete* $inf-sup$ *condition. We will study this property in Chapter 3.*

Boundary conditions

It is difficult to define the boundary conditions for the whole system. Therefore, we first impose boundary conditions for the hyperbolic part of the system and then we apply suitable boundary conditions for the elliptic equation governing the non-hydrostatic pressure p_{nh}.

Hyperbolic part The definition and the implementation of the boundary conditions used for the hyperbolic part have been presented in various papers of some of the authors. The reader can refer to [41].

Non-hydrostatic part For the non-hydrostatic part, we need to define boundary conditions for Eq. (2.98) and we adopt the following strategy. Notice that other solutions can be investigated since the coupling of the boundary conditions between a hyperbolic step and a parabolic step is far from being obvious.
Given flux When – for the hyperbolic part – the inflow is prescribed, we impose for the elliptic equation (2.98) a homogeneous Dirichlet type boundary condition. More precisely, if for $i = 0$ or $i = I$, $Hu|_{i+1/2}^{n+1/2} = Q_0$ is given then we impose $p_{nh,i+1/2}^{n+1} = 0$. This choice is imposed by the relation (2.96) in order to ensure $(Hu)^{n+1} = (Hu)^{n+1/2}$ on the neighbouring cell.
Given water depth If the water depth is prescribed for the hyperbolic part i.e. for $i = 0$ or $i = I$, $H|_{i+1/2}^{n+1/2} = H_0$ is given, then we impose for Eq. (2.98) a Neumann type boundary condition under the form $p_{nh,1/2} = p_{nh,3/2}$ or $p_{nh,I-1/2} = p_{nh,I+1/2}$.

2.4.4 The discrete $inf - sup$ condition

For the problems arising in incompressible fluid mechanics, the $inf - sup$ condition [40] (see also [3]) is a crucial point. The discretization we propose allows, in practice, the numerical resolution of the considered problem but we do not study the behavior of the solution when $\Delta x_i \to 0$. Let us give some hint of how this condition is involved in our approach.

Using a matrix notation for the shallow water gradient operator

$$\nabla_{sw}\, p_{nh}^{n+1} = B^T p_{nh}^{n+1},$$

we get

$$\mathrm{div}_{sw}\, \mathbf{u}^{n+1} = B\mathbf{u}^{n+1},$$

where suitable boundary conditions are assumed. Therefore, defining

$$\Lambda = \mathrm{diag}(H_i^{-1}),$$

the fully discrete scheme obtained from (2.90),(2.95)-(2.97) can be rewritten under the form

$$\begin{pmatrix} \frac{1}{\Delta t} & 0 & 0 \\ 0 & \frac{1}{\Delta t} & B^T \\ 0 & B\Lambda & 0 \end{pmatrix} \begin{pmatrix} H^{n+1} \\ (H\mathbf{u})^{n+1} \\ p_{nh}^{n+1} \end{pmatrix} = \begin{pmatrix} \frac{H^n}{\Delta t} + D_H(X^n) \\ \frac{(H\mathbf{u})^n}{\Delta t} + D_{H\underline{u}}(X^n) \\ 0 \end{pmatrix}, \tag{2.99}$$

where D_H,$D_{H\underline{u}}$ refer to the numerical discretization of the hyperbolic part. The system (2.99) admits a unique solution if the matrix $B\Lambda B^T$ is invertible which is related to the inf-sup condition. This property will be investigated in a forthcoming paper.

Remark 2.4.4. *Instead of the scheme* (2.99)*, a fully implicit version – including the hyperbolic part – may be considered. But such a discretization would imply to have an implicit treatment of the hyperbolic part of the proposed model corresponding to the Saint-Venant system. And an efficient and robust implicit solver for the Saint-Venant system is hardly accessible.*

2.4.5 Stability of the scheme

For the numerical scheme detailed in paragraphs 2.4.3 and 2.4.3 we have the following proposition.

Proposition 2.4.5. *Assuming a suitable CFL condition associated with the chosen numerical fluxes* (2.71) *for the hyperbolic part, the scheme* (2.90),(2.95)-(2.97)

(i) preserves the nonnegativity of the water depth $H_i^n \geq 0$, $\forall i$, $\forall n$,

(ii) preserves the steady state of the lake at rest,

(iii) is consistent with the model (2.1)-(2.4).

Proof of prop. 2.4.5. (i) The statement that $\mathcal{F}$ preserves the nonnegativity of the water depth means exactly that

$$\mathcal{F}_H(H_i = 0, u_i, H_{i+1}, u_{i+1}) - \mathcal{F}_H(H_{i-1}, u_{i-1}, H_i = 0, u_i) \leq 0,$$

for all choices of the other arguments. From (2.90),(2.91), we need to check that, with obvious notations

$$\mathcal{F}_H\left(X_{i+1/2-}^n, X_{i+1/2+}^n\right) - \mathcal{F}_H\left(X_{i-1/2-}^n, X_{i-1/2+}^n\right) \leq 0,$$

whenever $H_i^n = 0$. And this property holds since from (2.93),(2.94) $H_i = 0$ implies $H_{i+1/2-} = H_{i-1/2+} = 0$.

(ii) When $u_i^n = 0$ for all i, the properties of the hydrostatic reconstruction technique ensure

$$F_{i+1/2-}^n = F_{i-1/2+}^n,$$

in (2.90) and hence $X_i^{n+1/2} = X_i^n$ moreover the scheme (2.95),(2.96),(2.98) gives

$$X_i^{n+1} = X_i^{n+1/2},$$

proving that the scheme is well-balanced.

(iii) The numerical flux $\mathcal{F}$ being consistent with the homogeneous Saint-Venant system, the hydrostatic reconstruction associated with $\mathcal{F}$ gives a consistent discretization of the Saint-Venant system with the topography source term. The discretizations (2.96),(2.97) being obviously consistent with the remaining part, this proves the result. □

2.4.6 Wet-dry interfaces

When H tends to 0, the correction step (2.96) is no longer valid and we propose a modified version of (2.96),(2.97) under the form

$$\begin{aligned} \mathbf{u}_i^{n+1} &= \mathbf{u}_i^{n+1/2} - \Delta t^n \frac{1}{H_i^{n+1}} \nabla_{sw,i}^{\varepsilon} p_{nh}^{n+1}, \\ \mathrm{div}_{sw,i+1/2}\left(\mathbf{u}^{n+1}\right) &= 0, \end{aligned}$$

and

$$\begin{aligned} \frac{\Delta x_i}{H_i^{n+1}} \nabla_{sw,i}^{\varepsilon} p_{nh}^{n+1}\big|_1 &= p_{nh,i+1/2}^{n+1} - p_{nh,i-1/2}^{n+1} \\ &\quad + \frac{\mathbf{1}_{H_i^{n+1}\geq\varepsilon}}{H_i^{n+1}} \Big(p_{nh,i+1/2}^{n+1} \Big(\zeta_{i+1}^{n+1} - \zeta_i^{n+1}\Big) + p_{nh,i-1/2}^{n+1} \Big(\zeta_i^{n+1} - \zeta_{i-1}^{n+1}\Big) \Big), \\ \frac{\Delta x_i}{H_i^{n+1}} \nabla_{sw,i}^{\varepsilon} p_{nh}^{n+1}\big|_2 &= -\frac{1}{H_{i,\varepsilon}^{n+1}} \left(\Delta x_{i+1/2} p_{nh,i+1/2}^{n+1} + \Delta x_{i-1/2} p_{nh,i-1/2}^{n+1} \right), \end{aligned}$$

with ε being a constant $\varepsilon = cst > 0$ and $H_\varepsilon = \max(H, \varepsilon)$.

In order to ensure that the total pressure (2.5)

$$\overline{p} = \frac{g}{2} H + \overline{p}_{nh},$$

remains non negative, we add the constraint

$$\text{if} \quad \frac{g}{2} \min(H_i^{n+1}, H_{i+1}^{n+1}) + p_{nh,i+1/2}^{n+1} < 0 \quad \text{then} \quad p_{nh,i+1/2}^{n+1} = 0,$$

to the solution of the elliptic equation (2.98). Notice that in all the numerical tests presented in this paper this constraint is not active meaning the total pressure remains non negative.

2.5 Fully discrete entropy inequality

We have precised in paragraph 2.4.3 a general scheme for the resolution of the non-hydrostatic model. In this paragraph we study the properties of the proposed scheme in the context of one particular solver for the hyperbolic part, namely the kinetic solver, since it allows to ensure stability properties among which are entropy inequalities (semi-discrete and fully discrete) [8]. The presentation in the sequel follows closely that of [8].

Looking for a kinetic interpretation of the HR scheme, we would like to write down a kinetic scheme for Eq. (2.45) such that the associated macroscopic scheme is exactly (2.90)-(2.91) with the definitions (2.92)-(2.94).

We drop the superscript ^{n} and keep superscripts $^{n+1}$ and $^{n+1/2}$. We denote $M_i = M(H_i, u_i, \xi)$, $M_{i+1/2-} = M(H_{i+1/2-}, u_i, \xi)$, $M_{i+1/2+} = M(H_{i+1/2+}, u_{i+1}, \xi)$, $f_i^{n+1/2-} = f_i^{n+1/2-}(\xi)$ where M is defined by (2.39) and we consider the scheme

$$\begin{aligned} f_i^{n+1/2-} = M_i - \sigma_i \Big(& \xi frm[o] - - _{\xi<0} M_{i+1/2+} + \xi \mathbf{1}_{\xi>0} M_{i+1/2-} + \delta M_{i+1/2-} \\ & - \xi \mathbf{1}_{\xi>0} M_{i-1/2-} - \xi \mathbf{1}_{\xi<0} M_{i-1/2+} - \delta M_{i-1/2+} \Big). \end{aligned} \tag{2.100}$$

In this formula, $\delta M_{i+1/2\pm}$ are defined by

$$\delta M_{i+1/2-} = (\xi - u_i)(M_i - M_{i+1/2-}), \qquad \delta M_{i+1/2+} = (\xi - u_{i+1})(M_{i+1} - M_{i+1/2+}),$$

and are assumed to satisfy the moment relations

$$\int_{\mathbb{R}} \delta M_{i+1/2-} \, d\xi = 0, \quad \int_{\mathbb{R}} \xi \, \delta M_{i+1/2-} \, d\xi = g\frac{H_i^2}{2} - g\frac{H_{i+1/2-}^2}{2}, \tag{2.101}$$

$$\int_{\mathbb{R}} \delta M_{i-1/2+} \, d\xi = 0, \quad \int_{\mathbb{R}} \xi \, \delta M_{i-1/2+} \, d\xi = g\frac{H_i^2}{2} - g\frac{H_{i-1/2+}^2}{2}. \tag{2.102}$$

Defining the update as

$$\begin{pmatrix} H \\ Hu \end{pmatrix}_i^{n+1/2} = \int_{\mathbb{R}} \begin{pmatrix} 1 \\ \xi \end{pmatrix} f_i^{n+1/2-}(\xi) \, d\xi, \tag{2.103}$$

and using (2.72) we also define

$$(H_i w_i)^{n+1/2} = H_i w_i - \sigma_i \Big(w_{i+1/2} F_{H,i+1/2}^{kin} - w_{i-1/2} F_{H,i-1/2}^{kin} \Big), \tag{2.104}$$

with

$$F_{H,i+1/2}^{kin} = \int_{\mathbb{R}} \xi \big(\mathbf{1}_{\xi>0} M_{i+1/2-} + \mathbf{1}_{\xi<0} M_{i+1/2+} \big) d\xi.$$

Finally, relations (2.100)-(2.104) give an explicit formula for the prediction step (2.90) and

we have the following proposition that is proved in [8, Corollary 3.8] (the two constants v_m and C_β are precised therein).

Proposition 2.5.1. *For σ_i small enough, the numerical scheme* (2.90) *based on the kinetic description* (2.100)-(2.104) *and the HR technique* (2.93),(2.94) *satisfies the fully discrete entropy inequality*

$$\begin{aligned}\tilde{\eta}(X_i^{n+1/2}) \leq \tilde{\eta}(X_i) - \sigma_i\Big(\widetilde{G}_{i+1/2} - \widetilde{G}_{i-1/2}\Big) \\ + C_\beta(\sigma_i v_m)^2\bigg(g(z_{b,i+1}-z_{b,i})^2 + g(z_{b,i}-z_{b,i-1})^2\bigg),\end{aligned} \tag{2.105}$$

with $\widetilde{G}_{i+1/2} = \widetilde{G}_{hyd,i+1/2} + F_{H,i+1/2}\frac{w_{i+1/2}^2}{2}$ *and*

$$\widetilde{G}_{hyd,i+1/2} = \int_{\xi<0} \xi H(M_{i+1/2+}, z_{b,i+1/2})\, d\xi + \int_{\xi>0} \xi H(M_{i+1/2-}, z_{b,i+1/2})\, d\xi, \tag{2.106}$$

where v_m and C_β are two constants as defined in [8, Corollary 3.7].

Remark 2.5.2. *Let us notice that the quadratic error term in the right hand side of* (2.105) *has the following key properties: it vanishes identically when $z = cst$ (no topography) or when $\sigma_i \to 0$ (semi-discrete limit), and as soon as the topography is Lipschitz continuous, it tends to zero strongly when the grid size tends to 0 (consistency with the continuous entropy inequality* (2.6)*), even for non smooth solutions.*

For the correction step, we have the following discrete energy balance.

Proposition 2.5.3. *The numerical scheme* (2.96),(2.97) *satisfies the following inequality*

$$\begin{aligned}\tilde{\eta}(X_i^{n+1}) \leq \tilde{\eta}(X_i^{n+1/2}) \\ - \sigma_i\Big((Hu)_{i+1/2}^{n+1} p_{nh,i+1/2}^{n+1} - (Hu)_{i+1/2}^{n+1} p_{nh,i-1/2}^{n+1}\Big) - C_1^2\big((\Delta t^n)^2 - C_2(\Delta x_i)^3\big).\end{aligned}$$

Moreover, for Δt^n small enough and assuming suitable boundary conditions, we have

$$\sum_i \Delta x_i \left(\tilde{\eta}(X_i^{n+1}) - \tilde{\eta}(X_i^{n+1/2})\right) \leq 0.$$

Corollary 2.5.4. *The numerical scheme detailed in paragraphs 2.4.3 and 2.4.3 satisfies the fully discrete entropy inequality*

$$\begin{aligned}\tilde{\eta}(X_i^{n+1}) \leq \tilde{\eta}(X_i) - \sigma_i\Big(\widehat{G}_{i+1/2} - \widehat{G}_{i-1/2}\Big) \\ + C_\beta(\sigma_i v_m)^2\bigg(g(z_{b,i+1}-z_{b,i})^2 + g(z_{b,i}-z_{b,i-1})^2\bigg) - C_1^2(\sigma_i^2 + C_2\Delta t^n),\end{aligned}$$

with $\widehat{G}_{i+1/2} = \widetilde{G}_{i+1/2} + (Hu)_{i+1/2} p_{nh,i+1/2}$.

Proof of prop. 2.5.1. With $\eta_{hyd}(X)$ defined by (2.10), we start from the inequality

$$\begin{aligned}\tilde{\eta}_{hyd}(X_i^{n+1/2}) \leq \tilde{\eta}_{hyd}(X_i) - \sigma_i\Big(\widetilde{G}_{hyd,i+1/2} - \widetilde{G}_{hyd,i-1/2}\Big) \\ + C_\beta(\sigma_i v_m)^2\bigg(g(z_{b,i+1} - z_{b,i})^2 + g(z_{b,i} - z_{b,i-1})^2\bigg),\end{aligned} \tag{2.107}$$

that is proved in [8, Corollary 3.8]. Equation (2.107) corresponds to a fully discrete entropy inequality for the Saint-Venant system including the topography source term.

Multiplying (2.104) by w_i leads to

$$(H_i w_i)^{n+1/2} w_i = H_i w_i^2 - \sigma_i\Big(w_{i+1/2} w_i F_{H,i+1/2}^{kin} - w_{i-1/2} w_i F_{H,i-1/2}^{kin},\Big),$$

with

$$\begin{aligned}(H_i w_i)^{n+1/2} w_i - H_i w_i^2 = \frac{H_i^{n+1/2}}{2}\big(w_i^{n+1/2}\big)^2 - \frac{H_i}{2} w_i^2 \\ + \frac{w_i^2}{2}(H_i^{n+1/2} - H_i) - \frac{H_i^{n+1/2}}{2}(w_i^{n+1/2} - w_i)^2,\end{aligned}$$

and

$$\begin{aligned}w_{i+1/2} w_i F_{H,i+1/2}^{kin} - w_{i-1/2} w_i F_{H,i-1/2}^{kin} = \frac{w_{i+1/2}^2}{2} F_{H,i+1/2}^{kin} - \frac{w_{i-1/2}^2}{2} F_{H,i-1/2}^{kin} \\ + w_{i+1/2} F_{H,i+1/2}^{kin}\left(w_i - \frac{w_{i+1/2}}{2}\right) - w_{i-1/2} F_{H,i-1/2}^{kin}\left(w_i - \frac{w_{i-1/2}}{2}\right).\end{aligned}$$

The sum of the two previous relations gives

$$\begin{aligned}&\frac{H_i^{n+1/2}}{2}\big(w_i^2\big)^{n+1/2} - \frac{H_i}{2} w_i^2 + \sigma_i\Big(\frac{w_{i+1/2}^2}{2} F_{H,i+1/2}^{kin} - \frac{w_{i-1/2}^2}{2} F_{H,i-1/2}^{kin}\Big) \\ &\leq \frac{\sigma_i}{2}\left[F_{H,i+1/2}^{kin}\right]_- (w_{i+1} - w_i)^2 - \frac{\sigma_i}{2}\left[F_{H,i-1/2}^{kin}\right]_+ (w_i - w_{i-1})^2 + \frac{H_i^{n+1/2}}{2}(w_i^{n+1/2} - w_i)^2.\end{aligned} \tag{2.108}$$

It remains to estimate, when $H_i^{n+1/2} > 0$, the quantity

$$\frac{H_i^{n+1/2}}{2}(w_i^{n+1/2} - w_i)^2,$$

in the r.h.s. of Eq. (2.108).

We have

$$w_i^{n+1/2} - w_i \;=\; \frac{1}{H_i^{n+1/2}}\Big((Hw)_i^{n+1/2} - (Hw)_i - (H_i^{n+1/2} - H_i) w_i\Big)$$

$$= \frac{\sigma_i}{H_i^{n+1/2}}\Big(F^{kin}_{H,i+1/2}(w_i - w_{i+1/2}) - F^{kin}_{H,i-1/2}(w_i - w_{i-1/2})\Big),$$

and hence

$$\frac{H_i^{n+1/2}}{2}(w_i^{n+1/2} - w_i)^2 \leq \frac{\sigma_i^2}{H_i^{n+1/2}}\Big((F^{kin}_{H,i+1/2})^2(w_i - w_{i+1/2})^2 + (F^{kin}_{H,i-1/2})^2(w_i - w_{i-1/2})^2\Big).$$

Therefore, for σ_i small enough, the r.h.s. of Eq. (2.108) is non positive with

$$\frac{H_i^{n+1/2}}{2}\big(w_i^2\big)^{n+1/2} - \frac{H_i}{2}w_i^2 + \sigma_i\Big(\frac{w_{i+1/2}^2}{2}F^{kin}_{H,i+1/2} - \frac{w_{i-1/2}^2}{2}F^{kin}_{H,i-1/2}\Big) \leq -C_1^2\sigma_i(1 - C_2^2\sigma_i),$$

for some constants C_1 and C_2. The previous relation coupled with (2.107) gives the result. □

Proof of prop. 2.5.3. We start from relation (2.96) multiplied by $H_i^{n+1}\mathbf{u}_i^{n+1}$, this gives

$$\left(\frac{H_i}{2}|\mathbf{u}|_i^2\right)^{n+1} - \left(\frac{H_i}{2}|\mathbf{u}|_i^2\right)^{n+1/2} + \Delta t^n \nabla_{sw,i}\, p_{nh}^{n+1}.\mathbf{u}_i^{n+1} = -\frac{H_i^{n+1/2}}{2}\left|\mathbf{u}_i^{n+1} - \mathbf{u}_i^{n+1/2}\right|^2.$$

Omitting in this part the superscript $^{n+1}$ and as in the the proof of prop. 2.4.2, simple manipulations give

$$\Delta x_i \nabla_{sw,i}\, p_{nh}.\begin{pmatrix} u_i \\ w_i \end{pmatrix} = \Big((Hu)_{i+1/2}p_{nh,i+1/2} - (Hu)_{i-1/2}p_{nh,i-1/2}\Big) + d_{i+1/2} - d_{i-1/2},$$

with

$$\begin{aligned} d_{i+1/2} &= \frac{p_{nh,i+1/2}}{2}\Big(\Delta x_{i+1/2}(w_{i+1} - w_i) - \frac{u_{i+1} - u_i}{2}\big(H_{i+1} + 2z_{b,i+1} - (H_i + 2z_{b,i})\big)\Big), \\ d_{i-1/2} &= \frac{p_{nh,i-1/2}}{2}\Big(\Delta x_{i-1/2}(w_i - w_{i-1}) - \frac{u_i - u_{i-1}}{2}\big(H_i + 2z_{b,i} - (H_{i-1} + 2z_{b,i-1})\big)\Big), \end{aligned}$$

proving the result.

Assuming the variables are smooth enough, the quantities $d_{i+1/2}$,$d_{i-1/2}$ satisfy $d_{i+1/2} - d_{i-1/2} = \mathcal{O}(\Delta x^3)$ and we have

$$\Delta x_i \begin{pmatrix} u_i \\ w_i \end{pmatrix}.\nabla_{sw,i}\, p_{nh} = \Big((Hu)_{i+1/2}p_{nh,i+1/2} - (Hu)_{i-1/2}p_{nh,i-1/2}\Big) + \mathcal{O}(\Delta x)^3,$$

that completes the proof.

Notice that in the limit $\Delta t^n \to 0$, $\sigma_i \approx 1$, the inequality

$$-\frac{H_i^{n+1/2}}{2}\left|\mathbf{u}_i^{n+1} - \mathbf{u}_i^{n+1/2}\right|^2 + \sigma_i(d_{i+1/2} - d_{i-1/2}) \leq 0,$$

holds, meaning the correction step ensures a decrease of the entropy. □

Proof of corollary 2.5.4. The sum of the two inequalities obtained in props. 2.5.1 and 2.5.3 gives the result. □

2.6 Analytical solutions

Stationary and time dependent analytical solutions are available for the model (2.18)-(2.20), see [43] and references therein. In this section we only briefly recall some of them, they will be very useful to evaluate the properties of the proposed numerical scheme, see paragraph 2.7.

2.6.1 Time dependent analytical solution

Parabolic bowl

The functions defined by

$$H(x,t) = \max\left(H_0 - \frac{b_2}{2}\left(x - \int_{\tilde{t}^0}^{t} f(t_1)dt_1\right)^2, 0\right), \tag{2.109}$$

$$\overline{u}(x,t) = f(t)\mathbf{1}_{H>0}, \tag{2.110}$$

$$\overline{w}(x,t) = b_2 x f(t)\mathbf{1}_{H>0}, \tag{2.111}$$

$$z_b(x) = b_1 + \frac{b_2}{2}x^2, \tag{2.112}$$

$$\overline{p}_{nh}(x,t) = \frac{b_2 f^2}{2}H^2, \tag{2.113}$$

$$s(x,z,t) = b_2 x\frac{df}{dt}, \tag{2.114}$$

where $H_0 > 0, b_1, b_2$ are constants and where the function f satisfies the ODE

$$\frac{df}{dt} + b_2(g + b_2 f^2)\int_{\tilde{t}^0}^{t} f(t_1)dt_1 = 0, \quad f(t_0) = f^0, \ \ \tilde{t}^0 \in \mathbb{R}, \tag{2.115}$$

are solutions of the system

$$\frac{\partial H}{\partial t} + \frac{\partial}{\partial x}\big(H\overline{u}\big) = 0, \tag{2.116}$$

$$\frac{\partial}{\partial t}(H\overline{u}) + \frac{\partial}{\partial x}\left(H\overline{u}^2 + \frac{g}{2}H^2 + H\overline{p}_{nh}\right) = -(gH + 2\overline{p}_{nh})\frac{\partial z_b}{\partial x}, \tag{2.117}$$

$$\frac{\partial}{\partial t}(H\overline{w}) + \frac{\partial}{\partial x}(H\overline{w}\overline{u}) = 2\overline{p}_{nh} + Hs, \tag{2.118}$$

$$\frac{\partial(H\overline{u})}{\partial x} - \overline{u}\frac{\partial(H + 2z_b)}{\partial x} + 2\overline{w} = 0, \tag{2.119}$$

that corresponds to (2.18)-(2.19) completed with a source term Hs defined by (2.114) in the momentum equation (2.118).

Solitary wave solutions

The system (2.18)-(2.19) admits solitary waves having the form

$$H = H_0 + a\left(\operatorname{sech}\left(\frac{x - c_0 t}{l}\right)\right)^2, \tag{2.120}$$

$$\overline{u} = c_0\left(1 - \frac{d}{H}\right), \tag{2.121}$$

$$\overline{w} = -\frac{a c_0 d}{lH}\operatorname{sech}\left(\frac{x - c_0 t}{l}\right)\operatorname{sech}'\left(\frac{x - c_0 t}{l}\right), \tag{2.122}$$

$$\overline{p}_{nh} = \frac{a c_0^2 d^2}{2 l^2 H^2}\left((2H_0 - H)\left(\operatorname{sech}'\left(\frac{x - c_0 t}{l}\right)\right)^2 + H\operatorname{sech}\left(\frac{x - c_0 t}{l}\right)\operatorname{sech}''\left(\frac{x - c_0 t}{l}\right)\right), \tag{2.123}$$

where φ' denotes the derivative of function φ,

$$c_0 = \frac{l}{d}\sqrt{\frac{g H_0^3}{l^2 - H_0^2}}, \qquad a = \frac{H_0^3}{l^2 - H_0^2},$$

and $(d, l, H_0) \in \mathbb{R}^3$ are given constants with $l > H_0 > 0$.

2.7 Numerical simulations

A complete validation of the proposed numerical technique is not in the scope of this paper and will be investigated in a forthcoming paper. We focus on two typical situations, described in paragraphs 2.6.1 and 2.6.1 where analytical solutions exist.

For the numerical test, we use a formal 2^{nd} order extension of the space discretization for the prediction step and this second order extension is built as in [10], the correction step being kept unchanged. For the second order extension of the time scheme, we use a Heun type scheme, see [31]. Even if, the second order improvement (space and time) is only formal, we denote it "second order extension" in the following.

2.7.1 The parabolic bowl

At the discrete level, the analytical solution given in paragraph 2.6.1 (see also [43]) is particularly difficult to capture. Indeed, it is a non stationary solution and the flow exhibits wet/dry interfaces all along the simulation.

With the parameter values $H_0 = 1$, $a = 1$, $b_1 = 0$, $b_2 = 1$, $t^0 = 0$ over the geometrical domain $[-2, 2]$ and with the initial conditions (see Fig. 2.2)

$$\int_{\tilde{t}^0}^{t^0} f(t)\, dt = \frac{a}{\sqrt{gb_2}},$$
$$f(t_0) = f^0 = 0,$$

we have calculated – with a simple Runge-Kutta scheme – the solution of the ODE (2.115). The solution has been calculated with a very fine time discretization and thus can be considered as a reference solution, very close to the analytical solution of Eq. (2.115). This means we have at our disposal an analytical solution for the system (2.116)-(2.119).

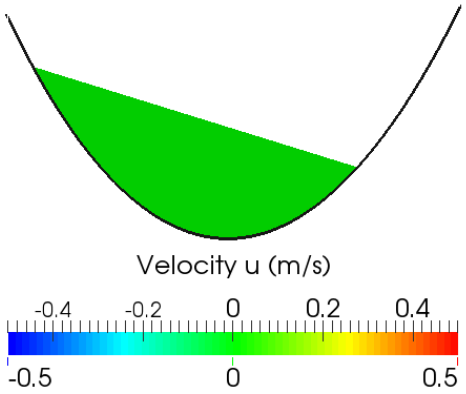

Figure 2.2: Initial conditions for the simulation of the "parabolic bowl" (parabolic bottom, water depth and null horizontal velocity).

To illustrate the behavior of the solution in such a situation, we give over Fig 2.3 the variations along time of the water depth at $x_0 = 0.8$ m for a mesh of 80 cells which is a rather coarse mesh.

In order to evaluate the convergence rate of the simulated solution H_{sim} towards the analytical one H_{anal}, we plot the error rate versus the space discretization. Over Fig 2.4, we have plotted the variations along time of the quantity

$$e_{x_0} : t \mapsto 100 \frac{|H_{sim}(x_0, t) - H_{anal}(x_0, t)|}{H_{sim}(x_0, t)}, \tag{2.124}$$

at node $x_0 = 0.8$ m. It appears that this quantity does not increase with time and remains bounded. Figure 2.5 is similar to Fig 2.4, we compare the variations of $t \mapsto e_{0.8}(t)$ for the 2^{nd} order scheme (space and time) obtained with 80 and 160 cells.

Over Fig 2.6, we have plotted the variations of the quantity

$$t \mapsto \frac{1}{t}\int_0^t e_{x_0}(t')dt', \tag{2.125}$$

obtained with a mesh of 80 cells.

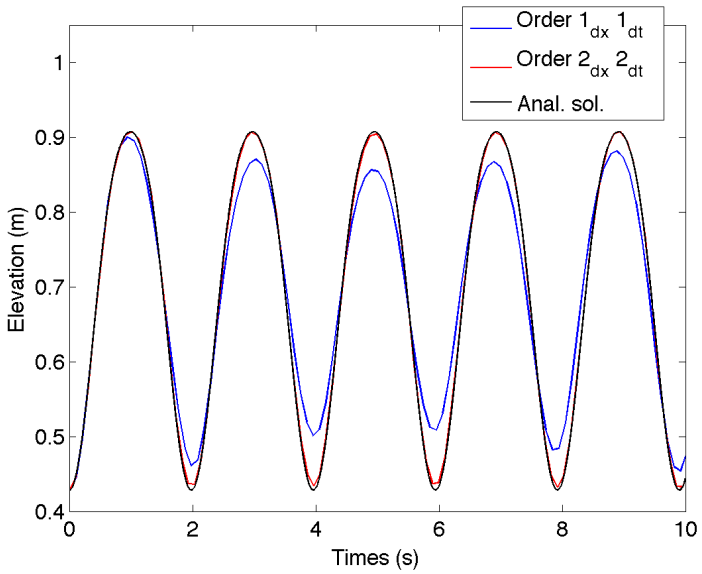

Figure 2.3: Parabolic bowl: variations of $t \mapsto H(0.8, t)$ - analytical solution and simulated one with the first order (space and time) and second order extension (space and time) schemes.

2.7.2 The solitary wave

As in the previous paragraph, we are able to examine the convergence rate of the simulated solution towards the analytical one (given in paragraph 2.6.1).

We consider the analytical solution corresponding to the choices $H_0 = 1$ m, $l = 1.7$ m, $d = 1$ m. These choices lead to $a = 0.5291$ m and $c_0 = 3.873$ m.s^{-1}. We compare the analytical solution and its simulated version at time $t = 6$ s.

We have plotted in Fig. 2.7 the $\log(L^1 - error)$ over the water depth at time $T = 6$ seconds versus $\log(h_0/h_i)$ for the first and second-order scheme and they are compared to the theoretical order. These errors have been computed on 7 meshes with 80, 120, 200, 400, 800, 1600 and 3200 cells.

For the curves obtained over Fig. 2.7, the soliton is – at the initial instant – in the fluid domain meaning the numerical treatment of the boundary condition does not play a crucial role. Figure 2.8 is similar to Fig. 2.7 except that the soliton is not within the fluid domain at the initial instant but enters the channel by the left boundary. The convergence

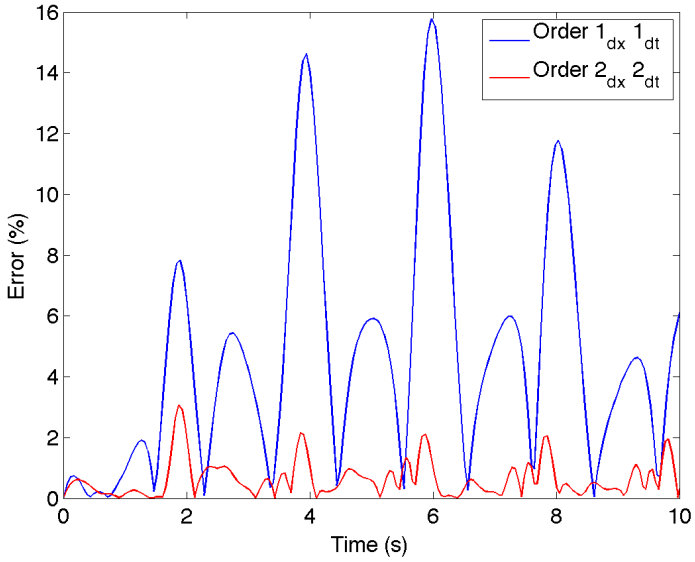

Figure 2.4: Parabolic bowl: variations along time of the error (2.124) at node $x_0 = 0.8$ m with 80 cells, 1^{st} order scheme (space and time) and 2^{nd} order scheme (space and time).

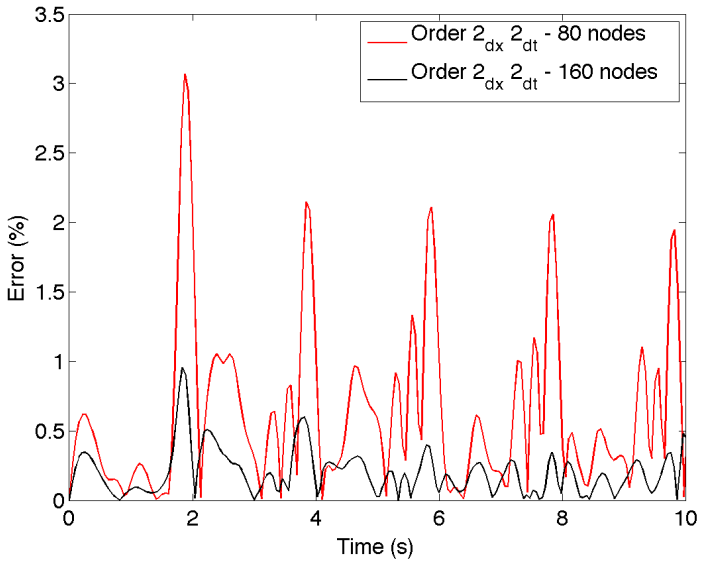

Figure 2.5: Parabolic bowl: variations along time of the error (2.124) at node $x_0 = 0.8$ m with 80 and 160 cells, 2^{nd} order scheme (space and time).

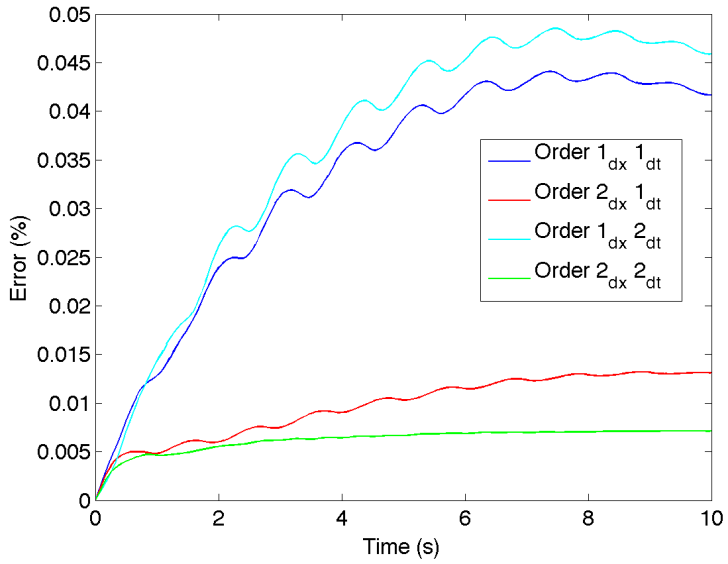

Figure 2.6: Parabolic bowl: variations along time of the quantity (2.125) at node $x_0 = 0.8$ m, 1^{st} and 2^{nd} order schemes (space and time) obtained with 80 cells.

order of the scheme is examined at time $T = 10$ seconds and the soliton arrives within the fluid domain after 4 seconds of simulation. Hence the soliton propagates during 6 seconds within the domain corresponding to the same situation as Fig. 2.7. Following 2.4.3, we have imposed a given flux at the entry of the domain. We notice that the convergence orders obtained over Figs. 2.7 and 2.8 are similar.

Remark 2.7.1. *This test case and the previous one concern non stationary solutions. The errors due to the time and space schemes are combined so the convergence rate of the simulated solution towards the analytical one is difficult to analyze. Indeed, for the second order scheme (space and time) and fine meshes, the error due to the time scheme becomes a significant part of the error so the convergence rate does not correspond to the theoretical one, see Figs. 2.7 and 2.8.*

2.8 Conclusion

In this paper we have proposed a robust and efficient numerical scheme for a non-hydrostatic shallow water type model approximating the incompressible Euler system with free surface.

The correction step is the key point of the scheme and especially the discretization of the shallow water type version of the gradient and divergence operators. A finite difference strategy has been used to discretize this correction step. In order to be able to treat 2d flows on unstructured meshes, a variational approximation of the correction step is required, it is presented and its numerical performance is evaluated in [3].

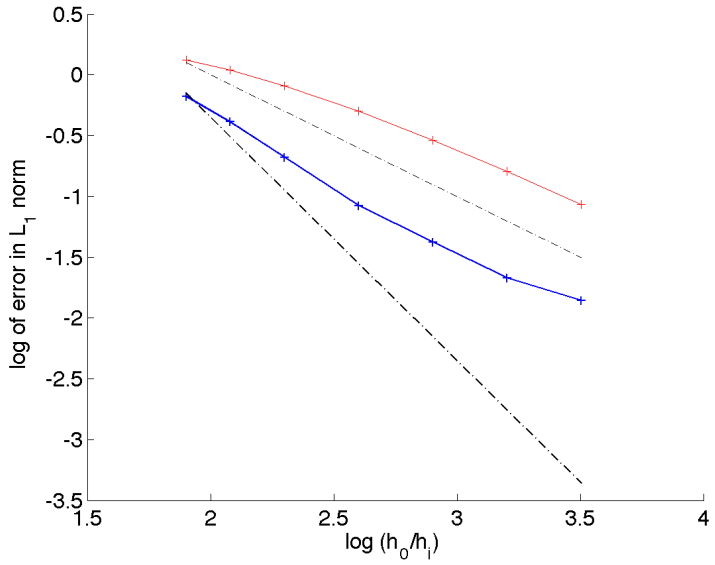

Figure 2.7: Soliton (interior of the domain): convergence rates to the reference solution, 1^{st} order scheme (space and time) and 2^{nd} order scheme (space and time), '-.' theoretical order.

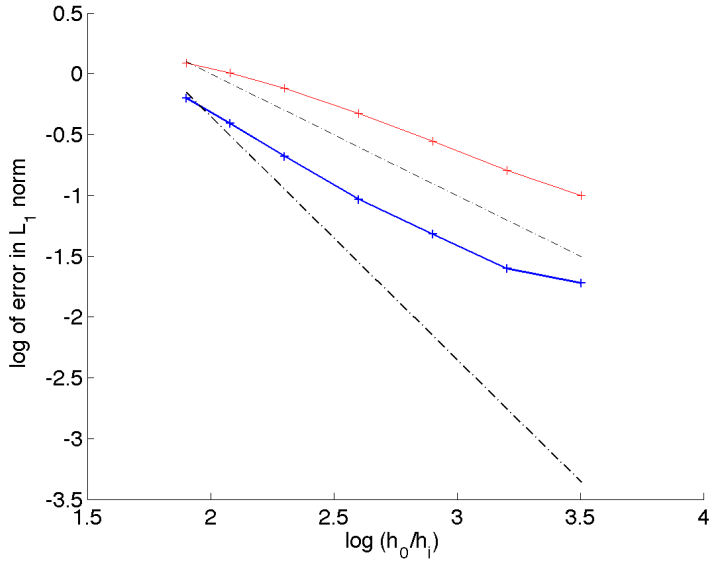

Figure 2.8: Soliton (entering the domain): convergence rates to the reference solution, 1^{st} order scheme (space and time) and 2^{nd} order scheme (space and time), '-.' theoretical order.

Chapter 3

A combined finite volume/ finite element method for a one-dimensional dispersive Shallow Water system

This work has been done in collaboration with Marie-Odile Bristeau, Edwige Godlewski and Jacques Sainte-Marie. It has been published in Networks and Heterogeneous Media.

3.1 Introduction

Starting from the incompressible Euler or Navier-Stokes system, the hydrostatic assumption consists in neglecting the vertical acceleration of the fluid. More precisely the momentum along the vertical axis of the Euler equation

$$\frac{\partial w}{\partial t} + u\frac{\partial w}{\partial x} + w\frac{\partial w}{\partial z} + \frac{\partial p}{\partial z} = -g,$$

reduces in the hydrostatic context to

$$\frac{\partial p}{\partial z} = -g, \tag{3.1}$$

where p is the pressure, g is the gravitational constant, and u (resp. w) is the horizontal (resp. vertical) component of the fluid velocity.

Such an assumption produces important consequences over the structure and complexity of the model. Indeed, Eq. (3.1) implies that the pressure p is no longer the Lagrange multiplier of the incompressibility constraint and p can be expressed, for free surface flows, as a function of the water depth of the fluid. Therefore, the hydrostatic assumption implies that the resulting model, even though it describes an incompressible fluid, has common features with models arising in compressible fluid mechanics.

In geophysical problems, the hydrostatic assumption coupled with a shallow water type description of the flow is often used. Unfortunately, these models do not represent phenomena containing dispersive effects for which the non-hydrostatic contribution cannot be neglected. More complex models have to be considered to take into account this kind of phenomena, together with numerical methods able to discretize the high order derivative terms coming from the dispersive effects. Many shallow water type dispersive models have been proposed such as KdV, Boussinesq, Green-Naghdi, see [86, 45, 26, 129, 131, 29, 48, 105, 4, 5, 44]. The modeling of the non-hydrostatic effects for shallow water flows does not raise insuperable difficulties but their discretization is more tricky. Numerical techniques for the approximation of these models have been recently proposed [48, 42, 108].

The depth-averaged Euler model studied in the present paper has been derived and studied in [43]. A numerical approximation based on a prediction-correction strategy [50] is described in Chapter 2, where the discretization of the elliptic part arising from the non-hydrostatic terms is carried out in a finite difference framework. It is worth noticing that the numerical scheme given in Chapter 2 is endowed with robustness and stability properties such as positivity, well-balancing, discrete entropy and wet/dry interfaces treatment.

Since the derivation in a 2d context of the model proposed in [43] does not raise difficulty, the objective is to have a numerical method that can be easily extended to the two-dimensional problem. In Chapter 2, a finite volume method is used for the prediction part, while a finite difference method is applied for the projection part, which is not easy to apply on an unstructured grid in the 2d framework. The main contents of this paper is the derivation and validation of the correction step in a variational framework allowing a finite element approximation. The results depicted in this paper pave the way for a discretization of the 2d model on an unstructured mesh.

Notice that the non-hydrostatic model we consider slightly differs from the well-known Green-Naghdi model [86], see remarks 3.2.1, 3.5.1 and [43] for more details.

Let $\Omega \subset \mathbb{R}$, be a 1d domain (an interval) and $\Gamma = \Gamma_{in} \cup \Gamma_{out}$ its boundary (see Figure 3.1). The non-hydrostatic depth-averaged Euler model derived in [43, 2] reads

$$\frac{\partial H}{\partial t} + \frac{\partial H\overline{u}}{\partial x} = 0, \tag{3.2}$$

$$\frac{\partial H\overline{u}}{\partial t} + \frac{\partial}{\partial x}(H\overline{u}^2 + g\frac{H^2}{2} + H\overline{p}_{nh}) = -(gH + 2\overline{p}_{nh})\frac{\partial z_b}{\partial x}, \tag{3.3}$$

$$\frac{\partial H\overline{w}}{\partial t} + \frac{\partial H\overline{w}\overline{u}}{\partial x} = 2\overline{p}_{nh}, \tag{3.4}$$

$$\frac{\partial H\bar{u}}{\partial x} - \bar{u}\frac{\partial(H + 2z_b)}{\partial x} + 2\bar{w} = 0, \tag{3.5}$$

where H is the water depth, z_b is the topography and p_{nh} is the non-hydrostatic part of the pressure. The variables denoted with a bar recall that this model is obtained performing an average along the water depth of the incompressible Euler system with free surface. The velocity field is denoted $\bar{\mathbf{u}} = (\bar{u}, \bar{w})^t$ with $\bar{u}$ (resp. $\bar{w}$) the horizontal (resp. vertical) component.

We denote $\eta = H + z_b$ the free surface of the fluid. In addition, we give the following notation

$$\mathbf{n} = \begin{pmatrix} n \\ 0 \end{pmatrix}, \tag{3.6}$$

with n the unit outward normal vector at Γ (in 1d, $n = \pm 1$), $\mathbf{n}$ represents the unit outward normal vector of the domain covered by the fluid, namely $\Omega \times [z_b, \eta]$. We also consider the gradient operator

$$\nabla_0 = \begin{pmatrix} \frac{\partial}{\partial x} \\ 0 \end{pmatrix}. \tag{3.7}$$

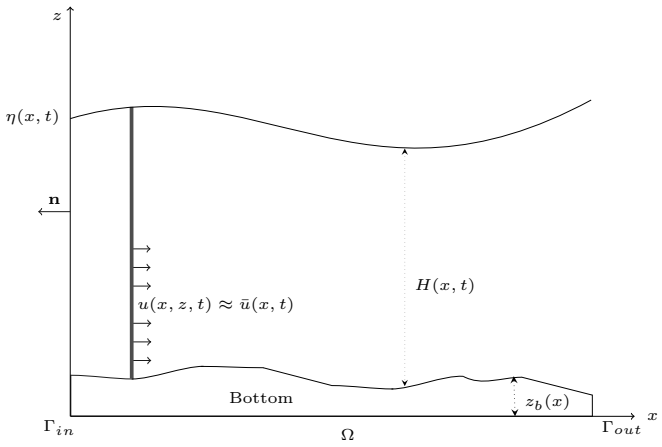

Figure 3.1: Notations and domain definition.

Moreover, the smooth solutions of the system (3.2)-(3.5) satisfy an energy conservation law, namely

$$\frac{\partial \bar{E}}{\partial t} + \frac{\partial}{\partial x}\left(\bar{u}\left(\bar{E} + \frac{g}{2}H^2 + H\bar{p}_{nh}\right)\right) = 0, \tag{3.8}$$

with

$$\bar{E} = \frac{H\left(\bar{u}^2 + \bar{w}^2\right)}{2} + \frac{gH\left(\eta + z_b\right)}{2}. \tag{3.9}$$

Equation (3.5) represents a shallow water version of the divergence free constraint, for which the non-hydrostatic pressure $\bar{p}_{nh}$ plays the role of a Lagrange multiplier. The reader can refer to [43] for more details. Notice that considering $\bar{p}_{nh} = 0$ and neglecting (3.4), the system (3.2)-(3.3),(3.5) reduces to the classical Saint-Venant system.

The paper is organized as follows. First we give a rewriting of the model and we present the prediction-correction method, the main part being the variational formulation of the correction part. Then in Section 3.3, we detail the numerical approximation. Finally, in Section 3.4.1 and 3.5, numerical simulations validating the proposed discretization techniques are presented.

3.2 The projection scheme for the non-hydrostatic model

Projection methods have been introduced by A. Chorin and R. Temam [138] in order to compute the pressure for incompressible Navier-Stokes equations. These methods, based on a time splitting scheme, have been widely studied and applied to treat the incompressibility constraint (see [92, 144, 143]). We develop below an analogue of this method for shallow water flow. In order to describe the fractional time step method we use, we propose a rewritting of the model (3.2)-(3.5).

3.2.1 A rewritting

Let us introduce the two operators ∇_{sw} and div_{sw} defined by

$$\nabla_{sw} f = \begin{pmatrix} H\frac{\partial f}{\partial x} + f\frac{\partial (H+2z_b)}{\partial x} \\ -2f \end{pmatrix}, \tag{3.10}$$

$$\mathrm{div}_{sw}(\mathbf{v}) = \frac{\partial H v_1}{\partial x} - v_1 \frac{\partial (H+2z_b)}{\partial x} + 2v_2, \tag{3.11}$$

with $\mathbf{v} = (v_1, v_2)^t$. We assume for a while that f and $\mathbf{v}$ are smooth enough. The shallow water form of the divergence operator div_{sw} (resp. of the gradient operator ∇_{sw}) corresponds to a depth-averaged version of the divergence (resp. gradient) appearing in the incompressible Euler and Navier-Stokes equations. Notice that the two operators ∇_{sw}, div_{sw} defined by (3.10)-(3.11) are H and z_b dependent and we assume that H and z_b are sufficiently smooth functions. One can check that these operators verify the fundamental duality relation

$$\int_\Omega \mathrm{div}_{sw}(\mathbf{v}) f \, dx = -\int_\Omega \nabla_{sw} f \cdot \mathbf{v} \, dx + [H v_1 \, f]_\Gamma . \tag{3.12}$$

These definitions allow to rewrite the model (3.2)-(3.5) as

$$\frac{\partial H}{\partial t} + \frac{\partial H\bar{u}}{\partial x} = 0, \tag{3.13}$$

$$\frac{\partial H\bar{\mathbf{u}}}{\partial t} + \frac{\partial}{\partial x}(\overline{u} H\overline{\mathbf{u}}) + \nabla_0\left(\frac{g}{2}H^2\right) + \nabla_{sw}\bar{p}_{nh} = -gH\nabla_0 z_b, \tag{3.14}$$

$$\mathrm{div}_{sw}(\bar{\mathbf{u}}) = 0, \tag{3.15}$$

with ∇_0 defined by (3.7).

Remark 3.2.1. *It has been established in [43] that, when $z_b = 0$, the Green Naghdi model can be written in the form* (3.2)-(3.4) *with a different coefficient in the right hand side of the equation* (3.4)*, which is replaced by*

$$\frac{\partial H\overline{w}}{\partial t} + \frac{\partial H\overline{wu}}{\partial x} = \frac{3}{2}\overline{p}_{nh}. \tag{3.16}$$

So, if we try to write the Green-Naghdi model in the form (3.13)-(3.15)*, the duality relation* (3.12) *is no longer satisfied. Therefore the energy balance will also differ by one coefficient and the stability results established in Chapter 2 and based on the energy balance does not apply to the Green-Naghdi model.*

The system (3.13)-(3.15) can be written in the compact form

$$\frac{\partial X}{\partial t} + \frac{\partial}{\partial x}F(X) + R_{nh} = S(X), \tag{3.17}$$

$$\mathrm{div}_{sw}\,(\bar{\mathbf{u}}) \;=\; 0, \tag{3.18}$$

where we denote

$$X = \begin{pmatrix} H \\ H\bar{u} \\ H\bar{w} \end{pmatrix}, \qquad F(X) = \begin{pmatrix} H\bar{u} \\ H\bar{u}^2 + \frac{g}{2}H^2 \\ H\bar{u}\bar{w} \end{pmatrix}, \tag{3.19}$$

and

$$R_{nh} = \begin{pmatrix} 0 \\ \nabla_{sw}\,\bar{p}_{nh} \end{pmatrix}, \qquad S(X) = \begin{pmatrix} 0 \\ -gH\nabla_0 z_b \end{pmatrix}. \tag{3.20}$$

Let be given time steps Δt^n and note $t^n = \sum_{k\leq n} \Delta t^k$. As detailed in Chapter 2, the projection scheme for system (3.17)-(3.18) consists in the following time splitting

$$X^{n+1/2} \;=\; X^n - \Delta t^n \,\frac{\partial}{\partial x} F(X^n) + \Delta t^n\, S(X^n), \tag{3.21}$$

$$X^{n+1} \;=\; X^{n+1/2} - \Delta t^n\, R_{nh}^{n+1}, \tag{3.22}$$

$$\mathrm{div}_{sw}\,\bar{\mathbf{u}}^{n+1} \;=\; 0, \tag{3.23}$$

with $\bar{\mathbf{u}}^{n+1} = \left(\frac{(H\bar{u})^{n+1}}{H^{n+1}}, \frac{(H\bar{w})^{n+1}}{H^{n+1}}\right)^t$.

The first two equations of (3.21) consist in the classical Saint-Venant system with topography and the third equation is an advection equation for the quantity $H\bar{w}$. Equations (3.22)-(3.23) describe the correction step allowing to determine the non-hydrostatic part of the pressure p_{nh}^{n+1} and hence giving the corrected state X^{n+1}. The numerical resolution of (3.21) – especially the first two equations – has received an extensive coverage and efficient and robust numerical techniques exist, mainly based on finite volume approach, see [32, 8]. The derivation of a robust and efficient numerical technique for the resolution of the correction step (3.22)-(3.23) is the key point. A strategy based on a finite difference approach has been proposed, studied and validated in Chapter 2. Unfortunately, the finite difference framework does not allow to tackle situations with unstructured meshes in 2 or 3 dimensions. It is the key point of this paper to propose a variational formulation of the correction step coupled with a finite volume discretization of the prediction step.

3.2.2 The correction step

In this part, we consider we have at our disposal a space discretization of Eq. (3.21) solving the hydrostatic part of the model and we focus on the correction step (3.22)-(3.23).

Variational formulation

The correction step (3.22)-(3.23) writes,

$$H^{n+1} = H^{n+1/2}, \tag{3.24}$$
$$(H\mathbf{u})^{n+1} + \Delta t^n \nabla_{sw}\, p_{nh}^{n+1} = (H\mathbf{u})^{n+1/2}, \tag{3.25}$$
$$\mathrm{div}_{sw}\,(\mathbf{u}^{n+1}) = 0. \tag{3.26}$$

For the sake of clarity, in the following we will drop the notation with a bar and we denote p instead of $\bar{p}_{nh}$. Likewise we drop the superscript $^{n+1}$ for the corrected states. The system of Equations (3.25)-(3.26) is a mixed problem in velocity/pressure, its approximation leads to a variational mixed problem.
First of all, we assume $z_b \in C^1(\bar{\Omega})$, and $H \in C^1(\bar{\Omega})$ is bounded below and above:

$$\alpha_1 < H < \alpha_2, \quad \alpha_1, \alpha_2 > 0. \tag{3.27}$$

We give two formulations of the problem depending on the boundary conditions, the first one is written with the operator div_{sw} (see (3.32)-(3.33) below) while the second one is written with the operator ∇_{sw} (see (3.38)-(3.39)).

Formulation with the operator div_{sw} : In this section, we give the variational formulation of the problem (3.25)-(3.26) using the shallow water divergence operator. We start by completing Equations (3.25)-(3.26) with homogeneous Dirichlet boundary conditions for the velocity at the inlet and Dirichlet boundary conditions for the pressure at the outlet:

$$u = 0 \text{ on } \Gamma_{in}, \tag{3.28}$$
$$p = 0 \text{ on } \Gamma_{out}. \tag{3.29}$$

Using the duality relation between the operators ∇_{sw} and div_{sw} given by (3.12), and introducing the bilinear forms:

$$a(\mathbf{u},\mathbf{v}) = \int_\Omega H\mathbf{u}\cdot\mathbf{v}\,dx, \quad \forall\,\mathbf{u},\mathbf{v}\in V_0,$$
$$b(\mathbf{v},q) = -\int_\Omega \mathrm{div}_{sw}\,(\mathbf{v})q\,dx, \quad \forall\mathbf{v}\in V_0, \forall\, q\in L^2(\Omega),$$

with:

$$V = \{\mathbf{v}=(v_1,v_2)\in (L^2(\Omega))^2 | \mathrm{div}_{sw}(\mathbf{v})\in L^2(\Omega)\}, \tag{3.30}$$
$$V_0 = \{\mathbf{v}\in V\ ,\ v_1|_{\Gamma_{in}} = 0\}, \tag{3.31}$$

The variational formulation of Equations (3.25)-(3.26) writes:
Find $\mathbf{u} \in V_0$ and $p \in L^2(\Omega)$ such that

$$\begin{aligned} \frac{1}{\Delta t^n} a(\mathbf{u}, \mathbf{v}) + b(\mathbf{v}, p) &= \frac{1}{\Delta t^n} a(\mathbf{u}^{n+1/2}, \mathbf{v}), \quad \forall \mathbf{v} \in V_0, & (3.32) \\ b(\mathbf{u}, q) &= 0, \quad \forall q \in Q. & (3.33) \end{aligned}$$

Now, if we consider non homogeneous boundary conditions for the velocity and the pressure:

$$\begin{aligned} u &= u_0 \text{ on } \quad \Gamma_{in}, & (3.34) \\ p &= p_0 \text{ on } \quad \Gamma_{out}, & (3.35) \end{aligned}$$

where $p_0 \in H^{-1/2}(\Gamma_{out})$, and we assume there exists a given velocity $\bar{\mathbf{u}}_0 \in V$, such that $u_0 = \bar{u}_0|_{\Gamma_{in}} \in H^{1/2}(\Gamma_{in})$ and $\int_\Omega \mathrm{div}_{sw}(\bar{\mathbf{u}}_0) q = 0\, dx$, $\forall q \in L^2(\Omega)$. We set $\mathbf{u} = \tilde{\mathbf{u}} + \bar{\mathbf{u}}_0$ with $\tilde{\mathbf{u}} \in V_0$, therefore, the problem writes:
Find $\tilde{\mathbf{u}} \in V_0$, $p \in L^2(\Omega)$ such that, $\forall\, \mathbf{v} \in V_0$,

$$\int_\Omega (H\tilde{\mathbf{u}} \cdot \mathbf{v} - \Delta t\, \mathrm{div}_{sw}(\mathbf{v})\, p)\, dx = \int_\Omega (H\mathbf{u})^{n+1/2} \cdot \mathbf{v}\, dx - \int_\Omega H\bar{\mathbf{u}}_\mathbf{0} \cdot \mathbf{v} - < H\, v_1\, n\, , p_0 >_{\Gamma_{out}} \quad (3.36)$$

$$-\int_\Omega \mathrm{div}_{sw}(\mathbf{u})\, q\, dx = 0 \quad \forall q \in L^2(\Omega). \quad (3.37)$$

where $< \cdot, \cdot >_{\Gamma_{out}}$ represents the duality product between $H^{-1/2}(\Gamma_{out})$ and $H^{1/2}(\Gamma_{out})$. In one dimension, $u_0 \in \mathbb{R}$ (imposed in Equation (3.34)), then we can take the lifting of boundary conditions $\bar{\mathbf{u}}_0 = (u_0, \frac{u_0}{2}\frac{\partial \zeta}{\partial x})^T$ to satisfy the shallow water version of the the free divergence condition (3.26). In Section (3.2.4), we will see that the problem with this formulation is well posed.

Formulation with the operator ∇_{sw} : We can also consider the problem using the shallow water gradient operator with the Dirichlet boundary conditions (3.34)-(3.35) where here, $u_0 \in H^{-1/2}(\Gamma_{in})$ and $p_0 \in H^{1/2}(\Gamma_{out})$. Using the duality relation (3.12), we have the following problem with homogeneous boundary conditions for the pressure:
Find $\mathbf{u} \in L^2(\Omega)$, $p \in Q_0$ such that

$$\begin{aligned} \int_\Omega (H\mathbf{u} \cdot \mathbf{v} + \Delta t \nabla_{sw}(p) \cdot \mathbf{v})\, dx &= \int_\Omega (H\mathbf{u})^{n+1/2} \cdot \mathbf{v}\, dx, \quad \forall\, \mathbf{v} \in (L^2(\Omega))^2, & (3.38) \\ \int_\Omega \nabla_{sw}(q) \cdot \mathbf{u}\, dx &= < H\, u_0\, n,\, q >_{\Gamma_{in}}, \quad \forall q \in Q_0. & (3.39) \end{aligned}$$

with :

$$Q = \{q \in L^2(\Omega),\ \nabla_{sw}(q) \in (L^2(\Omega))^2\}. \tag{3.40}$$

$$Q_0 = \{q \in Q,\ q|_{\Gamma_{out}} = 0\}. \tag{3.41}$$

To impose non homogeneous Dirichlet conditions for the pressure, we assume there exists a given pressure $\bar{p}_0 \in Q$ such that $p_0 = \bar{p}_0|_{\Gamma_{out}} \in H^{1/2}(\Gamma_{out})$. We set $p = \tilde{p} + \bar{p}_0$ with $\tilde{p} \in Q_0$. Finally, the variational problem writes:
Find $\mathbf{u} \in (L^2(\Omega))^2$, $\tilde{p} \in Q_0$ such that, $\forall\, \mathbf{v} \in (L^2(\Omega))^2$,

$$\begin{aligned} \int_\Omega (H\mathbf{u}\cdot\mathbf{v} + \Delta t \nabla_{sw}(\tilde{p})\cdot\mathbf{v})\ dx &= \int_\Omega (H\mathbf{u})^{n+1/2}\cdot\mathbf{v}\ dx - \Delta t \int_\Omega \nabla_{sw}(\bar{p}_0)\cdot\mathbf{v}\, dx, \\ \int_\Omega \nabla_{sw}(q)\cdot\mathbf{u}\, dx &= < H\, u_0\, n,\, q >_{\Gamma_{in}}, \quad \forall q \in Q_0. \end{aligned}$$

Finally, depending on the boundary conditions for the velocity or the pressure, we can choose the first or the second formulation.

The pressure equation

Now, we are interested in deriving an equation for the pressure. Instead of considering the problem in velocity/pressure under the coupled form, we consider an elliptic problem leading to an uncoupled equation for the pressure. This is in analogy with the Poisson equation derived from the Navier-Stokes equations by the projection scheme of Chorin-Temam [138, 50]. We start from the variational problem (3.38)-(3.39) using the shallow water gradient operator with homogenous boundary condition for the velocity and the pressure, *i.e.* $u_0 = 0$, $p_0 = 0$ in Equations (3.35)-(3.34)), which leads to search $\mathbf{u} \in V_0$, and $p \in Q_0$. In order to obtain the pressure equation, we take a specific value for $\mathbf{v}$. Formally, let us take $\mathbf{v}$ of the form $\mathbf{v} = \frac{\nabla_{sw}\, q}{H}$ with $q \in Q_0$ defined by (3.41).
Equation (3.38) gives, $\forall q \in Q_0$,

$$\int_\Omega H\mathbf{u}\cdot\frac{\nabla_{sw}\,(q)}{H}\,dx + \int_\Omega \Delta t \nabla_{sw}\,(p)\cdot\frac{\nabla_{sw}\,(q)}{H}\,dx = \int_\Omega H\mathbf{u}^{n+1/2}\cdot\frac{\nabla_{sw}\,(q)}{H}\,dx, \tag{3.42}$$

Then, using (3.39), we obtain:

$$\int_\Omega \Delta t \nabla_{sw}\,(p)\cdot\frac{\nabla_{sw}\,(q)}{H}\,dx = \int_\Omega H\mathbf{u}^{n+1/2}\cdot\frac{\nabla_{sw}\,(q)}{H}\,dx, \quad \forall q \in Q_0 \tag{3.43}$$

then:

$$\left(\frac{\nabla_{sw}\, q}{H}, \nabla_{sw}\, p\right) = \frac{1}{\Delta t^n}\left(\mathbf{u}^{n+1/2}, \frac{\nabla_{sw}\, q}{H}\right) \quad \forall q \in Q_0. \tag{3.44}$$

Let us introduce the shallow water version of the Laplacian operator Δ_{sw} defined by

$$\Delta_{sw}\, p = \mathrm{div}_{sw}\left(\frac{\nabla_{sw}\, p}{H}\right), \tag{3.45}$$

and the space

$$Q_{0,sw} = \{q \in Q_0 | \mathrm{div}_{sw}\left(\frac{\nabla_{sw}\, q}{H}\right) \in L^2(\Omega)\}.$$

Using (3.12) and (3.45), we get

$$(\Delta_{sw}\, p, q) \;=\; \frac{1}{\Delta t^n}\left(\mathrm{div}_{sw}\,(\mathbf{u}^{n+1/2}), q\right), \quad \forall q \in Q_{0,sw}. \tag{3.46}$$

From (3.46), we deduce

$$\Delta_{sw}\, p \;=\; \frac{1}{\Delta t^n}\mathrm{div}_{sw}\,(\mathbf{u}^{n+1/2}), \tag{3.47}$$

$$p|_{\Gamma=0} \;=\; 0. \tag{3.48}$$

The resolution of the equations (3.47)-(3.48) allows to compute p and then to update the velocity at the correction step (3.25). To obtain equation (3.47), which is independent of $\mathbf{u}$, it is equivalent to apply the operator div_{sw} to the equation (3.22) divided by H, and to use the shallow water free divergence condition (3.23) to eliminate $\mathbf{u}$.

Remark 3.2.2. *Notice that* $\mathrm{div}_{sw}\,(\mathbf{u}) = \nabla_0 \cdot (H\mathbf{u}) + \mathbf{u} \cdot (\mathbf{n_s} + \mathbf{n_b})$ *and* $\nabla_{sw}\, p = H\nabla_0(p) - p(\mathbf{n_s} + \mathbf{n_b})$ *with* ∇_0 *defined by* (3.7) *and* $\mathbf{n_s}$ *(resp.* $\mathbf{n_b}$*) the (non-unit) normal vector at the surface (resp. at the bottom)*

$$\mathbf{n_s} = \begin{pmatrix} -\frac{\partial \eta}{\partial x} \\ 1 \end{pmatrix}, \qquad \mathbf{n_b} = \begin{pmatrix} -\frac{\partial z_b}{\partial x} \\ 1 \end{pmatrix}.$$

With that notation, the relation (3.12) *rewrites*

$$\int_\Omega \mathrm{div}_{sw}\,(\mathbf{u})\; dx = \int_\Gamma H u\, n\, ds + \int_\Omega \mathbf{u} \cdot (\mathbf{n_s} + \mathbf{n_b})\, dx.$$

Hence, to satisfy the divergence free condition, the velocity $\mathbf{u}$ *should satisfy*

$$\int_\Gamma H u\, n\, ds = -\int_\Omega \mathbf{u} \cdot (\mathbf{n_s} + \mathbf{n_b})\, dx.$$

3.2.3 Boundary conditions

In this section, we still consider that the hydrostatic part is provided and we study the compatibility of the boundary conditions between the hydrostatic part and the projection part. Therefore, the compatibility between the pressure and velocity at boundary needs to be studied. To this aim, we first provide the conditions required to impose a Dirichlet

or a Neumann boundary condition for the pressure at the boundary on the variational formulation, and then, we couple these conditions with the hydrostatic part. Concerning the bathymetry, it is usual to impose a Neumann boundary condition for the bottom z_b at the hydrostatic level.

Neumann boundary condition for the pressure

The Neumann boundary condition for the projection scheme is not natural and to enforce such a condition, the elliptic problem (3.44)-(3.46) can be considered. Many studies have been done to choose an appropriate variational formulation for this problem. In [90] J-L. Guermond explores the different variational formulations in order to enforce a Neumann pressure boundary condition, in [96] some equivalent formulations are given to switch between Neumann and Dirichlet boundary conditions. As for the hyperbolic part, we still consider that we have imposed a Neumann boundary condition for the topography $\frac{\partial z_b}{\partial x}|_{\Gamma_i} = 0,\ \forall i = in, out$. Taking the normal component at the boundary Γ_i of the momentum equation at the second step of the splitting (3.25), it follows that

$$H\frac{\partial p}{\partial n}|_{\Gamma_i} + p|_{\Gamma_i}(\frac{\partial H}{\partial n}|_{\Gamma_i}) = \frac{H}{\Delta t^n}(u|_{\Gamma_i}^{n+1/2} - u|_{\Gamma_i}),$$

where the left hand side would correspond to the boundary terms of the elliptic problem (3.46) if we choose non homogeneous boundary condition for the pressure.

We denote $\frac{\partial H}{\partial n}|_{\Gamma_i} = \beta_i$, $i = in, out$.

- In case $\beta_i = 0$, a Neumann boundary condition for the pressure is deduced from a Dirichlet condition for u.

$$\frac{\partial p}{\partial n}|_{\Gamma_i} = \frac{1}{\Delta t^n}(u|_{\Gamma_i}^{n+1/2} - u|_{\Gamma_i}). \tag{3.49}$$

- In the other cases, it gives a mixed boundary condition

$$\frac{\partial p}{\partial n}|_{\Gamma_i} + \beta_i p|_{\Gamma_i} = \frac{1}{\Delta t^n}(u|_{\Gamma_i}^{n+1/2} - u|_{\Gamma_i}). \tag{3.50}$$

Then, in the two cases, we have imposed a Dirichlet velocity condition, that leads to solve the variational problem (3.36)-(3.37) with the shallow water divergence operator where we search $\mathbf{v} \in V_i$ and $q \in L^2(\Omega)$, with $i = in$ for the inflow or $i = out$ for the outflow defined by:

$$V_i = \{\mathbf{v} = (v_1, v_2) \in (L^2(\Omega))^2 | \mathrm{div}_{sw}(\mathbf{v}) \in L^2(\Omega), v_{1|\Gamma_i} = 0\}. \tag{3.51}$$

Let us now give the coupling boundary conditions between the prediction step and the

correction step. Indeed, in the projection part, boundary conditions need to be set in order to be consistent with the hydrostatic part.
Concerning the prediction step, we consider the well known Saint-Venant system and we assume that the Riemann invariant remains constant along the associated characteristic. This approach has been introduced in [41] and distinguishes fluvial and torrential boundaries depending on the Froude number $Fr = \frac{|u|}{c}$. Usual boundary conditions consist in imposing a flux $\mathbf{q}_0$ at the inflow boundary and a water depth at the outflow boundary. It is also classical to let a free outflow boundary, setting a Neumann boundary condition for the water depth and for the velocity. For both cases, we now give the boundary conditions that have to be set in the correction step.

We consider the first situation in which we set a flux at the inflow Γ_{in} and a given depth at the outflow Γ_{out}. Assuming a fluvial flow, this case consists in solving a Riemann problem at the interface Γ_{in} where the global flux is given by $\mathbf{q}_0 = (q_{01}, q_{02})^t = (Hu^{n+1/2}, Hw^{n+1/2})^t$. That gives the boundary values $H_0 = H_0^{n+1/2}$, $u_0 = \frac{q_{02}}{H_0^{n+1/2}}$ and $w_0 = \frac{q_{02}}{H_0^{n+1/2}}$ from the hyperbolic part. This leads to obtain a Dirichlet condition for the pressure at the left boundary of the correction part.
Moreover, if H is given for the outflow, we preconize to give a mixed condition for the pressure that corresponds to the boundary condition (3.50)

$$\begin{aligned} p|_{\Gamma_{in}} &= 0, \\ \left.\frac{\partial p}{\partial n}\right|_{\Gamma_{out}} + p\left.\frac{\partial H}{\partial n}\right|_{\Gamma_{out}} &= 0, \end{aligned}$$

that leads to the problem (3.36)-(3.37) and take $\mathbf{u} \in V_0$, with the definition (3.31) and $p \in L^2(\Omega)$.
We now consider the second situation in which we still impose a flux $\mathbf{q}_0$ at the inflow and we set a free outflow boundary. In this case, we assume the two Riemann invariants are constant along the outgoing characteristics of the hyperbolic part (see [41]), therefore, we have a Neumann boundary condition for $H^{n+1/2}$ and $u^{n+1/2}$.

$$\left.\frac{\partial H}{\partial n}\right|_{\Gamma_{out}} = 0, \qquad \left.\frac{\partial \mathbf{u}^{n+1/2}}{\partial n}\right|_{\Gamma_{out}} = 0.$$

Preserving these conditions at the correction step, it gives a Neumann boundary condition for the pressure of type (3.49)

$$\left.\frac{\partial p}{\partial n}\right|_{\Gamma_{out}} = 0.$$

For an inflow given and using the formulation with the shallow water divergence operator,

the functional spaces will be defined by

$$\mathbf{u} \in V_{out} = \{\mathbf{v} \in V,\ v_1|_{\Gamma_{out}} = 0\},\ p \in L^2(\Omega).$$

Notice that we can also impose the same conditions using the formulation with the shallow water gradient operator (3.42)-(3.42) and using a lifting of the boundary conditions for the pressure.

3.2.4 The inf-sup condition

We want to establish the inf-sup condition at the continuous level to ensure we have a well-posed problem. The so-called inf-sup condition was introduced by Ladyzhenskaya, Babuska and Brezzi in [18, 40, 103] to ensure the well-posedness of mixed problems for incompressible flows and has been studied for the finite element method for instance in [71]. We consider the variational formulation with the shallow water divergence operator div_{sw} given by Equations (3.42)-(3.42) with homogeneous Dirichlet boundary conditions for the velocity and Dirichlet boundary conditions for the pressure. The Hilbert space V_0 is equipped with inner product $(.,.)_{V_0}$ and induced norm $||.||_{V_0} = ||.||_{L^2(\Omega)} + ||\text{div}_{sw}(.)||_{L^2(\Omega)}$.
The problem reads:
Find $\mathbf{u} \in V_0$, $p \in L^2(\Omega)$ such that

$$\begin{aligned} a(\mathbf{u},\mathbf{v}) - \Delta t\, b(\mathbf{v},p) &= a(\mathbf{u}^{n+1/2},\mathbf{v}) - < H\mathbf{v}\cdot\mathbf{n}\,, p_0 >_{\Gamma_{out}}, \quad \forall \mathbf{v} \in V_0, \qquad (3.52)\\ b(\mathbf{u},q) &= 0, \quad \forall q \in L^2(\Omega). \qquad (3.53)\end{aligned}$$

where $< \cdot,\cdot >_{\Gamma_{out}}$ represents again the duality between $H^{-1/2}(\Gamma_{out})$ and $H^{1/2}(\Gamma_{out})$.
For all $\mathbf{v} \in W_0 = \{\mathbf{v} \in V_0\,, \text{div}_{sw}(\mathbf{v}) = 0\}$, the problem becomes:
Find $\mathbf{u} \in W_0$ such that

$$a(\mathbf{u},\mathbf{v}) = a(\mathbf{u}^{n+1/2},\mathbf{v}) - < H\mathbf{v}\cdot\mathbf{n}\,, p_0 >_{\Gamma_{out}}, \quad \forall \mathbf{v} \in W_0. \qquad (3.54)$$

Under the assumption (3.27), it is obvious that the bilinear form a is coercive, *i.e.* for all $\mathbf{v} \in W_0$:

$$a(\mathbf{v},\mathbf{v}) \geq \alpha_1 ||\mathbf{v}||^2_{L^2(\Omega)}, \ \ \alpha_1 > 0. \qquad (3.55)$$

In addition, b is bilinear. With the assumption (3.27), and given $q \in L^2(\Omega)$, if we choose $\mathbf{v} = (0,q)^T$, then

$$\frac{b(\mathbf{v},q)}{||q||_{L^2(\Omega)}} = 2||q||_{L^2(\Omega)}. \qquad (3.56)$$

This implies the existence and uniqueness of the solution of (3.52)-(3.53).

For the formulation with the operator ∇_{sw}, we can use a similar argument and take $\mathbf{v} = \nabla_{sw}(q)$.

3.3 Numerical approximation

3.3.1 Discretization

This section is devoted to the numerical approximation and gives mainly details about the correction step. Let us be given a subdivision of Ω with N vertices $x_1 < x_2 < ... < x_N$ and we define the space step $\Delta x_{i+1/2} = x_{i+1} - x_i$. We also note $\Delta x_i = x_{i+1/2} - x_{i-1/2}$ with $x_{i+1/2} = \frac{x_i + x_{i+1}}{2}$.

Prediction part

For the prediction step (3.21) i.e the hydrostatic part of the model, we use a finite volume scheme. We introduce the finite volume cells C_i centered at vertices x_i such that $\Omega = \cup_{i=1,N} C_i$. Then, the approximate solution X_i^n at time t^n

$$X_i^n \approx \frac{1}{\Delta x_i} \int_{C_i} X(x, t^n) dx,$$

is solution of the numerical scheme

$$X_i^{n+1} = X_i^n - \sigma_i^n \left(\mathcal{F}_{i+1/2}^n - \mathcal{F}_{i-1/2}^n \right) + \sigma_i^n \mathcal{S}_i^n,$$

where $\sigma_i^n = \frac{\Delta t^n}{\Delta x_i}$ and $\mathcal{F}$ (resp. $\mathcal{S}$) is a robust and efficient discretization of the conservative flux $F(X)$ (resp. the source term $S(X)$). The time step is determined through a classical CFL condition. Many numerical fluxes and discretizations are available in the literature [32, 83, 110], we choose a kinetic based solver [8] coupled with the hydrostatic reconstruction technique [7].

Correction part

Concerning the correction step (3.22)-(3.23), we consider the discrete problem corresponding to the mixed problem using the shallow water divergence operator div_{sw} described by Equations (3.32)-(3.33). We approach $(V_0,\ L^2(\Omega))$ by the finite dimensional spaces $(V_{0h},\ Q_h)$ and we note

$$N = \dim(V_{0h}), \qquad M = \dim(Q_h).$$

We also denote by $(\varphi_i)_{i=1,N}$ and $(\phi_l)_{l=1,M}$ the basis functions of V_{0h} and Q_h respectively. The finite dimensional spaces will be specified later on. We approximate $(\mathbf{u}, p) \in$

$(V_0, L^2(\Omega))$ by $(\mathbf{u}_h, p_h) \in (V_{0h}, Q_h)$ such that

$$\mathbf{u}_h(x) = \sum_{i=1}^{N} \begin{pmatrix} u_i \\ w_i \end{pmatrix} \varphi_i(x), \qquad p_h(x) = \sum_{l=1}^{M} p_l \, \phi_l(x).$$

Therefore, we consider the discrete problem corresponding to (3.32)-(3.33).
Find $\mathbf{u}_h \in V_{0h}$, $p_h \in Q_h$ such that

$$\begin{aligned} \frac{1}{\Delta t^n} a(\mathbf{u}_h, \mathbf{v}_h) + b(\mathbf{v}_h, p_h) &= \frac{1}{\Delta t^n} a(\mathbf{u}_h^{n+1/2}, \mathbf{v}_h), \quad \forall \mathbf{v}_h \in V_{0h}, & (3.57) \\ b(\mathbf{u}_h, q_h) &= 0, \quad \forall q_h \in Q_h. & (3.58) \end{aligned}$$

Let us introduce the mass matrix M_H given by

$$M_H = \left(\int_\Omega H \varphi_i \varphi_j dx \right)_{1 \le i,j \le N},$$

and the two matrices B^t, B defined by

$$B^t = \left(\int_\Omega \nabla_{sw}(\phi_l) \varphi_i dx \right)_{1 \le l \le M, 1 \le i \le N}, B = -\left(\int_\Omega \mathrm{div}_{sw}(\varphi_j) \phi_l dx \right)_{1 \le l \le M, 1 \le j \le N},$$

and we denote

$$U = \begin{pmatrix} u_1 \\ \vdots \\ u_N \\ w_1 \\ \vdots \\ w_N \end{pmatrix}, \qquad P = \begin{pmatrix} p_1 \\ \vdots \\ p_M \end{pmatrix},$$

Therefore, the problem (3.57)-(3.58) becomes

$$\begin{pmatrix} \frac{1}{\Delta t^n} A_H & B^t \\ B & 0 \end{pmatrix} \begin{pmatrix} U \\ P \end{pmatrix} = \begin{pmatrix} \frac{1}{\Delta t^n} A_H U^{n+1/2} \\ 0 \end{pmatrix},$$

with

$$A_H = \begin{pmatrix} M_H & 0 \\ 0 & M_H \end{pmatrix}.$$

Assuming that M_H is invertible and eliminating the velocity U, we obtain the following equation

$$B A_H^{-1} B^t P = \frac{1}{\Delta t^n} B U^{n+1/2}, \tag{3.59}$$

that is a discretization of the elliptic equation (3.47) of Sturm-Liouville type governing the pressure p. If one want to take the Dirichlet boundary condition for the pressure at the outlet, the problem becomes:

$$BA_H^{-1}B^tP = \frac{1}{\Delta t^n}B(U^{n+1/2} + C).$$

where the matrix $\Delta t^n C = \left(\int_{\Gamma_{out}} H\varphi_i\,\phi_l\,n\right)_{1\leq l\leq M, 1\leq i\leq N}$ contains the boundary terms.

This approach is suitable for the finite element approximation that is given in the next section. However, it implies to invert a mass matrix M_H that is not diagonal and depends on the water depth H. In practice, we use the mass lumping technique introduced by Gresho ([89]) to avoid inverting the mass matrix in projection methods for Navier-Stokes incompressible system.

3.3.2 Finite element $\mathbb{P}_1/\mathbb{P}_0$

It has been seen in Chapter 2 that the discrete entropy is satisfied if we use a finite difference scheme on a staggered grid, then we choose the specific pair $\mathbb{P}_1/\mathbb{P}_0$ in order to satisfy the entropy properties.

The problem is solved by the mixed finite element approximation $\mathbb{P}_1/\mathbb{P}_0$ (see [134]) on the domain $\Omega = \cup_{l=1}^{M} K_l$ ($M = N-1$ with N the number of nodes), where the velocity is approximated by a continuous linear function and the pressure is approximated by a discontinuous piecewise constant function over each element

$$\mathbf{u}_h \in V_h = \{\mathbf{v}_h \in (\mathcal{C}^0(\Omega))^2 \mid \ \mathbf{v}_h|_{K_l} \in \mathbb{P}_1^2, \forall l = 1, \ldots, N-1\},$$

and

$$p_h \in Q_h = \{q_h \mid q_h|_{K_l} \in \mathbb{P}_0\ ,\ \forall l = 1, \ldots, M-1\}.$$

Using the discretization given in 3.3.1, we denote by $K_{i+1/2}$ the finite element cell $[x_i, x_{i+1}]$, then the pressure is constant on the finite element $K_{i+1/2}$.

For the sake of clarity, in this situation, let $\left(\phi_{j+1/2}\right)_{1\leq j\leq M}$ be the basis functions for the pressure p_h, and $(\varphi_i)_{1\leq i\leq N}$ the basis functions for the velocity $\mathbf{u}_h$, and set

$$\mathbf{u}_h(x) = \sum_{i=1}^{N} \begin{pmatrix} u_i \\ w_i \end{pmatrix} \varphi_i(x), \quad p_h(x) = \sum_{j=1}^{M} p_{j+1/2}\,\phi_{j+1/2}(x).$$

We note $\zeta = H + 2z_b$ and assume ζ is approximated by a piecewise linear function ζ_h, namely $\zeta_h(x) = \sum_{i=i}^{N} \zeta_i\varphi_i(x)$. We also note $\frac{\partial \zeta_h}{\partial x}|_{i+1/2} = \frac{\zeta_{i+1}-\zeta_i}{\Delta x_{i+1/2}} = \frac{\chi_{i+1/2}}{\Delta x_{i+1/2}}$ the constant gradient of ζ_h on the element $K_{i+1/2}$.

Remark 3.3.1. *In the context of the discontinuous Galerkin method, using $\partial_x\phi_{j+1/2}(x) = \delta_j(x) - \delta_{j+1}(x)$ in the sense of distribution, it gives a distributional derivative for the*

pressure $\partial_x p_h(x) = \sum_j \left(p_{j+1/2} - p_{j-1/2}\right) \delta_j(x)$.

We denote $\underline{\varphi} = (\varphi, \varphi)^t$, then the shallow water gradient operator is written

$$\int_\Omega \nabla_{sw}(p_h) \cdot \underline{\varphi_i}\, dx = \begin{pmatrix} H_i(p_{i+1/2} - p_{i-1/2}) + \frac{p_{i-1/2}}{2}\chi_{i-1/2} + \frac{p_{i+1/2}}{2}\chi_{i+1/2} \\ -(\Delta x_{i+1/2} p_{i+1/2} + \Delta x_{i-1/2} p_{i-1/2}) \end{pmatrix}.$$

Similarly, after integrating by part, the shallow water divergence operator writes

$$\begin{aligned} \int_\Omega \mathrm{div}_{sw}\left(\mathbf{u}_h\right)\phi_{j+1/2}\, dx &= H_{j+1}u_{j+1} - H_j u_j - \frac{u_j + u_{j+1}}{2}\left(\zeta_{j+1} - \zeta_j\right) \\ &\quad + \Delta x_{j+1/2}(w_j + w_{j+1}). \end{aligned}$$

In one dimension, this approach corresponds to a staggered-grid finite-difference method where the velocity is computed at the nodes and the pressure is computed at the middle nodes. The discretization we obtain corresponds exactly to the finite difference scheme given in Chapter 2, and then, the properties established in Chapter 2are conserved.

3.3.3 Finite element $\mathbb{P}_1$-iso-$\mathbb{P}_2/\mathbb{P}_1$

In this part, we propose to give an approximation $\mathbb{P}_1$-iso-$\mathbb{P}_2$ for the velocity and $\mathbb{P}_1$ for the pressure. To satisfy the discrete entropy, as explained in Chapter 2, it is necessary to have a staggered grid, then, this pair has been chosen in order to prepare the two-dimensional method. We give here an analogy for the one-dimensional problem.

For the one-dimensional $\mathbb{P}_1$-iso-$\mathbb{P}_2/\mathbb{P}_1$, we consider two meshes $\mathcal{K}_h$ (the same as before) and $\mathcal{K}_{2h}$ with $K_{h,i+1/2} = [x_i, x_{i+1}]$ and $K_{2h,j} = [x_{2j-1}, x_{2j+1}]$ the finite elements defined on the respective meshes $\mathcal{K}_h$ and $\mathcal{K}_{2h}$ such that $\mathcal{K}_h = \cup_{i=1}^{N-1} K_{h,i+1/2}$ and $\mathcal{K}_{2h} = \cup_{j=1}^{M-1} K_{2h,j}$ with N the total number of vertices of $\mathcal{K}_h$ and $M = (N-1)/2$ (assuming N odd), the number of vertices of $\mathcal{K}_{2h}$. Therefore, the approximation spaces V_h and Q_h are defined by

$$\begin{aligned} V_h &= \left\{\mathbf{v}_h \in C^0(\Omega)^2 |\ \mathbf{v}_h|_{K_h,i} \in \mathbb{P}_1^2, \forall i = 1, \cdots, N-1\right\}, \\ Q_h &= \left\{q_h \in C^0(\Omega) |\ q_h|_{K_{2h,j}} \in \mathbb{P}_1, \forall j = 1, ..., M-1\right\}. \end{aligned}$$

Then, the velocity and the pressure are written

$$p_h(x) = \sum_{j=1}^{M} p_j \phi_j, \quad \mathbf{u}_h(x) = \sum_{i=1}^{N} \begin{pmatrix} u_i \\ w_i \end{pmatrix} \varphi_i. \tag{3.60}$$

where $(\phi_j)_{1\le j\le M}$ are the basis functions for the pressure p_h, and $(\varphi_i)_{1\le i\le N}$ the basis functions for the velocity $\mathbf{u}_h$.

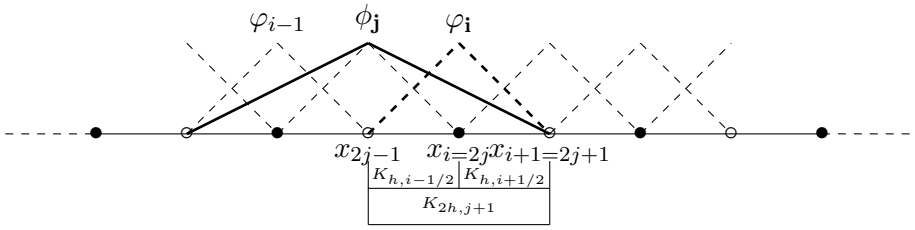

Figure 3.2: Representation of the basis functions.

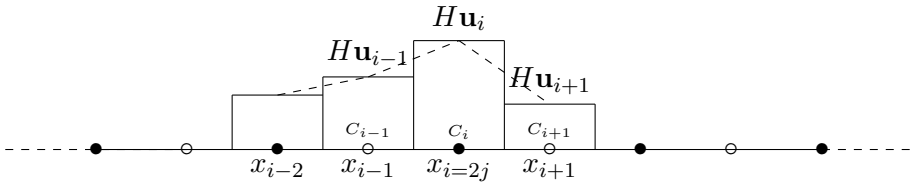

Figure 3.3: Representation of the discretization of the function $(H\mathbf{u})$ and representation of the finite volume cell $C_i = [x_{i-1/2}, x_{i+1/2}]$.

In figure 3.2, the dashed lines are the usual elementary basis functions of $\mathbb{P}_1$ on the mesh K_h, while the continuous lines are the basis functions on the mesh K_{2h}. The divergence operator, for all $j = 1, M$, writes

$$\int_\Omega \mathrm{div}_{sw}(\mathbf{u}_h)\phi_j \, dx = \sum_{K_h \in \mathcal{K}_h} \int_K \mathrm{div}_{sw}(\mathbf{u}_h)\phi_j \, dx.$$

We use a linear interpolation for $H\varphi_j$ in the computation of $\int_{K_{h,i+1/2}} H\varphi_i \, dx$, and we consider that $\Delta x_i = \Delta x \quad \forall i = 1, \ldots, N$ for the sake of simplicity. We still approximate ζ by ζ_h defined before.

The discrete shallow water divergence operator is computed for all nodes x_j of the mesh $\mathcal{K}_{2h}$ and therefore, denoting $i = 2j - 1$, it can be written, $\forall j = 1, M$

$$\begin{aligned}
\int_\Omega \mathrm{div}_{sw}(\mathbf{u}_h)\phi_j \, dx \;=\; & \left(\frac{1}{4}H_{i+2}u_{i+2} + \frac{H_{i+1}}{2}u_{i+1}\right) - \left(\frac{1}{4}H_{i-2}u_{i-2} + \frac{H_{i-1}}{2}u_{i-1}\right) \\
& - \left(\chi_{i-1/2}m_{i,j}^{i-1/2} + \chi_{i+1/2}m_{i,j}^{i+1/2}\right)u_i \\
& - \left(\chi_{i-3/2}m_{i-2,j}^{i-3/2}\right)u_{i-2} - \left(\chi_{i+3/2}m_{i+2,j}^{i+3/2}\right)u_{i+2} \\
& - \left(\chi_{i-1/2}m_{i-1,j}^{i-1/2} + \chi_{i-3/2}m_{i-1,j}^{i-3/2}\right)u_{i-1} \\
& - \left(\chi_{i+1/2}m_{i+1,j}^{i+1/2} + \chi_{i+3/2}m_{i+1,j}^{i+3/2}\right)u_{i+1} \\
& + (2m_{i,j}^{i+1/2})w_i \\
& + \left(m_{i-1,j}^{i-1/2} + m_{i-1,j}^{i-3/2}\right)w_{i-1} + \left(m_{i+1,j}^{i+1/2} + m_{i+1,j}^{i+3/2}\right)w_{i+1} \\
& + (m_{i-2,j}^{i-3/2})w_{i-2} + m_{i+2,j}^{i+3/2}w_{i+2},
\end{aligned}$$

with $m_{i,j}^{i+1/2} = \int_{K_{h,i+1/2}} \varphi_i \phi_j dx$.

Similarly, the shallow water gradient operator is obtained for all the nodes x_i of the mesh $\mathcal{K}_h$. However, we distinguish the gradient at the nodes of the elements K_{2h} from the ones at the interior. In other words, for all the nodes x_i of the mesh $\mathcal{K}_{2h}$, the gradient operator is defined by

$$\begin{aligned}
\int_\Omega \nabla_{sw} p_h \cdot \underline{\varphi}_{(i=2j-1)}\, dx\Big|_1 &= \frac{H_i}{4}\left(p_{j+1} - p_{j-1}\right) \\
&\quad + \chi_{i-1/2}\left(m_{i,j}^{i-1/2} p_j + m_{i,j-1}^{i-1/2} p_{j-1}\right) \\
&\quad + \chi_{j+1/2}\left(m_{i,j}^{i+1/2} p_j + m_{i,j+1}^{i+1/2} p_{j+1}\right), \\
\int_\Omega \nabla_{sw} p_h \cdot \underline{\varphi}_{(i=2j-1)}\, dx\Big|_2 &= -2m_{i,j}^{i+1/2} p_j - m_{i,j}^{i-1/2} p_{j-1} - m_{i,j}^{i+1/2} p_{j+1}.
\end{aligned}$$

On the other hand, for all the nodes x_i such that i is even

$$\begin{aligned}
\int_\Omega \nabla_{sw} p_h \cdot \underline{\varphi}_{(i=2j)}\, dx\Big|_1 &= \frac{H_i}{2}\left(p_{j+1} - p_j\right) \\
&\quad + \left(\chi_{i-1/2} m_{i,j}^{i-1/2} + \chi_{i+1/2} m_{i,j}^{i+1/2}\right) p_j \\
&\quad + \left(\chi_{i-1/2} m_{i,j+1}^{i-1/2} + \chi_{i+1/2} m_{i,j+1}^{i+1/2}\right) p_{j+1}, \\
\int_\Omega \nabla_{sw} p_h \cdot \underline{\varphi}_{(i=2j)}\, dx\Big|_2 &= -\left(m_{i,j}^{i-1/2} + m_{i,j}^{i+1/2}\right) p_j - \left(m_{i,j+1}^{i-1/2} + m_{i,j+1}^{i+1/2}\right) p_{j+1}.
\end{aligned}$$

With the discretization of the shallow water operators given above, we are able to validate the scheme for the first order method and the second order method.

3.3.4 Towards a second order approximation

In this section, we give some modifications of the previous scheme to improve the accuracy.

Second order approximation in space

A formally second order scheme in space has been developed for the hydrostatic shallow water system in [7], using a limited reconstruction of the variables. We use this reconstruction in the finite volume scheme applied to the hyperbolic part. For the correction part, we use the scheme presented in the previous section but a higher order accuracy could be used like a $\mathbb{P}_2 - \mathbb{P}1$ approximation for instance.

Second order approximation in time

For hyperbolic conservation laws, the second-order accuracy in time is usually recovered by the Heun method [31, 32] which is a slight modification of the second order Runge-Kutta method. The second order scheme presented here is an adaptation of the Heun scheme

which takes into account the CFL constraint for each time step. More precisely, for a system written under the simplified form

$$\frac{\partial y}{\partial t} = f(y), \tag{3.61}$$

the scheme writes

$$\begin{aligned} \tilde{y}^{n+1} &= y^n + \Delta t_1^n f(y^n), && (3.62)\\ \tilde{y}^{n+2} &= \tilde{y}^{n+1} + \Delta t_2^n f(\tilde{y}^{n+1}), && (3.63)\\ y^{n+1} &= \alpha y^n + \beta \tilde{y}^{n+2}, && (3.64) \end{aligned}$$

where Δt_1^n and Δt_2^n respectively satisfy the CFL conditions associated with y^n and $\tilde{y}^{n+1}$. Using a Taylor expansion, it can be verified that this is a second order scheme in time if the following relations hold

$$\begin{aligned} \Delta t^n &= \frac{2\Delta t_1^n \Delta t_2^n}{\Delta t_1^n + \Delta t_2^n}, && (3.65)\\ \beta &= \frac{(\Delta t^n)^2}{2\Delta t_1^n \Delta t_2^n}, && (3.66)\\ \alpha &= 1 - \beta. && (3.67) \end{aligned}$$

Since, $\alpha, \beta \geq 0$, $\tilde{y}^{n+1}$ is a convex combination of y^n and $\tilde{y}^{n+2}$ so the scheme preserves the positivity.

By analogy, the idea is to apply this method to the prediction-correction scheme. To this aim, we rewrite the system (3.17)-(3.18) under the form

$$\begin{aligned} \frac{\partial X}{\partial t} &= f(X) - R_{nh}, && (3.68)\\ \mathrm{div}_{sw}\,(\tilde{\mathbf{u}}) &= 0 && (3.69) \end{aligned}$$

where R_{nh} is defined by (3.20) and $f(x) = -\frac{\partial F(X)}{\partial x} + S(X)$ with F and S defined by (3.19) and (3.20). We replace each step (3.62)-(3.63) by the prediction-correction step (3.21)-(3.22)

$$\begin{aligned} \tilde{X}^{n+1-} &= X^n + \Delta t_1^n f(X^n), && (3.70)\\ \tilde{X}^{n+1} &= \tilde{X}^{n+1-} - \Delta t_1^n \tilde{R}_n^{n+1}, && (3.71)\\ \mathrm{div}_{sw}\,(\tilde{\mathbf{u}}^{n+1}) &= 0, && (3.72) \end{aligned}$$

$$\tilde{X}^{n+2-} = \tilde{X}^{n+1} + \Delta t_2^n f(\tilde{X}^{n+1}), \tag{3.73}$$

$$\tilde{X}^{n+2} = \tilde{X}^{n+2-} - \Delta t_2^n \tilde{R}_{nh}^{n+2}, \tag{3.74}$$

$$\mathrm{div}_{sw}\left(\tilde{\mathbf{u}}^{n+2}\right) = 0, \tag{3.75}$$

and then (3.64) becomes

$$X^{n+1} = \alpha X^n + \beta \tilde{X}^{n+2}. \tag{3.76}$$

Notice that the divergence free condition is not satisfied by X^{n+1} but it is satisfied for each intermediate steps (3.71) and (3.74).

With these modifications, we improve the accuracy of the global scheme, some parts of which are formally "second order". But the proof of the convergence orders is a difficult problem that we do not address here. These difficulties have been encountered and have been studied for the Navier-Stokes problem by J-L.Guermond and J.Shen in [92] (see also [67, 70]).

The convergence order has been computed for the elevation and the pressure in the figures 3.6, 3.7 and 3.8 (see section 3.4.1).

3.4 Analytical solutions

3.4.1 Validation with an analytical solution

In Chapter 2, (see also [43]) some analytical solutions of the model (3.2)-(3.5) have been presented and they allow to validate the numerical method. We consider the propagation of a solitary wave on a flat bottom ($z_b = cte$). This solution has the form

$$H = H_0 + a\left(\mathrm{sech}\left(\frac{x - c_0 t}{l}\right)\right)^2, \tag{3.77}$$

$$u = c_0\left(1 - \frac{d}{H}\right), \tag{3.78}$$

$$w = -\frac{a c_0 d}{lH}\mathrm{sech}\left(\frac{x - c_0 t}{l}\right)\mathrm{sech}'\left(\frac{x - c_0 t}{l}\right), \tag{3.79}$$

$$p = \frac{a c_0^2 d^2}{2 l^2 H^2}\left((2H_0 - H)\left(\mathrm{sech}'\left(\frac{x - c_0 t}{l}\right)\right)^2, + H\mathrm{sech}\left(\frac{x - c_0 t}{l}\right)\mathrm{sech}''\left(\frac{x - c_0 t}{l}\right)\right), \tag{3.80}$$

with $d, a, H_0 \in \mathbb{R}$, $H_0 > 0$, $a > 0$ and

$$c_0 = \frac{l}{d}\sqrt{\frac{gH_0^3}{l^2 - H_0^2}}, \quad l = \sqrt{\frac{H_0^3}{a} + H_0^2} \tag{3.81}$$

The solitary wave is a particular case where dispersive contributions are counterbalanced by non linear effects so that the shape of the wave remains unchanged during the propagation. The propagation of the solitary wave has been simulated for the parameters $a = 0.4\,m$, $H_0 = 1\,m$, and $d = 1\,m$ over a domain of $45\,m$ with 9000 nodes. At time $t = 0$, the solitary wave is positioned inside the domain. The results presented in figure 3.4 show the different fields, namely the elevation, the components of velocity and the total pressure at different times, and the comparison with the analytical solution at the last time.

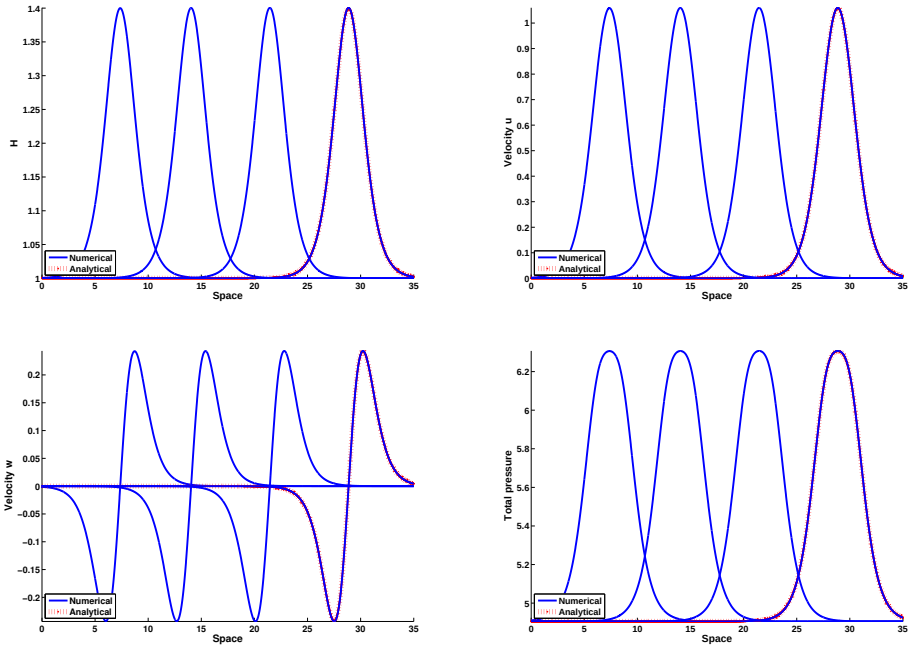

Figure 3.4: Propagation of the solitary wave at times $1.00008\,s, 1.9009\,s, 3.9017\,s$ and $5.9025\,s$. Comparison with analytical solution at time $t = 5.9025\,s$.

In the projection step, the greatest difficulty is to compute the pressure corresponding to the boundary conditions of the hyperbolic part (as seen in 3.2.3). The solution near the boundary has been confronted to the analytical solution. In the following result, we set a Neumann boundary condition on the non-hydrostatic pressure with the parameters given below. As shown in Figure 3.5, the pressure is well estimated at the outflow boundary and allows the wave to leave the domain with a good behavior. The inflow boundary condition has been tested with this same test case and gives similar results. We are able to let the solitary wave enter in the domain with a good approximation of the elevation.

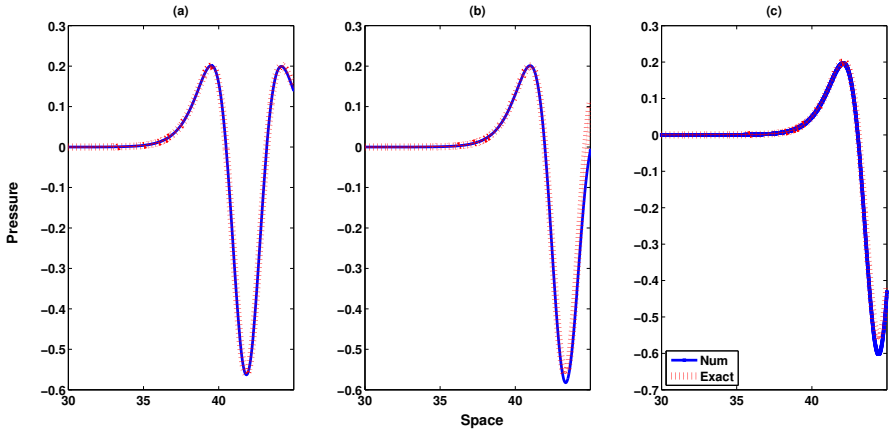

Figure 3.5: non-hydrostatic pressure profile at right boundary ($x = 45\,m$) (a): $t = 9.4044\,s$ (b): $t = 9.8046\,s$ (c): $t = 10.1048\,s$.

The numerical simulations for the first and the second order method are compared with the analytical solution and the L^2- error has been evaluated over different meshes of sizes from 395 nodes to 695 nodes (see Figures 3.6, 3.7 and 3.8).

With the parameters given above, for the first order method it gives a convergence rate for H close to 1 for the two computations, i.e $\mathbb{P}_1/\mathbb{P}_0$ and $\mathbb{P}_1$-iso-$\mathbb{P}_2/\mathbb{P}_1$. For the second order scheme, it gives a convergence order close to two (see Fig.3.6). Same results have been also obtained for the velocity (see Fig.3.7).

In Figure 3.8, the convergence rate has been computed for the pressure and we can observe that, for the first order method, the convergence rate of the pressure error is close to the first order, while the second order scheme gives a first order convergence rate for the pressure error.

Notice that the parameters set to validate the method lead to have a significant non-hydrostatic pressure (see the Figure 3.5) and then, the results show the ability of the method to preserve the solitary wave over the time.

The numerical results have also been obtained for the Thacker's test presented in Chapter 2, with the same convergence rate as the $\mathbb{P}_1/\mathbb{P}_0$ method.

3.4.2 Partial comparison with the Green-Naghdi model

In this part, we propose to compare the two models using an analytical solution of the Green-Naghdi model. As mentioned in Remark 3.2.1, the solution method presented in this paper does not apply immediately to the Green-Naghdi model. So, we just propose here a comparison with an analytical solution of the Green-Naghdi equations. In [43], it has been adduced that the analytical solitary wave of the Green-Naghdi model can be

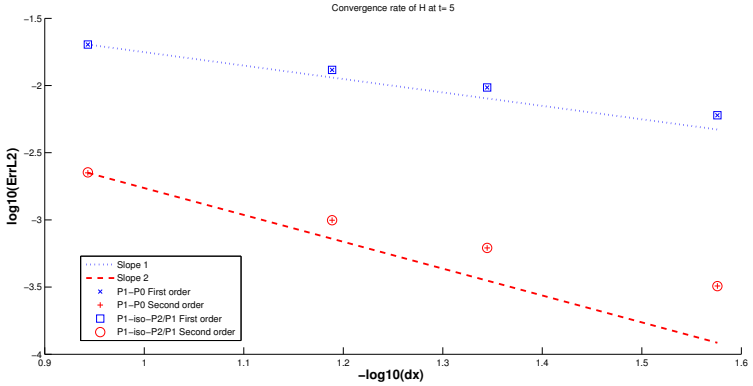

Figure 3.6: Convergence rate - Computation of the L_2-error of the solution H at time $t = 5s$ for the first and the second order scheme and comparison for $\mathbb{P}_1/\mathbb{P}_0$ and $\mathbb{P}_1$-iso-$\mathbb{P}_2/\mathbb{P}_1$ scheme.

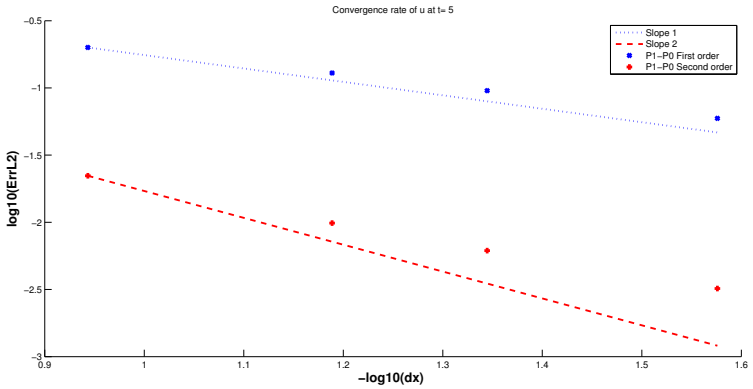

Figure 3.7: Convergence rate - Computation of the L_2-error of the solution u at time $t = 5s$ for the first and the second order scheme.

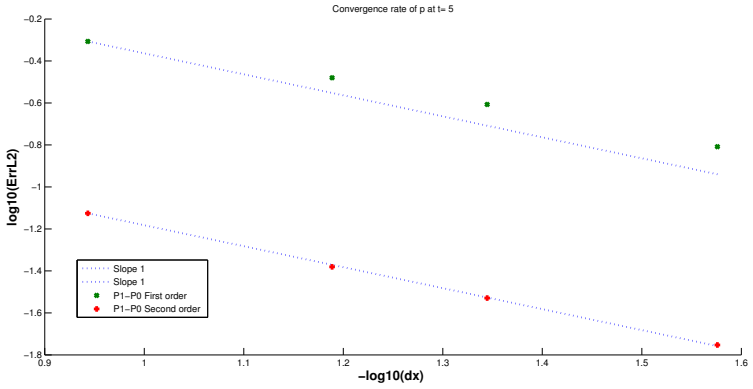

Figure 3.8: Convergence rate - Computation of the L_2-error of the solution p at time $t = 5s$ for the first and the second order scheme.

written in the same form as (3.77)-(3.80) with the parameters:

$$c_0 = \frac{2}{\sqrt{3}}\frac{l}{d}\sqrt{\frac{gH_0^3}{l^2 - H_0^2}}, \quad l = \frac{2}{\sqrt{3}}\sqrt{\frac{H_0^3}{a} + H_0^2}. \tag{3.82}$$

The idea is to initialize the simulation using the depth-averaged Euler model with the solitary wave of the Green-Naghdi model. Then, the aim is to compare after a long time lapse the analytical solution of the Green-Naghdi model and the simulated solution with the depth-averaged Euler model to see how the two models differ after a long time. We prescribe the amplitude $a = 0.2\,m$, the elevation $H_0 = 1.0\,m$ and the velocity $c_0 = 3.43\,m/s$ and, from (3.82), we deduce the values of l and d for the Green-Naghdi model.

Remark 3.4.1. *The parameters c_0 and a have been chosen such that, if we compute the solitary solution of the depth-averaged Euler model* (3.77)-(3.80) *with the parameters* (3.81)*, the two waves only slightly differ, as one can see in Figure 3.9.*

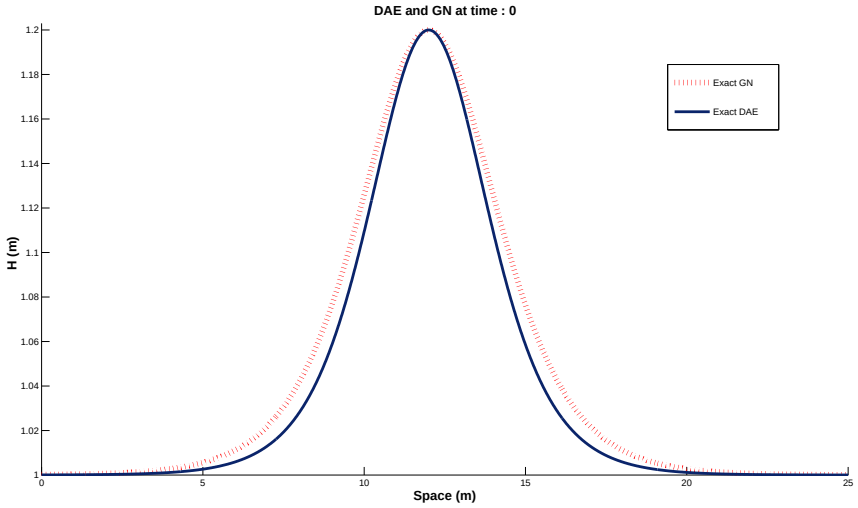

Figure 3.9: The solitary wave - Comparison of the two analytical solutions for the depth-averaged Euler system (DAE) and the Green-Naghdi model (GN) at time $t = 0$, for the same amplitude $a = 0.2\,m$ and the same velocity $c_0 = 3.43m/s$.

In Figure 3.10, the simulation in a long channel of $80\,m$ has been initialized with the solitary wave of the Green-Naghdi model. The elevation of the simulated wave is compared with the analytical solutions of the Green-Naghdi model at different times. There is a significant gap between the two curves after a long time lapse, showing the discrepancy between the solution of the two models.

Remark 3.4.2. *Another unsteady solution has been presented in [43] and generalizes the solution obtained by Thacker [148] for the shallow water equation. Although it is not studied*

in this paper, in the same way as the solitary wave, notice that the solution can be adapted for the Green-Naghdi model.

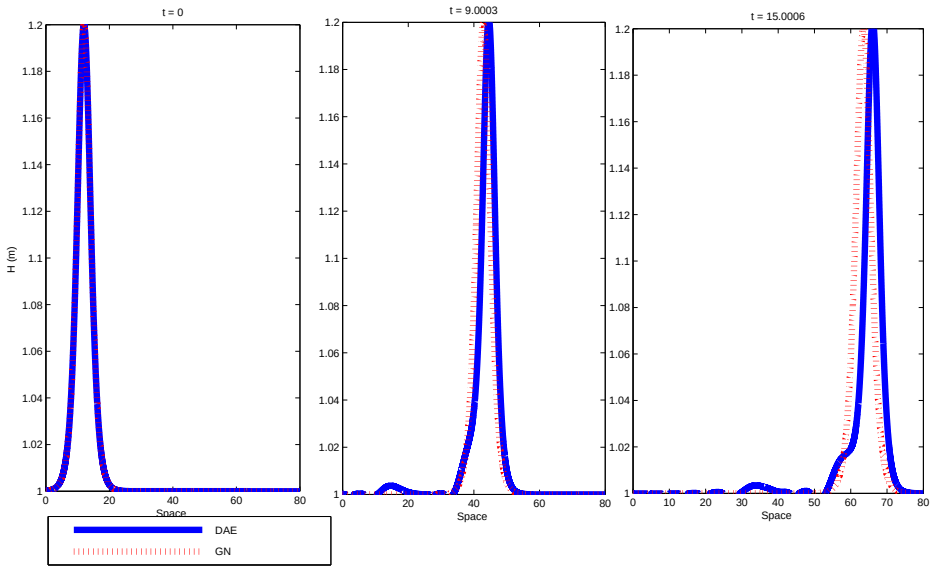

Figure 3.10: The solitary wave - Comparison of a DAE simulation with an analytical solution of the Green-Naghdi model at times : $t = 0\,s$, $t = 3.003\,s$, $t = 18.0008\,s$.

3.5 Numerical results

3.5.1 Dam break problem

We next study the dispersive effect on the classical dam break problem, which is usually modeled by a Riemann problem providing a left state (H_L, u_L) and a right state (H_R, u_R) on each side of the discontinuity x_d ([83]). However, our numerical dispersive model does not allow discontinuous solutions due to the functional spaces required for H (see also [43]), thus we provide an initial data numerically close to the analytical one

$$\begin{aligned} H(x,0) &= (H_R + a) - a \tanh\left(\frac{x - x_d}{\epsilon}\right), \\ a &= H_R - H_L. \end{aligned}$$

To evaluate the non-hydrostatic effect, the different fields have been compared with the shallow water solution with the initial data: $H_L = 1.8\,m$, $H_R = 1\,m$, $u_R = u_L = 0\,m.s^{-1}$, $\epsilon = 10^{-4}\,m$, $x_d = 300\,m$ over a domain of length $600\,m$ with 30000 nodes. In Figure 3.11, the evolution of the state is shown at time $t = 10\,s$ and $t = 45\,s$. The oscillations are due to the dispersive effects but the mean velocity does not change. These results are in

adequation with the analysis proposed by Gavrilyuk in [108] for the Green-Naghdi model with the same configuration.

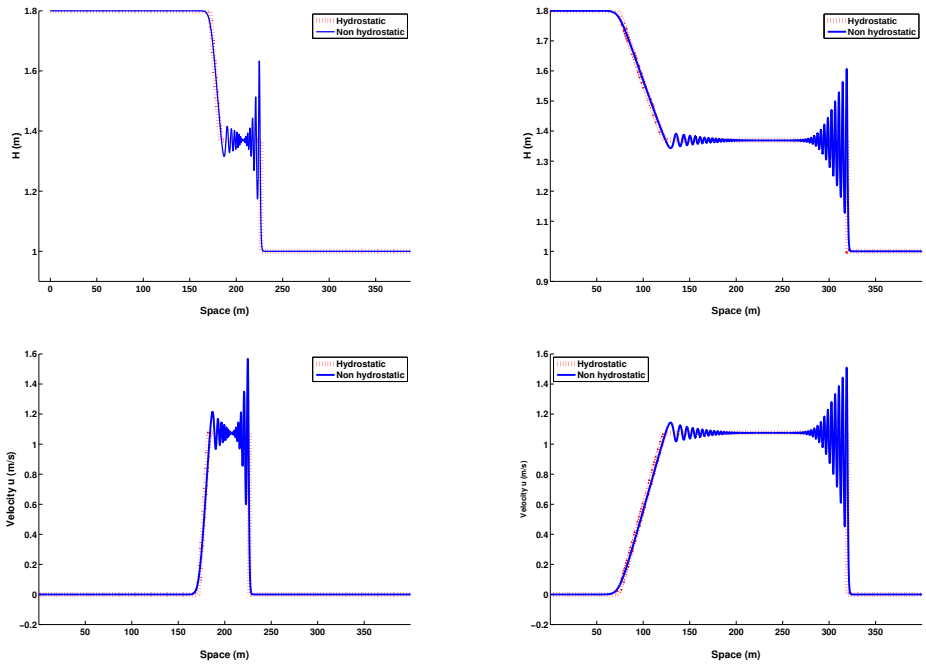

Figure 3.11: The dam break problem, elevation H and velocity u at times $t = 10\,s$ and $t = 45\,s$.

3.5.2 Wet-dry interfaces

The ability to treat the wet/dry interfaces is crucial in geophysical problems, since geophysicists are interested in studying the behavior of the water depth near the shorelines. This implies a water depth tending to zero at such boundaries. To treat the problem, we use the method introduced in Chapter 2, considering a minimum elevation H_ϵ.

Therefore, we confront the method with a coastal bottom at the right boundary over a domain of $35\,m$ with 3000 nodes. A wave is generated at the left boundary with an amplitude of $0.2\,m$ and an initial water depth $H_0 = 1\,m$. In Figure 3.12, the arrival of the wave at the coast is shown for times $t = 7.91\,s$, $9.92\,s$ and $10.42\,s$.

3.5.3 Comparison with experimental results

In this part, we confront the model with Dingemans experiments (detailed in [56, 57]) that consist in generating a small amplitude wave at the left boundary of a channel with topography as described in Figure 3.13.

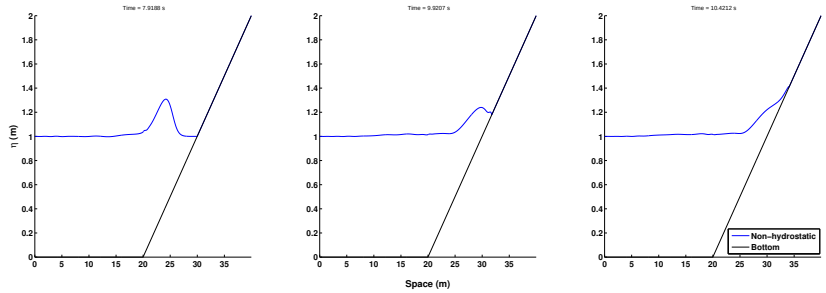

Figure 3.12: Propagation of a wave at a wet/dry interface.

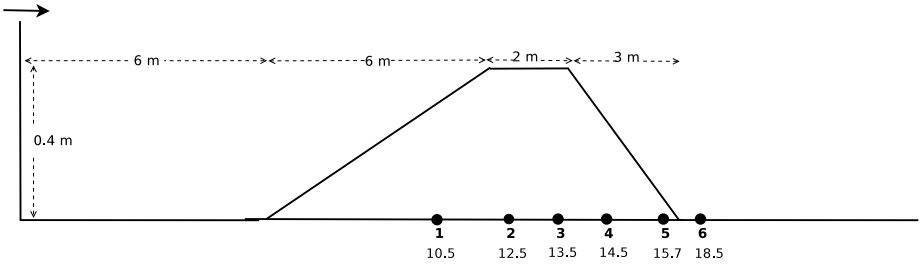

Figure 3.13: Configuration of Dingemans's test.

At the left boundary, a wave is generated with a period $T = 2.02\,s$ and an amplitude of $0.02\,m$. A free outflow condition is set at the right boundary. The initial free surface is set to be $\eta_0 = 0.4\,m$, and the measurement readings are saved at the following positions $10.5\,m$, $12.5\,m$, $13.5\,m$, $14.5\,m$,$15,7\,m$ and $17.3\,m$, placed at sensors 1 to 6 (Fig.3.13). In such a situation, the non-hydrostatic effects have a significant impact on the water depth that cannot be represented by a hydrostatic model. These effects result mainly from the slope of the bathymetry, 10% in this case. In Figure 3.14, the simulation has been run with the hydrostatic model and the elevation has been compared with measures at the sensor 5. As one can see, the non-hydrostatic pressure has to be taken in consideration to estimate the real water depth variation.

The numerical simulation with the non-hydrostatic model has been run with 15000 nodes on a domain of $49\,m$ over $25\,s$ and the comparisons are illustrated for each sensor (fig. 3.15). The goal of this last result is also to highlight the ability of the model to capture dispersive effects for a geophysical flow with a non negligible pressure.

Remark 3.5.1. *The reader can refer to [48, 62] to see the numerical results of the Green-Naghdi model on the Dingemans test. As expected, for the two models, the numerical results are close to the experimental data. Notice that the measured quantities contain experimental errors and uncertainties. Therefore, since the two models are very close and the generated perturbation during the experiment is small, it is complicated to evaluate if the differences are due to the uncertainty of the measures or the accuracy of the models.*

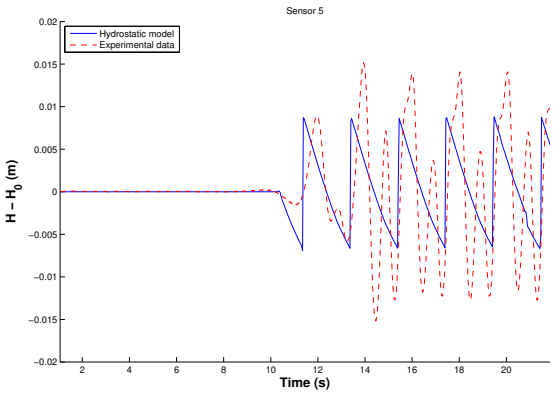

Figure 3.14: Comparison with hydrostatic model on sensor 5.

Nevertheless, it is expected that the difference between the models would be observable after a long time. Although this is not the scope of this paper, it would be interesting in a future study to compare the two models on the same experimental data.

3.5.4 Remark on iterative method

We recall that this formulation should allow to extend the method on two-dimensional unstructured grids. However, it requires to invert a system at each time iteration, which will become too costly in two dimensions. To anticipate the two-dimensional problem, this method has been tested using different iterative methods like conjugate gradient and Uzawa methods. In Figure 3.16, we show a comparison of the computing time for the implementation of the direct method and Uzawa method for $\mathbb{P}_1$-iso-$\mathbb{P}_2/\mathbb{P}_1$ approximation. In one dimension, it is not relevant to use one of these methods, while it will be necessary for the two dimension model.

3.6 Conclusion

In this paper, a variational formulation has been established for the one-dimensional dispersive model introduced in [43]. The main idea is to give a new framework in which it will be possible to extend the scheme to the two-dimensional model. To this aim, the finite-element method has been presented with two approximation spaces. First, the $\mathbb{P}_1/\mathbb{P}_0$ approximation has been done and we recover, as expected, the finite difference scheme, together with the good results proved in Chapter 2. Then, the $\mathbb{P}_1$-iso-$\mathbb{P}_2/\mathbb{P}_1$approximation has been studied to prepare the two-dimensional problem. We have validated the method using several numerical tests and studying the dispersive effect on geophysical situations.

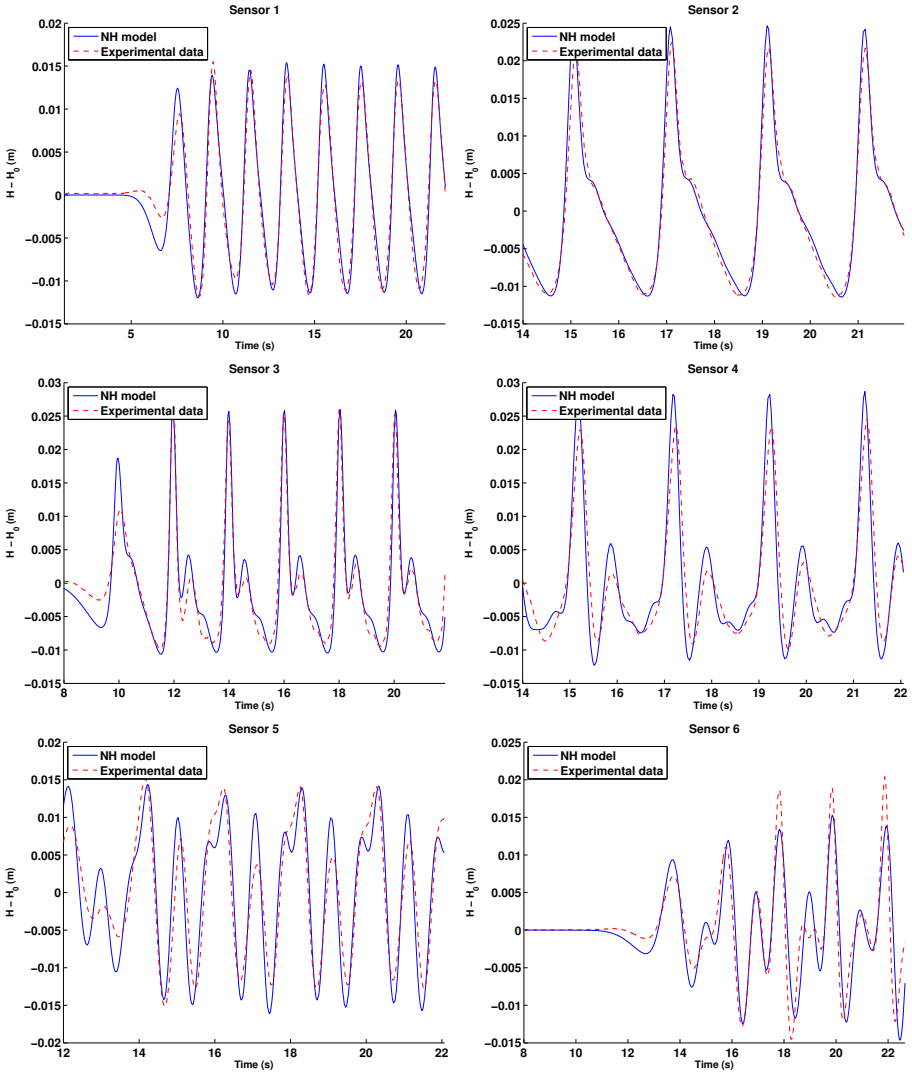

Figure 3.15: Comparison between measured and computed elevations on Dingemans test for the six first sensors.

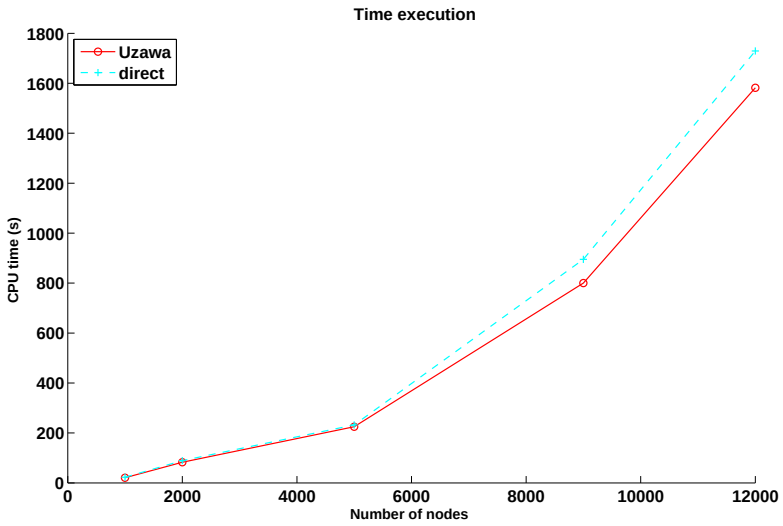

Figure 3.16: Comparison of the computing time (CPU) for the direct method and Uzawa method with $\mathbb{P}_1$-iso-$\mathbb{P}_2/\mathbb{P}_1$ approximation.

Chapter 4

A numerical method for a two-dimensional dispersive shallow water system on unstructured grids

This work has been done in collaboration with Marie-Odile Bristeau, Edwige Godlewski, Anne Mangeney, Carlos Parés and Jacques Sainte-Marie. To be submitted

4.1 Introduction

Mathematical models for free surface flows are widely studied, however one still needs to improve the existing models as well as develop robust numerical methods. The most common way to represent the physical behavior of the free surface is to compute the solutions of the Shallow Water equations. These equations are based on a shallowness assumption and lead to assuming the pressure is hydrostatic. Therefore, they are used for many geophysical flows on rivers, lakes, oceans where the characteristic horizontal length is much greater than the depth. This is the case when we want to simulate the propagation of tsunamis.

However, depending on the regime of the flow, this model can be inappropriate, in particular, when the hydrostatic assumption is no longer valid, what we call dispersive effects appear and then more complex models have to be used to represent these effects. Many free surface models are available to take into consideration this dispersive effect, see [86] for the classical Green-Naghdi (GN) model and [29, 48, 62, 43] for other kinds of non hydrostatic models with bathymetry. One of the difficulties of these models arises in the development of robust numerical methods. In this paper, we propose a new numerical scheme for a depth-averaged model derived in [43] and which is based on the minimization of the energy (see [112], this property provides a consistency with the Euler system [43] in terms of energy.

The non linear Shallow Water model with topograpphy is a hyperbolic system with source term, which has been studied extensively and the literature provides efficient algorithms for this model, see [83, 32] for the theory of hyperbolic systems with source term and [7, 12, 11, 9, 14] for numerical methods for the Shallow Water system with topography. Since non hydrostatic models are no longer hyperbolic, it is necessary to propose new numerical algorithms. Several approaches have been proposed to solve these kinds of models, especially in one dimension or in two dimensions with a structured grid (see [51, 29, 48, 72, 108]). A discretization with a Galerkin method has been proposed in [62] to treat the high order terms of the dispersive part, and more recently (2016), A. Duran and F. Marche performed an hybrid method [63] for the two-dimensional GN model. Indeed, there is a real need of methods to capture dispersion with a good accuracy and for real cases.

In this paper, we propose a new approach dealing with a formuation without high order terms, we treat the depth-averaged Euler system developed in [43] where the non-hydrostatic pressure is an unknown of the system. The aim is to provide a robust numerical method for the two-dimensional model on an unstructured grid. The objective is to have a stable method to simulate real cases where the topography can be complex and needs an irregular mesh. Moreover, it gives the possibility to perform adaptative meshes if one wants to refine the mesh in the areas where the dispersive effects are expected. For

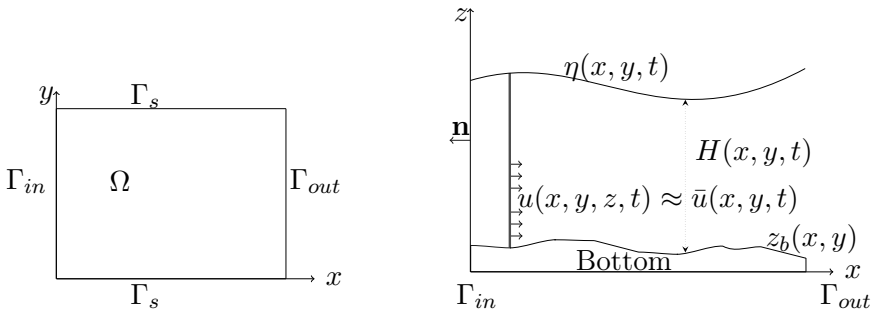

(a) View from above. (b) Vertical cross section.

Figure 4.1: Model domain and notations.

instance, the dispersive contribution can have a significant impact in the water depth for the propagation of tsunamis [81],[22]. We start with the formulation proposed in Chapter 3, where the authors have combined a finite-volume scheme with a finite element scheme for the one dimensional non-hydrostatic model using a Chorin-Temam splitting method (initially described in [138]).

The paper is organized as follows. In the next section, we recall the depth-averaged Euler system completed with standard boundary conditions. The Section 4.2 is devoted to the Chorin-Temam approach (prediction-correction scheme) applied for the model problem, while in Section 4.4, we focus on the mixed problem which corresponds in this case to the correction part of the prediction-correction scheme. In Section 4.5, we propose two approximation spaces (P1/P1 and P1-isoP2/P1) for the finite element scheme applied to the mixed problem. Finally we validate the implementations using comparisons with analytical solutions, and then we give a geophysical application.

4.2 The model

4.2.1 The averaged Euler system

We consider a two-dimensional domain $\Omega \subset \mathbb{R}^2$ delimited by the boundary $\Gamma = \Gamma_{in} \cup \Gamma_{out} \cup \Gamma_s$ as described in Figure 4.1a. We denote by $H(x,y,t)$ the water depth, $z_b(x,y)$ the topography, $\mathbf{u}(x,y,t)$ the averaged velocity of the fluid $\mathbf{u} = (u,v,w)^t$ and p the non hydrostatic pressure (see Figure 4.1b).

The two-dimensional depth-averaged Euler system described in [43], [141] reads:

$$\frac{\partial H}{\partial t} + \frac{\partial Hu}{\partial x} + \frac{\partial Hv}{\partial y} = 0, \tag{4.1}$$

$$\frac{\partial Hu}{\partial t} + \frac{\partial}{\partial x}(Hu^2) + \frac{\partial}{\partial y}(Huv) + \frac{\partial}{\partial x}(g\frac{H^2}{2} + Hp) = -(gH + 2p)\frac{\partial z_b}{\partial x}, \tag{4.2}$$

$$\frac{\partial Hv}{\partial t} + \frac{\partial}{\partial x}(Huv) + \frac{\partial}{\partial y}(Hv^2) + \frac{\partial}{\partial y}(g\frac{H^2}{2} + Hp) = -(gH + 2p)\frac{\partial z_b}{\partial y}, \tag{4.3}$$

$$\frac{\partial Hw}{\partial t} + \frac{\partial Huw}{\partial x} + \frac{\partial Hvw}{\partial y} = 2p, \tag{4.4}$$

completed with the incompressibility condition:

$$\frac{\partial Hu}{\partial x} + \frac{\partial Hv}{\partial y} - u\frac{\partial(H + 2z_b)}{\partial x} - v\frac{\partial(H + 2z_b)}{\partial y} + 2w = 0. \tag{4.5}$$

Equation (4.5) is obtained by an average of the free divergence condition of the Euler system.

The model (4.1)-(4.5) can be written in a more condensed form:

$$\frac{\partial H}{\partial t} + \nabla_0 \cdot (H\mathbf{u}) = 0, \tag{4.6}$$

$$\frac{\partial H\mathbf{u}}{\partial t} + \nabla_0 \cdot (H\mathbf{u} \otimes \mathbf{u}) + \nabla_0(\frac{g}{2}H^2) + \nabla_{sw}(p) = -gH\nabla_0(z_b), \tag{4.7}$$

$$\mathrm{div}_{sw}(\mathbf{u}) = 0, \tag{4.8}$$

where we define the operators ∇_0 and div_0 by

$$\nabla_0 f = \begin{pmatrix} \frac{\partial f}{\partial x} \\ \frac{\partial f}{\partial y} \\ 0 \end{pmatrix}, \quad \mathrm{div}_0 \mathbf{v} = \nabla_0 \cdot \mathbf{v}. \tag{4.9}$$

Also, we give an interpretation of the non-hydrostatic contribution by defining a shallow water version of the pressure gradient ∇_{sw} and the divergence operator div_{sw}. Assuming that f and $\mathbf{v} = (v_1, v_2, v_3)^T$ are smooth enough:

$$\nabla_{sw} f = \begin{pmatrix} H\frac{\partial f}{\partial x} + f\frac{\partial \zeta}{\partial x} \\ H\frac{\partial f}{\partial y} + f\frac{\partial \zeta}{\partial y} \\ -2f \end{pmatrix}, \tag{4.10}$$

$$\mathrm{div}_{sw}(\mathbf{v}) = \frac{\partial Hv_1}{\partial x} + \frac{\partial Hv_2}{\partial y} - v_1\frac{\partial \zeta}{\partial x} - v_2\frac{\partial \zeta}{\partial y} + 2v_3 \tag{4.11}$$

where we use the notation

$$\zeta = H + 2z_b. \tag{4.12}$$

Notice that we consider the non-hydrostatic pressure p as an unknown of the model, but we can write the total pressure p_{tot} as:

$$p_{tot} = g\frac{H}{2} + p, \tag{4.13}$$

where we take into account the hydrostatic pressure $g\frac{H}{2}$. An important property is that the operators div_{sw} and ∇_{sw} satisfy the duality relation

$$\int_\Omega \nabla_{sw}(f)\cdot\mathbf{v} = -\int_\Omega \mathrm{div}_{sw}(\mathbf{v})f + \int_\Gamma Hf\mathbf{v}\cdot\mathbf{n}, \tag{4.14}$$

where $\mathbf{n}$ is the outward unit normal vector to the boundary Γ. This property is crucial for the algorithm presented in the following since we will consider a mixed problem in velocity/pressure (see Section 4.4), which will lead, at the numerical level, to having an operator for the pressure and its transpose for the velocity.

4.2.2 The boundary conditions

The model problem (4.6)-(4.8) is completed with the following boundary conditions. Since we are considering a channel as the model domain with an inlet Γ_{in} and an outlet Γ_{out}, we impose specific conditions on each boundary. The inflow is set by imposing a given discharge $\mathbf{q_g}(x,t)$ on Γ_{in}, and a water depth $h_g(x,t)$ is imposed on Γ_{out}. Finally, we prescribe slip boundary conditions for the velocity at the walls of the channel Γ_s:

$$H\mathbf{u}(\mathbf{x},t) = \mathbf{q_g}(\mathbf{x},t) \quad \text{on } \Gamma_{in}, \tag{4.15}$$

$$H(\mathbf{x},t) = h_g(\mathbf{x},t) \quad \text{on } \Gamma_{out}, \tag{4.16}$$

$$\mathbf{u}(\mathbf{x},t)\cdot\mathbf{n} = 0 \quad \text{on } \Gamma_s. \tag{4.17}$$

In most cases, we keep these boundary conditions in the numerical experiment, but we can also change the outflow boundary condition to have a free outflow by imposing a Neumann boundary condition for the elevation:

$$\nabla H\cdot\mathbf{n} = 0 \quad \text{on } \Gamma_{out}. \tag{4.18}$$

4.3 Time and space discretizations

As for the one dimensional system (see Chapter 3), the problem (4.6)-(4.8) is solved using a Chorin-Temam splitting scheme (see [50, 138, 90, 92]). Let us recall here the general idea of the splitting scheme.

4.3.1 Prediction - Correction scheme

The prediction-correction method is widely used to approximate the Navier-Stokes equations and is based on a time-splitting scheme. For each time step, the problem is solved in two steps, in the first one, we use a finite-volume method to solve the hyperbolic part which is a Shallow Water system with topography (where the non hydrostatic pressure p is not evaluated). This allows us to get a first predicted state which is not divergence free.

In the second step, we update the predicted state with the shallow water version of the gradient pressure evaluated in such a way that the velocity satisfies the divergence free condition (4.5).
Let us denote by X the vectors of unknowns:

$$X = \begin{pmatrix} H \\ Hu \\ Hv \\ Hw \end{pmatrix}$$

and $F(X)$ the matrix:

$$F(X) = \begin{pmatrix} Hu & Hv \\ Hu^2 + \frac{g}{2}H^2 & Huv \\ Huv & Hv^2 + \frac{g}{2}H^2 \\ Huw & Hvw \end{pmatrix}, \tag{4.19}$$

and set

$$S(X) = \begin{pmatrix} 0 \\ -gH\frac{\partial z_b}{\partial x} \\ -gH\frac{\partial z_b}{\partial y} \\ 0 \end{pmatrix} \quad \text{and} \quad R_{nh} = \begin{pmatrix} 0 \\ \nabla_{sw}(p) \end{pmatrix}. \tag{4.20}$$

Then, the system (4.6)-(4.8) can be written

$$\frac{\partial X}{\partial t} + \mathrm{div}_0 F(X) + R_{nh} = S(X), \tag{4.21}$$

$$\mathrm{div}_{sw}(\mathbf{u}) = 0. \tag{4.22}$$

We set t^0 the initial time and $t^{n+1} = t^n + \Delta t^n$ where Δt^n satisfies a stability condition (CFL) and the state X^n will denote an approximation of $X(t^n)$. For each time step, we consider an intermediate state which will be denoted with the superscript $^{n+1/2}$. So the first step leads to solving the hyperbolic system with source terms in order to get the state $X^{n+1/2} = (H^{n+1/2}, (Hu)^{n+1/2}, (Hv)^{n+1/2}, (Hw)^{n+1/2})^T$. Finally, the semi discretization in time can be summarized in the following steps:

$$X^{n+1/2} = X^n - \Delta t^n \mathrm{div}_0 F(X^n) + \Delta t S(X^n), \tag{4.23}$$

$$X^{n+1} = X^{n+1/2} - \Delta t^n R_{nh}^{n+1}, \tag{4.24}$$

$$\mathrm{div}_{sw}\,\mathbf{u}^{n+1} = 0. \tag{4.25}$$

Equation (4.24) allows us to correct the predicted value $X^{n+1/2}$ in order to obtain a state which satisfies the divergence free condition (4.25). The equation satisfied by the pressure is then an elliptic equation which is obtained by applying the shallow water divergence operator to the equation (4.24) and reads:

$$\mathrm{div}_{sw}\left(\frac{\nabla_{sw}\ p^{n+1}}{H^{n+1}}\right) = \frac{1}{\Delta t^n}\mathrm{div}_{sw}\left(\frac{(H\mathbf{u})^{n+1/2}}{H^{n+1/2}}\right). \tag{4.26}$$

Once the pressure has been determined by an elliptic equation (4.26), the correction step (4.24) gives the final step X^{n+1}.
In this paper, we will focus on the second step of the scheme, namely Equations (4.23)-(4.25), which we discretize by a finite element method. Therefore, we will consider the state $X^{n+1/2}$ as a given state and the state X^{n+1} as the unknown. The operator $\mathrm{div}_{sw}\left(\frac{\nabla_{sw}}{H}\right)$ is a shallow water version of the Laplacian operator and is denoted by $\triangle_{sw}$, it is written

$$\begin{aligned}\triangle_{sw}\ p \ &= \ H\ \triangle\ p + \frac{\partial p}{\partial x}\frac{\partial H}{\partial x} + \frac{\partial p}{\partial y}\frac{\partial H}{\partial y} \\ &\quad + p\left(\triangle\ \zeta - \frac{1}{H}\left(\left(\frac{\partial \zeta}{\partial x}\right)^2 + \left(\frac{\partial \zeta}{\partial y}\right)^2 + 4\right)\right),\end{aligned} \tag{4.27}$$

with ζ given by (4.12). The operator (4.27) can be written in the form of a Sturm-Liouville operator, but it is still a tricky task to study the equation (4.26) since it requires studying the differential term in factor of p: $\triangle\ \zeta - \frac{1}{H}\left(\left(\frac{\partial \zeta}{\partial x}\right)^2 + \left(\frac{\partial \zeta}{\partial y}\right)^2 + 4\right)$.

4.3.2 Space discretization

Concerning the space discretization, each step, prediction step and correction step, is solved with its own scheme. The method relies on a combination between a finite volume scheme for the hyperbolic part (4.23) and a finite element scheme for the elliptic part (see the correction step in Section 4.3.1). The idea is to start with a primal mesh which is triangular, then a dual mesh is built by the finite volume cells centered on the vertices.
Let us consider Ω the computational domain with boundary Γ, which is assumed to be polygonal. Let $\mathscr{T}$ be a triangulation of Ω. We denote by S_h the set of the vertices of the mesh:

$$S_h = \{s_i = (x_i, y_i) \in \mathscr{T}\}. \tag{4.28}$$

We recall here the general formalism of finite volumes on unstructured meshes, and the finite element method we use for the correction part will be detailed in Section 4.5.
Let us define the finite volume cell C_i associated to the vertex s_i. The cells C_i are built by joining the centers of mass of the triangles surrounding each vertex s_i. We use the

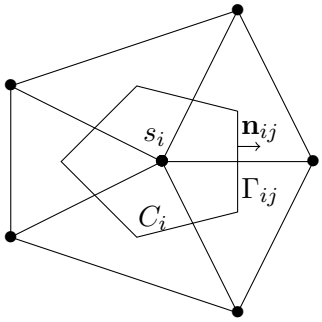

Figure 4.2: Representation of the dual mesh

following notations (see Figure 4.2):

- $|C_i|$, area of C_i,
- Γ_{ij}, boundary edge between the cells C_i and C_j,
- L_{ij}, length of Γ_{ij},
- $\mathbf{n}_{ij}$, unit normal to Γ_{ij}, outward to C_i ($\mathbf{n}_{ji} = -\mathbf{n}_{ij}$),
- $\mathscr{K}_i$ the set of nodes connected to the node s_i.

Remark 4.3.1. *The variables $H, H\mathbf{u}$ are estimated first as constant mean values on the cells C_i by the finite volume scheme, which gives the intermediate state $X^{n+1/2}$. For the finite element scheme, the state X^{n+1} is approximated at the vertices of the triangles, and for the required value of $X^{n+1/2}$ at the node s_i, we use the constant mean value computed on the cell C_i. Similarly, for the next finite volume step, the required value X^{n+1} at cell C_i is given by the value at node s_i. Therefore, combining the finite volume and the finite element approximations, we will denote by X_i both the constant mean value on cell C_i and the value at node s_i.*

4.3.3 Finite volume scheme for the prediction part

We denote by X_i^n the approximation of $X(t^n)$ on a finite volume cell C_i, the state X_i^n is the approximation of the cell average of $X(t^n, \mathbf{x})$:

$$X_i^n \simeq \frac{1}{mes(C_i)} \int_{C_i} X(\mathbf{x}, t^n) d\mathbf{x}. \tag{4.29}$$

Then, the approximation of the prediction step (4.23) can be summarized as follows:

$$H_i^{n+1/2} = H_i^n - \sum_{j \in \mathscr{K}_i} \sigma_{ij} \mathcal{F}_H(H_i^n, H_j^n) - \sigma_i \mathcal{F}_H(H_i^n, H_{e,i}^n), \tag{4.30}$$

$$
\begin{aligned}
(H\mathbf{u})_i^{n+1/2} &= (H\mathbf{u})_i^n - \sum_{j\in\mathscr{K}_i} \sigma_{ij}\mathcal{F}_{(H\mathbf{u})}((H\mathbf{u})_i^n,(H\mathbf{u})_j^n) \\
&\quad -\sigma_i\mathcal{F}_{(H\mathbf{u})}((H\mathbf{u})_i^n,(H\mathbf{u})_{e,i}^n),
\end{aligned} \tag{4.31}
$$

where σ_{ij} depends on $mes(C_i)$, Δt^n and the length of the edges of cells and ensures the stability of the scheme. Similarly, $\sigma_i = \sigma_{ii}$ is computed for the boundary cells of the domain and $X_{e,i}^n$ is a fictive state associated to a cell C_i at the boundary of the domain (see [41]). The numerical fluxes $\mathcal{F}_H$ (resp. $\mathcal{F}_{(H\mathbf{u})}$) are the numerical fluxes corresponding to H (resp. $H\mathbf{u}$). We do not give details on the flux $\mathcal{F}$. For the numerical results presented in this paper, the numerical fluxes are computed by a kinetic solver with a hydrostatic reconstruction for the water depth (see [10]) but it is not the only possible choice. This ensures the well balanced property of the scheme (see [10]). In this part, the boundary conditions (4.15)-(4.17) are treated as a Riemann problem at the interface (see [41] for more details about the treatment of the boundary conditions for the Shallow Water system).

4.4 The mixed problem

In this section, $X^{n+1/2}$ is given following the Chorin-Temam approach, by (4.23) as explained in Section 4.3.1. We now study the mixed problem corresponding to the correction step, that is to say the system (4.24)-(4.25), and we give a variational formulation of the problem together with an appropriate treatment of the boundary conditions at the continuous level in order to be compatible with the hyperbolic part. This will make it possible to construct the finite element scheme for this problem. To do so, we consider the model domain Ω of Figure 4.1 with classical boundary conditions (4.15). The correction step consists in computing the shallow water pressure in order to satisfy the shallow water divergence free condition (4.8). Notice that the water elevation is not corrected and is given by the hyperbolic part, then the equation (4.24) reads

$$H^{n+1} = H^{n+1/2}, \tag{4.32}$$

$$(Hu)^{n+1} + \Delta t^n \left(H^{n+1}\frac{\partial p^{n+1}}{\partial x} + p\frac{\partial \zeta^{n+1}}{\partial x}\right) = (Hu)^{n+1/2}, \tag{4.33}$$

$$(Hv)^{n+1} + \Delta t^n \left(H^{n+1}\frac{\partial p^{n+1}}{\partial y} + p\frac{\partial \zeta^{n+1}}{\partial y}\right) = (Hv)^{n+1/2}, \tag{4.34}$$

$$(Hw)^{n+1} - 2\Delta t^n\, p^{n+1} = (Hw)^{n+1/2}, \tag{4.35}$$

completed with the divergence free condition (4.25) and the boundary conditions (4.15)-(4.17). From now on, we drop the superscript $^{n+1}$ and note Δt for Δt^n, thus the system (4.33)-(4.35) and (4.25) is written:

$$H\mathbf{u} + \Delta t \nabla_{sw}\, p = H\mathbf{u}^{n+1/2}, \tag{4.36}$$

$$\mathrm{div}_{sw}\,(\mathbf{u}) \;=\; 0, \tag{4.37}$$

where H denotes the unique value $H^{n+1} = H^{n+1/2}$. This mixed problem in velocity/pressure leads to solving the pressure equation (4.26), and then to updating the velocity with the equation (4.36). Equations (4.36)-(4.37) are the "grad-div" formulation of the problem. The boundary conditions need to be detailed since they have to be consistent with the prediction part. This is the object of the next section.

4.4.1 Compatible boundary conditions

In geophysical models such as the Shallow Water model, it is usual to impose an inflow condition on the inlet Γ_{in}, namely $H\mathbf{u}$, and the water depth at the outflow or a free outflow, as defined by (4.15) and (4.16). At the hyperbolic level, this choice depends on the Froude number $Fr = \frac{|\mathbf{u}|}{\sqrt{gH}}$ which characterizes the flow (fluvial or torrential). In this part, we apply compatible boundary conditions on the mixed system depending on the regime chosen for the Saint-Venant problem at the prediction step. The mixed formulation will allow us to impose boundary conditions on the velocity or the pressure.

Inflow /outflow

Let us take the two-dimensional inflow $\mathbf{Q}_0 = ((Hu)_0^{n+1/2}, (Hv)_0^{n+1/2})^t$ which is imposed at the hyperbolic part; the vertical velocity w_0 will be treated independently. Many strategies can be applied to satisfy compatible boundary conditions. As can be seen in the equations (4.33)-(4.34), a natural choice is to keep $\mathbf{Q}_0$ the same as in the hyperbolic part, then we will impose a condition on the inlet velocity $\mathbf{u}\cdot\mathbf{n} = (u_0, v_0)^T \cdot \mathbf{n}$, with $\mathbf{n} = (n_x, n_y, 0)^T$. on Γ_{in}.
Considering the pressure equation (4.26) and following the same procedure detailed in Chapter 3, we can deduce that this corresponds to apply a shallow water version of a Neumann boundary condition for the pressure:

$$\nabla_{sw}\, p \cdot \mathbf{n} = 0 \text{ on } \Gamma_{in}. \tag{4.38}$$

In contrast, for the outflow, we impose the water depth in the hyperbolic step and recommend a homogeneous Dirichlet boundary condition for the pressure in order to let the discharge free at the outlet, namely $p|_{\Gamma_{out}} = 0$.

Slip boundary conditions

For the wall of the channel represented by Γ_s in Figure 4.1a , we assume a slip condition for the hyperbolic part $\mathbf{u}^{n+1/2}\cdot\mathbf{n}|_{\Gamma_s} = 0$ with a Neumann boundary condition for H (see [41]) and we maintain this condition in the dispersive part, namely $\mathbf{u}\cdot\mathbf{n}|_{\Gamma_s} = 0$. Still from the pressure equation (4.26) and in the same spirit as in Chapter 3, we deduce that this leads

to having $\nabla_{sw}(p)\cdot\mathbf{n}|_{\Gamma_s}=0$. Since $\frac{\partial H}{\partial x}|_{\Gamma_s}=0$, it gives a Neumann boundary condition for the pressure $\frac{\partial p}{\partial \mathbf{n}}=0$ on Γ_s.

4.4.2 The variational formulation

In this section, we distinguish two variational formulations using the shallow water divergence or gradient operator and we explain how to chose the most judicious one in practice.

Formulation with the shallow water divergence operator

First of all, we assume $\nabla\zeta\in(L^\infty(\Omega))^2$, $p_0\in H^{-1/2}(\Gamma)$ and $H\in L^\infty(\Omega)$ is bounded below and above:

$$\alpha_1<H<\alpha_2,\quad \alpha_1,\alpha_2>0, \tag{4.39}$$

We consider the variational problem with Dirichlet boundary conditions for the pressure. We introduce the spaces:

$$\mathbf{V} = \{\mathbf{v}\in L^2(\Omega)^3,\ \mathrm{div}_{sw}(\mathbf{u})\in L^2(\Omega)\} \tag{4.40}$$

$$\mathbf{W} = \{\mathbf{w}\in\mathbf{V},\ \mathbf{w}\cdot\mathbf{n}=0 \text{ on } \Gamma_{in}\cup\Gamma_s\}. \tag{4.41}$$

The Hilbert space $\mathbf{W}$ is equipped with inner product $(.,.)_{\mathbf{W}}$ and induced norm $||.||_{\mathbf{W}} = ||.||_{\mathbf{L(\Omega)^2}} + ||\mathrm{div}_{sw}(.)||_{\mathbf{L^2(\Omega)}}$. Then the problem reads:
Find $\mathbf{u}\in\mathbf{W}$, $p\in L^2(\Omega)$ such that, $\forall\,\mathbf{v}\in\mathbf{W}$

$$\int_\Omega H\mathbf{u}\mathbf{v}\,d\mathbf{x}-\Delta t\int_\Omega \mathrm{div}_{sw}(\mathbf{v})\,p\,d\mathbf{x} = \int_\Omega H\mathbf{u}^{n+1/2}\cdot\mathbf{v}\,d\mathbf{x}-\int_{\Gamma_{out}} H\mathbf{v}\cdot\mathbf{n}\,p_0 ds, \tag{4.42}$$

$$\int_\Omega \mathrm{div}_{sw}(\mathbf{u})q\,d\mathbf{x} = 0,\quad \forall q\in L^2(\Omega), \tag{4.43}$$

where we assume $\mathbf{u}^{n+1/2}\in\mathbf{W}$. We introduce the bilinear forms

$$a(\mathbf{u},\mathbf{v}) = <H\mathbf{u},\mathbf{v}>, \tag{4.44}$$

$$b(\mathbf{v},q) = -\int_\Omega \mathrm{div}_{sw}(\mathbf{v})\,q\,d\mathbf{x},\quad \forall\mathbf{v}\in\mathbf{W}\ ,\forall q\in L^2(\Omega), \tag{4.45}$$

where $<\cdot,\cdot>_\Omega=(\cdot,\cdot)_{L2(\Omega)}$.
The problem reads:
Find $\mathbf{u}\in\mathbf{W}$, $p\in L^2(\Omega)$ such that

$$a(\mathbf{u},\mathbf{v})-\Delta t\,b(\mathbf{v},p) = <H\mathbf{u}^{n+1/2},\mathbf{v}>_\Omega - <H\mathbf{v}\cdot\mathbf{n}\,,p_0>_{\Gamma_{out}},\quad \forall\mathbf{v}\in\mathbf{W}, \tag{4.46}$$

$$b(\mathbf{u},q) = 0,\quad \forall q\in L^2(\Omega). \tag{4.47}$$

where $< \cdot, \cdot >_{\Gamma_{out}}$ represents the duality between $H^{-1/2}(\Gamma_{out})$ and $H^{1/2}(\Gamma_{out})$. For all $\mathbf{v} \in \mathbf{W}_0 = \{\mathbf{v} \in \mathbf{W}\ ,\ \mathrm{div}_{sw}(\mathbf{v}) = 0\}$, the problem becomes:
Find $\mathbf{u} \in \mathbf{W}_0$ such that

$$a(\mathbf{u}, \mathbf{v}) = < H\mathbf{u}^{n+1/2}, \mathbf{v} >_{\Omega} - < H\mathbf{v} \cdot \mathbf{n}\ , p_0 >_{\Gamma_{out}}, \quad \forall \mathbf{v} \in \mathbf{W}_0. \tag{4.48}$$

To impose a slip boundary condition on Γ_s for the velocity $\mathbf{u}$, we choose $\mathbf{u} - \bar{\mathbf{u}}_0 \in \mathbf{W}$ where $\bar{\mathbf{u}}_0$ is defined on $\bar{\Omega}$ such that $\bar{\mathbf{u}}_0|_{\Gamma_s} = \bar{\mathbf{u}}^{n+1/2}|_{\Gamma_s}$. In practice, this formulation requires to choose basis functions satisfying the slip condition in (4.41). Therefore, if we want to have a domain with a specific boundary, we will prefer the formulation using the shallow water gradient operator, which is described in the following.

Formulation using the shallow water gradient operator

In this section we give the variational formulation of the mixed problem (4.36)-(4.37) using the shallow water gradient operator, and completed with appropriate boundary conditions:

$$\begin{array}{rcll} \mathbf{u} \cdot \mathbf{n} & = & \mathbf{u}^{n+1/2} \cdot \mathbf{n} & \text{on } \Gamma_{in}, \\ \mathbf{u} \cdot \mathbf{n} & = & 0 & \text{on } \Gamma_s, \\ p & = & p_0 & \text{on } \Gamma_{out}. \end{array} \tag{4.49}$$

In (4.49), to give a general formulation, we have considered a non-homogeneous Dirichlet boundary condition for the pressure. We assume there exists $\bar{p}_0 \in Q$ a given pressure such that $p_0 = \bar{p}_0|_{\Gamma_{out}} \in H^{1/2}(\Gamma_{out})$. We define the spaces:

$$Q = \{q \in L^2(\Omega), \nabla_{sw}(q) \in L^2(\Omega)^3\}, \tag{4.50}$$

$$Q_0 = \{q \in Q\ ,\ q|_{\Gamma_{out}} = 0\}. \tag{4.51}$$

Using the duality relation (4.14), we have:

$$\int_{\Omega} \nabla_{sw}(q) \cdot \mathbf{u}\ d\mathbf{x} - \int_{\Gamma} qH\mathbf{u} \cdot \mathbf{n}\ ds = 0 \quad \forall q \in Q,$$

then writing

$$\int_{\Gamma} qH\mathbf{u} \cdot n\ ds = \int_{\Gamma_{in}} qH\mathbf{u} \cdot \mathbf{n}\ ds + \int_{\Gamma_s} qH\mathbf{u} \cdot \mathbf{n}\ ds + \int_{\Gamma_{out}} qH\mathbf{u} \cdot \mathbf{n}\ ds, \tag{4.52}$$

and, using the boundary conditions (4.49), we have

$$\int_{\Gamma} qH\mathbf{u} \cdot \mathbf{n}\ ds = \int_{\Gamma_{in}} qH\mathbf{u}^{n+1/2} \cdot \mathbf{n}\ ds, \tag{4.53}$$

where the slip boundary condition is imposed in the weak form $\int_{\Gamma_s} qH\mathbf{u}\cdot\mathbf{n} = 0$. We apply the procedure proposed for the Navier-Stokes equations in [94]. Therefore, the problem (4.36)-(4.37) completed with (4.49) reads:
Find $\tilde{p} = p - \bar{p}_0 \in Q_0$, $p \in Q$, $\mathbf{u} \in (L^2(\Omega))^3$ such that,

$$\int_\Omega (H\mathbf{u} + \Delta t \nabla_{sw}\tilde{p})\cdot\mathbf{v}\, d\mathbf{x} = \int_\Omega H\mathbf{u}^{n+1/2}\cdot\mathbf{v}\, d\mathbf{x} \quad \forall \mathbf{v} \in (L^2(\Omega))^3, \tag{4.54}$$

$$\int_\Omega \nabla_{sw}(q)\ \mathbf{u}\, d\mathbf{x} = \int_{\Gamma_{in}} qH\mathbf{u}^{n+1/2}\cdot\mathbf{n}\, ds \quad \forall q \in Q_0. \tag{4.55}$$

Finally, we consider the following problem:
Find $\mathbf{u} \in (L^2(\Omega))^3$, with $p \in Q$ such that, $\forall \mathbf{v} \in (L^2(\Omega))^3$,

$$\int_\Omega (H\mathbf{u} + \Delta t \nabla_{sw} p)\cdot\mathbf{v}\, d\mathbf{x} = \int_\Omega H\mathbf{u}^{n+1/2}\cdot\mathbf{v}\, d\mathbf{x} - \Delta t\int_\Omega \nabla_{sw}\bar{p}_0\cdot\mathbf{v}\, d\mathbf{x} \quad , \tag{4.56}$$

$$\int_\Omega \nabla_{sw}(q)\ \mathbf{u}\, d\mathbf{x} = \int_{\Gamma_{in}} qH\mathbf{u}^{n+1/2}\cdot\mathbf{n}\, ds \quad \forall q \in Q_0. \tag{4.57}$$

Notice that we use the formulation with the shallow water gradient operator instead of divergence in order to avoid choosing basis functions satisfying the slip boundary condition. This last formulation allows the problem to be solved using a finite element method (see Section 4.5) with the appropriate boundary conditions (4.49) and is equivalent to solving the elliptic problem (4.26).

The inf-sup condition For the two formulations "div_{sw}" (*i.e* Equations (4.42)-(4.43)) and "∇_{sw}" (*i.e* Equations (4.54)-(4.55)), we can prove the inf-sup condition to ensure the problems are well posed. This is detailed in 3.

The pressure equation Following the procedure of the one-dimensional problem in Chapter 3, we set $\mathbf{v} = \frac{\nabla_{sw}(q)}{H}$ and take homogeneous boundary conditions for the pressure on Γ, it leads to a variational formulation of the problem in the form:

$$(\Delta_{sw}\, p, q) = \frac{1}{\Delta t^n}\left(\mathrm{div}_{sw}(\mathbf{u}^{n+1/2}), q\right) - \frac{1}{\Delta t^n}, \quad \forall q \in Q_{0,sw}, \tag{4.58}$$

where

$$Q_{sw} = \{q \in Q, |\mathrm{div}_{sw}\left(\frac{\nabla_{sw}\, q}{H}\right) \in L^2(\Omega)\},$$

$$Q_{sw} = \{q \in Q,\ \ q|_\Gamma = 0\}.$$

The operator Δ_{sw} is the Laplacian operator defined by (4.26).

4.5 Finite element approximations for the mixed problem

In this part, we apply the finite element method for the correction part (4.36)-(4.37), using the formulation with the shallow water gradient operator (4.56)-(4.57). We need two discrete spaces, one for the velocity and one for the approximation of the pressure. We propose two implementations, the first one is the P1/P1 and the second one is the P1-isoP2/P1 spaces. For both, we give the discrete formulation and we provide a comparison of the numerical results (see Section 4.7.1) in order to choose the most accurate solution. As usual, P_k denotes the space of polynomials of two variables of degree $\leq k$, and P_j/P_i denotes the pair of approximation spaces where P_j is related to the velocity and P_i is related to the pressure.

4.5.1 A P1/P1 approximation

For this first implementation, we choose a P1/P1 finite element approximation (see [134, 71]) on the primal mesh $\mathscr{T}$ introduced in 4.3.3, on which we approximate the variables at the nodes of the triangles (see Figure 4.2). Let us introduce the discrete spaces of approximation:

$$\begin{aligned} V_h &= \{v_h \in C_0(\Omega_h), v_h|_T \in \mathrm{P1}\ \forall\ T \in \mathscr{T}\}, \\ Q_h &= \{q_h \in C_0(\Omega_h), q_h|_T \in \mathrm{P1}\ \forall\ T \in \mathscr{T}\ ,\ q_h|_{\Gamma_{out}} = 0\}, \end{aligned}$$

with the dimensions $\dim(Q_h) = M$, $\dim(V_h) = N$. For the sake of clarity, we denote the vectors in bold characters and $\mathbf{V_h} = (V_h)^3$. We take $\mathbf{u}_h \in \mathbf{V_h}$, $p_h \in Q_h$ the piecewise linear approximations of $\mathbf{u}$, p on the triangles of $\mathscr{T}$. In addition, we assume $H_h \in V_h$, $\zeta_h \in V_h$, so we introduce:

$$p_h(\mathbf{x}) = \sum_{j \in \mathcal{J}_M} p_j \varphi_j(\mathbf{x}) \quad , \quad H_h = \sum_{i \in \mathcal{I}_N} H_i \varphi_i(\mathbf{x}), \tag{4.59}$$

$$(H\mathbf{u})_h = \sum_{i \in \mathcal{I}_N} (H\mathbf{u})_i \varphi_i(\mathbf{x}), \qquad \zeta_h = \sum_{i \in \mathcal{I}_N} \zeta_i \varphi_i, \tag{4.60}$$

where $\mathcal{I}_N$ (resp. $\mathcal{J}_M$) is the set of indices of the space V_h (resp. Q_h) and $\{\varphi_j\}_{j \in \mathcal{J}_M}$ (resp. $\{\varphi_i\}_{i \in \mathcal{I}_N}$) are the basis functions of Q_h (resp. V_h) and

$$\mathbf{u}_h(\mathbf{x}) = \sum_{i \in \mathcal{I}_N} \mathbf{u}_i \varphi_i(\mathbf{x}), \tag{4.61}$$

with

$$\mathbf{u}_i = \begin{pmatrix} u_i \\ v_i \\ w_i \end{pmatrix} = \frac{1}{H_i} \begin{pmatrix} (Hu)_i \\ (Hv)_i \\ (Hw)_i \end{pmatrix}. \tag{4.62}$$

We use the definitions (4.62) in accordance with the finite volume approximation (4.30)-(4.31) (see Remark 4.3.1); we will use mass lumping in the integrals to be consistent with these definitions.
The discrete formulation of problem (4.42)-(4.43) reads:
Find $\mathbf{u}_h \in \mathbf{V_h}$, $p_h \in Q_h$ such that:

$$\begin{aligned}\int_\Omega H_h\mathbf{u}_h\cdot\mathbf{v}_h\,d\mathbf{x}+\Delta t\int_\Omega \nabla_{sw}p_h\cdot\mathbf{v}_h\,d\mathbf{x} &= \int_\Omega H_h\mathbf{u}_h^{n+1/2}\cdot\mathbf{v}_h\,d\mathbf{x}\\ &\quad -\Delta t\int_\Omega \nabla_{sw}p_0\cdot\mathbf{v}_h\,d\mathbf{x},\quad \forall\mathbf{v}_h\in\mathbf{V_h}, \quad (4.63)\\ \int_\Omega \nabla_{sw}\,q_h\cdot\mathbf{u}_h\,d\mathbf{x} &= \int_{\Gamma_{in}} q_hH_h\mathbf{u}_h^{n+1/2}\cdot\mathbf{n}\,ds,\quad \forall q_h\in Q_h. \quad (4.64)\end{aligned}$$

In order to describe the method, we introduce the following notations:

- $S_h=\{s_i=(x_i,y_i)\in\mathscr{T}\}$: the vertices of the triangular mesh (see (4.28)),
- $K_{h,i}=\{T\in\mathscr{T}|s_i\in T\}$: the triangles connected to a vertex s_i.

Using definitions (4.59)-(4.62), equations (4.63)-(4.64) become:

$$\begin{aligned}&\sum_{i\in\mathcal{I}_N}\left(\int_\Omega H_i\mathbf{u}_i\varphi_i(\mathbf{x})\cdot\mathbf{v}_h(\mathbf{x})\,dx\right)-\sum_{j\in\mathcal{J}_M}\Delta t\left(\int_\Omega\nabla_{sw}\,\varphi_j(\mathbf{x})\cdot\mathbf{v}_h(\mathbf{x})\,d\mathbf{x}\right)p_j\\ &=\sum_{i\in\mathcal{I}_N}\left(\int_\Omega H_i\mathbf{u}_i^{n+1/2}\varphi_i(\mathbf{x})\cdot\mathbf{v}_h(\mathbf{x})\,d\mathbf{x}\right),\quad\forall\mathbf{v}_h\in\mathbf{V_h}, \qquad (4.65)\end{aligned}$$

completed with the divergence free condition:

$$\sum_{i\in\mathcal{I}_N}\left(-\int_\Omega\nabla_{sw}\,q_h\,\cdot\varphi_i\mathbf{u}_i\,d\mathbf{x}\right)=\sum_{i\in\mathcal{I}_N}\int_{\Gamma_{in}}q_hH_i\mathbf{u}_i^{n+1/2}\varphi_i\cdot\mathbf{n},\quad\forall q_h\in Q_h. \qquad (4.66)$$

We introduce the pressure vector $P=(p_j)_{1\le j\le M}$ and the velocity vector $U=\begin{pmatrix}U_1, & U_2, & U_3\end{pmatrix}^t$, with $U_1=(u_i)_{1\le i\le N}$, $U_2=(v_i)_{1\le i\le N}$, and $U_3=(w_i)_{1\le i\le N}$. Then the problem (4.65)-(4.66) can be written as:

$$\begin{aligned}A_HU+\Delta t\tilde{B}P &= A_HU^{n+1/2}, \qquad (4.67)\\ \tilde{B}^tU-CU^{n+1/2} &= 0, \qquad (4.68)\end{aligned}$$

with the classical notations (see [134]) for the mass matrix A_H, the divergence operator matrix $\tilde{B}^t$, and the matrix of the boundary conditions C. The matrix A_H depends on the

water depth H and is composed of the three diagonal matrices M_H:

$$A_H = \begin{pmatrix} M_H & 0 & 0 \\ 0 & M_H & 0 \\ 0 & 0 & M_H \end{pmatrix},$$

with M_{Hji} the approximation of $\sum_{T\in K_{h,i}} \int_T H_i\varphi_i\varphi_j d\mathbf{x}$. More precisely, using mass lumping we obtain:

$$M_{Hji} = \sum_{T\in K_{h,i}} \frac{mes(T)}{3} H_i\delta_{ij}. \tag{4.69}$$

We have denoted by $\tilde{B}^t$ the shallow water divergence operator defined by (4.66):

$$\tilde{B} = \begin{pmatrix} \tilde{B}_1^t & \tilde{B}_2^t & \tilde{B}_3^t \end{pmatrix},$$

and using the definition of the shallow water operator ∇_{sw} in (4.10), we obtain:

$$\begin{aligned}
\tilde{B}^t_{1\,ji} &= \sum_{T\in K_{h,i}} \int_T \frac{\partial\varphi_j}{\partial x} H_i\varphi_i d\mathbf{x} + \sum_{T\in K_{h,i}} \int_T \varphi_i\varphi_j \frac{\partial\zeta_h}{\partial x} d\mathbf{x}, \\
\tilde{B}^t_{2\,ji} &= \sum_{T\in K_{h,i}} \int_T \frac{\partial\varphi_j}{\partial y} H_i\varphi_i d\mathbf{x} + \sum_{T\in K_{h,i}} \int_T \varphi_i\varphi_j \frac{\partial\zeta_h}{\partial y} d\mathbf{x}, \\
\tilde{B}^t_{3\,ji} &= 2 \sum_{T\in K_{h,i}} \int_T \varphi_i\varphi_j d\mathbf{x}.
\end{aligned}$$

And, the matrix C contains the discretization of the boundary terms:

$$\int_{\Gamma_{in}} qH\mathbf{u}^{n+1/2} \cdot \mathbf{n}\, ds, \tag{4.70}$$

which is made up with the three blocks:

$$C_{1,ji} = \int_{\Gamma_{in}} H_h\varphi_j\varphi_i n_1\, ds, \tag{4.71}$$

$$C_{2,ji} = \int_{\Gamma_{in}} H_h\varphi_j\varphi_i n_2\, ds, \tag{4.72}$$

$$C_{3,ji} = 0, \tag{4.73}$$

with $\mathbf{n} = (n_1, n_2, 0)$ the outward normal vector of the boundary Γ_{in}. Finally, the algebraic system (4.67)-(4.68) reads:

$$\begin{pmatrix} \frac{1}{\Delta t}M_H & 0 & 0 & \tilde{B}_1 \\ 0 & \frac{1}{\Delta t}M_H & 0 & \tilde{B}_2 \\ 0 & 0 & \frac{1}{\Delta t}M_H & \tilde{B}_3 \\ \tilde{B}_1^t & \tilde{B}_2^t & \tilde{B}_3^t & 0 \end{pmatrix} \begin{pmatrix} U_1 \\ U_2 \\ U_3 \\ P \end{pmatrix} = \begin{pmatrix} \frac{1}{\Delta t}M_H & 0 & 0 \\ 0 & \frac{1}{\Delta t}M_H & 0 \\ 0 & 0 & \frac{1}{\Delta t}M_H \\ C_1 & C_2 & C_3 \end{pmatrix} \begin{pmatrix} U_1^{n+1/2} \\ U_2^{n+1/2} \\ U_3^{n+1/2} \\ 0 \end{pmatrix} \quad (4.74)$$

By analogy with the continuous problem, applying the matrix $\tilde{B}^t$ to the equation (4.67), we obtain the discrete elliptic equation of the pressure:

$$\tilde{B}^t A_H^{-1} \tilde{B} P = (\tilde{B}^t - C) U^{n+1/2}, \quad (4.75)$$

which is the discretization of the pressure equation (4.58). We now give some numerical approximations of the integrals we use for each matrix. The matrix $\tilde{B}^t$ is computed with the following formulas:

$$\begin{aligned} \tilde{B}^t_{1\,ji} &= \sum_{T \in K_{h,i}} \frac{\partial \varphi_j}{\partial x}\Big|_T \int_T H_h \varphi_i \, d\mathbf{x} - \sum_{T \in K_{h,i}} \frac{\partial \zeta_h}{\partial x}\Big|_T \int_T \varphi_i \varphi_j \, d\mathbf{x}, \\ \tilde{B}^t_{2\,ji} &= \sum_{T \in K_{h,i}} \frac{\partial \varphi_j}{\partial y}\Big|_T \int_T H_h \varphi_i \, d\mathbf{x} - \sum_{T \in K_{h,i}} \frac{\partial \zeta_h}{\partial y}\Big|_T \int_T \varphi_i \varphi_j \, d\mathbf{x}, \\ \tilde{B}^t_{3\,ji} &= 2 \sum_{T \in K_{h,i}} \frac{mes(T)}{3} \delta_{ij}. \end{aligned}$$

In the first terms of $\tilde{B}^t_{1\,ji}$ and $\tilde{B}^t_{2\,ji}$, we use definition (4.59) of H_h with mass lumping, and we obtain the following formula:

$$\int_T H_h \varphi_i \, dx = \sum_k \int_T H_k \varphi_k \varphi_i \, d\mathbf{x} = \int_T H_i \varphi_i \, d\mathbf{x} = \frac{mes(T)}{3} H_i. \quad (4.76)$$

The projection of the shallow water divergence on a vertex of the mesh is defined by:

$$\mathrm{div}_{sw}\,(\mathbf{u}_h)|_j = \frac{3}{Supp(\varphi_j)} \sum_{i \in \mathcal{I}_N} \int_\Omega \nabla_{sw}\, \varphi_j(\mathbf{x}) \cdot \boldsymbol{\varphi}_i(\mathbf{x}) \, d\mathbf{x}\, \mathbf{u}_i \quad \forall \boldsymbol{\varphi}_i \in \boldsymbol{V}_h, \varphi_j \in Q_h,$$

where $Supp(\varphi_j)$ is the area of the support of the function φ_j and is computed by: $Supp(\varphi_j) = \sum_{T \in K_{h,j}} mes(T)$.

Remark 4.5.1. *Notice that mass lumping is chosen for the approximation of M_H in order to be consistent at the update step:*

$$A_H U + \Delta t B P = A_H U^{n+1/2},$$

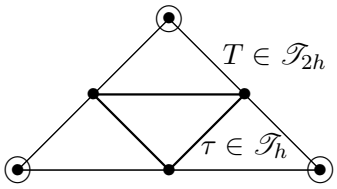

Figure 4.3: Representation of the triangulation. The velocity is evaluated on the black nodes, while the pressure is evaluated on the circles.

since $U^{n+1/2}$ is not written in the same approximation space in the finite volume part, it is more convenient to have a diagonal matrix in practice.

4.5.2 A P1-isoP2/P1 approximation

In this part, we propose another approximation by finite elements, using this time the spaces P1-iso-P2/ P2 (see [134]) in which we define a coarse triangular mesh $\mathscr{T}_{2h}$ and a fine mesh $\mathscr{T}_h$. The fine mesh corresponds to the primal mesh introduced for the finite volume method 4.3.3. Unlike the previous approximation, the velocity and the pressure are defined in two different spaces. Let us introduce the discrete spaces of approximation:

$$\begin{aligned} V_h &= \{v_h \in C_0(\Omega_h),\ \mathbf{v}_h|_\tau \in \mathrm{P1},\ \forall\, \tau \in \mathscr{T}_h\}, \\ Q_h &= \{q_h \in C_0(\Omega_h),\ q_h|_T \in \mathrm{P1},\ \forall\, T \in \mathscr{T}_{2h}\ ,\ q_h|_{\Gamma_{out}} = 0\}, \end{aligned}$$

with the dimensions $\dim(V_h) = N$ and $\dim(Q_h) = M$. In addition, we assume $H_h \in V_h$. In practice, the triangulation $\mathscr{T}_h$ is obtained by subdividing each triangle $T \in \mathscr{T}_{2h}$ into four triangles τ by joining the middle of the edges, as shown in Figure 4.3. In these spaces of approximation, the velocity on the coarse mesh is evaluated with the same degree of freedom as the P2 space. Then we expect a better approximation using P1-isoP2/P1 rather than P1/P1 on the coarse mesh.
In order to describe the method, we introduce the following notations:

- $S_h = \{s_i = (x_i, y_i) \in \mathscr{T}_h\}$: the vertices of the fine mesh,
- $S_{2h} = \{s_j = (x_j, y_j) \in \mathscr{T}_{2h}\}$: the vertices of the coarse mesh,
- $K_{h,i} = \{\tau \in \mathscr{T}_h | s_i \in \tau\}$: the triangles of the fine mesh connected to node s_i,
- $K_{2h,j} = \{T \in \mathscr{T}_{2h} | s_j \in T\}$: the triangles of the coarse mesh connected to node s_j.

We take $\mathbf{u}_h \in \mathbf{V_h}$ and $p_h \in Q_h$:

$$p_h(\mathbf{x}) = \sum_{j \in \mathcal{J}_M} p_i \phi_j(\mathbf{x}) \quad , \quad H_h = \sum_{i \in \mathcal{I}_N} H_i \varphi_i(\mathbf{x}) \quad , \quad (H\mathbf{u})_h = \sum_{i \in \mathcal{I}_N} (H\mathbf{u})_i \varphi_i(\mathbf{x}),$$

where ϕ_j (resp. φ_i) are the basis functions of Q_h (resp. V_h) and

$$\mathbf{u}_h(\mathbf{x}) = \sum_{i \in \mathcal{I}_N} \mathbf{u}_i \varphi_i(\mathbf{x}),$$

with $\mathbf{u}_i$ defined as in (4.61). Then matrix $\tilde{B}^t$ is computed with the following approximation

$$\begin{aligned}
\tilde{B}^t_{1\,ji} &= \sum_{T \in K_{2h,i}} \left.\frac{\partial \phi_j}{\partial x}\right|_T \sum_{\tau \in T} \int_\tau H_h \varphi_i \, d\mathbf{x} - \sum_{T \in K_{2h,i}} \sum_{\tau \in T} \left.\frac{\partial \zeta_h}{\partial x}\right|_\tau \int_\tau \varphi_i \phi_j \, d\mathbf{x}, \\
\tilde{B}^t_{2\,ji} &= \sum_{T \in K_{2h,i}} \left.\frac{\partial \phi_j}{\partial y}\right|_T \sum_{\tau \in T} \int_\tau H_h \varphi_i \, d\mathbf{x} - \sum_{T \in K_{2h,i}} \sum_{\tau \in T} \left.\frac{\partial \zeta_h}{\partial y}\right|_\tau \int_\tau \varphi_i \phi_j \, d\mathbf{x}, \\
\tilde{B}^t_{3\,ji} &= 2 \sum_{T \in K_{2h,i}} \sum_{\tau \in T} \int_\tau \varphi_i \phi_j d\mathbf{x},
\end{aligned}$$

and the boundary terms (4.71)-(4.72) become:

$$\begin{aligned}
C_{1,ji} &= \int_{\Gamma_{in}} H_h \phi_j \varphi_i n_1 \, ds, \\
C_{2,ji} &= \int_{\Gamma_{in}} H_h \phi_j \varphi_i n_2 \, ds.
\end{aligned}$$

Then as for (4.76), we choose H_h and ζ_h linear on each triangle $\tau \in \mathcal{T}_h$ and we use mass lumping:

$$\int_\tau H_h \varphi_i \mathbf{x} = \sum_{\mathbf{x} \in s(\tau)} H_i(\mathbf{x}) \varphi_i(\mathbf{x}),$$

where $s(\tau) = \{v_0, v_1, v_2\}$ are the three vertices of the triangle τ, also

$$\int_\tau \varphi_i \phi_j d\mathbf{x} = \frac{mes(\tau)}{3} \sum_{\mathbf{x} \in \bar{s}(\tau)} \varphi_i(\mathbf{x}) \phi_j(\mathbf{x}),$$

where $\bar{s}(\tau) = \{\mathbf{x} = \frac{v_i + v_j}{2}, \forall v_i, v_j \in s(\tau)\}$ are the vertices corresponding to the middle of the edges of τ. Finally, the discrete version of the shallow water divergence operator is defined for each vertex of the coarse mesh by:

$$\mathrm{div}_{sw}\, \mathbf{u}_j = \frac{3}{Supp(\phi_j)} \sum_{i \in \mathcal{I}_N} \int_\Omega \nabla_{sw}\, \phi_j \cdot \varphi_i \, d\mathbf{x}\, \mathbf{u}_i. \tag{4.77}$$

This definition is used numerically and can be seen as a diagonal preconditioner to solve Equation (4.75).

4.6 Numerical algorithm

In this section, we give details on the algorithm we use to combine the finite volume method and the finite element method in practice. For the sake of clarity, we just give an overview of the steps of the algorithm. Assuming we know $H^n, H\mathbf{u}^n$, the combined finite volume/finite element method (4.23)-(4.25) can be summarized by the following steps:

- Solve the hyperbolic part (4.23) with the finite volume scheme (4.30)-(4.31) and get $(H^{n+1/2}, H\mathbf{u}^{n+1/2})$. Because of equation (4.32), we obtain H^{n+1} as well.
- Solve the elliptic problem (4.75) to obtain p^{n+1}. We use the iterative method described below.
- Update the velocity $\mathbf{u}^{n+1}$ in the correction step (4.67) using $\nabla_{sw}\, p^{n+1}$.

4.6.1 Iterative methods

Whenever possible, the linear problem (4.67)-(4.68) leading to (4.75), is solved in practice with iterative methods. Several algorithms allow us to solve the classical mixed problem (4.36)-(4.37) in the grad-div form. This is usually applied to the finite element method for the Navier-Stokes equations, see [134, 94]. We describe here the Conjugate Gradient method and the Uzawa algorithm (see [107, 134]) which uses the duality between the operators. In practice, to take the boundary conditions into account, the matrix is built in two blocks in which one part contains the elements of $\tilde{B}^t A_H^{-1} \tilde{B}$ for all the nodes that have to be solved and another diagonal part which is the Identity and corresponds to impose Dirichlet conditions for the pressure. Then the contribution of matrix $\tilde{B}$ associated with the given pressure is affected on the right hand side. The matrix problem can be written:

$$\begin{pmatrix} \mathcal{A} & 0 \\ 0 & Id \end{pmatrix} P = \begin{pmatrix} \frac{1}{\Delta t}\mathcal{D} - (\mathcal{A}_G) P_G \\ P_G \end{pmatrix}, \tag{4.78}$$

where $\mathcal{A}$ is the matrix extracted from $\tilde{B}^t A_H^{-1} \tilde{B}$ corresponding to the fact that we restrict to the nodes of unknowns, $\mathcal{A}_G$ to the nodes of the given pressure P_G respectively. The matrix $\mathcal{D}$ is the shallow water divergence vector of the unknown nodes at the prediction part. This reduces the size of the problem and allows us to apply the Conjugate Gradient algorithm. The initialization is done with the state $(Hu, Hv, Hw)^{n+1/2}$ computed at the hyperbolic step. For the sake of clarity, we drop the superscripts $^{n+1/2}$ and we denote with the superscript $^{(k)}$ the index iteration of the iterative method. In addition, we use the notation: $f = \frac{1}{\Delta t}\mathcal{D} - \mathcal{A}_G P_G$. Then the CG algorithm can be summarized as:
Initialization:

$$r^{(0)} \;=\; f - \mathcal{A}P^{(0)},$$

$$d^{(0)} = -r^{(0)}.$$

For $k > 0$

$$\begin{aligned}
\rho &= \frac{(r^{(k)}, d^{(k)})}{(d, \mathcal{A}d^{(k)})}, \\
P^{(k+1)} &= P^{(k)} + \rho d^{[k)}, \\
r^{(k+1)} &= r^{(k)} + \rho \mathcal{A} d^{(k)}, \\
\gamma^{(k)} &= \frac{||r^{k+1}||^2}{||r^k||^2}, \\
d^{(k+1)} &= -r^{(k)} + \gamma^{(k)} d^{(k)}.
\end{aligned}$$

Then, the correction is applied to the velocity.
For the description of the Uzawa problem, let us now use the duality between the operators (4.26) and (4.11), keeping the notations

$$\begin{aligned}
&U^{(0)}, P^{(0)} given, \\
A_H U^{(k+1)} &= A_H U^{n+1/2} - \Delta t \tilde{B} P^{(k+1)}, \\
P^{(k+1)} &= P^{(k)} + \alpha \tilde{B}^t U^{(k)},
\end{aligned}$$

with α chosen such that $0 < \alpha < \frac{2}{\max \lambda_i}$ with λ_i the eigenvalues of $B A_H^{-1} B^t$. The CG algorithm adapted for problem (4.67)-(4.68) in the form of the Uzawa algorithm reads:
Initialization:

$$\begin{aligned}
U^0 &= U^{n+1/2}, \\
d^{(0)} &= -r^{(0)} = \tilde{B}^t U^{(0)},
\end{aligned}$$

$k > 0$:

$$\alpha^k = \frac{(r^{(k)}, d^k)}{(\tilde{B} d^k, A_H^{-1} \tilde{B} d^k)},$$

$$\begin{aligned}
P^{(k+1)} &= P^{(k)} + \alpha^k d^{(k)}, \\
Z &= A_H U^{(k)} - \Delta t \tilde{B} P^{(k+1)}.
\end{aligned}$$

Solve the system $A_H U^{(k+1)} = Z$ (We recall that the matrix A_H is diagonal since we have used mass lumping).

Compute $\tilde{B}^t U$:

$$r^{(k+1)} = \tilde{B}^t U^{(k+1)},$$

$$\gamma^{(k)} = \frac{||r^{(k+1)}||^2}{||r^{(k)}||^2},$$
$$d^{(k+1)} = r^{(k)} + \gamma^{(k)} d^{(k)}.$$

In accordance with Equation (4.77) and Equation (4.77), the norm $||.||$ used in the iterative algorithms above take into account the normalization of the operators.

4.6.2 Wet-dry interface

As one can see, the method presented above only applies for non-negative water depth. The main problem comes from the shallow water equation of the pressure (4.26), which requires dividing the shallow water gradient by H. At the discrete level, this difficulty arises in the mass matrix (4.69). Yet, in the geophysical context, it is necessary to allow a dry/wet transition to model, for instance, a propagation over obstacles like islands or a wave reaching a coast line. In practice, we set the pressure p to zero when H tends to zero. This can be viewed as a Dirichlet condition on the dry zone of the domain, such that the pressure equation is solved only on the wet domain. In the iterative solver, this leads to testing the value of the water depth for each node s_j of the mesh (or for the coarse mesh if the P1-isoP2/P1 approximation is used). However, in order to avoid selecting a list of dry nodes at each time step, which would require significant computation time, we solve the whole problem and we introduce a threshold

$$\epsilon << 1, \tag{4.79}$$

under which the water depth is redefined by ϵ, namely $H_\epsilon = \max(H, \epsilon)$. Since the mass matrix M_H is weighted with H and needs to be inverted in the correction step, to avoid having singularities, the matrix is redefined with respect of H_ϵ as

$$M_{H_\epsilon ji} = \sum_{T \in K_{h,i}} \int_T H_\epsilon \varphi_i \varphi_j d\mathbf{x}.$$

Then, at the correction step, the shallow water gradient is redefined by

$$\nabla^\epsilon_{sw}(p)|_i = \frac{1}{Supp(\varphi_i)} \sum_j \int_\Omega \nabla_{sw}(\varphi_j) \cdot \boldsymbol{\varphi}_i d\mathbf{x}\, p_j \mathbb{1}_{H_i > H_\epsilon}, \tag{4.80}$$

so the velocity is not updated at these nodes by step (4.24). In equation (4.80), the function φ_j is replaced by ϕ_j if we use P1-isoP2 /P1 space approximation. Notice that

introducing H_ϵ does not change the result since it appears only in the terms of degree zero for the derivative of the pressure. It only prevents us from redefining wet/dry zones at each iteration. With these definitions, the Laplacian operator written in (4.27) becomes:

$$\begin{aligned} \triangle_{sw}^{\epsilon}(p) &= \mathrm{div}_{sw}\left(\frac{\nabla_{sw}}{H_\epsilon}\right), && (4.81)\\ &= H \triangle(p) + \frac{\partial p}{\partial x}\left(\frac{\partial H}{\partial x}\right) + \frac{\partial p}{\partial y}\left(\frac{\partial H}{\partial y}\right), && (4.82)\\ &\quad + p\left(\triangle\zeta - \frac{1}{H_\epsilon}\left(\left(\frac{\partial \zeta}{\partial x}\right)^2 + \left(\frac{\partial \zeta}{\partial y}\right)^2 + 4\right)\right). && (4.83) \end{aligned}$$

4.6.3 An improved method

The numerical methods presented in the previous sections can be improved if we apply a Heun scheme, which is based on a Runge-Kutta method, to the Saint-Venant model and the correction part. This improvement has been detailed for the one-dimenional problem in Chapter 3 and can be straightforwardly applied to the two-dimensional case. The Heun scheme is slightly modified so that the stability (CFL) condition remains valid. For this system, our scheme is second order accurate in time and, if we use a reconstruction algorithm (see [10]) in the hyperbolic step, it is formally second order accurate in space (see [10]). However, with the correction step, the resulting scheme is no longer of order two, but introducing the Heun scheme and the reconstruction in the hyperbolic step can improve the global accuracy of the scheme. This will be illustrated in the next section.

4.7 Validation with analytical solutions

In this part, we propose a validation of the method using a comparison of the numerical results for two non-stationary analytical solutions.

4.7.1 A solitary wave

The solitary wave is a one-dimensional non-stationary analytical solution of the model. This solution has been proposed to validate the one-dimensional model in Chapter 3 and has the form:

$$\begin{aligned} H &= H_0 + a\left(\mathrm{sech}\left(\frac{x - c_0 t}{l}\right)\right)^2,\\ u &= c_0\left(1 - \frac{d}{H}\right),\\ w &= -\frac{a c_0 d}{lH}\mathrm{sech}\left(\frac{x - c_0 t}{l}\right)\mathrm{sech}'\left(\frac{x - c_0 t}{l}\right), \end{aligned}$$

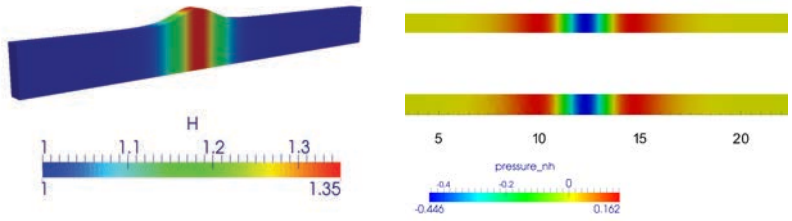

(a) Computed water depth.

(b) non hydrostatic pressure: Analytical field at the top, numerical field at the bottom.

Figure 4.4: Illustration of the solitary wave propagation at $t = 1.99s$.

$$\begin{aligned} p &= \frac{ac_0^2d^2}{2l^2H^2}\left((2H_0 - H)\left(\text{sech}'\left(\frac{x - c_0t}{l}\right)\right)^2,\right. \\ &+ \left. H\text{sech}\left(\frac{x - c_0t}{l}\right)\text{sech}''\left(\frac{x - c_0t}{l}\right)\right), \end{aligned}$$

with $d, a, H_0 \in \mathbb{R}$, $H_0 > 0$, $a > 0$ and $c_0 = \frac{l}{d}\sqrt{\frac{gH^3}{l^2 - H_0^2}}$, $l = \sqrt{\frac{H_0^3}{a} + H_0^2}$.
This analytical solution is extended to two dimensions in a rectangular channel and we add $v = 0$ in the equations.
We consider a channel of dimension 30 m $\times$1 m, the water elevation H_0 is set to 1 m with significant wave amplitude $a = 0.35$m and $d = 1$m. On the model domain in Figure 4.1a, we set a slip boundary condition for Γ_s, a given discharge for the inlet (4.15) and a water elevation at the outlet (4.16) with a homogeneous Dirichlet boundary condition for the pressure at the correction step. The test case is initialized with the analytical solution in the domain and we observe the propagation of the wave over time. In Figure 4.4, we show the computed water depth (4.4a) and the computed and analytical pressures (4.4b). This has been obtained with the P1-isoP2/P1 approximation and the wave covered approximately one wavelength.

Comparison of the approximation spaces

A numerical comparison of the P1/P1 and P1-isoP2/P1 approximations is proposed in order to choose the most accurate one for practical applications. In Figure 4.5, we compare the numerical solutions, computing the P1/P1 solution on the fine mesh of the P1-isoP2/P1, here an unstructured mesh of 7277 nodes. After a short time, the P1/P1 method provides a less accurate solution than the P1-isoP2/P1 approximation, since we observe the amplitude of the wave obtained by the P-isoP21/P1 method is closer to the analytical solution than the P1/P1 approximation.

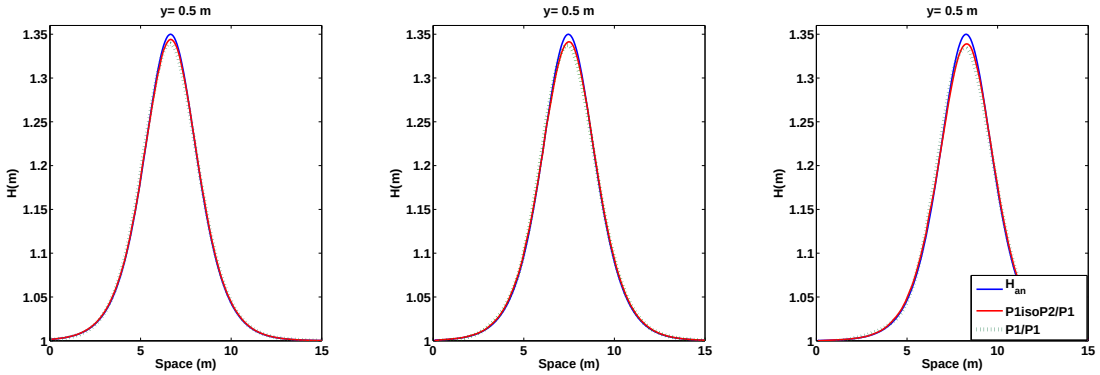

(a) H at time t=0.444213 s (b) H at time t=0.665963 s (c) H at time t=0.888782 s

Figure 4.5: Comparision between the P1isoP2/1 and the P1P1 approximation on the solitary wave propagation

Validation with P1-isoP2/P1

As the comparison gives better results with the P1-isoP2 / P1 spaces, we opt for this approximation to validate the method. We apply the "improved" method presented in 4.6.3 and obtain a good approximation of the soliton all over the propagation (see Figure 4.6). In Figure 4.6, we observe that the solitary wave conserves its amplitude over the time. The simulation shown in Figure 4.6 was computed with 251330 nodes for the fine mesh. We study the convergence rate of the computed solutions, computing the L^2 error at time $t = 1.99s$ for different meshes of triangle's mean edges of $h_0 = 0.0493528\,m$, $h_1 = 0.0250468\,m$ and $h_2 = 0.016781\,m$. Figure 4.7 shows the logarithm of the error L^2 between the analytical solution and the numerical solution in function of $\log\left(\frac{h_0}{h}\right)$ where $h = h_i, i = 0, 1, 2$. We observe a convergence rate close to 1 for the first order method, while with the improved scheme we still obtain approximately a first order convergence rate, although the error computed is smaller.

4.7.2 A periodic solution with a wet-dry interface

In this section the objective is to validate the method with a non stationary analytical solution where the free surface oscillates over the time. Such solutions have been introduced by Thacker in [148] for the Shallow Water equations and can be obtained over a paraboloid topography with a velocity (u, v) varying with respect to time. To obtain this kind of solution for the non hydrostatic model (4.6)-(4.8), we slightly modify this model by adding a given source term $s(x, y, t)$ in the third equation of the system (4.7), which becomes

$$\frac{\partial Hw}{\partial t} + \frac{\partial Huw}{\partial x} + \frac{\partial Hvw}{\partial y} - 2p = Hs.$$

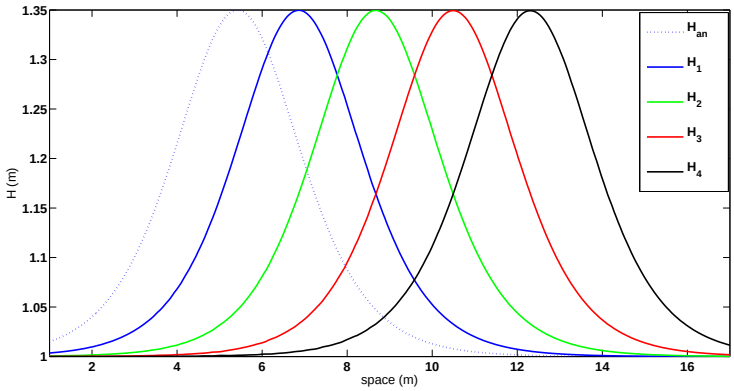

Figure 4.6: Cross section at the center of the channel $y = 0.5$ m; water depth of the analytical solution at initial time $H_0 = H_{an}$ and computed solution for $H_i, i = 1, ..., 4$ with $t_0 = 0, t_1 = 0.499805\, s$, $t_2 = 0.999871\, s$, $t_3 = 1.49983\, s$, $t_4 = 1.99993\, s$ for the P1-isoP2/P1 approximation for the improved method (Heun scheme).

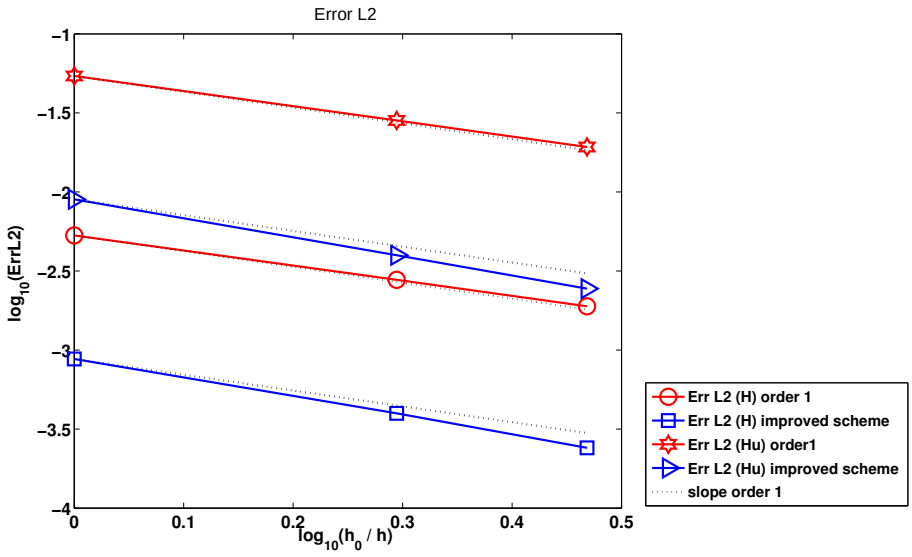

Figure 4.7: Convergence rate for the P1-isoP2/P1 approximation for the classical scheme (order 1 in time and space) and the improved method (Heun scheme and reconstruction in the prediction step). The L^2 is computed at time $t = 1.99s$

Then an analytical solution of this modified system can be written under the form

$$\begin{aligned}
H(x,y,t) &= \max(0, H_0 - \frac{\alpha}{2}\left(x - a\cos(\sqrt{r}t)\right)^2 - \frac{\beta}{2}\left(y - a\sin(\sqrt{r}t)\right)^2), \\
u(x,y,t) &= -a\sqrt{r}\sin(\sqrt{r}t), \\
v(x,y,t) &= a\sqrt{r}\cos(\sqrt{r}t), \\
w(x,y,t) &= -\alpha a\sqrt{r}\sin(\sqrt{r}t)x + \alpha a\sqrt{r}\cos(\sqrt{r}t)y, \\
p(x,y,t) &= \frac{a^2\alpha r}{2}H, \\
s(x,y,t) &= \alpha a r\sin(\sqrt{r}t)x - \alpha a r\cos(\sqrt{r}t)y, \\
z_b(x,y) &= \frac{\alpha}{2}(x^2+y^2),
\end{aligned}$$

where $a, \alpha > 0$ with $a\alpha < 1$, and

$$r = \frac{\alpha g}{1 - \alpha^2 a^2}.$$

We run this test on a disc domain centered in $(x, y) = (0, 0)$ with a radius of $5\,m$, with $\alpha = 0.3\,m^{-1}$, $a = 1.6\,m$ and $H_0 = 1.0\,m$ as shown in Figure 4.8. This case is simulated with 440746 nodes for the fine mesh (and 110588 for the coarse mesh). We use the strategy proposed in Section 4.6.2 to treat the wet-dry front with ϵ defined by (4.79) set to 10^{-5} and impose a discharge equal to zero at the boundary conditions (4.15) and a Dirichlet boundary condition for the pressure on Γ. In Figure 4.8, the representation of the free surface oscillating in the bowl is shown for different time steps. The Figure 4.9 presents the profile of the elevation for $y = 0$ at different time steps compared with the analytical solution. This is a crucial test case for the validation of the method since we test the dry/wet - wet/dry transitions and strong variation of the free surface. We also compute the convergence rate with the same formula described for the solitary case 4.7.1 for different meshes where $h_0 = 0.0551138\,m$, $h_1 = 0.0412458\,m$, $h_2 = 0330043\,m$, $h_3 = 0.0274674\,m$, with $h, i = 0, ..., 3$ are the mean edges of the meshes. In Figure 4.10 and 4.11 we observe the convergence rate is close to one for the water depth, the velocity hw and the non-hydrostatic pressure p. These simulated results are computed with the improved method described in (4.6.3) and as expected, we obtain a similar slope for Hw and p and a better convergence for H which is not corrected in the second step of the scheme 4.24.

4.8 Numerical results

In this section we test the depth-averaged model (4.6)-(4.8) on a numerical application. We generate small amplitude waves at the inlet of a domain of dimensions $[0, 10] \times [0, 6]$ and we observe the propagation of the waves over an obstacle. The channel is also ended by a slope of 40%. This simulation allows us to confront our method to a test case where

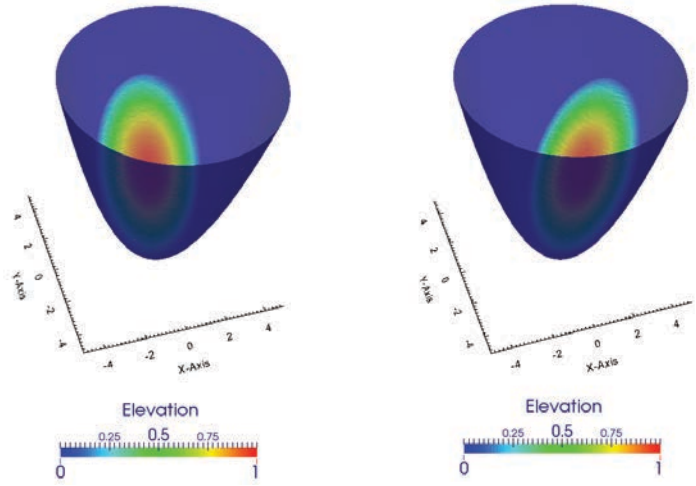

Figure 4.8: Simulation of the free surface oscillations in a paraboloid at different time steps.

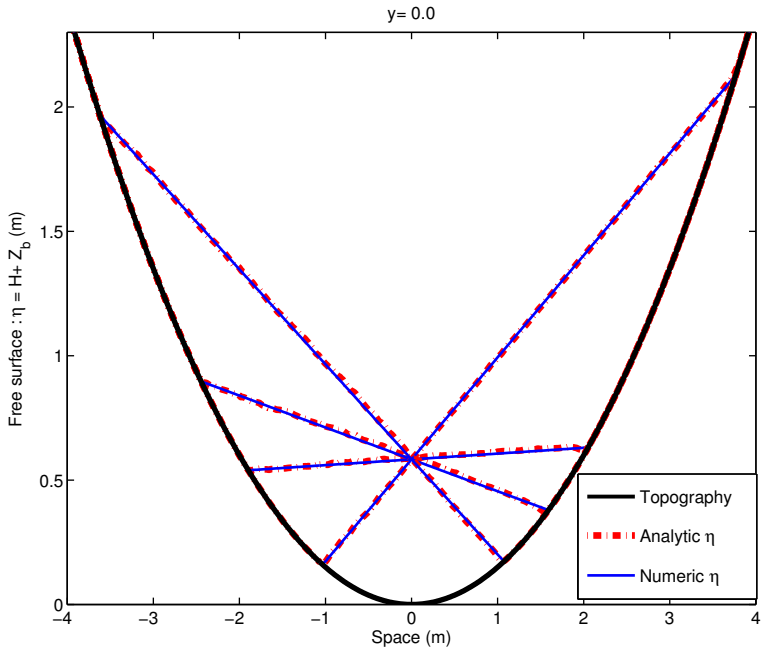

Figure 4.9: Cross section of the solution at $y = 0$ of the free surface $H + z_b$ compared with the analytical solution at different times: $t_0 = 0.277222\,s$, $t_1 = 0.431123\,s$, $t_2 = 0.739382\,s$, $t_3 = 0.893419\,s$, $t_4 = 1.20134\,s$

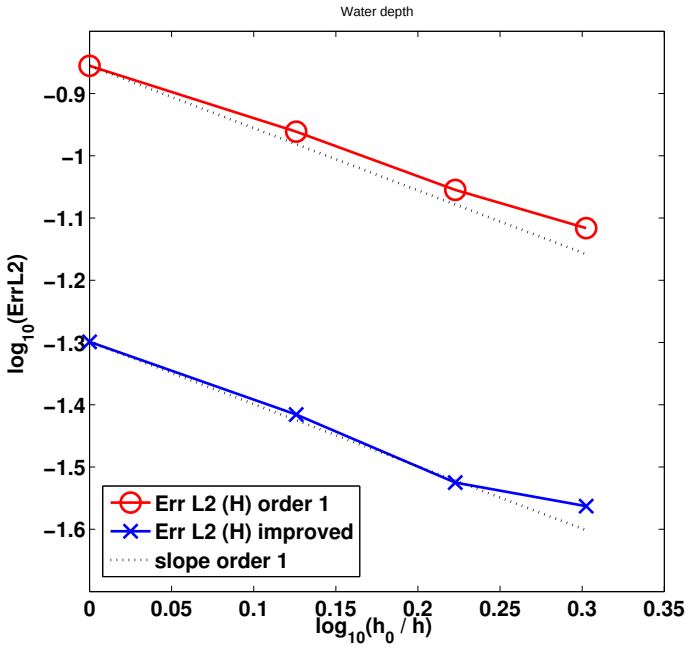

Figure 4.10: Convergence rate of the water depth, and the pressure

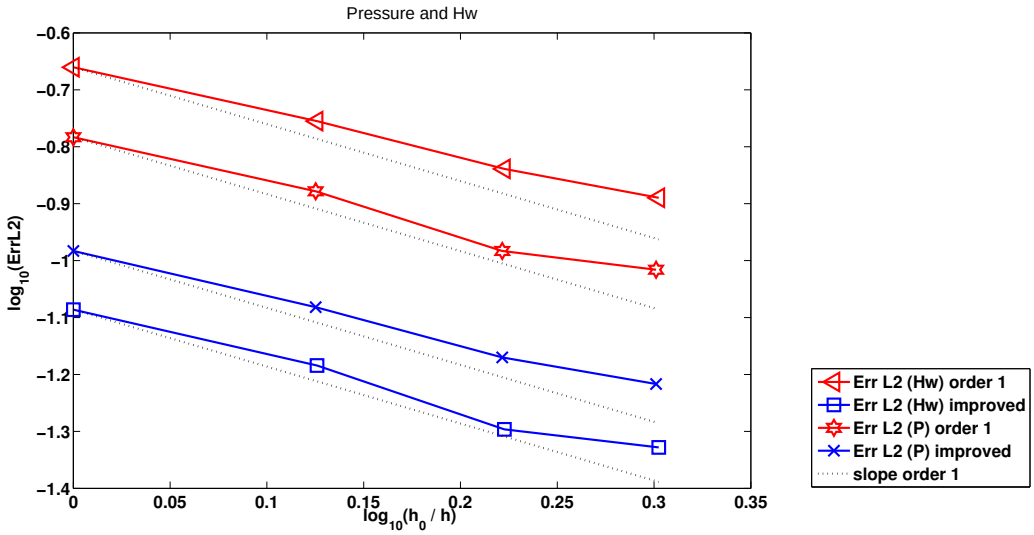

Figure 4.11: Convergence rate of the velocity

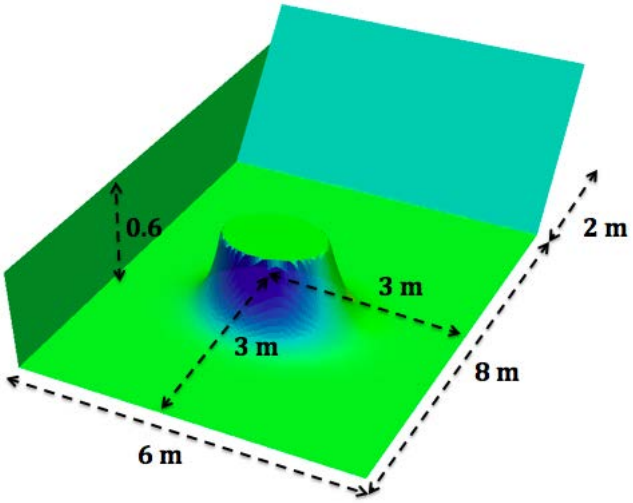

Figure 4.12: Dimension of the test case

we have a variable bottom with strong variations of the elevation and wet/dry interfaces. The dimensions of the case are described in Figure 4.12 and the obstacle is defined by the topography function:

$$z_b = \min\left(z_m, Ae^{-\left((a(x-x_0)^2)+b(y-y_0)^2\right)}\right), \tag{4.84}$$

where we set $z_m = 0.5\,m$, $A = 2\,m$, $a = 3.3\,m$, $b = 1.51\,m$ and $x_0 = 3\,m$, $y_0 = 3\,m$. We set an initial free surface $\eta_0 = 0.6\,m$ and a sinusoidal wave given at the inlet with an amplitude of $0.02\,m$. The test is performed over an unstructured mesh of 45506 nodes for the fine mesh. The numerical solution is computed with the P1-iso-P2/P1 approximation and we use the improved scheme described in Section 4.6.3. We compare the solutions obtained using the Shallow Water model and using the DAE model (4.6)-(4.8) to observe the effects on the dispersion on the propagation and the wave interactions. Figure 4.13 shows the simulations at different instants $t_1 = 4.54531\,s$ (4.13a and 4.13b), $t_2 = 7.07028\,s$ (4.13c and 4.13d), $t_3 = 9.59589\,s$ (4.13e and 4.13f) for the Shallow Water model (left) and the dispersive model (right). The figures represent the free surface η. We clearly observe the impact of the dispersive effects around the obstacle and on the forms of the waves. In Figure 4.14 we show the free surface over the time at different points around the obstacle and compare the solution obtained for the Shallow Water model and the depth averaged model.

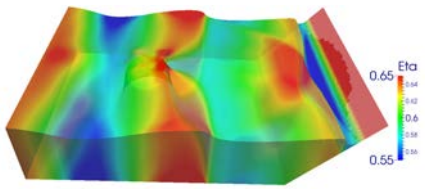

(a) Hydrostatic simulation at time t=4.54531 s

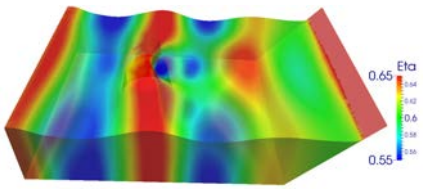

(b) Non-hydrostatic simulation at time t=4.54531 s

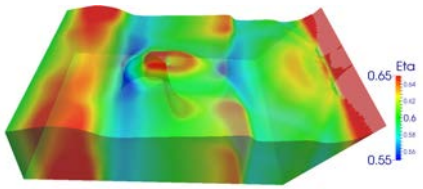

(c) Hydrostatic simulation at time t=7.07028 s

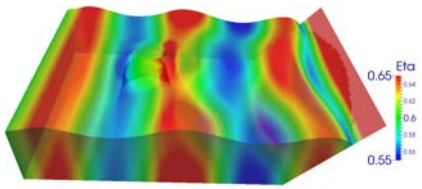

(d) Non-hydrostatic simulation at time t=7.07028 s

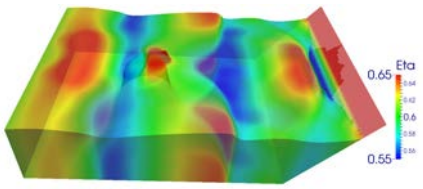

(e) Hydrostatic simulation at time t=9.59589 s

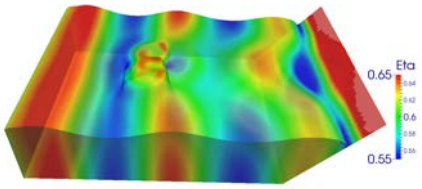

(f) Non-hydrostatic simulation at time t=9.59589 s

Figure 4.13: Free surface obtained with a hydrostatic simulation and a non-hydrostatic simulation

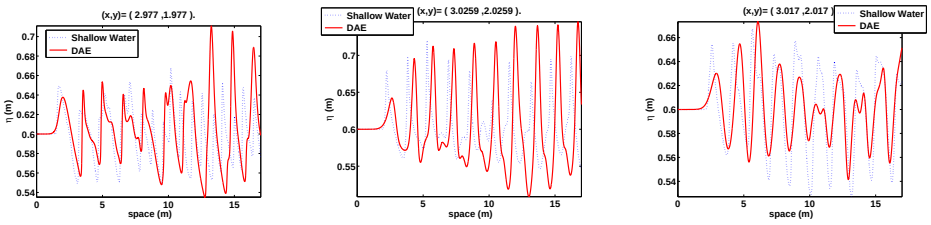

(a) Point 1 (b) Point 2 (c) Point 3

Figure 4.14: Comparison of the free surface over the time for the selected points between solutions computed with a hydrostatic model (···) and the depth-averaged model (—).

4.9 Conclusion

In this paper, we have presented a new method for the two-dimensional dispersive shallow water system on unstructured meshes using a combined finite volume / finite element method. We have provided a numerical validation with two analytical solutions. The algorithm uses an iterative method of Uzawa type to solve the elliptic problem.

In a future work, we intend to optimize the computational cost in order to make the numerical method applicable to larger real domains, by focusing on the preconditioning of the iterative solver. Concerning the method, we would like to extend it to other dispersive models, in particular to a multilayer model.

Chapter 5

Supplementary results

5.1 Introduction

This Chapter is devoted to a supplementary study of the depth-averaged Euler (DAE) problem (3.2)-(3.4) concerning some modeling and numerical aspects.
We want to study the stationary solutions of the DAE model, and to compare these solutions with the Shallow Water model. We search for analytical solutions for the DAE model [43] and we give a comparison between an analytical and a computed solution. This allows us to provide a validation of the method we use.

Then, we are interested in the hydraulic jump. This phenomenon has been widely studied by physicists and mathematicians for the Shallow Water model [54]. We give a comparison between the two models for the hydraulic jump to show up the dispersive effects in this case.

It is classical to study the dispersion relation of dispersive models to evaluate its validity with respect to the linearized Euler system. We provide the dispersion relation of the linearized DAE model (1.34)-(1.34) and give a comparison with the Airy theory [1].

In contrast to the Shallow Water system, dispersive models as the DAE system do not give a good approximation of the wave propagation after the breaking point. Many strategies have been investigated in the literature and we can distinguish two main techniques. The first one consists in switching from a dispersive model to a hydrostatic model, while the second method consists in adding an artificial viscosity after the breaking [99, 139, 29]. In the two methods, a breaking criteria is needed to detect the breaking point and there is again a large choice of criteria proposed by the literature [30, 19]. In this Chapter, we apply one of the method performed in [99] and confront the results with experimental data. We also compare the solution obtained without any treatment for the breaking.

This Chapter is organized as follow. In Section 5.2, we study the steady states of the DAE system and give a validation of the numerical method implemented in this case. We propose a comparison of the numerical solution of a non-hydrostatic hydraulic jump with the hydrostatic one. Then, we provide a common analytical solution with the Euler system. In the third section , we give the dispersion relation of the linearized DAE equations and look for analytical solution of the Euler equations and the DAE system. Finaly, in Section 5.5 we modify the scheme to detect the breaking waves and we propose a comparison of a computed solution with data from laboratory experiment. The additional results presented in this Chapter are still an on-going work, which will be the object of a forthcoming paper.

5.2 Stationary solutions for the one-dimensional problem

In this section, we wish to study the steady states of the dispersive system (3.2)-(3.4). We search the solutions $H, H\mathbf{u}, p$ of the DAE system satisfying $\frac{\partial H}{\partial t} = 0$ and $\frac{\partial H\mathbf{u}}{\partial t} = 0$ and we denote $Q_0 = H\bar{u}$. In this case, it is also interesting to compare the computed solution with an analytical solution. There are many possible strategies to find a "pseudo" analytical solution of this problem, that is to say a solution which is not given explicitly and requires solving numerically an ODE equation. The more suitable way to proceed is to set the velocity w because it involves an ODE that we can solve numerically with a simple Runge Kutta scheme. The stationary solutions of the system (3.2)-(3.4) satisfy:

$$\frac{\partial}{\partial x}\left(\frac{Q_0^2}{H} + \frac{g}{2}H^2 + p\right) = -\left(g + 2p\right)\frac{\partial z_b}{\partial x}, \tag{5.1}$$

$$H\bar{w} = \frac{Q_0}{2}\frac{\partial}{\partial x}\left(H + 2z_b\right), \tag{5.2}$$

$$\tag{5.3}$$

$$p = \frac{Q_0}{2}\frac{\partial \bar{w}}{\partial x}. \tag{5.4}$$

$$\tag{5.5}$$

Setting a velocity $\bar{w}(x)$ of the form:

$$w = 2c(x-a)e^{-b(x-a)^2}, \tag{5.6}$$

in (5.2)-(5.4), and using these equations, Equation (5.1) becomes an ODE in term of the variable H. We set $Q_0 = 0.5\,m.s^{-1}$, $a = 5.0\,m$, $b = 5.0\,m$, $c = 1\,m$ and an initial free surface $\eta = 1.0\,m$ on a channel with a length of 10 m. We show the solution with these parameters in Figure 5.1. We compute the numerical solution by imposing a discharge Q_0 at the inlet and a free outflow. The solution converges to the steady state after about 200 s and we show the comparison between the analytical and the numerical solution in Figure 5.2. We compute the convergence rate for the finite difference method as explained in Chapter 2 and the finite element method with a P1-isoP2/P1 approximation as in Chapter 3. To do so, we compute the error L^2 between the analytical solution and the numerical solution for the water depth H and we obtain, a convergence rate close to 1, as shown in Figure 5.3.

It is clear that in practice it is more convenient to set a topography and compute a stationary solution. We propose to define the bottom z_b by:

$$z_b = A\,e^{(-\frac{(x-B)^2}{C})}, \tag{5.7}$$

with $A = 0.5\,m$, $B = 15.0\,m$, $C = 5.0\,m$ and we choose an initial elevation $\eta = H + z_b = 1\,m$ and a discharge $Q_0 = 1.3m.s^{-1}$. These choices provide a solution where the regime switches

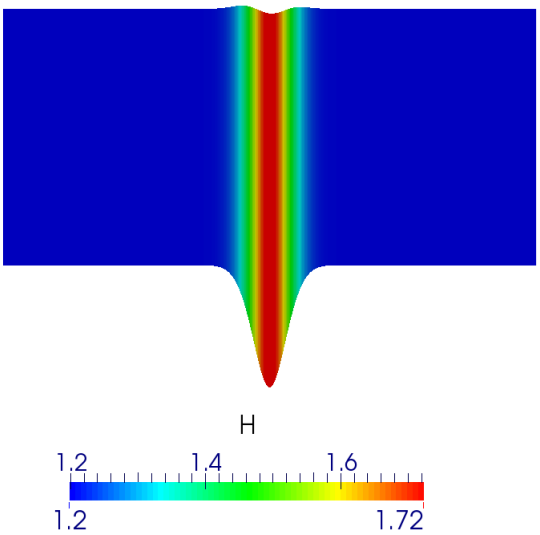

Figure 5.1: Analytical non-stationary solution

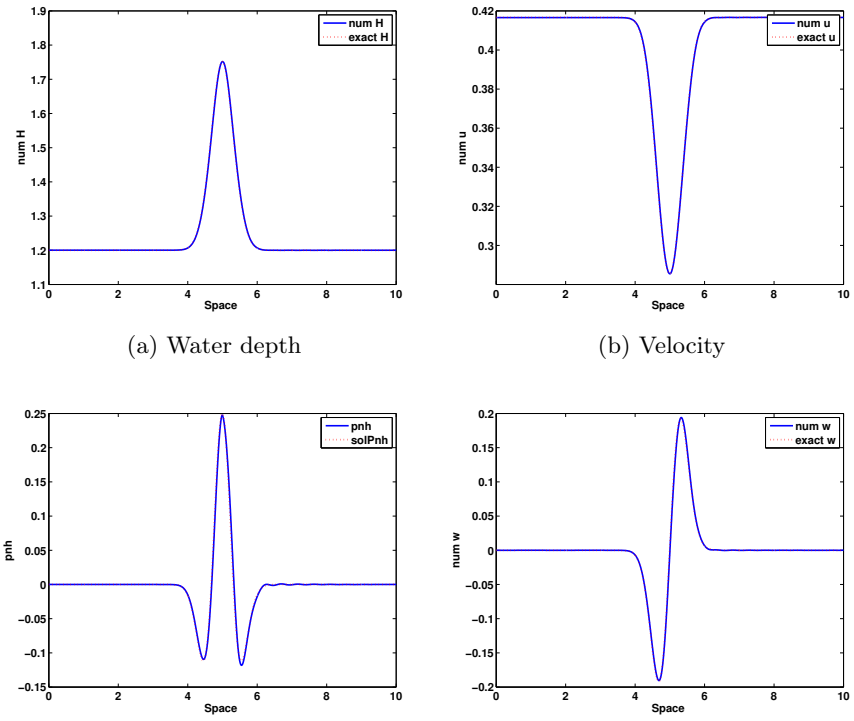

(a) Water depth

(b) Velocity

(c) Pressure

(d) Velocity

Figure 5.2: Comparison of the analytical solution and the computed solution for H,$\bar{u}, \bar{w}, p$ on a domain of 10 m and with a mesh of 3000 nodes.

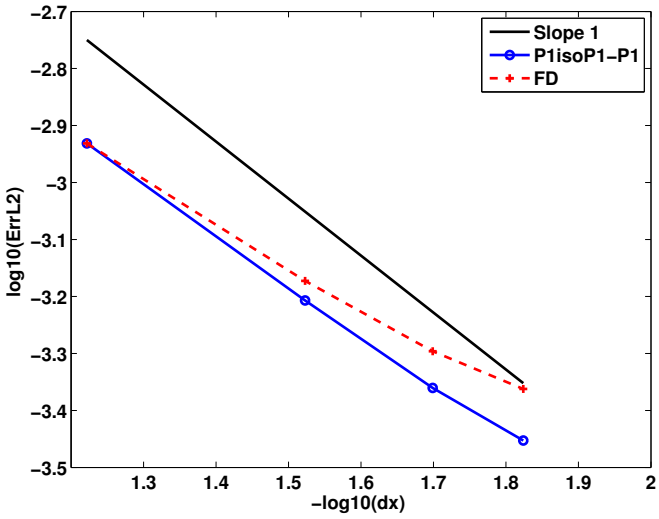

Figure 5.3: Error L^2 : comparison between the analytical solution and the computed solution for the finite difference (FD) method and the finite element method P1-isoP2/P1.

from a fluvial regime ($Fr < 1$) to a torrential regime ($Fr > 1$) on the top of the bump. In Figure 5.4 we compare the computed solution using the dispersive model (3.2)-(3.4) and the solution of the Saint-Venant system. This simulates a hydraulic jump. This phenomenon has been widely studied and experimented in laboratory. In Figure 5.5 is illustrated an experiment where a discharge has been injected in a channel over an obstacle. The reality is much more complicated than a shock at the interface since it involves turbulence for instance. Any way, it is interesting to observe the result computed with a non-hydrostatic system, where the dispersive effects appear here instead of the shock.

Remark 5.2.1. *Notice that it is also possible to find a "pseudo" analytical solution if we impose a topography z_b. However, it implies that a non linear boundaries value problem has to be solved.*

$$\left(-\frac{Q_0^2}{H^2}+gH+p\right)\frac{\partial H}{\partial x}+H\frac{\partial \overline{p}_{nh}}{\partial x} = -(gH+2p)\frac{\partial z_b}{\partial x}, \tag{5.8}$$

$$\frac{\partial w}{\partial x} = \frac{2}{Q_0}p, \tag{5.9}$$

$$\frac{\partial H}{\partial x} = \frac{H}{Q_0}\overline{w}-2\frac{\partial z_b}{\partial x}. \tag{5.10}$$

This problem can be solved numerically with an iterative method (gradient, newton etc..), we do not develop an algorithm here for this problem but we highlight the difficulty to obtain an analytical solution, if we provide the topography.

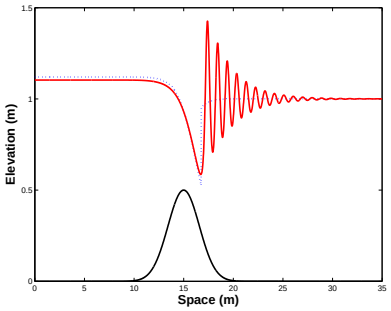

(a) Water depth

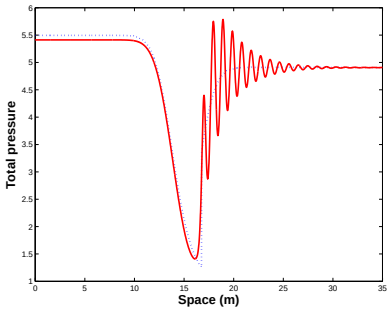

(b) Total pressure

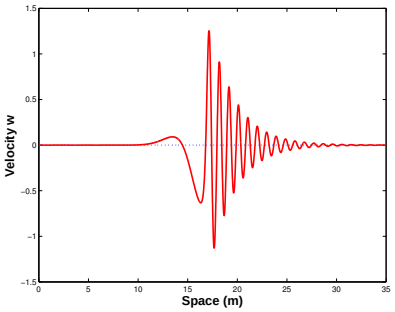

(c) Vertical velocity

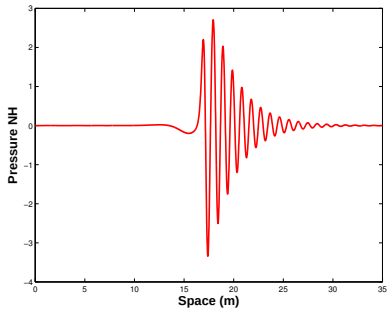

(d) Non-hydrostatic pressure

Figure 5.4: Hydraulic jump: comparison between the hydrostatic simulation (···) and non-hydrostatic simulation (—).

Figure 5.5: Hydraulic jump experiment

5.3 Another analytical solution

For some particular cases, analytical solutions of the Euler system are also solutions of the DAE system 1.34-(1.38). We recall the Euler system in two dimensions:

$$\frac{\partial u}{\partial x} + \frac{\partial w}{\partial z} = 0, \tag{5.11}$$

$$\frac{\partial u}{\partial t} + u\frac{\partial u}{\partial x} + w\frac{\partial u}{\partial z} + \frac{\partial p}{\partial x} = 0, \tag{5.12}$$

$$\frac{\partial w}{\partial t} + u\frac{\partial w}{\partial x} + w\frac{\partial w}{\partial z} + \frac{\partial p}{\partial z} = -g, \tag{5.13}$$

and it is completed with the one-dimensional kinematic boundary conditions (as (1.13)-(1.14) for the two-dimensional model). The dynamic boundary condition at the free surface reduces to

$$p_s = p(x, \eta, t) = p^a(x, t). \tag{5.14}$$

where p^a is the atmospheric pressure. This is the case for the adapted version of the Thacker's solution (see parabolic bowl explained in Section 1.5.1). This is also the case of the following solution:
For some $\alpha \in \mathbb{R}_+$, $t_0 \in \mathbb{R}$, let us consider the functions u, w, H, p defined for $t > t_0$ by

$$H(x,t) = \frac{\alpha}{t - t_0}, \tag{5.15}$$

$$u(x,z,t) = \frac{x}{t - t_0}, \tag{5.16}$$

$$w(x,z,t) = -\frac{z}{t - t_0}, \tag{5.17}$$

$$p(x,z,t) = g(H - z) + \frac{H^2 - z^2}{(t - t_0)^2}, \tag{5.18}$$

with a flat bottom $z_b = z_{b,0}$. Then u, w, H, p satisfy the two-dimensional Euler system (5.11)-(5.13) completed with the free surface boundary conditions (1.13)-(1.14) and are also solution of the one-dimensional DAE system (3.2)-(3.4).
This analytical solution can be easily extended to three dimensions. With obvious notations, the functions u, v, w, H, p defined by

$$\begin{aligned}
H(x,y,t) &= \frac{\alpha}{t - t_0}, \\
u(x,y,z,t) &= \frac{\cos(\theta)x + \sin(\theta)y}{t - t_0}, \\
v(x,y,z,t) &= \frac{1 - \cos(\theta)}{\sin(\theta)} \frac{\cos(\theta)x + \sin(\theta)y}{t - t_0}, \\
w(x,y,z,t) &= -\frac{z}{t - t_0},
\end{aligned}$$

$$p(x,y,z,t) = g(H-z) + \frac{H^2 - z^2}{(t-t_0)^2},$$

with $\theta \in [0, 2\pi]$, are solutions of the three-dimensional incompressible free surface Euler system (5.19)-(5.19), completed with the boundary conditions (1.13)-(1.14) and are also solution of the DAE system (1.34)-(1.37). These solutions can be used for a future validation of the model in one and two dimensions.

5.4 Dispersion relation

We consider the two-dimensional Euler system (5.11)-(5.13). Assuming the velocities u and w are such that $u, w = \mathcal{O}(\varepsilon)$ with $\varepsilon \ll 1$, the approximation in $\mathcal{O}(\varepsilon^2)$ of the Euler system (5.11)-(5.13) gives

$$\frac{\partial u}{\partial x} + \frac{\partial w}{\partial z} = 0, \tag{5.19}$$

$$\frac{\partial u}{\partial t} + \frac{\partial p}{\partial x} = 0, \tag{5.20}$$

$$\frac{\partial w}{\partial t} + \frac{\partial p}{\partial z} = -g, \tag{5.21}$$

completed with the boundary conditions (as in two dimensions for the surface and the bottom (1.13)-(1.14)), and (5.14). Now we consider a flat bottom i.e. $z_b(x) = z_{b,0} = 0$ and a water depth having the form

$$H = H_0 + \varepsilon f(x,t), \tag{5.22}$$

with $\varepsilon \ll H_0$ and $f(x,t)$ represents the variations of the water depth around the equilibrium at rest of the fluid. Up to $\mathcal{O}(\varepsilon^2)$ terms, the linearized Euler system (5.19)-(5.21) also gives

$$\frac{\partial H}{\partial t} + \frac{\partial}{\partial x}\int_0^{H_0} u \; dz = 0, \tag{5.23}$$

$$w = -\frac{\partial}{\partial x}\int_0^{z} u \; dz, \tag{5.24}$$

$$\frac{\partial u}{\partial t} + \frac{\partial p}{\partial x} = 0, \tag{5.25}$$

$$p = p^a(x,t) + g(H-z) + \int_z^{H_0} \frac{\partial w}{\partial t} dz, \tag{5.26}$$

which is an approximation in $\mathcal{O}(\varepsilon^2)$ of the Euler system (5.11)-(5.13), completed with the kinematic boundary condition and (5.14). Equation (5.23) results from a vertical integration of Eq. (5.19) coupled with the boundary conditions at the surface and at the bottom (as in (1.13)-(1.14)). Using the boundary condition (5.14) and the assumption $\varepsilon \ll H_0$ in (5.22), the vertical integration of (5.21) gives (5.26). Notice that, as in the Airy

theory, the fluid pressure at the free surface does not vanish. Indeed, from Eq. (5.26) we get $p_s = p(x, H, t) = p^a(x, t) + \mathcal{O}(\varepsilon^2)$ with

$$p_s = p^a(x,t) + \int_H^{H_0} \frac{\partial w}{\partial t} dz = p^a(x,t) + \mathcal{O}(\varepsilon^2).$$

The linearized model (5.23)-(5.26) is widely used in the literature especially for the study of water waves problems [104, 150] and the dispersion relation associated corresponds to the Airy theory [1].

$$\frac{\omega}{k} = \sqrt{\frac{g}{k}\tanh(kH_0)} \tag{5.27}$$

Dispersion relation of the depth-averaged Euler model

Considering a flat bottom $z_b(x) = z_{b,0}$ and assuming

- the velocities $\overline{u}$ and $\overline{w}$ are such that $\overline{u}, \overline{w} = \mathcal{O}(\varepsilon)$,
- a water depth having the form

$$H = H_0 + \varepsilon e^{i(kx-\omega t)}, \tag{5.28}$$

with $H_0 = cst$ and $\varepsilon \ll 1$, then the approximation in $\mathcal{O}(\varepsilon^2)$ of the non-hydrostatic model (2.1)-(2.4) gives

$$\frac{\partial H}{\partial t} + \frac{\partial}{\partial x}\big(H\overline{u}\big) = 0, \tag{5.29}$$

$$H_0\frac{\partial \overline{u}}{\partial t} + H_0\frac{\partial}{\partial x}\left(gH + \overline{p}_{nh}\right) = 0, \tag{5.30}$$

$$H_0\frac{\partial \overline{w}}{\partial t} = 2\overline{p}_{nh}, \tag{5.31}$$

$$H_0\frac{\partial \overline{u}}{\partial x} + 2\overline{w} = 0. \tag{5.32}$$

And it is straightforward to obtain the linear dispersion relation for the system (5.29)-(5.32) under the form

$$\frac{\omega}{k} = \sqrt{\frac{gH_0}{1+\frac{k^2H_0^2}{4}}}. \tag{5.33}$$

The formula (5.33) has to be compared with the dispersion relation (5.27) coming from the Airy wavetheory and the Green-Naghdi model given by

$$\frac{\omega}{k} = \sqrt{\frac{gH_0}{1+\frac{k^2H_0^2}{3}}}.$$

Over Fig. 5.6, we compare the two previous dispersion relations with the dispersion relation (5.27). We observe that under the hypothesis of the linearized model, the Green-Naghdi model give a better approximation of the dispersion relation from Airy that the DAE model (1.34)-(1.37). However, we expect that non-linearities play an important role in the phenomena studied. Depending on the regime, the validity of the model is still an open question.

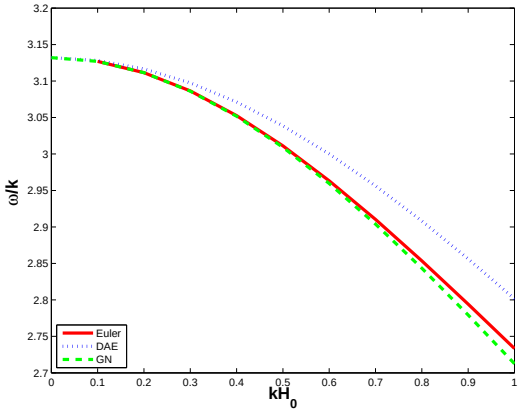

Figure 5.6: The linear dispersion relation for the Airy wave model, the Green-Naghdi system and the DAE model.

5.5 Breaking wave

This work was done in collaboration with Manuel Castro, Tomas Morales and Cipriano Escalante, carried out during a scientific stay financed by Fondation Ledoux in the team headed by Professor Carlos Parés of the University of Malaga.

The non-hydrostatic models and the numerical methods developed to approach the equations are not devoted to represent the breaking wave, which can occur when the wave reaches the coast. Despite the treatment we do for the wet/dry interface, many experiments in laboratory confirm us that we can not recover the behavior of the surface at the coast. To have an accurate result at the coast, it is necessary to propose a breaking detection and modify the numerical method. In this part, we apply the approach proposed in [99] and also applied in [72] for Yamazaki's model, the principle is to add an artificial viscosity when a breaking is detected, to enforce the dissipation of energy.

5.5.1 Modified model

We start with the one-dimensional model (3.2)-(3.4) and add a viscosity term to the momentum equation depending on the breaking criteria. For the sake of clarity, we denote $q = Hu$. We define R_b by:

$$R_b = \frac{\partial}{\partial x}(\mu H \frac{\partial u}{\partial x}), \tag{5.34}$$

with

$$\mu = -\beta H |\frac{\partial q}{\partial x}|,$$

and β is defined by the breaking criteria:

$$\beta = \begin{cases} 1 - \frac{1}{|u_1|}\frac{\partial q}{\partial x} & \text{if } |\frac{\partial q}{\partial x}| \geq u_2, \\ 0 & \text{else,} \end{cases}$$

with u_1, u_2 two characteristic wave speeds set empirically by

$$u_1 = B_1\sqrt{gH}, \quad u_2 = B_2\sqrt{gH}, \quad B1, B2 \in \mathbb{R}. \tag{5.35}$$

The parameters B_1, B_2 are chosen empirically and strongly depend of the model and case [139]. Re-writing Equations (3.2)-(3.4) with the viscosity term R_b, we obtain:

$$\begin{aligned}
\frac{\partial H}{\partial t} + \frac{\partial Hu}{\partial x} &= 0, && (5.36)\\
\frac{\partial Hu}{\partial t} + \frac{\partial Hu^2}{\partial x} + \frac{\partial}{\partial x}(\frac{g}{2}H^2) + \frac{\partial Hp}{\partial x} + 2p\frac{\partial z_b}{\partial x} + R_b &= -gH\frac{\partial z_b}{\partial x}, && (5.37)\\
\frac{\partial Hw}{\partial t} + \frac{\partial Huw}{\partial x} - 2p &= 0, && (5.38)\\
\mathrm{div}_{sw}(\mathbf{u}) &= 0, && (5.39)
\end{aligned}$$

In order to use the same numerical method presented in Chapter 3, we rewrite Equation (5.37) as:

$$\frac{\partial Hu}{\partial t} + \frac{\partial Hu^2}{\partial x} + \frac{\partial}{\partial x}(\frac{g}{2}H^2) + \frac{\partial}{\partial x}\left(H(p + \mu\frac{\partial u}{\partial x})\right) + 2p\frac{\partial z_b}{\partial x} = -gH\frac{\partial z_b}{\partial x}.$$

This allows us to write the system depending on a new non-hydrostatic pressure. To do so, we introduce a new pressure $\tilde{p} = p + \mu\frac{\partial u}{\partial x}$, which takes into consideration the viscosity. The idea is to keep the splitting method in time detailed in Section 3.2. Hence, Equations (5.37)-(5.38) become:

$$\frac{\partial Hu}{\partial t} + \frac{\partial Hu^2}{\partial x} + \frac{\partial}{\partial x}(\frac{g}{2}H^2) + H\frac{\partial}{\partial x}\tilde{p} + \tilde{p}\frac{\partial \zeta}{\partial x} = -gH\frac{\partial z_b}{\partial x} + 2\mu\frac{\partial u}{\partial x}\frac{\partial z_b}{\partial x},$$

$$\frac{\partial Hw}{\partial t} + \frac{\partial Huw}{\partial x} + -2\tilde{p} = -2\mu\frac{\partial u}{\partial x}.$$

Denoting

$$\tilde{R} = \begin{pmatrix} 2\mu\frac{\partial u}{\partial x}\frac{\partial z_b}{\partial x} \\ -2\mu\frac{\partial u}{\partial x} \end{pmatrix},$$

and using the formulation (3.13)-(3.15), it writes:

$$\frac{\partial H}{\partial t} + \frac{\partial Hu}{\partial x} = 0, \tag{5.40}$$

$$\frac{\partial H\mathbf{u}}{\partial t} + \frac{\partial}{\partial x}\left(uH\mathbf{u}\right) + \nabla_0\left(\frac{g}{2}H^2\right) + \nabla_{sw}\,\tilde{p} = -gH\nabla_0 z_b + \tilde{R}, \tag{5.41}$$

$$\mathrm{div}_{sw}\left(\mathbf{u}\right) = 0. \tag{5.42}$$

5.5.2 Discretization

In this section, we focus on the discretization in time using the numerical method described in Chapter 3. We use the combined finite volume / finite element method to solve the problem (5.40)-(5.42) and add the artificial viscosity by adding $\tilde{R}$ (defined by (5.5.1)) in both the prediction and the projection step. First, in the hydrostatic part and then in the correction part where the right hand side of the elliptic equation contains the viscosity term. The term $2\mu\frac{\partial u}{\partial x}\frac{\partial z_b}{\partial x}$ in Equation (5.41) is discretized in the finite volume part as a source term (we use a centered scheme for the disretization of this term). We focus here on the correction part detailed in Equations (3.24) (3.26) for the DAE problem (3.2)-(3.2). Applying the same procedure to Equations (5.40)-(5.42), we obtain:

$$\begin{aligned} H^{n+1} &= H^{n+1/2}, \\ Hu^{n+1} &= Hu^{n+1/2} - \Delta t\nabla_{sw}\left(\tilde{p}^{n+1}\right)|_1, \\ Hw^{n+1} &= Hw^{n+1/2} - \Delta t\nabla_{sw}\left(\tilde{p}^{n+1}\right)|_2 - \Delta t 2\mu\frac{\partial u^{n+1/2}}{\partial x}, \end{aligned}$$

completed with the free divergence condition:

$$\mathrm{div}_{sw}\left(\mathbf{u}^{n+1}\right) = 0. \tag{5.43}$$

Applying the shallow water version of the divergence operator (5.43) to Equations (5.43)-(5.43), it leads to the following pressure equation:

$$\triangle_{sw}\left(\tilde{p}\right) = \frac{1}{\Delta t}\mathrm{div}_{sw}\left(\mathbf{u}^{n+1/2}\right) - \frac{1}{H^{n+1/2}}\mathrm{div}_{sw}\left(\left(\left(0, 2\mu\frac{\partial u^{n+1/2}}{\partial x}\right)^T\right)\right).$$

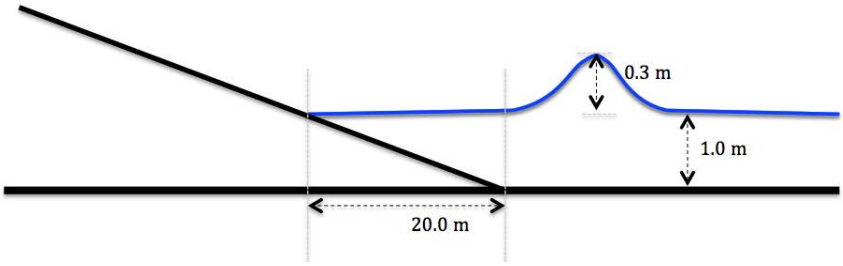

Figure 5.7: Topography of the experiment domain of length $70m$ and a slope of $1/20$.

Using the definition of div_{sw} in (3.11), we obtain:

$$\triangle_{sw}(\tilde{p}) = \frac{1}{\Delta t}\mathrm{div}_{sw}(\mathbf{u}^{n+1/2}) + 4\frac{\mu}{H^{n+1/2}}\frac{\partial u^{n+1/2}}{\partial x}$$

with $\triangle_{sw}(\tilde{p})$ is a shallow water version of the Laplacien operator and is defined by:

$$\triangle_{sw}(\tilde{p}) = \mathrm{div}_{sw}\left(\frac{1}{H}\nabla_{sw}(\tilde{p})\right)$$

Remark 5.5.1. *In two dimensions, the splitting in time applies with*

$$\tilde{R} = \begin{pmatrix} 2\mu\frac{\partial u}{\partial x}\frac{\partial z_b}{\partial x} \\ 2\mu\frac{\partial v}{\partial y}\frac{\partial z_b}{\partial y} \\ -2\mu(\frac{\partial u}{\partial x} + \frac{\partial v}{\partial y}) \end{pmatrix},$$

and $\tilde{p} = p + \mu(\frac{\partial u}{\partial x} + \frac{\partial v}{\partial y})$. *The approach can be extended and only the discretization in space differs from the one-dimensional part.*

5.5.3 Numerical Results

In this section, we propose a numerical test where we reproduce the experiment described in [147]. It consists in propagating a solitary wave in a long channel ending by a slope with the dimensions depicted in Figure 5.7. We initialize the numerical test with a solitary wave of the form (3.77)-(3.80) where we set the intial depth $H_0 = 1\,m$ and an amplitude $a = 0.3\,m$. For this case, the parameters B_1, B_2 introduced by (5.35) have been chosen as $B_1 = 0.5$ and $B_2 = 0.2$. The solitary wave is positioned over the flat bottom at the initialization. Data have been observed at different positions over the slope and every five seconds. In Figure 5.8, we compare the data with the numerical solution obtained using the DAE model for both with a breaking criteria and without. We can observe that we recover the amplitude of the wave when it reaches the slope only with the breaking criteria technique. In Figure 5.8a, we observe the detetion of the the breaking just started, while

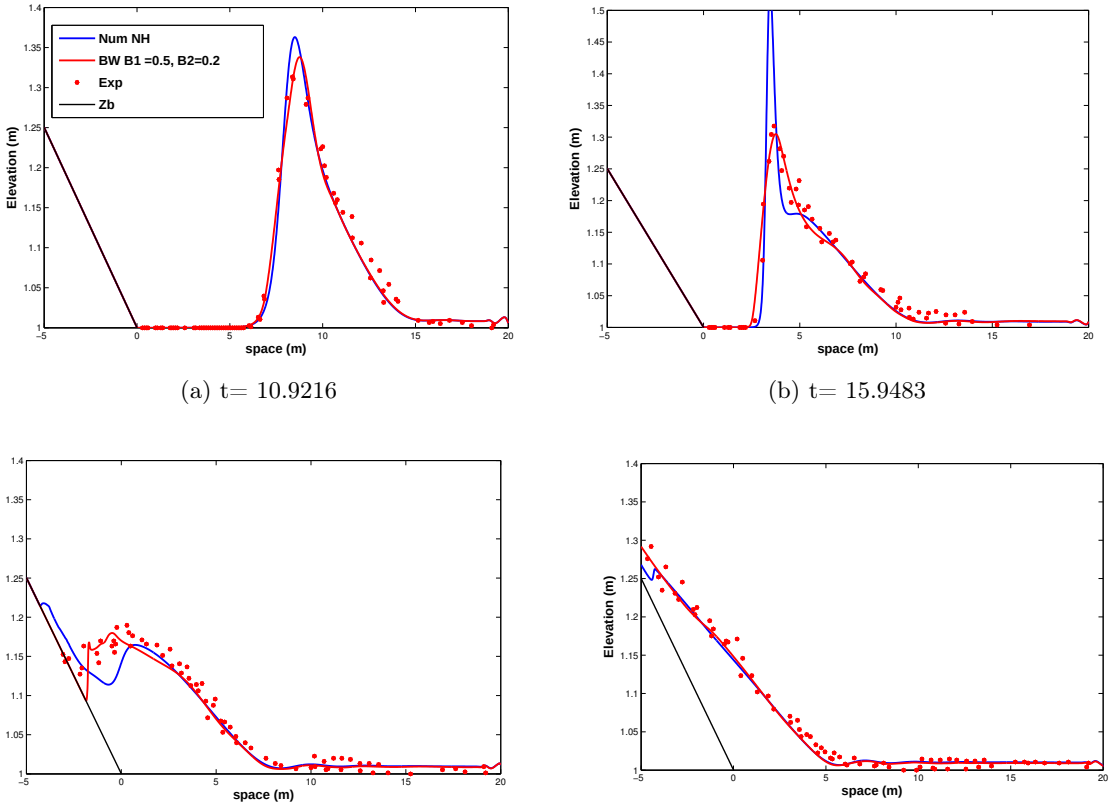

(a) t= 10.9216

(b) t= 15.9483

(c) t= 20.965

(d) t= 25.9834

Figure 5.8: Comparison with data on a domain of length $70m$ and a slope of $1/20$. Simulation run with 8000 nodes.

in Figure 5.8b, we observe a more significant differences between the classical method and the modified method. In Figure 5.8c and 5.8d, we observe a different behavior of the two methods and for both, we use the same treatment of the wet/dry interface given in 2.4.6 and 3.5.2. Notice that the amplitude obtained with the DAE model without a breaking detection can be obtained only with a very fine mesh, indeed, due to the complexity of the non-hydrostatic pressure, it is necessary to run simulations with a significant size of mesh.

5.6 Conclusion

In this Chapter, we studied the one-dimensional problem regarding some new numerical aspects. We give an other validation of the numerical method using a stationary analytical solution. We compared the linearized DAE model with the linearized Euler system in order to compare the dispersion relation. Finally, we apply a standard breaking wave detection in order to simulate a wave reaching the coast and to confront the numerical results with experimental data. This last approach gives relevant results and we plan to apply this method for the two-dimensional model.

Appendix A

A coupled Exner/ Stokes model for the sediment transport

This work has been done in collaboration with Tarik Amtout, Matthieu Brachet, Emmanuel Frenod, Romain Hild, Christophe Prud'homme, Antoine Rousseau and Stephanie Salmon and will be published in the proceedings of CEMRACS 2015.

A.1 Introduction

Many hydrodynamic studies have been done to understand and predict the dynamics of sediments at the bottom of flows which is a significant and complex process for many geophysical situations. Morphodynamics modelling is a broad subject whose principles can be found in several references [126],[127]. We can distinguish two types of sediment transport, the suspended load and the bedload. In this proceeding, we focus on the bedload transport and its impact on the hydrodynamics. The difficulty remains in the necessity to couple the sediment transport models with the hydrodynamic models, and then to develop a robust and stable numerical method.

On the one hand, the sediment transport is usually modeled by the classical Exner equation [130] and several laws of transport have been proposed (see [75] to have delails on some classical laws) by physical arguments or closure relations. On the other hand, models as shallow water equations are used to model the hydrodynamics, and recently in [46, 75] a model derived from the Navier-Stokes equations that has an energy balance.

Concerning the numerical methods that have been established for these models, the main numerical schemes are developed for the hyperbolic systems with source terms for the hydrodynamic flow (see [32], [83]). Therefore, finite volume schemes are applied for the shallow water system [7, 133, 79, 6]. The problem lies in the coupling of the numerical schemes. Indeed, in the shallow water models, the topography is a source term and the Exner equation gives the evolution of the bottom in terms of the fluid velocity. Then, two strategies are distinguished, the splitting one and the non-splitting one (see [16]). The splitting methods are easier to implement but generate instabilities in specific situations (see [53]). On the contrary, more complicated models, for instance involving relaxation, have to be used to take into consideration the fully coupled model [93, 15].

Notice that the shallow water model is based on a hydrostatic assumption. It is deduced from the Navier Stokes equations, neglecting the vertical acceleration (see [79]). Many other free surface models have been developed to take into account non-hydrostatic effects with vertically averaged models: see [30, 42, 106, 43, 62]. Contrariwise, for this study we choose to conserve the z coordinate in our model, which raises the question of time-depending domain when the bathymetry changes with time: this coupling between fluid motion (including vertical effects) and domain evolution is at the core of this paper.

This objective being stated, we start with the simplest possible model, a 2D $(x - z)$ Stokes equation. We couple this equation for the fluid with the Exner model since our computational domain moves as times goes by. We choose to use the Grass law for the

bedload formula (see Equation (A.10)) which is one possible law among others. As for the time coupling between hydrodynamical and morphological processes, we choose to use a monolithic scheme rather than a splitting method: such refinements (that can prove to be very important, see [53]) are beyond the scope of our work.
Let us now focus on the main feature of this work: the use of fluid-structure interaction techniques (see [84, 47]) for the coupling between Stokes and Exner equations. From the numerical viewpoint, we decided to use finite elements and the open software Feel++ [136, 137] that are well adapted to fluid-structure interaction (ALE implementation, see [84]) and parallelization for large 3D computations. The article is organized as follows, the first part is devoted to the description of the fluid model and the sediment model at the bottom. In a second part, it is explained why a method like the ALE is necessary to couple the models. The third part establishes a complete ALE formulation of the Stokes-Exner model. Then, a variational formulation is given with the different boundary conditions that we explore. Finally, some numerical results are presented to evaluate the model and the method used to solve the problem.

A.2 The model

In this part, we introduce various equations for our coupled system. Section 1.1 is devoted to the unsteady Stokes equations (dimension 2, $x-z$) that we supplement with appropriate boundary conditions. Section 1.2 is dedicated to the bottom boundary condition, located at the (moving) boundary where the fluid model is coupled with the Exner equation for bedload. Before recalling the complete coupled system in section 1.4, we present in Section 1.3 the ALE implementation of our model.

We start with a model domain $\Omega(t)$ and a specific boundary to represent the topography. We consider the domain as a moving domain depending on the bottom. Let us introduce the domain with the following definitions:

$$\Omega(t) = \{(x,z) \in \mathbb{R}^2 \quad | \quad 0 \leq x \leq l, \quad b_z(x,t) \leq z \leq 1\} \tag{A.1}$$

where $l > 0$ is the cavity length and $b_z(x,t)$ is the bottom topography in x at time t. We also denote by $\Gamma(t) = \Gamma_{in}(t) \cup \Gamma_{out}(t) \cup \Gamma_s \cup \Gamma_b(t)$ the boundaries (see Figure A.1):

- $\Gamma_{in}(t) = \{0\} \times [b_z(0,t), 1]$
- $\Gamma_{out}(t) = \{l\} \times [b_z(l,t), 1]$
- $\Gamma_s = [0,l] \times \{1\}$
- $\Gamma_b(t) = \{(x,z) \in \mathbb{R}^2 \text{ s.t. } z = b_z(x,t), x \in [0,l]\}$

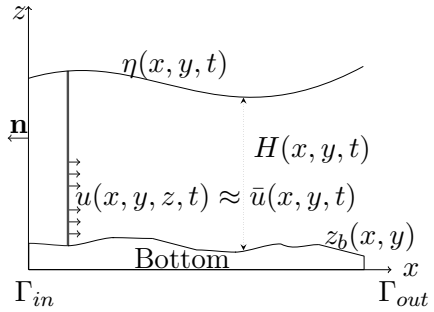

Figure A.1: Definition of the domain

The coupled model leads to solving the non-steady Stokes problem in the fluid domain $\Omega(t)$ and the Exner equation to give the boundary $\Gamma_b(t)$. The issue is to model the fluid process in interaction with the sediment transport at the bottom. To do so, we describe in the following sections the equations chosen for the fluid in the domain $\Omega(t)$ with usual boundary conditions for the boundary Γ. Then we propose to use Exner equation to make the boundary Γ_b move.

A.2.1 Hydrodynamical Model

We consider the unsteady Stokes problem on the domain $\Omega(t)$

$$\rho\frac{\partial \mathbf{u}}{\partial t} - \mu\triangle\mathbf{u} + \nabla p = 0 \text{ on } \Omega(t), \tag{A.2}$$

$$\text{div}\,(\mathbf{u}) = 0 \text{ on } \Omega(t), \tag{A.3}$$

where $\mathbf{u} = (u, w)^T$ is the velocity of the fluid, p is the pressure, $\mu > 0$ is the dynamic viscosity and ρ is the density. From now on, we will use $\rho = 1$. This problem is completed by the conditions detailed hereafter.

A crucial issue is to have judicious boundary conditions at the interface between the fluid and the topography. The physical behavior of the sediment transport studied here implies an impermeability boundary condition, then a constraint on the normal component of the velocity has to be done. Concerning the other boundaries, one can consider a model test case on which one wants to simulate a flow on the pseudo free surface (Γ_s in our case), we impose the velocity on the surface boundary by a Dirichlet condition and free boundary conditions, using Neumann conditions, at the inlet and outlet.

$$\mathbf{u} = \mathbf{g}_1 \text{ on } \Gamma_s \tag{A.4}$$

$$\boldsymbol{\sigma}\mathbf{n} = \mu\frac{\partial \mathbf{u}}{\partial \mathbf{n}} - p\mathbf{n} = \mathbf{g}_2 \text{ on } \Gamma_{in}(t) \cup \Gamma_{out}(t) \tag{A.5}$$

$$\mathbf{u}\cdot\mathbf{n} = 0 \quad \text{on } \Gamma_b(t) \tag{A.6}$$

$$\boldsymbol{\sigma}\mathbf{n}\cdot\boldsymbol{\tau} = \mu\frac{\partial \mathbf{u}}{\partial \mathbf{n}}\cdot\boldsymbol{\tau} = g_3 \text{ on } \Gamma_b(t) \tag{A.7}$$

where $\boldsymbol{\sigma}$ is the stress tensor defined by:

$$\boldsymbol{\sigma} = (\mu\nabla\mathbf{u} - p\mathbb{I}d). \tag{A.8}$$

The condition (A.4) imposes the force by using Dirichlet condition.
The condition (A.5) lets free the velocity at the inlet and at the outlet.
The condition (A.6) imposes the normal component of the velocity to be null at the bottom. It is the condition of impermeability of the domain.
The condition (A.7) lets free the tangential component of the velocity at the bottom. It is needed to have a displacement of the bottom.

A.2.2 Morphodynamics model

The sediment dynamics is based on the formulation of a sediment continuity equation stating that the time variation of the sediment layer in a certain volume is due to the net variation of the solid transport through the boundaries of the volume. The mathematical expression of such law is known as the Exner equation [125] presented in this form:

$$\frac{\partial b_z}{\partial t} + \xi\frac{\partial Q}{\partial x} = 0 \quad \forall x \in [0,l], \forall t \in [0,T] \tag{A.9}$$

where $b_z(x,t)$ is the bed elevation, ξ is defined by $(1-p)^{-1}$ where p is the material porosity and Q denotes the solid transport discharge along the x coordinate influenced by the velocity $\mathbf{u}$. The formulation of the bedload discharge Q can be based on deterministic laws ([17],[68],[145]) or in probabilistic methods ([69],[97]), often supported by experimentation. Grass [85] discussed one of the most basic sediment transport laws that can be written in one dimension as:

$$Q = a|\mathbf{u}|^{3/2} \tag{A.10}$$

where $0 < a < 1$ is an empirical parameter depending of the type of the sediments, it takes into account the effects due to the grain size and the kinematic viscosity . For the problem studied in this work, the velocity taken into consideration in the Grass formula is reduced to the tangential part $\mathbf{u}_\tau$ since we impose an impermeability condition on the interface, see the boundary condition (A.6).

For the sake of clarity, we will consider the Exner equation under the form:

$$\frac{\partial b_z}{\partial t} + \frac{\partial Q}{\partial x} = 0 \quad \forall x \in [0,l], \forall t \in [0,T] \tag{A.11}$$

where $Q = \alpha|\mathbf{u}_\tau|^{3/2}$ and $\alpha = \xi a$.

A.2.3 Arbitrary Lagrangian Eulerian (ALE) Method

We now want to couple the two models previously described. The issue is to solve the unsteady Stokes equations with a moving boundary Γ_b. In fluid mechanics, one can enumerate two ways to represent a problem: Lagrangian and Eulerian formulation. On the one hand, Lagrangian formulation is similar to keep track of the location of each fluid particles. The velocity $\mathbf{u}$ and the density ρ depend only on $\mathbf{x_0}$ the initial position of the particles and on t the time. Then, the time derivative of a quantity F is given by the total time derivative :

$$\frac{DF}{Dt}$$

On the other hand, the main idea of the Eulerian method is to fix a system of coordinates and follow the flux of particles. In this case, the velocity $\mathbf{u}$ and the density ρ depend on $\mathbf{x}$ the position in a global system of coordinates and t the time. Now, for a function F, the time derivative is given by :

$$\frac{\partial F}{\partial t} + \mathbf{u} \cdot \nabla F$$

The relation between the Eulerian and the Lagrangian time derivatives is:

$$\frac{D}{Dt} = \frac{\partial}{\partial t} + \mathbf{u} \cdot \nabla \tag{A.12}$$

Then, the idea of the ALE method is to combine the Eulerian and the Lagrangian method in order to take into consideration the boundary displacement at each iteration, which represents the bottom in our case. The goal is to avoid remeshing the domain at each time iteration. This method was first developped for finite difference in [128, 78] and scope to finite element methods in [59, 60] and [24]. In 2004, [47] built a method for great order elements. This has been widely used in Fluid Structure Interaction (FSI) on which it is usual to have a fluid equation like unsteady Stokes or Navier Stokes in the fluid domain and an elasticity equation for the structure. This is used in the simulation of blood flow in arteries for instance (see [47], [84]). In the context of the sediment transport, the bottom plays the role of the structure in the classical methods. Then the idea is to use the analogy of these methods for the coupled Stokes Exner model.

As the goal is to avoid remeshing the domain, the clue is to use a Lagrangian description to describe the bottom displacement and a Eulerian description for the fluid model. First, we define a reference domain on which the topography is described by a Lagrangian description. Secondly, we consider the moving mesh $\Omega(t)$ on which the equations of the fluid evoluates. Then, it is necessary to define an application able to make the link between the two domains. In the following, we write $\widehat{\cdot}$ all quantities concerning the reference domain. For the sake of clarity, we choose $\widehat{\Omega}$ the rectangular domain $[0, l] \times [0, 1]$ and the following boundaries :

- $\widehat{\Gamma}_{in} = \{0\} \times [0, 1]$,

- $\widehat{\Gamma}_s = [0, l] \times \{1\}$,
- $\widehat{\Gamma}_{out} = \{l\} \times [0, 1]$,
- $\widehat{\Gamma}_b = [0, l] \times \{0\} = \widehat{\gamma}_b \times \{0\}$ where $\widehat{\gamma}_b = [0, l]$.

The relation between the reference domain $\widehat{\Omega}$ and the physical domain $\Omega(t)$, is made by an ALE map (see figure A.2), defined by :

$$\mathcal{A}^t : \begin{cases} \widehat{\Omega} & \longrightarrow & \Omega(t) \\ \widehat{\mathbf{x}} & \longmapsto & \mathbf{x}(\widehat{\mathbf{x}}, t) \end{cases} \tag{A.13}$$

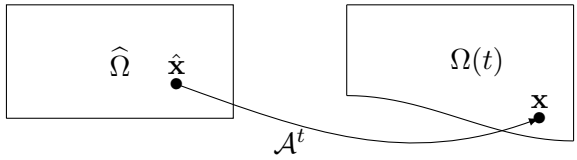

Figure A.2: The ALE map

Therefore the point $\mathbf{x}(t) \in \Omega(t)$ is obtained by:

$$\mathbf{x}(t) = \mathcal{A}^t(\widehat{\mathbf{x}}) = \widehat{\mathbf{x}} + \widehat{\mathbf{d}}_\delta(\widehat{\mathbf{x}}, t) \tag{A.14}$$

where $\widehat{\mathbf{d}}_\delta(\widehat{\mathbf{x}}, t)$ is the displacement of $\widehat{\mathbf{x}}$ between $\widehat{\Omega}$ and $\Omega(t)$. Notice that $\mathbf{x}(t)$ is time dependent. Then, we can define the velocity of the mesh:

$$\widehat{\mathbf{w}}(\widehat{\mathbf{x}}, t) = \frac{\partial \mathcal{A}^t}{\partial t}(\widehat{\mathbf{x}}) = \frac{\partial \widehat{\mathbf{d}}_\delta}{\partial t}(\mathbf{x}, t) \tag{A.15}$$

where $\widehat{\mathbf{w}}(\hat{\mathbf{x}}, t) \in \mathbb{R}^d$ is defined for $\hat{\mathbf{x}} \in \widehat{\Omega} \times \mathbb{R}^+$. To take into consideration the velocity of the mesh into the fluid equation, it is necessary to define it in the fluid domain $\Omega(t)$, namely:

$$\mathbf{w} \quad : \quad (\mathbf{x}, t) \in \Omega(t) \times \mathbb{R}^+ \to \mathbb{R}^d \tag{A.16}$$

$$\mathbf{w} \quad = \quad \widehat{\mathbf{w}} \circ \left(\mathcal{A}^t\right)^{-1}. \tag{A.17}$$

This definition will allow us to rewrite the fluid equation with a Eulerian description, taking into account the displacement of the mesh. The last step of the method leads to determine the equation of the displacement $\widehat{\mathbf{d}}_\delta$ in $\widehat{\Omega}$. In practice, $\mathbf{d}_\delta$ is the solution of a PDE like harmonic or Wislow equation. For the sake of simplicity, we will work with harmonic extension that allows to have a smooth mesh. We often need to transport an equation from $\widehat{\Omega}$ to $\Omega(t)$ and mutually. Let $u : \Omega(t) \times \mathbb{R}^+ \longrightarrow \mathbb{R}^d$, then the corresponding map in $\widehat{\Omega}$ is $\widehat{u} = u \circ \mathcal{A}^t$.

If $\mathcal{D}\mathbf{u}/\mathcal{D}t$ is the time-derivative of u in ALE, we have the following equation:

$$\frac{\mathcal{D}\mathbf{u}}{\mathcal{D}t} = \left.\frac{\partial \mathbf{u}}{\partial t}\right|_x + \mathbf{w}\cdot\nabla\mathbf{u} \tag{A.18}$$

- Notice that if $\mathbf{w} = \mathbf{u}$, the mesh is moving with the particles so the description is Lagrangian.
- If $\mathbf{w} = \mathbf{0}$, the mesh does not move and the description is Eulerian.

A.2.4 Coupled model

In this part, we focus on the coupled model. We denote by $\widehat{\mathbf{x}}$ a point in the reference domain $\widehat{\Omega}$ and by $\Omega(t)$ the deformed domain after the transformation. The deformation of the mesh leads to consider the derivative $\mathcal{D}$ defined by (A.18) which is also called the ALE derivative where the velocity $\mathbf{w}$ is defined as: $\widehat{\mathbf{w}} = \left.\frac{\partial \widehat{\mathbf{d}}_\delta}{\partial t}\right|_{\hat{x}}$ and represents the velocity of the displacement of the mesh, that is to say the velocity of the particle in the referential domain. This allows to write the fluid model with a moving mesh on $\Omega(t)$. Concerning the boundary conditions, we still consider a slip boundary condition at the interface between the topography and the fluid. The complete model is composed of the equation of the fluid in two dimensional domain, the equation of the topography in one dimensional domain and the ALE equation in two dimensional domain. According to (A.18), the coupled model is written as follows :

Fluid equation

The fluid equation is given by :

$$\frac{\mathcal{D}\mathbf{u}}{\mathcal{D}t} - (\mathbf{w}\cdot\nabla)\mathbf{u} - \mu\,\triangle\,\mathbf{u} + \nabla p = \mathbf{F} \quad \text{on } \Omega(t) \tag{A.19}$$

$$\operatorname{div}(\mathbf{u}) = 0 \quad \text{on } \Omega(t) \tag{A.20}$$

$$+\mathbf{BC} \tag{A.21}$$

where the boundary conditions are those of section A.2.1. In particular, condition (A.7) depends on the bottom topography.

Bottom equation

We consider the one dimensional domain $\widehat{\gamma}_b = [0, l]$, on which the bottom topography at position $\widehat{x} \in \widehat{\gamma}_b$ and time $t > 0$ is defined by the Exner equation (A.9):

$$\frac{\partial \hat{b}_z(\hat{x},t)}{\partial t} + \frac{\partial \hat{Q}(\hat{x},t)}{\partial \hat{x}} = 0 \quad \forall \hat{x} \in \widehat{\gamma}_b, t > 0 \tag{A.22}$$

$$\hat{b}_z(\hat{x},0) = \hat{b}_{z,0}(\hat{x}) \tag{A.23}$$

Using (A.10), the sediment law $\hat{Q}$ depends on the fluid velocity and can be written in the reference domain by:

$$\hat{Q}(\hat{x},t) = Q\left(\hat{x}+\hat{b}(\hat{x}),t\right) \quad \forall \hat{x}\in\widehat{\gamma}_b \tag{A.24}$$

$$= \alpha u_\tau \left(\hat{x}+\hat{b}(\hat{x})\right)^{3/2} \tag{A.25}$$

Displacement equation

This displacement needs to be extended in the fluid domain to associate a new ALE map over the mesh. In order to do this, we use a classical harmonic extension (see [47] for more details).

$$-\triangle\,\hat{\mathbf{d}}_\delta = 0 \quad \text{on } \hat{\Omega} \tag{A.26}$$

$$\hat{\mathbf{d}}_\delta = 0 \quad \text{on } \hat{\Gamma}_s \tag{A.27}$$

$$\frac{\partial\hat{\mathbf{d}}_\delta}{\partial\mathbf{n}} = 0 \quad \text{on } \hat{\Gamma}_{in}\cup\hat{\Gamma}_{out} \tag{A.28}$$

$$\hat{\mathbf{d}}_\delta = (0,\hat{b}_z(\hat{x},t))^T \quad \text{on } \hat{\Gamma}_b \tag{A.29}$$

This allows us to have a given displacement defined on $\hat{\Gamma}_b$, to let free the boundaries $\hat{\Gamma}_{in}$ and $\hat{\Gamma}_{out}$, and to fix the boundary $\hat{\Gamma}_s$. The harmonic problem spreads the displacement $\hat{\mathbf{d}}_\delta$ on all the domain.

Equation for w

We denote by $\hat{\mathbf{w}}$ the velocity of the displacement

$$\hat{\mathbf{w}}(\widehat{\mathbf{x}},t) = \frac{\partial\hat{\mathbf{d}}(\hat{\mathbf{x}},t)}{\partial t} \tag{A.30}$$

Then, using the ALE transformation, we can compute the velocity $\mathbf{w}$ in the domain $\Omega(t)$:

$$\mathbf{w}(\mathbf{x},t) = \hat{\mathbf{w}}\left((\mathcal{A}^t)^{-1}(\mathbf{x}),t\right) \tag{A.31}$$

A.3 Variational formulation

This part is devoted to the variational formulation of the problem taking the ALE description into account.

A.3.1 Variational formulation of the Exner equation

By multiplying the Exner equation and integrating over $\hat{\gamma}_b$, we have the following variational formulation for equations (A.22)-(A.23): Taking a test function $\phi\in H^1(\hat{\gamma}_b)$, we

have:

$$\frac{d}{dt}\int_{\hat{\gamma}_b} \hat{b}_z(\hat{x},t)\phi(\hat{x})\,d\hat{x} + \int_{\hat{\gamma}_b} \frac{\partial \hat{Q}(\hat{x},t)}{\partial \hat{x}}\phi(\hat{x})\,d\hat{x} = 0 \tag{A.32}$$

$$\frac{d}{dt}\int_{\hat{\gamma}_b} \hat{b}_z(\hat{x},t)\phi(\hat{x})\,d\hat{x} - \int_{\hat{\gamma}_b} \hat{Q}(\hat{x},t)\phi'(\hat{x})\,d\hat{x} + \Big[\hat{Q}(\hat{x},t)\phi(\hat{x})\Big]_{\hat{\gamma}_b} = 0 \quad \forall \phi \in H^1(\gamma_b) \tag{A.33}$$

The problem becomes: find $\hat{b}_z$ such that for all $\phi \in H^1(\hat{\gamma}_b)$

$$\frac{d}{dt}\int_{\hat{\gamma}_b} \hat{b}_z(\hat{x},t)\phi(\hat{x})\,d\hat{x} = \int_{\hat{\gamma}_b} \hat{Q}(\hat{x},t)\phi'(\hat{x})\,d\hat{x} - \Big[\hat{Q}(\hat{x},t)\phi(\hat{x})\Big]_{\hat{\gamma}_b} \tag{A.34}$$

A.3.2 Variational formulation of unsteady Stokes Equation

The problem leads to find $\mathbf{u} \in \mathbf{V}$ and $p \in Q$ such that the fluid equation (A.19) is satisfied. Let $\mathbf{X}$ be the functional set of test functions. Notice that the sets $\mathbf{V}$, $\mathbf{X}$ and W will be defined later. In practice, the sets $\mathbf{V}$ and $\mathbf{X}$ can be different, they depend on the boundary conditions. Multiplying (A.19) with a test function $\mathbf{v} \in \mathbf{X}$ and (A.20) with a test function $q \in Q$, and then integrating by part, we get:

$$\int_\Omega \frac{\mathcal{D}\mathbf{u}}{\mathcal{D}t}\cdot\mathbf{v} - \int_\Omega [(\mathbf{w}\cdot\nabla)\mathbf{u}]\cdot\mathbf{v} + \mu\int_\Omega \nabla\mathbf{u} : \nabla\mathbf{v} - \mu\int_\Gamma \frac{\partial\mathbf{u}}{\partial\mathbf{n}}\cdot\mathbf{v} - \int_\Omega p\,\mathrm{div}(\mathbf{v}) + \int_\Gamma p\mathbf{n}\cdot\mathbf{v} = \int_\Omega \mathbf{F}\cdot\mathbf{v} \tag{A.35}$$

$$\int_\Omega \mathrm{div}(\mathbf{u})\,q = 0 \tag{A.36}$$

Then, using the Reynolds transport formula on the first term of (A.35):

$$\begin{aligned} \frac{\mathrm{d}}{\mathrm{d}t}\int_\Omega \mathbf{u}\cdot\mathbf{v} - \int_\Omega (\nabla\cdot\mathbf{w})\mathbf{u}\cdot\mathbf{v} - \int_\Omega [(\mathbf{w}\cdot\nabla)\mathbf{u}]\cdot\mathbf{v} & \\ + \mu\int_\Omega \nabla\mathbf{u} : \nabla\mathbf{v} - \mu\int_\Gamma \frac{\partial\mathbf{u}}{\partial\mathbf{n}}\cdot\mathbf{v} & \\ - \int_\Omega p\,\mathrm{div}(\mathbf{v}) + \int_\Gamma p\mathbf{n}\cdot\mathbf{v} &= \int_\Omega \mathbf{F}\cdot\mathbf{v} \end{aligned} \tag{A.37}$$

$$\int_\Omega \mathrm{div}(\mathbf{u})\,q = 0 \tag{A.38}$$

We define the following forms:

$$a_1(\mathbf{u},\mathbf{v}) = \int_{\Omega(t)} \mu\nabla\mathbf{u} : \nabla\mathbf{v}\,dx \qquad \forall \mathbf{u}\in\mathbf{V}, \mathbf{v}\in\mathbf{X} \tag{A.39}$$

$$a_2(\mathbf{u},\mathbf{v}) = -\int_\Omega (\nabla\cdot\mathbf{w})\mathbf{u}\cdot\mathbf{v} - \int_\Omega [(\mathbf{w}\cdot\nabla)\mathbf{u}]\cdot\mathbf{v}\,dx \quad \forall \mathbf{u}\in\mathbf{V}, \mathbf{v}\in\mathbf{X} \tag{A.40}$$

$$a(\mathbf{u},\mathbf{v}) = a_1(\mathbf{u},\mathbf{v}) + a_2(\mathbf{u},\mathbf{v}) \tag{A.41}$$

$$b(\mathbf{u},q) = \int_{\Omega(t)} q\,\mathrm{div}(\mathbf{u})\,dx \qquad \forall \mathbf{u}\in\mathbf{V}, q\in Q \tag{A.42}$$

$$L(\mathbf{v}) = \int_{\Omega(t)} F(t)\cdot\mathbf{v}\,dx \qquad \forall \mathbf{v}\in\mathbf{X} \tag{A.43}$$

We now need to treat the boundary conditions.

$$\mathbf{u} = \mathbf{g}_1 \text{ on } \Gamma_s \tag{A.44}$$

$$\boldsymbol{\sigma}\mathbf{n} = \mu\frac{\partial\mathbf{u}}{\partial\mathbf{n}} - p\mathbf{n} = \mathbf{g}_2 \text{ on } \Gamma_{in}(t)\cup\Gamma_{out}(t) \tag{A.45}$$

$$\mathbf{u}\cdot\mathbf{n} = 0 \quad \text{on } \Gamma_b(t) \tag{A.46}$$

$$\boldsymbol{\sigma}\mathbf{n}\cdot\boldsymbol{\tau} = \mu\frac{\partial\mathbf{u}}{\partial\mathbf{n}}\cdot\boldsymbol{\tau} = g_3 \text{ on } \Gamma_b(t) \tag{A.47}$$

Dirichlet and Neumann boundary conditions

We impose the Dirichlet condition in a strong way, the condition is embedded directly into the space in which we search the solution. We introduce the spaces:

$$\mathbf{V} = \{\mathbf{u}\in(\mathbf{H}^1(\Omega(t)))^2, \quad \mathbf{u} = \mathbf{g}_1 \text{ on } \Gamma_s\}$$
$$\boldsymbol{X} = \{\mathbf{v}\in(\mathbf{H}^1(\Omega(t)))^2, \quad \mathbf{v} = 0 \text{ on } \Gamma_s\}$$
$$Q = L^2_0(\Omega(t)) = \{q\in L^2(\Omega(t)), \quad \int_{\Omega(t)} q\,dx = 0\}$$

The Neumann condition on $\Gamma_{in}\cup\Gamma_{out}$ comes naturally into the formulation. Indeed, the boundary terms can be written with $\mathbf{v}\in\boldsymbol{X}$:

$$\int_{\Gamma_s}\left(p\mathbf{n}-\mu\frac{\partial\mathbf{u}}{\partial\mathbf{n}}\right)\cdot\underbrace{\mathbf{v}}_{0} + \int_{\Gamma_{in}\cup\Gamma_{out}}\underbrace{\left(p\mathbf{n}-\mu\frac{\partial\mathbf{u}}{\partial\mathbf{n}}\right)}_{\mathbf{g}_2}\cdot\mathbf{v} + \int_{\Gamma_b}\underbrace{\left(p\mathbf{n}-\mu\frac{\partial\mathbf{u}}{\partial\mathbf{n}}\right)}_{\boldsymbol{\sigma}\mathbf{n}}\cdot\mathbf{v} \tag{A.48}$$

Then, the problem writes:
Find $\mathbf{u}\in\mathbf{V}$, $p\in Q$ such that

$$\frac{\mathrm{d}}{\mathrm{d}t}\int_\Omega \mathbf{u}\cdot\mathbf{v} - \int_\Omega[(\mathbf{w}\cdot\nabla)\mathbf{u}]\cdot\mathbf{v} - \int_\Omega(\nabla\cdot\mathbf{w})\mathbf{u}\cdot\mathbf{v} + \mu\int_\Omega\nabla\mathbf{u}:\nabla\mathbf{v} - \int_\Omega p\,\mathrm{div}(\mathbf{v})$$
$$= \int_\Omega\mathbf{F}\cdot\mathbf{v} + \int_{\Gamma_{in}\cup\Gamma_{out}}\mathbf{g}_2\cdot\mathbf{v} + \int_{\Gamma_b}\boldsymbol{\sigma}\mathbf{n}\cdot\mathbf{v} \quad \forall\mathbf{v}\in\boldsymbol{X} \tag{A.49}$$

$$\int_\Omega \mathrm{div}(\mathbf{u})\,q = 0 \quad \forall q\in Q \tag{A.50}$$

With the notations (A.39)- (A.42), the problem writes :
Find $\mathbf{u} \in \mathbf{V}, p \in Q$ such that :

$$\frac{\mathrm{d}}{\mathrm{d}t}\int_\Omega \mathbf{u}\cdot\mathbf{v} + a(\mathbf{u},\mathbf{v}) + b(\mathbf{v},q) = L(\mathbf{v}) \qquad \forall \mathbf{v}\in\mathbf{X} \tag{A.51}$$

$$b(\mathbf{u},q) = 0 \qquad \forall q \in Q \tag{A.52}$$

The bilinear forms a and b are defined by (A.41)-(A.42), and L is defined by:

$$L(\mathbf{v}) = \int_{\Omega(t)} \mathbf{F}\cdot\mathbf{v} + \int_{\Gamma_{in}\cup\Gamma_{out}} \mathbf{g}_2\cdot\mathbf{v} + \int_{\Gamma_b} \boldsymbol{\sigma}\mathbf{n}\cdot\mathbf{v} \tag{A.53}$$

Slip boundary conditions

In this section, we are interested in the interface between the fluid and the topography and we preconise to have a slip boundary condition on Γ_b, which is physically consistent with the sediment transport model chosen in this study, namely the bedload transport. Then, we give the variational formulation with slip boundary condition $\mathbf{u}\cdot\mathbf{n} = 0$ on Γ_b. It is not natural to impose a slip boundary condition in the Stokes problem, and this problem has been widely studied:

- **First variational strategy**
  A first strategy, studied in [58], consists in giving a condition on the stress tensor $\boldsymbol{\sigma}\mathbf{n}\cdot\boldsymbol{\tau} = g_3$. We rewrite the test function $\mathbf{v} = (\mathbf{v}\cdot\mathbf{n})\,\mathbf{n} + (\mathbf{v}\cdot\boldsymbol{\tau})\,\boldsymbol{\tau}$ where $\mathbf{n}$ is the normal component and $\boldsymbol{\tau}$ is the tangential component on Γ_b. Taking $g_3 = 0$ and

  $$\mathbf{u}\in\mathbf{W} = \{\mathbf{v}\in\mathbf{V}, \quad \mathbf{v} = 0 \text{ on } \Gamma_s, \quad \mathbf{v}\cdot\mathbf{n}|_{\Gamma_b} = 0\}, \tag{A.54}$$

  $$\mathbf{Y} = \{\mathbf{v}\in\mathbf{X}, \quad \mathbf{v} = 0 \text{ on } \Gamma_s, \quad \mathbf{v}\cdot\mathbf{n}|_{\Gamma_b} = 0\} \tag{A.55}$$

  it is straightforward to verify that the variational formulation writes

  $$\frac{\mathrm{d}}{\mathrm{d}t}\int_\Omega \mathbf{u}\cdot\mathbf{v} - \int_\Omega (\nabla\cdot\mathbf{w})\mathbf{u}\cdot\mathbf{v} - \int_\Omega [(\mathbf{w}\cdot\nabla)\mathbf{u}]\cdot\mathbf{v} \tag{A.56}$$

  $$+\mu\int_\Omega \nabla\mathbf{u} : \nabla\mathbf{v} - \int_\Omega p\,\mathrm{div}(\mathbf{v}) = \int_\Omega \mathbf{F}\cdot\mathbf{v} + \int_{\Gamma_{in}\cup\Gamma out} \mathbf{g}_2\cdot\mathbf{v} \quad \forall \mathbf{v}\in\mathbf{Y}$$

  $$\int_\Omega \mathrm{div}(\mathbf{u})\,q = 0 \qquad \forall q\in Q. \tag{A.57}$$

- **Second variational strategy**
  A second strategy consists in giving a condition on the velocity at the boundary, see [91], as follows $\mu\dfrac{\partial\mathbf{u}}{\partial\mathbf{n}}\cdot\boldsymbol{\tau} + \alpha(\mathbf{u}\cdot\boldsymbol{\tau}) = g$ with $\alpha > 0$. To this aim, we notice that

  $$\int_{\Gamma_b} \boldsymbol{\sigma}\mathbf{n}\cdot\mathbf{v} = \int_{\Gamma_b} (\boldsymbol{\sigma}\mathbf{n}\cdot\mathbf{n})(\mathbf{v}\cdot\mathbf{n}) + (\boldsymbol{\sigma}\mathbf{n}\cdot\boldsymbol{\tau})(\mathbf{v}\cdot\boldsymbol{\tau}) \tag{A.58}$$

and we rewrite the test function $\mathbf{v}$ in terms of the normal component and the tangential component, as for the previous case. Taking

$$\mathbf{u} \in \mathbf{W} = \{\mathbf{v} \in \mathbf{V}, \quad \mathbf{v} = 0 \text{ on } \Gamma_s, \quad \mathbf{v}\cdot\mathbf{n}|_{\Gamma_b} = 0\},$$

the variational formulation writes:

$$\begin{aligned} &\frac{\mathrm{d}}{\mathrm{d}t}\int_\Omega \mathbf{u}\cdot\mathbf{v} - \int_\Omega (\nabla\cdot\mathbf{w})\mathbf{u}\cdot\mathbf{v} - \int_\Omega [(\mathbf{w}\cdot\nabla)\mathbf{u}]\cdot\mathbf{v} \\ &+\mu\int_\Omega \nabla\mathbf{u} : \nabla\mathbf{v} - \int_\Omega p\,\mathrm{div}(\mathbf{v}) + \int_{\Gamma_b}\alpha(\mathbf{u}\cdot\boldsymbol{\tau})(\mathbf{v}\cdot\boldsymbol{\tau}) \;=\; \int_\Omega \mathbf{F}\cdot\mathbf{v} + \int_{\Gamma_b} g(\mathbf{v}\cdot\boldsymbol{\tau}) \quad \text{(A.59)} \\ &\qquad\qquad + \int_{\Gamma_{in}\cup\Gamma out}\mathbf{g}_2\cdot\mathbf{v} \qquad \forall\mathbf{v}\in\mathbf{Y} \\ &\int_\Omega \mathrm{div}(\mathbf{u})\,q \;=\; 0 \qquad \forall q\in Q. \quad \text{(A.60)} \end{aligned}$$

- **Third variational strategy**

  An other alternative leads to using a penalty method. As in a previous case, we take $\boldsymbol{X} = \{\mathbf{v}\in(\mathbf{H}^1(\Omega(t)))^2, \quad \mathbf{v}=0 \text{ on } \Gamma_s\}$. In order to impose the condition $\mathbf{u}\cdot\mathbf{n}=0$ for the velocity which is not natural in the variational formulation, we consider the formulation (A.51) and penalize the natural boundary condition :

$$\boldsymbol{\sigma}\mathbf{n}|_{\Gamma_b} \;=\; -\frac{1}{\varepsilon}(\mathbf{u}\cdot\mathbf{n})\mathbf{n}$$

  where $\varepsilon \ll 1$. The variational formulation becomes:
  Find $\mathbf{u}\in\mathbf{V}$ and $p\in Q$ such that:

$$\begin{aligned} \frac{\mathrm{d}}{\mathrm{d}t}\int_\Omega \mathbf{u}\cdot\mathbf{v} + \tilde{a}(\mathbf{u},\mathbf{v}) + b(\mathbf{v},p) &= L(\mathbf{v}) \quad \forall\mathbf{v}\in\mathbf{X} && \text{(A.61)} \\ b(\mathbf{u},q) &= 0 \quad \forall q\in Q && \text{(A.62)} \end{aligned}$$

  with the bilinear form b defined by (A.42), L and $\tilde{a}$ defined by

$$\tilde{a}(\mathbf{u},\mathbf{v}) = a_1(\mathbf{u},\mathbf{v}) + a_2(\mathbf{u},\mathbf{v}) + \frac{1}{\varepsilon}\int_{\Gamma_b}(\mathbf{u}\cdot\mathbf{n})(\mathbf{v}\cdot\mathbf{n})\,d\sigma \quad \text{(A.63)}$$

$$L(\mathbf{v}) = \int_\Omega \mathbf{F}\cdot\mathbf{v} + \int_{\Gamma_{in}\cup\Gamma out}\mathbf{g}_2\cdot\mathbf{v} \quad \text{(A.64)}$$

  It is proved by Dione in [58] that this problem converges to the problem with slip boundary conditions when ε tends to zero.

A.4 Numerical tests

A.4.1 Validation with analytical solutions of the Stokes equations

In order to validate the numerical method proposed and implemented with Feel++, we compare the numerical results with analytical solutions of the Stokes problem.

Solution of Bercovier-Engelman

First of all, in order to validate the implementation of the Stokes problem only, we use the solution of Bercovier-Engelman [25], which consists in finding a velocity that satisfies the free divergence condition and is null on the whole boundary. From this velocity and a source term $\mathbf{f}$, we deduce gradient pressure, and then a pressure.

$$\mathbf{v} = \begin{pmatrix} -256z(z-1)(2z-1)x^2(x-1)^2 \\ 256x(x-1)(2x-1)z^2(z-1)^2 \end{pmatrix}$$

$$p = (x-0.5)(z-0.5)$$

$$\mathbf{f} = \begin{pmatrix} 256(x^2(x-1)^2(12z-6) + z(z-1)(2z-1)(12x^2-12x+2)) + (z-0.5) \\ -256(z^2(z-1)^2(12x-6) + x(x-1)(2x-1)(12z^2-12z+2)) + (x-0.5) \end{pmatrix}$$

We can compare the exact solution and the approximation in Fig A.3.

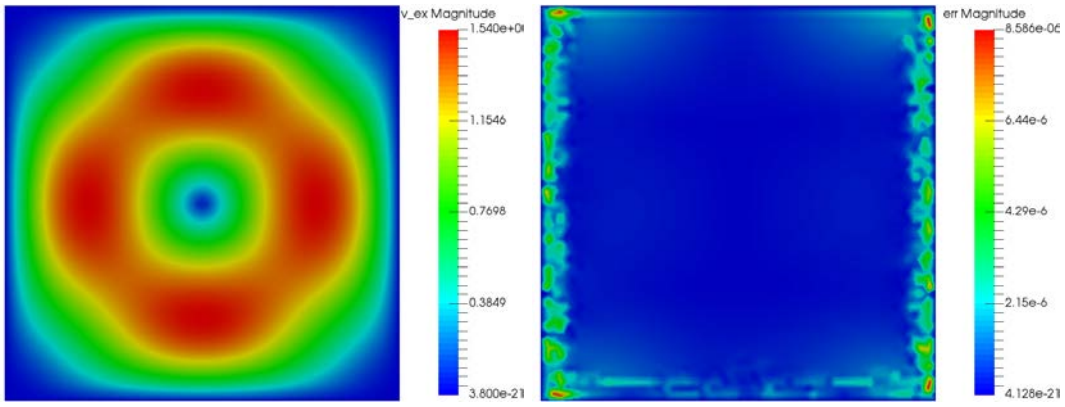

(a) Exact solution (b) Error

Figure A.3: Velocity field of the exact solution and error with the numerical solution.

In Figure A.4, we compute the errors between the exact and the computed solution and plot these errors versus the mesh size (in log-log scale). We can then verify that the method converges and that the convergence orders are 3 for the L2-norm of the velocity and 2 for the pressure, which are those expected by the theory with the finite elements chosen here.

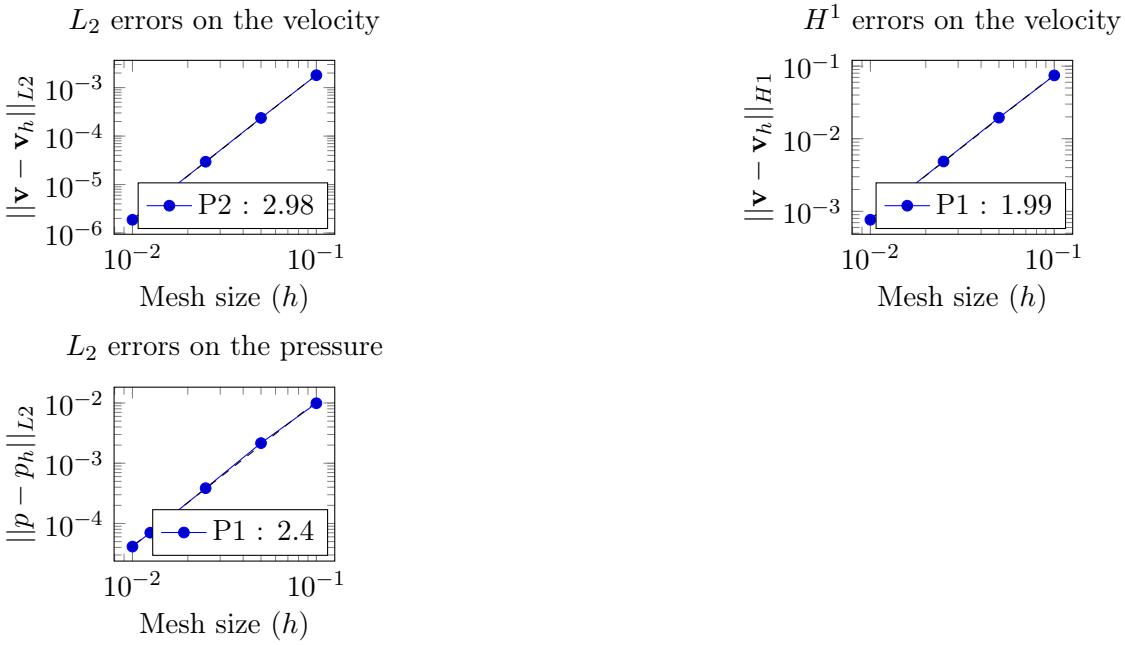

Figure A.4: Convergence rates for the Bercovier-Engelman solution.

Driven cavity

The second test case, the driven cavity, is a very classical test case in fluid dynamics. We verify again that the Stokes problem is well solved but with more physical boundary conditions that will be useful in the sequel. Indeed, to obtain this solution, we impose $v|_{\Gamma_{in} \cup \Gamma_{out} \cup \Gamma_b} = 0$ and $v|_{\Gamma_s} = (1, 0)^T$. The numerical results are shown in Figure A.5.

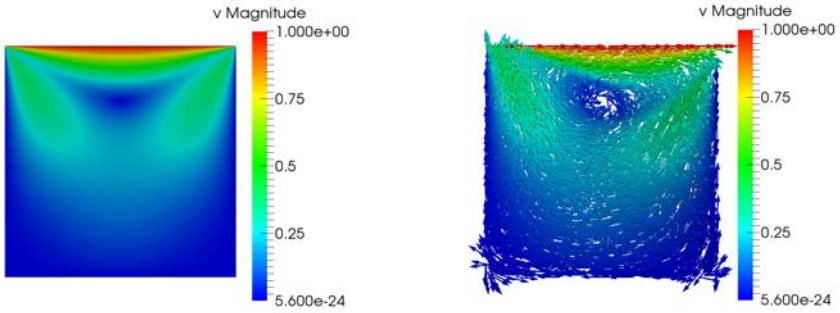

(a) Magnitude field (b) Velocity field

Figure A.5: Driven cavity.

Notice that the discontinuity of the velocity of the corners of the cavity is due to the discontinuity of the velocity imposed by the Dirichlet condition. It does not infer on the training, but to avoid this result, a polynomial function can be set instead of the constant.

A.4.2 Fluvial dune test case

To validate our complete coupled model with the Exner equation, we take an initial dune given by the equation :

$$b_z(x,0) = 0.2 \times e^{-\frac{(x-2.5)^2}{0.2}}, \forall x \in [0,l] \tag{A.65}$$

with $l = 5$.

For the unsteady Stokes equation, we use the slip boundary condition (A.4)-(A.7) and let free the velocity at the inlet and outlet with a Neumann boundary condition (A.5) with $\mathbf{g}_2 = \mathbf{0}$. On the top, we impose the same Dirichlet condition than in the driven cavity $\mathbf{u} = (1,0)^T$, driven the fluid to the right.

For the Exner model, we use the Grass formula (A.10) and the initial data given by (A.65).

We use the numerical method presented above : finite element method for spacial discretization and Implicit Euler method for time discretization for all the parts equations. As the cavity is driven with a moving bottom, we add the ALE formulation and obtain the results showed in Figure A.6. We use the penalty method for bottom condition.

The result is given in figure A.6 and is similar to that of E. J. Kubatko and J. J. Westerink [102] (Fig. 2 of their paper). The same test case has been tested with multiple dunes and a similar result (distortion to the right) was obtained. This kind of solution can be difficult to represent with a numerical scheme because the solution becomes discontinuous but the algorithm stays stable during the simulation. This test case allows us to evaluate the relevance of our method but a comparison with an analytical solution is necessary to validate the method.

A.5 Conclusion

In this note, we consider a coupling between the Exner equation and the Stokes equations to model the transport sediments in flow phenomena. We focus on a model without free surface and use some numerical tests to evaluate the relevance of the method. The fluid structure interaction theory and method have been applied and the objective is to te st the proposed method which can be extend to a free surface model. The library Feel++ and the high computing performance embedded have been used to test the solution method. Therefore, the final goal of this project is to understand the impact of the sediment transport on the flow using Navier-Stokes with a free surface system coupled with the standard Exner equation.

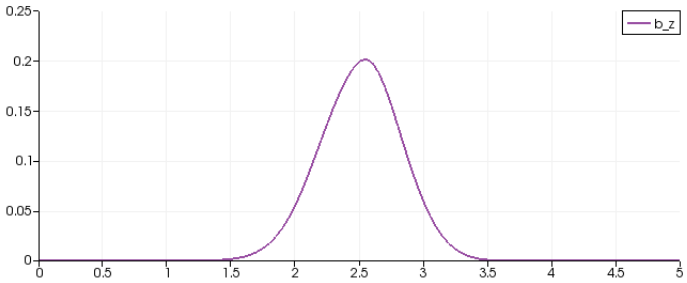

(a) $t = 0s$

(b) $t = 8s$

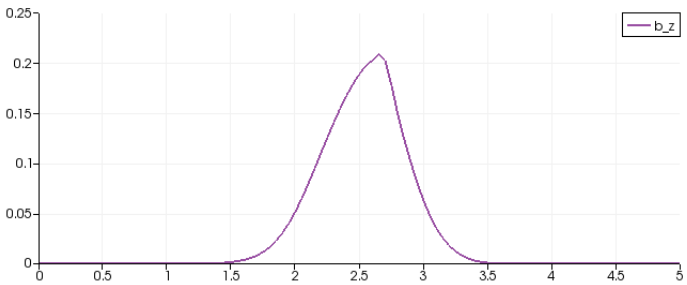

(c) $t = 16s$

Figure A.6: Bottom topography at different times

Bibliography

[1] G. Airy. Tides and waves. *Encycl. Metropolitana*, 5:291–369, 1845.

[2] N. Aïssiouene, M. O. Bristeau, E. Godlewski, and J. Sainte-Marie. A robust and stable numerical scheme for a depth-averaged euler system. *Submitted*, pages –, 2015.

[3] N. Aïssiouene, M.-O. Bristeau, E. Godlewski, and J. Sainte-Marie. A combined finite volume - finite element scheme for a dispersive shallow water system. *Networks and Heterogeneous Media*, 11(1):1–27, 2016.

[4] B. Alvarez-Samaniego and D. Lannes. Large time existence for 3D water-waves and asymptotics. *Invent. Math.*, 171(3):485–541, 2008.

[5] B. Alvarez-Samaniego and D. Lannes. A Nash-Moser theorem for singular evolution equations. Application to the Serre and Green-Naghdi equations. *Indiana Univ. Math. J.*, 57(1):97–131, 2008.

[6] E. Audusse. A multilayer Saint-Venant model: Derivation and numerical validation. *Discret. Contin. Dyn. Syst. Ser. B*, 5(2):189–214, 2005.

[7] E. Audusse, F. Bouchut, M.-O. Bristeau, R. Klein, and B. Perthame. A fast and stable well-balanced scheme with hydrostatic reconstruction for Shallow Water flows. *SIAM J. Sci. Comput.*, 25(6):2050–2065, 2004.

[8] E. Audusse, F. Bouchut, M.-O. Bristeau, and J. Sainte-Marie. Kinetic entropy inequality and hydrostatic reconstruction scheme for the Saint-Venant system. Published online in Math. Comp. http://dx.doi.org/10.1090/mcom/3099, March 2016.

[9] E. Audusse and M.-O. Bristeau. Transport of pollutant in shallow water flows : A two time steps kinetic method. *ESAIM: M2AN*, 37(2):389–416, 2003.

[10] E. Audusse and M.-O. Bristeau. A well-balanced positivity preserving second-order scheme for Shallow Water flows on unstructured meshes. *J. Comput. Phys.*, 206(1):311–333, 2005.

[11] E. Audusse and M.-O. Bristeau. Finite-volume solvers for a multilayer Saint-Venant system. *Int. J. Appl. Math. Comput. Sci.*, 17(3):311–319, 2007.

[12] E. Audusse, M.-O. Bristeau, and A. Decoene. Numerical simulations of 3d free surface flows by a multilayer Saint-Venant model. *Internat. J. Numer. Methods Fluids*, 56(3):331–350, 2008.

[13] E. Audusse, M.-O. Bristeau, M. Pelanti, and J. Sainte-Marie. Approximation of the hydrostatic Navier-Stokes system for density stratified flows by a multilayer model. Kinetic interpretation and numerical validation. *J. Comp. Phys.*, 230:3453–3478, 2011.

[14] E. Audusse, M.-O. Bristeau, and B. Perthame. Kinetic schemes for Saint-Venant equations with source terms on unstructured grids. Technical Report 3989, INRIA, Unité de recherche de Rocquencourt, FRANCE, 2000. http://www.inria.fr/rrrt/rr-3989.html.

[15] E. Audusse, C. Chalons, O. Delestre, N. Goutal, M. Jodeau, J. Sainte-Marie, J. Giesselmann, and G. Sadaka. Sediment transport modelling : relaxation schemes for Saint-Venant - Exner and three layer models. *ESAIM: Proceedings*, 38:78–98, 2012.

[16] E. Audusse, C. Chalons, and P. Ung. A simple three-wave Approximate Riemann Solver for the Saint-Venant–Exner equations. working paper or preprint, Sept. 2015.

[17] M. L. B. Camenen. A general formula for non-cohesive bed load sediment transport. *Estuarine Coastal Shelf Sci*, pages 249–260, 2005.

[18] I. Babuska. The finite element method with lagrangian multipliers. *Numerische Mathematik*, 20:179–192, 1972/73.

[19] P. Bacigaluppi, M. Ricchiuto, and P. Bonneton. *A 1D Stabilized Finite Element Model for Non-hydrostatic Wave Breaking and Run-up*, pages 779–790. Springer International Publishing, Cham, 2014.

[20] A.-J.-C. Barré de Saint-Venant. Sur la houle et le clapotis. *C. R. Acad. Sci. Paris*, 73:521–528,589–593, 1871.

[21] A.-J.-C. Barré de Saint-Venant. Théorie du mouvement non permanent des eaux avec applications aux crues des rivières et à l'introduction des marées dans leur lit. *C. R. Acad. Sci. Paris*, 73:147–154, 1871.

[22] J. Behrens and F. Dias. New computational methods in tsunami science. *Philos Trans A Math Phys Eng Sci.*, Oct 28(373):(2053), 2015.

[23] S. Bellec, M. Colin, and M. Ricchiuto. Discrete asymptotic equations for long wave propagation. Research Report RR-8806, Inria Bordeaux Sud-Ouest, Nov. 2015.

[24] T. Belytschko and J. M. Kennedy. Computer models for subassembly simulation. *Nuclear Engineering and Design*, 49, 1978.

[25] M. Bercovier and M. Engelman. A finite element for the numerical solution of viscous incompressible flows. *Journal of Computational Physics*, 30(2):181–201, 1979.

[26] J.-L. Bona, T.-B. Benjamin, and J.-J. Mahony. Model equations for long waves in nonlinear dispersive systems. *Philos. Trans. Royal Soc. London Series A*, 272:47–78, 1972.

[27] J.-L. Bona, M. Chen, and J.-C. Saut. Boussinesq equations and other systems for small-amplitude long waves in nonlinear dispersive media: Part I. Derivation and linear theory. *J. Nonlinear Sci.*, 12:283–318, 2002.

[28] J.-L. Bona, M. Chen, and J.-C. Saut. Boussinesq equations and other systems for small-amplitude long waves in nonlinear dispersive media: Part II. Nonlinear theory. *Nonlinearity*, 17:925–952, 2004.

[29] P. Bonneton, E. Barthelemy, F. Chazel, R. Cienfuegos, D. Lannes, F. Marche, and M. Tissier. Recent advances in Serre-Green Naghdi modelling for wave transformation, breaking and runup processes. *European Journal of Mechanics - B/Fluids*, 30(6):589 – 597, 2011. Special Issue: Nearshore Hydrodynamics.

[30] P. Bonneton, F. Chazel, D. Lannes, F. Marche, and M. Tissier. A splitting approach for the fully nonlinear and weakly dispersive Green–Naghdi model. *Journal of Computational Physics*, 230(4):1479 – 1498, 2011.

[31] F. Bouchut. An introduction to finite volume methods for hyperbolic conservation laws. *ESAIM Proc.*, 15:107–127, 2004.

[32] F. Bouchut. *Nonlinear stability of finite volume methods for hyperbolic conservation laws and well-balanced schemes for sources.* Birkhäuser, 2004.

[33] F. Bouchut, A. Mangeney-Castelnau, B. Perthame, and J.-P. Vilotte. A new model of Saint-Venant and Savage-Hutter type for gravity driven shallow water flows. *C. R. Math. Acad. Sci. Paris*, 336(6):531 – 536, 2003.

[34] F. Bouchut and T. Morales de Luna. An entropy satisfying scheme for two-layer shallow water equations with uncoupled treatment. *M2AN Math. Model. Numer. Anal.*, 42:683–698, 2008.

[35] F. Bouchut and M. Westdickenberg. Gravity driven shallow water models for arbitrary topography. *Comm. in Math. Sci.*, 2:359–389, 2004.

[36] J.-V. Boussinesq. Théorie de l'intumescence liquide appelée onde solitaire ou de translation se propageant dans un canal rectangulaire. *C. R. Acad. Sci. Paris*, 72:755–759, 1871.

[37] J.-V. Boussinesq. Théorie générale des mouvements qui sont propagés dans un canal rectangulaire horizontal. *C. R. Acad. Sci. Paris*, 73:256–260, 1871.

[38] J.-V. Boussinesq. Théorie des ondes et des remous qui se propagent le long d'un canal rectangulaire horizontal, en communiquant au liquide contenu dans ce canal des vitesses sensiblement pareilles de la surface au fond. *J. Math. Pures Appl.*, 17:55–108, 1872.

[39] Y. Brenier. Homogeneous hydrostatic flows with convex velocity profiles. *Nonlinearity*, 12(3):495–512, 1999.

[40] F. Brezzi. On the existence, uniqueness and approximation of saddle-point problems arising from Lagrangian multipliers. *Rev. Française Automat. Informat. Recherche Opérationnelle Sér. Rouge*, 8(R-2):129–151, 1974.

[41] M.-O. Bristeau and B. Coussin. Boundary Conditions for the Shallow Water Equations solved by Kinetic Schemes. Rapport de recherche RR-4282, INRIA, 2001. Projet M3N.

[42] M.-O. Bristeau, N. Goutal, and J. Sainte-Marie. Numerical simulations of a non-hydrostatic Shallow Water model. *Computers & Fluids*, 47(1):51–64, 2011.

[43] M.-O. Bristeau, A. Mangeney, J. Sainte-Marie, and N. Seguin. An energy-consistent depth-averaged euler system: Derivation and properties. *Discrete and Continuous Dynamical Systems - Series B*, 20(4):961–988, 2015.

[44] M.-O. Bristeau and J. Sainte-Marie. Derivation of a non-hydrostatic shallow water model; Comparison with Saint-Venant and Boussinesq systems. *Discrete Contin. Dyn. Syst. Ser. B*, 10(4):733–759, 2008.

[45] R. Camassa, D. Holm, and J. Hyman. A new integrable shallow water equation. *Adv. Appl. Math.*, 31:23–40, 1993.

[46] M. J. Castro Diaz, E. D. Fernandez, C. Pares, and a. M. Ferreiro. Two-dimensional sediment transport models in shallow water equations. A second order finite volume approach on unstructured meshes. *Computer Methods in Applied Mechanics and Engineering*, 198:2520–2538, 2009.

[47] V. Chabannes. *Vers la simulation des écoulements sanguins.* PhD thesis, Université de Grenoble, 2013.

[48] F. Chazel, D. Lannes, and F. Marche. Numerical simulation of strongly nonlinear and dispersive waves using a Green–Naghdi model. *J. Sci. Comput.*, 48(1-3):105–116, July 2011.

[49] Y. Chisti. Biodiesel from microalgae. *Biotechnol Adv.*, 25(3):294–306, 2007.

[50] A. J. Chorin. Numerical solution of the Navier-Stokes equations. *Math. Comp.*, 22:745–762, 1968.

[51] R. Cienfuegos, E. Barthélemy, and P. Bonneton. A fourth-order compact finite volume scheme for fully nonlinear and weakly dispersive Boussinesq-type equations. Part I: Model development and analysis. *Internat. J. Numer. Methods Fluids*, 51(11):1217–1253, 2006.

[52] D. Clamond, D. Dutykh, and D. Mitsotakis. Conservative modified Serre-Green-Naghdi equations with improved dispersion characteristics. *ArXiv e-prints*, Nov. 2015.

[53] S. Cordier, M. Le, and T. Morales de Luna. Bedload transport in shallow water models: Why splitting (may) fail, how hyperbolicity (can) help. *Adv. Water Resour.*, 34(8):980–989, 2011.

[54] R. Dasgupta and R. Govindarajan. The hydraulic jump and the shallow-water equations. *International Journal of Advances in Engineering Sciences and Applied Mathematics*, 3(1):126–130, 2011.

[55] E. M. de Jager. On the origin of the Korteweg-de Vries equation. *ArXiv Mathematics e-prints*, Feb. 2006.

[56] M. Dingemans. Comparison of computations with Boussinesq-like models and laboratory measurements. Technical Report H1684-12, AST G8M Coastal Morphodybamics Research Programme, 1994.

[57] M.-W. Dingemans. *Wave propagation over uneven bottoms.* Advanced Series on Ocean Engineering - World Scientific, 1997.

[58] I. Dione. *Analyse théorique et numérique des conditions de glissement pour les fluides et les solides par la méthode de pénalisation.* PhD thesis, Université de Laval, 2013.

[59] J. Donéa. Analysis of the levelling process based upon an analytic forming model. *Advances Science Publishers*, 3, 1978.

[60] J. Donéa, S. Giuliani, and J.-P. Halleux. An arbitrary lagrangian-eulerian fem for transient dynamic fluid-structure interactions. *Computer Methods in Applied Mechanics and Engineering*, 33, 1982.

[61] M. Dumbser and M. Facchini. A space-time discontinuous galerkin method for boussinesq-type equations. *Appl. Math. Comput.*, 272(P2):336–346, Jan. 2016.

[62] A. Duran and F. Marche. Discontinuous-Galerkin discretization of a new class of Green-Naghdi equations. *Communications in Computational Physics*, page 130, Oct. 2014.

[63] A. Duran and F. Marche. A discontinuous Galerkin method for a new class of Green-Naghdi equations on simplicial unstructured meshes. *ArXiv e-prints*, Apr. 2016.

[64] D. Dutykh. *Mathematical modelling of tsunami waves.* Theses, École normale supérieure de Cachan - ENS Cachan, Dec. 2007.

[65] D. Dutykh, D. Clamond, P. Milewski, and D. Mitsotakis. Finite volume and pseudo-spectral schemes for the fully nonlinear 1d serre equations. *European Journal of Applied Mathematics*, 24(5):761–787, 005 2013.

[66] D. Dutykh, T. Katsaounis, and D. Mitsotakis. Finite volume methods for unidirectional dispersive wave models. *Internat. J. Numer. Methods Fluids*, 71(6):717–736, 2013.

[67] W. E and J.-G. Liu. Projection Method I: Convergence and Numerical Boundary Layers. *SIAM J. Numer. Anal.*, 32(4):1017–1057, 1995.

[68] R. M. E. Meyer-Peter. Formulae for bed-load transport. *Report on the 2nd Meeting International Association Hydraulic Structure Research*, pages 39–64, 1948.

[69] H. Einstein. The bed-load function for sediment transportation in open channel flows. *Tech. Rep. 1026,US Department of Agriculture, Technical Bulletin*, 1950.

[70] A. Ern and S. Meunier. A posteriori error analysis of euler-galerkin approximations to coupled elliptic-parabolic problems. *ESAIM Math. Model. Numer. Anal.*, 43:353–375, 2009.

[71] G. Ern. *Theory and Practice of Finite Elements.* Springer-Verlag New York, 2004.

[72] C. Escalante, T. Morales, and M.-J. Castro. Weakly dispersive shallow water flows: an efficient implementation using a finite-volume finite-difference scheme. In *Proceedings of the XXIV congress on differential equations and applications XIV congress on applied mathematics*, pages 255–259, Cadiz, 2015.

[73] R. Eymard, D. Hilhorst, and M. Vohralík. A combined finite volume–finite element scheme for the discretization of strongly nonlinear convection–diffusion–reaction problems on nonmatching grids. *Numerical Methods for Partial Differential Equations*, 26(3):612–646, 5 2010.

[74] E. Fernandez-Nieto, M. Parisot, Y. Penel, and J. Sainte-Marie. Layer-averaged approximations for inviscid flow models. -, 2016.

[75] E. D. Fernández-Nieto, T. M. de Luna, G. Narbona-Reina, and J. D. Zabsonré. Formal deduction of the Saint-Venant-Exner model including arbitrarily sloping sediment beds and associated energy. *ArXiv*, pages 1–44, 2015.

[76] E. D. Fernández-Nieto, E. H. Koné, and T. Chacón Rebollo. A multilayer method for the hydrostatic navier-stokes equations: A particular weak solution. *Journal of Scientific Computing*, 60(2):408–437, 2014.

[77] S. Ferrari and F. Saleri. A new two-dimensional Shallow Water model including pressure effects and slow varying bottom topography. *M2AN Math. Model. Numer. Anal.*, 38(2):211–234, 2004.

[78] R. M. Frank and R. B. Lazarus. Mixed eulerian-lagrangian method. *Academic Press*, 3, 1964.

[79] J.-F. Gerbeau and B. Perthame. Derivation of Viscous Saint-Venant System for Laminar Shallow Water; Numerical Validation. *Discrete Contin. Dyn. Syst. Ser. B*, 1(1):89–102, 2001.

[80] V. Girault and P.-A. Raviart. *Finite element methods for Navier-Stokes equations*, volume 5 of *Springer Series in Computational Mathematics*. Springer-Verlag, Berlin, 1986. Theory and algorithms.

[81] S. Glimsdal, G. K. Pedersen, C. B. Harbitz, and F. Løvholt. Dispersion of tsunamis: does it really matter? *Natural Hazards and Earth System Sciences*, 13(6):1507–1526, 2013.

[82] E. Godlewski and P.-A. Raviart. *Hyperbolic systems of conservation laws*, volume 3/4 of *Mathématiques & Applications (Paris) [Mathematics and Applications]*. Ellipses, Paris, 1991.

[83] E. Godlewski and P.-A. Raviart. *Numerical approximations of hyperbolic systems of conservation laws*. Applied Mathematical Sciences, vol. 118, Springer, New York, 1996.

[84] C. Grandmont. *Analyse mathématique et numérique de problèmes d'interaction fluide-structure.*

Application à la modélisation de l'appareil respiratoire. Habilitation à diriger des recherches, Université Pierre et Marie Curie - Paris VI, Nov. 2009. Dans le cadre de l'ANR M3RS (ANR-08-JCJC-0013-01).

[85] J. Grass. Sediments transport by waves and currents. *SERC London Cent. Mar. Technol., Report No. FL29*, 1981.

[86] A. Green and P. Naghdi. A derivation of equations for wave propagation in water of variable depth. *J. Fluid Mech.*, 78:237–246, 1976.

[87] A. E. Green, N. Laws, and P. M. Naghdi. On the theory of water waves. *Proc. Roy. Soc. (London) Ser. A*, 338:43–55, 1974.

[88] E. Grenier. On the derivation of homogeneous hydrostatic equations. *ESAIM: M2AN*, 33(5):965–970, 1999.

[89] P. Gresho and S. Chan. Semi-consistent mass matrix techniques for solving the incompressible Navier-Stokes equations. *First Int. Conf. on Comput. Methods in Flow Analysis*, 1988. Okayama University, Japan.

[90] J.-L. Guermond. Some implementations of projection methods for Navier-Stokes equations. *ESAIM: Mathematical Modelling and Numerical Analysis*, 30(5):637–667, 1996.

[91] J. L. Guermond and P. D. Minev. A new class of massively parallel direction splitting for the incompressible Navier-Stokes equations. *Computer Methods in Applied Mechanics and Engineering*, 200(23-24):2083–2093, 2011.

[92] J.-L. Guermond and J. Shen. On the error estimates for the rotational pressure-correction projection methods. *Math. Comput.*, 73(248):1719–1737, 2004.

[93] P. H. Gunawan and X. Lhébrard. Hydrostatic relaxation scheme for the 1D shallow water - Exner equations in bedload transport. *Comput. Fluids*, 121:44–50, 2015.

[94] F. Hecht and C. Pares. NSP1B3 : un logiciel pour resoudre les equations de Navier Stokes incompressible 3D. Research Report RR-1449, INRIA, 1991. Projet MENUSIN.

[95] S. Israwi and A. Mourad. An explicit solution with correctos for the Green-Naghdi equations. *Mediterr. J. Math.*, 11:519–532, 2013.

[96] H. Johnston and J.-G. Liu. Accurate, stable and efficient Navier–Stokes solvers based on explicit treatment of the pressure term. *Journal of Computational Physics*, 199(1):221 – 259, 2004.

[97] A. Kalinske. Movement of sediment as bed load in rivers. *Earth and Space Sciences News*, pages 615–620, 1947.

[98] D. Kazerani. Global existence for small data of the viscous Green-Naghdi type equations. *Journal of Differential Equations*, 261(1):762–796, July 2016.

[99] M. Kazolea, A. Delis, and C. Synolakis. Numerical treatment of wave breaking on unstructured finite volume approximations for extended boussinesq-type equations. *Journal of Computational Physics*, 271:281 – 305, 2014. Frontiers in Computational PhysicsModeling the Earth System.

[100] D. J. Korteweg and G. de Vries. On the change of form of long waves advancing in a rectangular canal, and on a new type of long stationary waves. *Philosophical Magazine*, 39:422–443, 1895.

[101] M. D. Kruskal and N. J. Zabusky. Exact invariants for a class of nonlinear wave equations. *J. Mathematical Phys.*, 7:1256–1267, 1966.

[102] E. J. Kubatko and J. J. Westerink. Exact Discontinuous Solutions of Exner's Bed Evolution Model : Simple Theory for Sediment Bores. *Journal of Hydraulic Engineering*, 2007.

[103] O. Ladyzhenskaya. *The mathematical theory of viscous incompressible flow.* New York: Gordon and Breach, 1969.

[104] D. Lannes. *The water waves problem*, volume 188 of *Mathematical Surveys and Monographs*. American Mathematical Society, Providence, RI, 2013. Mathematical analysis and asymptotics.

[105] D. Lannes and P. Bonneton. Derivation of asymptotic two-dimensional time-dependent equations for surface water wave propagation. *Physics of Fluids*, 21(1):016601, 2009.

[106] D. Lannes and F. Marche. A new class of fully nonlinear and weakly dispersive Green-Naghdi models for efficient 2D simulations. *Journal of Computational Physics*, pages 238–268, Dec. 2014.

[107] P. Lascaux and R. Theodor. *Analyse numérique matricielle appliquée à l'art de l'ingénieur*. Masson, 1986.

[108] O. Le Métayer, S. Gavrilyuk, and S. Hank. A numerical scheme for the Green-Naghdi model. *J. Comput. Phys.*, 229(6):2034–2045, 2010.

[109] R. LeVeque. *Numerical methods for conservation laws.* Birkhauser, 1999.

[110] R.-J. LeVeque. *Finite Volume Methods for Hyperbolic Problems*. Cambridge University Press, 2002.

[111] R. J. LeVeque, D. L. George, and M. J. Berger. Tsunami modelling with adaptively refined finite volume methods*. *Acta Numerica*, 20:211–289, 004 2011.

[112] C. Levermore and M. Sammartino. A shallow water model with eddy viscosity for basins with varying bottom topography. *Nonlinearity*, 14(6):1493–1515, 2001.

[113] C. D. Levermore. Entropy-based moment closures for kinetic equations. In *Proceedings of the International Conference on Latest Developments and Fundamental Advances in Radiative Transfer (Los Angeles, CA, 1996)*, volume 26, pages 591–606, 1997.

[114] X. Lhebrard. *Analysis of several numerical scheme designed for shallow water problems*. Theses, Université Paris-Est, Apr. 2015.

[115] A. Lucas, A. Mangeney, and J. P. Ampuero. Frictional weakening in landslides on earth and on other planetary bodies. *Nature Communication*, 5(3417), 2014.

[116] M. P. M. Tonelli. Hybrid finite volume-finite difference scheme for 2dh improved boussinesq equations. *Coastal Engineering*, 56:609–620, 2009.

[117] P. Madsen and O. R. Sørensen. A new form of the boussinesq equations with improved linear dispersion characteristics. part 2: A slowing varying bathymetry. *Coastal Engineering*, 18:183–204, 1992.

[118] N. Makarenko. A second long-wave approximation in the Cauchy-Poisson problem (in Russian). *Dyn. Contin. Media*, 77:56–72, 1986.

[119] A. Mangeney, F. Bouchut, N. Thomas, J. P. Vilotte, and M.-O. Bristeau. Numerical modeling of self-channeling granular flows and of their levee-channel deposits. *Journal of Geophysical Research - Earth Surface*, 112(F02017), 2007.

[120] A. Mangeney-Castelnau, F. Bouchut, J. P. Vilotte, E. Lajeunesse, A. Aubertin, and M. Pirulli. On the use of Saint-Venant equations to simulate the spreading of a granular mass. *Journal of Geophysical Research: Solid Earth*, 110(B09103), 2005.

[121] F. Marche. Derivation of a new two-dimensional viscous shallow water model with varying topography, bottom friction and capillary effects. *European Journal of Mechanic /B*, 26:49–63, 2007.

[122] N. Masmoudi and T. Wong. On the Hs theory of hydrostatic Euler equations. *Archive for Rational Mechanics and Analysis*, 204(1):231–271, 2012.

[123] J. Miles and R. Salmon. Weakly dispersive nonlinear gravity waves. *J. Fluid Mech.*, 157:519–531, 1985.

[124] D. Mitsotakis, B. Ilan, and D. Dutykh. On the galerkin/finite-element method for the serre equations. *J. Sci. Comput.*, 61(1):166–195, 2014.

[125] P. Nielsen. Movement of sediment as bed load in rivers. *Cambridge University Press*, pages 615–620, 1947.

[126] P. Nielsen. Coastal Bottom Boundary Layers and Sediment Transport. *Advanced Series on Ocean Engineering*, vol. 4, 1992.

[127] P. Nielsen. Erosion and Sedimentation. *Cambridge University Press*, 1998.

[128] W. F. Noh. CEL : a time-dependent two-space-dimensional. Coupled Eulerian-Lagrangian code. *Academic Press*, 3, 1964.

[129] O. Nwogu. Alternative form of Boussinesq equations for nearshore wave propagation. *Journal of Waterway, Port, Coastal and Ocean Engineering, ASCE*, 119(6):618–638, 1993.

[130] G. Parker, C. Paola, and S. Leclair. Probabilistic Exner Sediment Continuity Equation for Mixtures with No Active Layer, 2000.

[131] D. Peregrine. Long waves on a beach. *J. Fluid Mech.*, 27:815–827, 1967.

[132] B. Perthame. *Kinetic formulation of conservation laws.* Oxford University Press, 2002.

[133] B. Perthame and C. Simeoni. A kinetic scheme for the Saint-Venant system with a source term. *Calcolo*, 38(4):201–231, 2001.

[134] O. Pironneau. *Méthodes des éléments finis pour les fluides.* Masson, 1988.

[135] A. Prosperetti. *Navier-Stokes Numerical Algorithms for Free-Surface Flow Computations: An Overview*, pages 237–257. Springer Vienna, Vienna, 2002.

[136] C. Prud'Homme, V. Chabannes, V. Doyeux, M. Ismail, A. Samake, and G. Pena. Feel++: A Computational Framework for Galerkin Methods and Advanced Numerical Methods. *ESAIM: Proceedings*, 38:429–455, Dec. 2012. CEMRACS'11: Multiscale Coupling of Complex Models in Scientific Computing.

[137] C. Prud'Homme, V. Chabannes, V. Doyeux, M. Ismail, A. Samake, and G. Pena. Feel++: A computational framework for galerkin methods and advanced numerical methods. In *ESAIM: Proceedings*, volume 38, pages 429–455. EDP Sciences, 2012.

[138] R. Rannacher. On Chorin's projection method for the incompressible Navier-Stokes equations. In G. Heywood, John, K. Masuda, R. Rautmann, and A. Solonnikov, Vsevolod, editors, *The Navier-Stokes Equations II — Theory and Numerical Methods*, volume 1530 of *Lecture Notes in Mathematics*, pages 167–183. Springer Berlin Heidelberg, 1992.

[139] V. Roeber, K. F. Cheung, and M. H. Kobayashi. Shock-capturing boussinesq-type model for nearshore wave processes. *Coastal Engineering*, 57(4):407 – 423, 2010.

[140] G. Russo. *Central schemes for conservation laws with application to shallow water equations*, pages 225–246. Springer Milan, Milano, 2005.

[141] J. Sainte-Marie. Vertically averaged models for the free surface Euler system. Derivation and kinetic interpretation. *Math. Models Methods Appl. Sci. (M3AS)*, 21(3):459–490, 2011.

[142] Serre. Contribution à l'étude des écoulements permanents et variables dans les cannaux. *Houille Blanche*, 8:374–388, 2011.

[143] J. Shen. Pseudo-compressibility methods for the unsteady incompressible Navier-Stokes equations. *11th AIAA Computational Fluid Dynamic Conference*, 1993. Orlando, FL, USA.

[144] J. Shen. On error estimates of the penalty method for unsteady Navier-Stokes equations. *SIAM J. Numer. Anal.*, 32(2):386–403, 1995.

[145] G. Smart. Sediment transport formula for steep channels. *J. Hydraul*, 3:267–276, 1984.

[146] C. H. Su and C. S. Gardner. Korteweg-de Vries equation and generalizations. III. Derivation of the Korteweg-de Vries equation and Burgers equation. *J. Mathematical Phys.*, 10:536–539, 1969.

[147] C. E. Synolakis. The runup of solitary waves. *Journal of Fluid Mechanics*, 185:523–545, 04 2006.

[148] W. C. Thacker. Some exact solutions to the non-linear shallow-water wave equations. *J. Fluid Mech.*, 107:499–508, 1981.

[149] E. van Brummelen, H. Raven, and B. Koren. Efficient numerical solution of steady free-surface Navier-Stokes flow. *Journal of Computational Physics*, 174(1):120 – 137, 2001.

[150] G. B. Whitham. *Linear and nonlinear waves*. Pure and Applied Mathematics (New York). John Wiley & Sons, Inc., New York, 1999. Reprint of the 1974 original, A Wiley-Interscience Publication.

[151] Y. Xing and C.-W. Shu. A new approach of high order well-balanced finite volume weno schemes and discontinuous galerkin methods for a class of hyperbolic systems with source terms. *Commun. Comput. Phys.*, 1:100–134, 2006.

[152] Y. Yamazaki, Z. Kowalik, and K. F. Cheung. Depth-integrated, non-hydrostatic model for wave breaking and run-up. *Internat. J. Numer. Methods Fluids*, 61(5):473–497, 2009.